EPSILON AURIGAE
A Mysterious Star System

by

Jeffrey L. Hopkins
Hopkins Phoenix Observatory
and
Robert E. Stencel
University of Denver

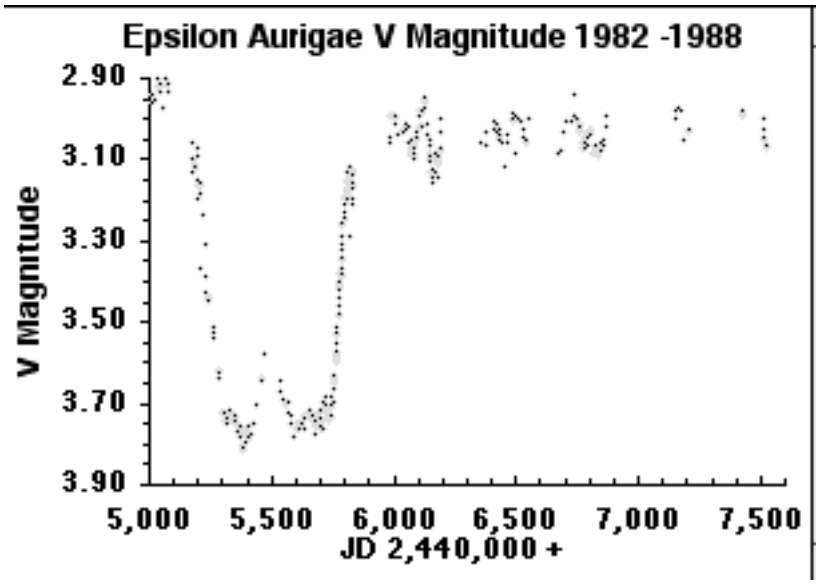

Copyright © 2008
Jeffrey L. Hopkins
and
Robert E. Stencel

All Rights Reserved

Reproduction or translation of any part of this work [except where specifically noted] beyond that permitted by sections 107 or 108 of the 1976 United States Copyright Act, without permission of the Copyright Owner, is unlawful. Requests for permission or further information should be addressed to: HOPKINS PHOENIX OBSERVATORY, 7812 West Clayton Drive, Phoenix, Arizona 85033-2439 U.S.A.

First Edition – First Printing September 2008
ISBN: 978-0-615-24022-0

Published in the United States of America
by
Hopkins Phoenix Observatory
7812 West Clayton Drive
Phoenix, Arizona 85033-2439 U.S.A.
http://www.hposoft.com

All photographs and figures are by the authors unless otherwise noted. Adirondack Astro Video, All Electronics, and Scope Stuff are copyrighted© trademarks® of their respective businesses. Astrodon and Schuler Photometric Filters are copyrighted© trademarks® of Astrodon, Inc. ATIK is a copyrighted© trademark® of ATIK, Inc. FileMaker Pro and FileMaker Developer are copyrighted© trademarks® of FileMaker, Inc. Autostar Suite, Deep Sky Imager, DSI, DSI Pro, Envisage, LX200 GPS, and the Meade logo are copyrighted© trademarks® of Meade Instruments Corporation. Microsoft Office, Word, Excel, PowerPoint, and NotePad are copyrighted© trademarks® of Microsoft Corporation.

Dedication

To all those who have contributed to the understanding of the epsilon Aurigae star system, especially those who are no longer with us and those about to make the next discoveries.

Table of Contents

	Page
Dedication	i
Table of Contents	iii
List of Tables and Figures	ix
Preface	xv
Acknowledgments	xvii
I. Introduction	1
1.1 Variable Stars	2
1.2 Auriga, Capella and the Kids	2
1.3 Epsilon Aurigae	3
1.4 Backyard Astronomers	4
II. History	5
2.1 First Observations	5
2.2 Disagreeable Spectra	6
2.3 Alternative Models	7
2.4 Observational Progress Preceding the 1982-84 Eclipse	8
2.5 The 1982-84 Eclipse and Theoretical Progress	10
2.6 Inter-eclipse Milestones on the Approach to 2009	15
2.7 References	18
III. 1982/1984 Campaign	21
3.1 The Campaign	21
3.2 American Astronomical Society Meeting	22
3.3 Workshop Invited Papers	22
3.4 Workshop Contributed Papers	23
3.5 Workshop Attendees	23
3.6 Workshop Photographs	24
3.7 Workshop Attendee Photograph	28
3.8 Photometry Data	29
3.8.1 Out-of-eclipse magnitudes	29
3.8.2 1982 -1984 Totality Magnitudes	29
3.8.3 1982 -1984 Depths Magnitudes	29
3.8.4 Contact Times	29
3.8.5 1982 -1984 Eclipse Summary of Event Durations	30
3.8.6 Photometry Data Plots	30
3.9 Spectroscopy	36
3.10 Polarimetry	37
3.10.1 Introduction	37
3.10.2 Interpretation	37
3.11 References	38

IV. Post 1984 Observations 39

4.0 Introduction 39
4.1 Photometry Data 39
4.1.1 HPO UBV Photometric Data 1982 - 1988 40
4.1.2 HPO UBV Photometric Data 2003 - 2008 43
4.1.3 HPO JH Photometric Data 2006 - 2007 47
4.1.4 Boyd UBV Photometric Data 1987 - 2005 48
4.1.5 Frequency Domain Data 52
4.1.5.1 Introduction 52
4.1.5.2 HPO V Band Frequency Domain Data 52
4.1.5.3 HPO V Band Prominent Period Data 56
4.2 Spectroscopy Data 58
4.2.1 Hydrogen Alpha Lines 58
4.2.2 Be Stars Hα Line 59
4.2.3 Epsilon Aurigae Hα Line 60
4.3 Polarimetry Data 64
4.4 Interferometry Data 64
4.4.1 Introduction 64
4.4.2 Navy Prototype Optical Interferometer 64
4.5 References 65

V. Current Interpretations 66

5.1 Epsilon Aurigae System Schematic 66
5.2 Next Eclipse Timing 66
5.3 Past Eclipse Timing 67
5.3.1 Timing Changes 67
5.3.1.1 Duration and Totality Change 68
5.3.1.2 Ingress and Egress Change 70
5.3.1.3 Eclipse Period Change 70
5.3.1.4 Eclipse Magnitude Change 71
5.3.2 Out-of-Eclipse Changes 71
5.3.2.1 Photometric Changes 71
5.3.2.2 Spectroscopic Changes 72
5.3.2.2 Spectroscopic Changes 72
5.3.3 Summary and Predictions 72
5,4 References 75

VI. 2009 Campaign 76

6.1 Campaign Web Site 76
6.2 Photometry Contact Time Predictions 76
6.3 Spectroscopy 77
6.4 Polarimetry 77
6.5 Interferometry 78
6.5.1 Palomar Testbed Interferometer 78
6.5.2 Preliminary Results 79
6.6 References 81

VII. Similar Star Systems 82

7.1 Introduction 82
7.2 Zeta Aurigae 82
7.2.1 Introduction 82
7..2.2 Zeta Aurigae Data 82
7.2.3 Zeta Aurigae Comparison Star 83
7.2.5 References 84
7.3 VV Cephei 84
7.3.1 Introduction 84
7.3.2 VV Cephei Data 85
7.3.3 VV Cephei Comparison Star 85
7.3.4 References 86
7.4 EE Cephei 87
7.4.1 Introduction 87
7.4.2 EE Cephei Data 87
7.4.3 EE Cephei Comparison Star 88
7.4.4 HPO EE Cephei Data 89
7.4.5 References 90
7.5 BM Orionis 90
7.5.1 Introduction 90
7.5.2 Theta 1 Orionis Data 91
7.5.3 BM Orionis Comparison Star 92
7.5.4 References 92

VIII. Prospects 94

8.1 Interferometry Diameter Measurements. 94
8.2 Changing Eclipse Timings 94
8.3 Out-of-Eclipse Variations 95
8.4 Hα Emission Wing Variability 95
8.5 Polarimetry 96
8.6 Your Role 96

IX. Observational Methods 97

9.0 Magnitudes 97
9.1 Naked Eye Techniques 98
9.2 Photometry 100
9.2.1 Introduction 100
9.2.2 Photomultiplier Tubes 100
9.2.3 Solid State Detectors 107
9.2.4 Charge-Coupled Device (CCD) Detectors 107
9.2.5 Photometric Filters 108
9.2.6 Photometric Techniques 110
9.2.7 Photometry Equipment 110
9.2.7.1 Single Channel Photometry Equipment 110
9.2.7.1.1 PMT Based Photometers 110
9.2.7.1.1.1 HPO Photon Counter Photometer 110
9.2.7.1.1.2 Optec SSP-5 Analog Photometer 111

9.2.7.1.1.3 PMT Saturation 112
9.2.7.1.1.4 Dead Time 113
9.2.7.1.1.5 Threshold Adjustment 115
9.2.7.1.1.6 Photon Counting Data Reduction 115
9.2.7.1.2 Single Channel Solid State Photometers 121
9.2.7.1.2.1 Optec SSP-3 PIN Diode Photometer 121
9.2.7.1.2.1.2 Optec SSP-4 Infrared Photometer 122
9.2.7.2 Potential Problems 127
9.2.8 CCD Photometry 128
9.2.8.1 CCD Observing 129
9.2.8.1.1 AutoStar Software 129
9.2.8.1.2 CCD Photometry Technique 130
9.2.8.1.2.1 Darks 130
9.2.8.1.2.2 Exposure 131
9.2.8.1.2.3 Defocusing 131
9.2.8.1.2.4 Flats 131
9.2.8.2 Image processing 132
9.2.8.2.1 AutoStar Image Processing 132
9.2.8.2.1.1 Differential Magnitude 133
9.2.7.2.1.2 Setting the Reference Magnitude 134
9.2.7.2.1.3 Raw Magnitude Determination 136
9.2.7.2.2 AIP4WIN Image Processing 138
9.2.9 Data Reduction 142
9.2.9.1 Star Information 143
9.2.9.2 Observatory and Equipment Information 144
9.2.9.3 Observation Data Entry 145
9.2.9.4 Final Data Reduction 146
9.2.10 Data Analysis 147
9.2.10.1 Plotting Data 147
9.2.10.2 Time Domain 147
9.2.10.3 Phase 148
9.2.10.4 Frequency Domain 149
9.2.10.4.1 Sine wave 150
9.2.10.4.2 Square Wave 150
9.2.10.4.3 Triangular Wave 151
9.2.10.4.4 Sawtooth Wave 151
9.2.910.4.5 Peranso 152
9.3 Spectroscopy 155
9.3.1 Introduction 155
9.3.2 Spectra 155
9.3.3 Types of Spectra 160
9.3.3.1 Continuous Spectra 160
9.3.3.2 Emission Spectra 160
9.3.3.3 Absorption Spectra 160
9.3.3.4 Stellar Spectroscopy 161
9.3.4 The Shape of a Spectral Line 161
9.3.4.1 Collisional Broadening 162
9.3.4.2 Doppler Broadening 162
9.3.4.3 Rotational Broadening 162

9.3.4.4 Zeeman Effect 163
9.3.4.5 Stark Effect 163
9.3.5 Stellar Spectra Classification 163
9.3.5.1 Spectral Type 164
9.3.5.2 Luminosity Classes 164
9.3.5.3 Chemical Composition 165
9.3.5.4 Radial Velocities 166
9.3.6 Spectroscopy Equipment 166
9.3.6.1 Introduction 166
9.3.6.2 Star Analyser 100 167
9.3.6.3 SBIG SGS 168
9.3.6.4 SBIG DSS-7 170
9.3.6.5 Shelyak Instruments Lhires III Spectrograph 173
9.3.7 Spectroscopy Techniques 176
9.3.7.1 Introduction 176
9.3.7.2 Obtaining a Spectrum 176
9.3.7.3 Spectroscopy Software 177
9.3.7.3 Plancks Law 178
9.3.7.4 Full Width Half Mean (FWHM) 179
9.3.7.4 Equivalent Width (EW) 179
9.3.7.5 Atmospheric Lines (Telluric Lines) 181
9.3.7.6 Spectral Resolution 182
9.3.7.7 Spectral Intensity 182
9.4 Polarimetry 184
9.4.1 Introduction 184
9.4.2 Polarimetry Techniques 187
9.5.3 Polarimetry Equipment 188
9.4.3 References 188
9.5 Interferometry 189
9.5.1 Introduction 189
9.5.2 Interferometry Techniques 189
9.5.3 Interferometry Equipment 190
9.5.4 References 192
9.6 Astronomical Dates 192
9.6.1 Julian Date 192
9.6.2 Heliocentric Julian Date 194
9.6.3 Modified, Reduced and Partial Julian Date 195
9.6.4 Julian Date List 196

Glossary 199
Meet the Authors 207
Index 209

List of Tables and Figures

Tables

Page

II. History
Table 2.1 Model Comparison 17

III. 1982/1984 Campaign
Table 3.1 1982-84 Eclipse Contact Times 29
Table 3.2 1982-84 Eclipse Event Durations 30

IV. Post 1984 Observations
Table 4.1 HPO V Photometric Data Summary 44
Table 4.2 Boyd V Photometric Data Summary 49

V. Current Interpretations
Table 5.1 Past Eclipse Timing Summary 68

VI. 2009 Campaign
Table 6.1 Official Predicted Contact Times PJD + 2,450,000 76
Table 6.2 Unofficial Predicted First Contact Time For UBV Bands 76

VII. Similar Star Systems
Table 7.1 Zeta Aurigae Basic Data 82
Table 7.2 Zeta Aurigae Magnitudes Out-of-Eclipse 83
Table 7.3 Lambda Aurigae Magnitudes 83
Table 7.4 EE Cephei Magnitudes Out-of-Eclipse 88
Table 7.5 Star b Magnitudes 89
Table 7.6 Star c Magnitudes 89
Table 7.7 BM Ori Magnitudes Out-of-Eclipse 91
Table 7.8 Theta 1 Ori B Ori Magnitudes 91
Table 7.9 Theta 1 Ori C Ori Magnitudes 92
Table 7.10 Theta 1 Ori D Ori Magnitudes 92

IX. Observational Methods
Table 9.1 Sample SSP-4 Data 125
Table 9.2 Hydrogen Series 158
Table 9.3 MK of Spectral Types 164
Table 9.4 Luminosity Classes 165
Table 9.5 Lhires III Parameters 175
Table 9.6. Lhires III Performance 175

Figures

Page

I. Introduction
Figure 1.1 Aurigae and the Kids 3

II. History
Figure 2.1 Shu-Shu Huang Model 8

III. 1982/1984 Campaign
Figure 3.1 Newsletter #5 Cover 21
Figure 3.2 AAS Tucson, Arizona Meeting Billing 22
Figure 3.3 AAS Poster Paper 24
Figure 3.4 Ronald Webbick Preparing Talk 25
Figure 3.5 Bruce Altner 25
Figure 3.6 Webbink and Stencel 26
Figure 3.7 F.B. Wood 26
Figure 3.8 D.S. Hall 27
Figure 3.9 R.E. Stencel Introducing a Speaker 27
Figure 3.10 J.L. Hopkins 28
Figure 3.11 Epsilon Aurigae Workshop Gang 28
Figure 3.12 Stig Ingvarsson TAO - Sweden 30
Figure 3.13 1982 -1984 U Band Data Plot 31
Figure 3.14 1982 -1984 B Band Data Plot 32
Figure 3.15 1982 -1984 V Band Data Plot 33
Figure 3.16 1982 -1984 (U - B) Data Plot 34
Figure 3.17 1982 -1984 (B - V) Data Plot 35
Figure 3.18 1982 -1984 (U - B) vs. (B -V) Data Plot 36
Figure 3.19 Kemp, 1985 Workshop Diagram 37

IV. Post 1984 Observations
Figure 4.1 HPO V Band Data 1982 - 1988 40
Figure 4.2 HPO B Band Data 1982 - 1988 41
Figure 4.3 HPO U Band Data 1982 - 1988 42
Figure 4.4 HPO V Band Data 2003 - 2008 43
Figure 4.5 HPO B Band Data 2003 - 2008 45
Figure 4.6 HPO U Band Data 2003 - 2008 46
Figure 4.7 2006 - 2007 Season HPO J Band Data 47
Figure 4.8 2006 - 2007 Season HPO H Band Data 47
Figure 4.9 Boyd V Band Data 1987 - 2005 48
Figure 4.10 Boyd B Band Data 1987 -2005 50
Figure 4.11 Boyd U Band Data 1987 - 2005 51
Figure 4.12 HPO V Frequency Domain 1984 - 1985 52
Figure 4.13 HPO V Frequency Domain 2003 - 2004 53
Figure 4.14 HPO V Frequency Domain 2003 - 2008 54
Figure 4.15 HPO V Frequency Domain 2007 - 2008 55
Figure 4.16 HPO V Prominent Periods 2003 - 2008 56
Figure 4.17 HPO V Prominent Periods 2003 - 2008 56
Figure 4.18 HPO V Prominent Periods 2003 - 2008 57

Figure 4.19 HPO V Prominent Periods 2007 - 2008 57
Figure 4.20 Sample Hα Spectrum 58
Figure 4.21 Be Star Hydrogen α Lines 59
Figure 4.22 Hydrogen α Line Horns 59
Figure 4.23 Hydrogen α Line Parts 60
Figure 4.24a Epsilon Aurigae Hα Spectra 12 December 2005 61
Figure 4.24b Epsilon Aurigae Hα Spectra 24 November 2006 61
Figure 4.25 Epsilon Aurigae Primary Star Ring 62
Figure 4.26 Schematic of Epsilon Aurigae Primary Star 63
Figure 4.27 NPOI Flagstaff, Arizona 65

V. Current Interpretations
Figure 5.1 Epsilon Aurigae System Schematic 66
Figure 5.2 2009/2011 Eclipse Timing 66
Figure 5.3 Past Eclipse Duration and Totality Time Changes 69
Figure 5.4 Past Eclipse Ingress and Egress Time Changes 70
Figure 5.5 Eclipse Periods 70
Figure 5.6 Eclipse Δ Magnitudes 71

VI. 2009 Campaign
Figure 6.1 Palomar Observatory 78
Figure 6.2 Palomar Observatory and PTI Aerial View 78
Figure 6.3 PTI Aerial View 79
Figure 6.4 Optical Delay Lines 79
Figure 6.5 FFT Image and Diffraction Pattern July 2009 80
Figure 6.6 FFT Image and Diffraction Pattern October 2009 81
Figure 6.7 FFT Image and Diffraction Pattern July 2010 81

VII. Similar Star Systems
Figure 7.1 Zeta Aurigae Image 83
Figure 7.2 U Band Plot of 1985 Zeta Aurigae Eclipse 84
Figure 7.3 VV Cephei System Diagram 85
Figure 7.4 HPO EE Cephei V Filter Image 88
Figure 7.5 EE Cephei Detail 88
Figure 7.6 Theta 1 Orionis Detail 90
Figure 7.7 Theta 1 Orionis HPO V Image 91
Figure 7.8 Eclipse of BM Orionis 93

IX. Observational Methods
Figure 9.1 The Stars of Aurigae 99
Figure 9.2 1P21 Photomultiplier Tube 100
Figure 9.3 PMT Pulse Forming Voltage Divider 102
Figure 9.4 PMT Spectral Response 103
Figure 9.5 HPO Photon Counting Photometer 104
Figure 9.6 HPO Photometer on C-8 105
Figure 9.7 Inside HPO Photometer 106
Figure 9.8 UBVRI Band Passes 108
Figure 9.9 Photometric UBVRIYJHK Filter Bands. 109

Figure 9.10 HPO C-8 UBV Photon Counting System 111
Figure 9.11 Optec PMT Analog SSP-5 System 112
Figure 9.12 HPO UBV Photon Counting Data Entry Form 116
Figure 9.13 FMP UBV Data Entry 117
Figure 9.14 FMP Data Summary Screen 118
Figure 9.15 FMP UBV Data Reduction 119
Figure 9.16 FMP UBV Data Report 120
Figure 9.17 Optec SSP-3 Photometer 121
Figure 9.18 Optec SSP-4 Photometer 122
Figure 9.19 HPO 12" LX200 GPS and SSP-4 123
Figure 9.20 SSP-4 Detector Comparison 124
Figure 9.21 FMP JH Band Summary Data 126
Figure 9.22 DSI Pro/Mogg Adapter/Camera Lens 128
Figure 9.23 HPO Wide Angle BVRI Photometry 129
Figure 9.24 Wide Angle Field of View 130
Figure 9.25 AutoStar Histogram 131
Figure 9.26 AutoStar Photometry Cursor 134
Figure 9.27 Setting Reference Magnitude 135
Figure 9.28 Setting Aperture and Annulus Diameters 136
Figure 9.29 Selecting Determine Magnitude 137
Figure 9.30 Determine Max Pixel and Total Flux 137
Figure 9.31 AIP4WIN Initial Display 138
Figure 9.32 AIP4WIN Single Image Selection 139
Figure 9.33 Single Image Photometry Window 139
Figure 9.34 AIP4WIN Aperture and Annulus Settings 140
Figure 9.35 AIP4WIN Photometry Results 141
Figure 9.36 AIP4WIN Photometry Results Detail 141
Figure 9.37 FMP Star Data 143
Figure 9.38 FMP Observatory and Equipment Data 144
Figure 9.39 FMP Data Entry 145
Figure 9.40 FMP Final Data Reduction 146
Figure 9.41 Time Domain Plot 147
Figure 9.42 Phase Plot 148
Figure 9.43 Frequency Domain Plot 149
Figure 9.44 100 Hz Sine Wave 150
Figure 9.45 100 Hz Square Wave 150
Figure 9.46 100 Hz Triangular Wave 151
Figure 9.47 100 Hz Sawtooth Wave 151
Figure 9.48 Peranso V Data 152
Figure 9.49 DFT Frequency Domain 153
Figure 9.50 Prominent Periods 153
Figure 9.51 p/o Hydrogen Transition Series 159
Figure 9.52 Hydrogen Balmer Spectrum 159
Figure 9.53 Star Analyser 100 168
Figure 9.54 Star Analyser Spectra 168
Figure 9.55 SBIG SGS Spectrograph 169
Figure 9.56 Sample High Resolution Spectra 170
Figure 9.57 SBIG DSS-7 Spectrograph 171
Figure 9.58 Spectrum of Nova Scorpii-2 171

Figure 9.59 Inside the DSS-7 172
Figure 9.60 Lhires III Spectrograph 173
Figure 9.61 Inside the Lhires III Spectrograph 174
Figure 9.62 Lhires III with DSI Pro CCD Cameras 175
Figure 9.63 Lhires III on 12" LX200 GPS 177
Figure 9.64 Black Body Spectrum 178
Figure 9.65 Full Width Half Mean 179
Figure 9.66 Equivalent Width 180
Figure 9.67 Equivalent Widths of Hydrogen α 181
Figure 9.68 Atmospheric (Telluric) Lines 182
Figure 9.69 Electromagnetic Spectrum 183
Figure 9.70 Polarized Light 184
Figure 9.71 Astronomical Polarimeter 187
Figure 9.72 Optical Interferometer 190
Figure 9.73 Mt. Wilson Interferometer 191
Figure 9.74 Mt. Wilson Interferometer Detail 191

Preface

People buy their first telescope and spend years looking at the wonders of the night sky. Some of those people then have a desire to do more. The first thing that comes to mind is usually to take pictures with the telescope. With the new CCD cameras this is much easier than in the days of film photography.

Still some of these people tire of taking pictures. It is nice to have astro images of deep sky objects, galaxies, nebulae, star clusters planets and more, but soon realization hits that while these pictures can be satisfying, they are just pictures and not of much real value.

In the early 1980's an organization was formed to help amateur astronomers contribute real science using their modest backyard astronomical equipment. A new organization, called International Amateur-Professional Photoelectric Photometry or I.A.P.P.P. was formed in June 1980 in Fairborn, Ohio by Douglas S. Hall and Russell M. Genet. This inspired many amateur astronomers to become involved with photoelectric photometry. Hundreds of papers were published with data from these amateurs. This was before the CCD came onto the scene and before the personal computer became popular. Data reduction calculations were done by hand and when available a handheld or pocket calculator provided great relief from all the calculations. Times have changed.

Telescopes have improved, computers are many times more powerful than ever thought possible in the 1980's and in many cases now less than what was paid for the pocket calculator. The Internet has changed the way information gets spread and provides near instantaneous publication of results accessible by most anyone in the world. New telescopes now align and track by themselves with precision only seen at professional observatories of the 1980's. While some of the original photometric equipment is still in use today providing excellent data, many people now choose CCD detectors for photometric work.

What is even more remarkable is that many amateurs are now doing high quality spectroscopy with modest backyard setups.

A detailed section on the History of epsilon Aurigae is presented along with a list of further reading articles.

This book is dedicated to the study of the epsilon Aurigae star system. It is designed for use by both professional and advanced amateur astronomers. There is information on observational techniques to help an amateur astronomer contribute valuable data using backyard astronomical equipment. This next eclipse of epsilon Aurigae will be observed with equipment vastly more powerful than any previous eclipse. With such advances, even amateur astronomers may contribute valuable data toward the understanding of this mysterious star system.

Acknowledgments

A very important part of the success of this book will be due to the reviewers who have spent time to go through the manuscript and point out errors and make comments.

We wish to thank:

Lothar Schanne of Völklingen, Deutschland (Germany) for his expertise on spectroscopy and valuable comments on the book.

And.

Brian McCandless of the Grand View Observatory in Elkton, MD, USA for his expertise in photometry, spectroscopy and polarimetry and his valuable comments. We also wish to thank Brian for his contribution to the Polarimetry section 9.4.

I. Introduction

Since the beginning people have looked at the night sky with wonder. At first glance it appeared the nigh sky was fixed except for the Moon's movement. The points of light we know as stars were thought to be embedded in a celestial sphere. The Greeks were the first to devise a system for determining the brightness of the stars. While they used a system of just six magnitudes it was at least a start. A magnitude 1 star was considered the brightest they could see while magnitude 6 was the faintest, 100 times fainter in fact. We now know there are stars much brighter than magnitude 1 (our Sun is a star and is magnitude -26.8, Sirius, the brightest star in the night sky is magnitude -1.47 and Vega is magnitude 0.03). There are also billions of stars fainter than magnitude 6. One must remember that the lower the magnitude number and extending into negative numbers, the brighter the star. A magnitude -2 is many times brighter than a magnitude +2 star.

Studying the heavens became full time jobs for some people. Most of these people considered the stars fixed in position, but it wasn't long before it was discovered that some stars moved with respect to others. These were called wanderers which we now know are not stars at all, but planets.

To better talk about the stars and identify where they are, patterns of stars where grouped into constellations. The Greeks may have been the first to specify certain groups of stars and give them names. Most cultures also grouped stars into constellations, but used different star groupings and different names. While constellations are not real, they do help identify where in the sky a star or object is located.

Today there are 88 official constellations. Some of these can only be seen in the Northern Hemisphere while others only in the Southern Hemisphere.

1.1 Variable Stars

At first it was thought that stars were fixed in brightness and unchanging. Those who studied the stars night after night discovered some of the stars seemed to remain fixed in the sky, but varied in brightness. At the time observers had no idea what they were seeing. One star, known as Algol, dimmed down very noticeably for a few hours every few days and created much fear. The fading every few days was known as the "wink of the demon."

Variable stars are stars seen from Earth that vary in brightness over a period of time from minutes to decades. There are several mechanisms that can cause this variation. Some stars pulse. As the nuclear fuel is consumed the star expands a bit and gets brighter. It then falls back to a dimmer mode. Other star systems have more than one star in them. If the orbits of the stars are such that one star passes in front of another as seen from Earth, a decrease in brightness from that star system will be seen. This type of variable star is known as an eclipsing binary star system. Even the closest eclipsing binary systems are too far away to easily be resolved into the individual stars. However, much can be determined about the star system by noting the variation of brightness. This is known as photometry [light-metering] of stars. Photometers are used to measure these changes and are special very sensitive light meters.

1.2 Auriga, Capella and the Kids

The constellation Auriga is visible from the Northern Hemisphere and the northern part of the Southern Hemisphere. It is highest in the early evening sky during the northern hemisphere winter months. Auriga is the Latin name for the Charioteer. Mythology portrayed Auriga as a charioteer with three children on his arm. Aurigae was also known as Erechtheus, son of Hephaestus. The Romans called him Vulcan. Hephaestus, who was crippled as a child, was believed to have invented the chariot for his son so his son could move him about more easily.

The brightest star in the constellation Auriga is Capella or alpha Aurigae. To the Northeast of Capella is a triangle of stars with the closest star epsilon Aurigae (Almaaz or Al Anz, the he-goat) at the

vertex and zeta (Haedi) and eta (Hoedus II) at the bottom of the triangle. Sometimes zeta and eta are referred to as Haedus I and Haedus II respectively. The triangle forms an asterism known as the Kids. The Kids are the three children on the arm of Auriga. These stars are all bright (around 3rd magnitude) and easily visible with the naked eye even in light polluted areas. Both epsilon and zeta Aurigae are long period eclipsing binary star systems and even eta varies a little (an unconfirmed 24-day period), but not due to a companion.

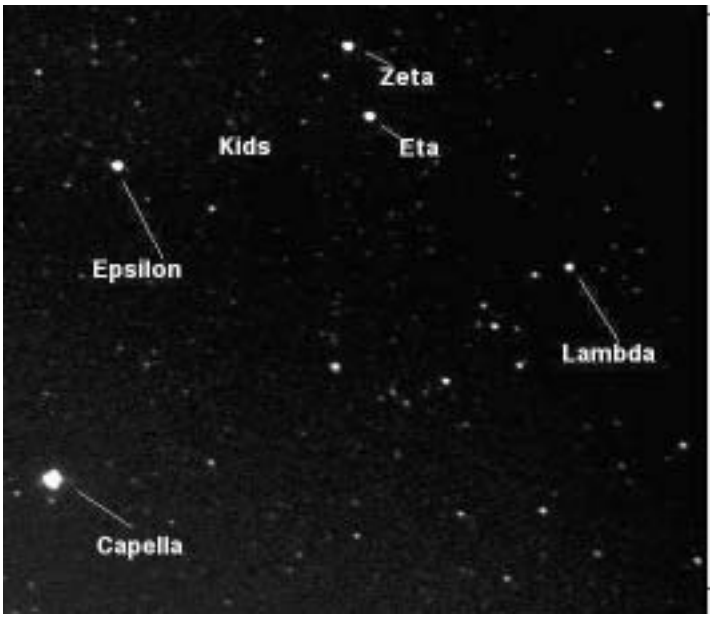

Figure 1.1 Aurigae and the Kids

1.3 Epsilon Aurigae

Epsilon Aurigae (pronounced awe reggie) is one of the most mysterious star systems known. It has the longest period of all known eclipsing binary systems with a period of a little over 27 years. To add further to the mystery while one would think that such a long period would produce a fairly short eclipse, the surprise is that the eclipse lasts nearly 2 years. While those two facts are interesting by themselves things get even more interesting during the middle of the eclipse. What happens is the star system gets brighter at mid-eclipse. Some astronomers have likened the object causing the eclipse to a gigantic paving brick with a hole in the middle.

While professional astronomers are interested in understanding the system, the long period between eclipses, the fact that it is a 3rd magnitude system and one that requires many continuous nights of observations all tend to preclude most professional observations. Indeed many astronomers are lucky to observe one eclipse during their career and usually two is about it. In part due to the high level of brightness, the object does not require large telescopes, so observations of it tend to be of lower priority for major observatories except during the eclipse.

1.4 Backyard Astronomers

Photometry of variable stars is ideal for backyard astronomers. Even with modest telescopes and equipment much can be learned and epsilon Aurigae presents an ideal project. Because of the star system's brightness it is easily observed and quality data can be taken even in a light polluted area. In addition, being able to pop out back each clear night and make observations with no need to petition a major observatory, makes continuous following of this system ideal for the backyard astronomer. This is an area where it is relatively easy for a backyard astronomer to do real science.

In addition to astronomical photometry, there are other techniques that are used to gather data about a star system. These include spectroscopy, polarimetry and interferometry. While advanced backyard astronomers can do spectroscopy these techniques have been beyond the capability of a backyard astronomer until recently.

In this book, we will review the historical context surrounding epsilon Aurigae and some related systems, discuss observational methods associated with the science of eclipsing binaries and then discuss the eclipse of 1982-84, the work done since and the pre-status of the eclipse of 2009-11. Given that science often leads to more questions, conclusions from the 2009-11 eclipse will set the stage for studies of the next eclipse cycle, forecast to begin in the year 2036, whether or not Earth dodges impact by asteroids like Apophis.

II. History

2.1 First Observations

Epsilon Aurigae has fascinated astronomers for parts of three centuries -- so far. The NASA Astrophysical Database Service keeps track of publications related to stars like this one. For the period prior to 1930, 23 papers are on record; for 1930-1960, 54 papers appeared, for 1961-1990 there were 200 papers, reflecting the explosion of interest surrounding the 1983 eclipse (with 173 of those during 1981-1990); most recently (1991-2007) there were 37 papers, thus far. While we can't summarize every last report, we attempt to describe here the story told by some of these.

The fifth-brightest bright star in the constellation Auriga, epsilon, northernmost of the group called The Kids, is defined by its Algol-like eclipsing character. Algol stars derive their name from the prototype, The Demon Star, in nearby constellation Perseus, that undergoes a striking, several hour decrease in light each 2.89 days. This behavior is successfully explained as an eclipsing binary star, where a larger, cooler component hides the smaller, hotter star on a fixed orbital period. The duration and shape of eclipses enables astronomers to deduce parameters of the stars, the size and separations. Algol has been noted as a variable star for centuries, but its periodicity was finally documented in 1782, and evidence for its binary star characteristic is credited to Edward Pickering of Harvard and H.C. Vogel of Potsdam Observatory in the late 19th century. Twentieth century American astronomer, Henry Norris Russell was first to systematically construct numeric models for eclipsing binary stars and apply it to Algol and related systems, including epsilon Aurigae – which is when the trouble began.

Following Galileo, the widespread adoption of the telescope along with interest in the natural sciences, many amateur observers carefully recorded phenomena of the night sky: comets, meteors, sunspots and variable stars. One such observer was J. Fritsch of Germany, who noted a minimum in brightness during 1821. During the 19th century, Fritsch and others compiled hundreds of visual

observations and noted minima during 1847-48 and 1874-75. These were analyzed by Hans Ludendorff in 1904, who provided evidence that the epsilon Aurigae light curve follows the Algol-like eclipsing binary characteristic with a 27.1 year period and with a "dark cloud of meteors" causing the dimming. However, in a more complete discussion in 1912, he too questioned the eclipse theory because of discrepancy between photometry showing variations, and spectra that were unchanged during minimum light.

2.2 Disagreeable Spectra

Harlow Shapley, who would later gain fame for using globular clusters to identify the center of the Milky Way, during 1915 elaborated the Russell method for the study of eclipsing binaries and included epsilon Aurigae in the analysis. He found the F star diameter to be 79-169 solar radii and that the binary had a nearly equal mass ratio – despite the invisibility of the secondary! He was not completely satisfied with the solutions, but did comment on the out-of-eclipse light variations, of up to 0.3 magnitudes. The spectra of epsilon Aurigae yield an orbital solution implying the secondary has mass equal to the primary star, but remains "invisible" – this facet, plus the long period, is what has made epsilon Aurigae the center of attention for decades.

The 1928-30 eclipse was reported to be underway by D.B.McLaughlin at Michigan, who noted the light decrease, along with radial velocity changes consistent with a rotating disk - in analogy with other Algol-like systems: positive at ingress, negative at egress. Hence, although the secondary was not directly seen, its influence in spectra was present. A problem with the disk model is that it requires a strong central gravitational field to keep it stable – and a suitably massive central star should have revealed its presence. Many Algol systems have an accretion disk due to mass transfer between the binary star components, but both stars can be seen in their combined spectrum.

2.3 Alternative Models

As Gerald Kuiper, Otto Struve and Bengt Stromgren eloquently phrased it in their 1937 Astrophysical Journal paper on epsilon Aurigae, "The combination of photometric and spectroscopic data seems to lead to contradictions unparalleled in the study of eclipsing binaries." These contradictions include the extreme ratio of surface brightness for a similar mass ratio binary and constant spectral type eclipse, leading some to postulate electron scattering from a transparent stellar shell was required, perhaps in a grazing eclipse.

An extended, ionized stellar atmosphere is plausible, but normally the central star remains detectable at some wavelength in those cases, as in the highly evolved OH-IR stars. Also, an extended region might be expected to relate to mass transfer in the binary. Struve in 1956 published answers to some of the criticisms of this model, including the lack of infrared excess that might be expected, proposing instead that both components contribute to an extended nebula similar to models for beta Lyrae.

Struve's student, Shu-Shu Huang in 1965 published the disk model still viable today. He cites the idea originating with Zdenek Kopal who in 1954 published a model featuring a semitransparent flat ring consisting of large solid particles in orbit around a secondary star, which resolves many of the observational issues. Huang then developed his model for a transiting opaque gaseous ring, based on the success of a similar model with beta Lyrae, which preserves the spectrum of the primary, adds rotationally-varying spectral features, plus can account for Hα and light variations.

From light curve considerations, Huang deduces that the F star radius is 6.5 percent of the binary separation, the disk radius is 17.1 percent thereof and the disk thickness is 5.5 percent of the binary separation. Adopting a = 27.6 AU, this means the F star radius would be 1.8 AU, or 385 solar radii. The disk radius is 4.7 AU and the disk thickness is 1.5 AU, as required to remove 0.75 magnitudes during total eclipse. Light curve asymmetries suggest to

Huang that a gaseous stream is present in the system connecting the F star and the trailing side of the disk. In commenting on the nature of the disk, Huang argues that dust particles could survive in the disk near the F star, perhaps replenished with mass transfer material. An important modification to this basic model was proposed by Wilson (1971) who argues that a dust ring with a semitransparent central opening best represents the eclipse observations and features of the secondary spectrum. Based on this, Wilson then proposed that 1956 mid-eclipse light curve structure argues for an eclipse of the F star by its true secondary object in the center of the dust ring. Cameron suggested this central object is a black hole, although it has never been detected in X-rays thereafter. Several more papers have elaborated on the basic Huang model (e.g. Hack and Selvelli 1979; Lissauer and Backman 1985), but it still remains the template against which observations are tested (see Guinan and Dewarf 2002). Figure 2.1 is a redrawn diagram of Huang's model.

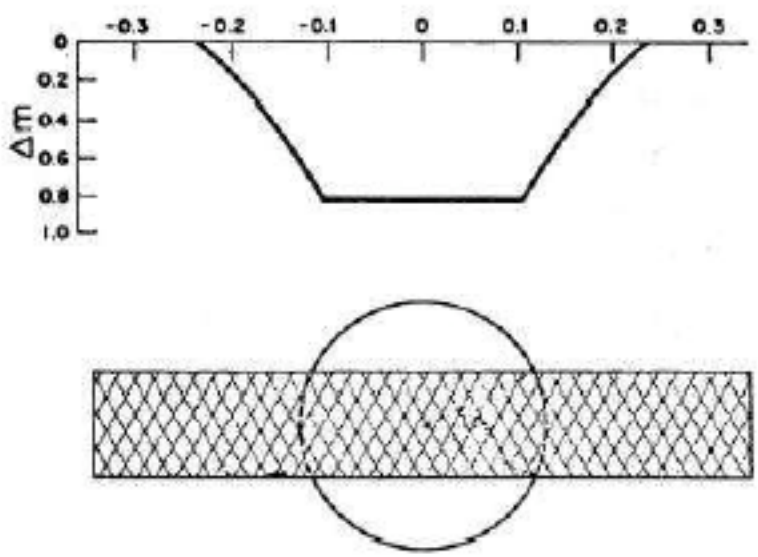

Figure 2.1 Shu-Shu Huang's Model

2.4 Observational Progress Preceding the 1982-84 Eclipse

An important synthesis of observations was published in 1970 by K. Gyldenkerne. Photometric results of the then recent 1954 eclipse were discussed providing the first clear evidence for mid-

eclipse brightening between JD 2,435,550 and 2,435,700. He also showed a correlation between differences from mean values of V magnitude and B-V color, being up to 0.05 magnitude redder when V is 0.1 magnitude fainter. Gyldenkerne also comments on changes to duration of portions of eclipse: decreasing to 670 days in 1956, compared with a mean value of 714 days from prior eclipses, whereas the duration of totality increase to 394 days compared with 330 days previously, coming at the expense of partial phase duration. The 1983 eclipse follows this trend, and emphasizes the need to closely monitor the 2010 events. An important re-discussion of the photometry was provided by R. Canavaggia in 1980 who examined the wavelength dependency of low level light fluctuations of epsilon Aurigae both in and out of eclipse. These were explained as originating from both intrinsic fluctuations of the F star primary and extinction variations of absorbing variations associated with the secondary. Several observers had noticed the maximum extinction occurs near egress, with B-V about 0.05 magnitudes redder than mean values.

In the late 1970s, cold-war driven detector and space technologies were being applied to new observations in astronomy, including ultraviolet and infrared work. The 1978 launch of the International Ultraviolet Explorer (IUE) satellite, which functioned for over 15 years, enabled coverage of the 1983 eclipse in detail – beginning with the first report of the UV spectrum of epsilon Aurigae by Hack and Selvelli (1979). They observed UV output to be stronger than expected for an F0 star, ascribing the excess energy to a 15,000K hot object, along with atomic oxygen emission indicating the presence of a large shell of ionized hydrogen, and Mg II line widths supportive of high luminosity, supergiant star characteristics. New technology associated with the 1983 launch of the Infrared Astronomical Satellite, IRAS, during mid-eclipse, along with ground based infrared measurements, made possible detection of new evidence about the nature of the dusty disk in epsilon Aurigae.

2.5 The 1982-84 Eclipse and Theoretical Progress

The 'Baby Boom' generation in the USA was ready for the 1982-1984 eclipse of epsilon Aurigae. A record number of PhD astronomers were graduating in those days, and opportunities with new ground and space telescopes were rampant – spanning X-ray to radio wavelengths. IUE and IRAS in particular were pressed into service to expand the optical measurements of epsilon Aurigae already underway. IUE observed at wavelengths shortward of visible light, while IRAS observed longward thereof. Visible light we see spans wavelengths 400 to 700 nano-meters. The measure of light, the nano-meter (nm), is one billionth of a meter in length. While IUE was ultraviolet-sensitive from 350nm down to 120nm, IRAS measured the mid and far-infrared, 12,000nm to 100,000nm. The smaller the wavelength, the higher the energy and temperatures measured, and vice-versa.

Several authors were able to confirm and extend the Hack and Selvelli results with IUE, confirming the UV excess and demonstrating eclipse variations. Tom Ake in 1985 reported results of eclipse monitoring with IUE, indicating that the eclipse was asymmetric, deepening toward 3rd contact. Also, fluctuations and brightenings were frequent, and the interstellar 2,200A extinction was consistent with the E(B-V) = 0.35, reported previously. His report, like many, appears in a 1985 special meeting on the results of the eclipse campaign – see below.

In the emerging infrared studies, the first IRAS results were by Dana Backman in 1984, who claimed detection of the secondary as a 500K object, based on 5 to 20 micron photometry. From geometrical arguments, he deduced that the secondary subtends a solid angle of about 9 x 10^{-16} ster-radians (think, square degrees), with a 2:1 elliptical aspect ratio. Considering the advances in infrared technology since the 1980s, confirmation of these results remains a priority during the first eclipse of the new millennium. That same year, Dana Backman and collaborator Jack Lissauer published the now widely adopted solution for stabilizing the massive disk, by proposing that an embedded binary of B type

stars inside the disk could provide the secondary with high mass, but limited total luminosity compared to the F supergiant star.

Dana Backman and many of the active observers were able to gather in Tucson in January 1985 for a special meeting connected with the American Astronomical Society. For more information on this see Section IV of this book. The proceedings were published in NASA Conference Publication series #2384, edited by one of us (Stencel). While this was circulated nationally to libraries, it may be easier to find on the Internet than at your local government repository. Papers by Frank Bradshaw Wood, Jeff Hopkins, James Kemp, Tom Ake, Steno Ferluga and others appear in their most complete form only in these proceedings. Kemp's polarimetry is unique among the papers, in showing a highly asymmetric signature of the disk, with polarization changes becoming maximum toward 3rd contact, and significant variations on timescales as short as a few days. He argues that these measurements require a disk tilted relative to the orbital plane. If so, precession of the disk seems unavoidable, and could account for eclipse to eclipse duration changes. Another of these is an important paper by Ronald Webbink, on the theory for formation and evolution of binaries like epsilon Aurigae. His evolutionary models span a dizzying range. Single star models included considering the early F supergiant to be a pre-main sequence star, or in post-main sequence states ranging from shell hydrogen burning to shell helium burning. Binary star models included mass transfer from core and shell helium burning states, and pre-white dwarf (post AGB) stars. Webbink preferred the solution involving either helium shell burning or pre-white dwarf mass transfer, and proposed observational tests. These are: better distance and orbit solutions, better stellar atmospheric abundance and surface gravity determination derived from spectroscopy. Observers should consider these to be key challenges. Recent parallax determinations include 600 pc by Heintz et al. in 1994, and 625 pc with Hipparcos (Perryman et al., 1997).

Photometry of the eclipse played a central role. Definitive UBV photometry of the eclipse was reported by Jeff Hopkins at the

1985 Workshop, and is discussed elsewhere in this book. Paul Schmidtke studying Hopkins and Tjorn Island data, noted a dramatic U-B rise during 4th contact, which deserves renewed attention. Many other observers compiled light curves, and among the reports was that of I-S. Nha at Yonsei Observatory, who in 1983 reported a 0.4 magnitude 'flare' over a fraction of one hour on JD 2,445,356 (21 Jan. 1983).

After the 1985 eclipse workshop, a series of important reports appeared, beginning with Lambert and Sawyer's high resolution spectroscopic radial velocity study in 1986, wherein they found strong velocity and strength variation in the 766 and 770 nm lines of potassium (K I) due to the passage of the secondary (detectable 200 days after end of eclipse!), and clear association of lines of neutral nitrogen (N I) near 871 nm tracking the primary star motion. They concluded, based on comparing the velocity variations of different groups of lines, that these arise from an 'atmosphere' about the periphery of an opaque secondary disk, asymmetrically trailing the center of mass. Detection of CO lines during the latter half of eclipse by Hinkle and Simon, reported in 1987, agree with these points. The overall asymmetry in radial velocities at start (+20 km/sec) and end (-40 km/sec) of eclipse admits either a large mass ratio, or an off-centered object in an elliptical disk, and/or an asymmetrically heated disk. Polarimetry by Kemp et al. reported in 1986, is supportive of the asymmetric facets of the disk. For Keplerian motions in the Huang-Wilson eclipse geometry, they deduce that the primary is most likely a post-AGB star with residual mass under 3 solar masses, with the secondary up to twice as massive, in agreement with the "low mass solution" also presented by Saito et al. in 1987. These results favor models advanced by Wolff (1971) and Eggleton & Pringle in 1985 for mass transfer and evolution from a binary of 6 and 3 solar masses and initial period of 1500 days. Key to demonstrating correctness of these models remains better determination of gravity, abundances and, if possible, detection of motions associated with the object(s) in the disk, using either mid-infrared or far-ultraviolet high resolution spectra.

Mamoru Saito is cited by Lambert and Sawyer as proposing the low mass solution, but the report appeared finally in 1987, wherein is reported analysis of high dispersion spectra and the conclusion that the system mass is far lower than traditionally deduced. By dividing eclipse spectra with pre-eclipse ones, Saito and colleagues find inverse P Cygni profiles during ingress, and P Cygni profiles during egress – associated with the secondary, along with unaffected lines ascribed to the primary star. The line profile types are named after those seen in P Cygni (Nova Cyg 1600, 34 Cyg), which is a star that brightened greatly during 1600 and later showed a spectroscopic signature of a fast, dense outflow causing apparently redshifted emission due to blueshifted absorption line profiles. The lines from the secondary tend to appear among lower temperature atomic transitions, and are stronger during egress than ingress. The radial velocities show the same story – rotation of the secondary as it passes the primary averages about 30 km/sec. The temperatures deduced from the secondary spectrum also appear asymmetric: 4,000K for the lower ionizations either side of central eclipse, but 7,500K for the ionized lines during ingress, dropping to 4,000K during egress. This suggests the leading side of the secondary disk is heated. The inferred density is 10^9 cm^{-3}. They further note the great increase in Hα absorption strength during mid-eclipse and provide evidence for the central object being slightly displaced toward the egress side of the secondary disk. The Keplerian model for the secondary results in rotational speeds of 38 km/sec and 43 km/sec for the ingress and egress limbs of the disk, respectively. This results in a model for the system with nebular extensions 15% in radius to either side of the F star, plus an asymmetric disk with an ingress side shock due to Lyman photons from the primary that decelerates the rotating gas by 10 km/sec. The masses of the components are deduced to be ~ 2 solar masses for the primary and ~6 solar masses for the secondary and disk. This places the primary star near the "Eddington limit" which is the brightness at which the radiation pressure begins to overcome gravity and the star evaporates.

The proposed distribution of matter around the secondary component in the orbital plane includes rotating dust and metallic

gas which defines the disk, plus rotating hydrogen gas surrounding same and a more rarefied, non-rotating hydrogen zone existing outside the disk. At ingress, there is a shocked gas region on the leading face influencing the light and spectrum.

Saito and collaborators also reported pre-eclipse radial velocities and found singular events like a velocity change of about 40 km/s during October 1977, indicating a decrease of 0.07 AU in the radius over three days and an overall decrease of radius of about 16% (0.2 AU) over the preceding 27 years. They suggest that changes in eclipse duration can be explained by a shrinking primary star – again supportive of the post-AGB, low mass scenario. However, changes in the disk could account for these variations.

As mentioned above, Backman and Lissauer proposed a solution to stabilizing a massive disk by adding a pair of B stars orbiting within the secondary. While the lower mass solutions advocated by Lambert and Sawyer do not require this invention, the higher mass solutions may need it. Two studies of the disk in epsilon Aurigae include Sanjiv Kumar's 1987 disk model that includes precession effects due to the embedded binary, resulting in a twisted disk structure. However, the postulated inclination (20 degrees) and short period (a few days) of the binary inside the disk implies observational signatures not yet seen, although the binary effectively slows any accretion losses from the disk, thus providing disk longevity. The combined effect of forced precession, regression of nodes and the quadrupole moment of the close binary are to doubly twist the disk structure and thicken the disk in the line of sight. Tomographic methods might be applied during the coming eclipse to investigate this model.

Norio Saito's 1989 time-dependent models of the irradiated accretion disks applied to epsilon Aurigae, predicts thermal instabilities from ionizing radiation on the interior of the disk from a single B star, with ~2-3 year timescales. Although UV monitoring has been sporadic, the observations do not seem to support the prediction of recurring bursts. However, the interior of the disk remains of great interest and clever observations are needed to

penetrate that zone. A post-eclipse light curve monitoring effort also was reported by Nha and collaborators in 1993, who show 7 years of UBV data (1982-89) and found a 95.5 day periodicity prominent in their data, which they associated with pulsations of the primary. They too note the steady increase in duration of totality, from less than 350 days in 1928-30, to nearly 400 days in 1955-57 and almost 450 days in 1982-84.

2.6 Inter-eclipse Milestones on the Approach to 2009

After the excitement of the 1982-84 eclipse of epsilon Aurigae began to wind down, most astronomers moved on to other topics, but a few papers appeared during the 1990s that advanced the subject. Noteworthy among these are spectroscopic studies by Steno Ferluga, collaborator with Margarita Hack, from Trieste Observatory, Sheffer and Lambert's use of the Hubble Space Telescope and Tom Ake's use of the Far-UV Spectroscopic Explorer satellite.

A remarkable pair of papers were authored by Steno Ferluga in 1990 and 1991. In the first, he demonstrated by light curve fitting that the eclipsing body must consist of at least two rings and a central annulus, with asymmetric centers. Great care was taken to remove the out-of-eclipse light variations, and the UBV colors constrain disk structure parameters for the 1983 eclipse, and using broadband information for the 1956 and 1929 disks. In the 1956 disk, the outer semitransparent band is wider and the central hole is shifted 0.7 AU back. The 1929 eclipse data shows a more nearly flat totality, so the constraints on disk sub-structure are weaker. From this exercise, Ferluga deduced the size of the central hole is 1.3 +/- 0.4 AU, which constrains an embedded binary separation to less than 0.6 AU. The outer radius of the disk is 5.2 or 4.4 AU for the high mass and low mass models, respectively. Although the origin for the Cassini-like gap in the ring system is not explained, his analysis also favored the high mass model.

In Ferluga's second paper, 1991, he ratioed high resolution optical spectra obtained before, during and after eclipse to present the first

detailed view of the shell spectrum due to the eclipsing secondary disk. Spectra outside of eclipse are averaged to minimize the F star variation effect on the ratios. An excitation temperature of 4,500K is derived, and an electron density of 10^{11} cm^{-3}, which is similar to the density of the solar atmosphere, He comments on the "well-known" UV bump at 3rd contact, possibly referring to the UV study presented by Tom Ake at the 1985 Workshop. From line strengths, Ferluga also derived line blanketing effect variations. From the set of constraints provided by variation of the shell spectrum through eclipse, he derived the disk radius, 8.1 +/- 0.4 AU (for the high mass model) and thickness, 0.9 +/- 0.3 AU. The detection of the shell spectrum on 25 Jan 1985, after end of eclipse (21 April 1984), is used as strong evidence for the high mass model, as the shell lines occur with zero velocity shift, consistent with position near the Roche lobe (but could not be stationary in the low mass model, far from its Roche limits). Steno Ferluga ends his article with a plea that we should pursue "regularly monitoring the spectroscopic behavior of the primary star to obtain a clear record of out of eclipse variability and possible correlations with key spectral features." We salute Lothar Schanne and others who have taken up this challenge.

An unpublished effort by Dana Backman, one of us (Stencel) and collaborators involved an attempt to observe secondary eclipse in the infrared – predicted to occur during the mid/late 1990s. Using a bolometer at IRTF and the Denver mid-infrared camera at the Wyoming IR Observatory and Mt. Lemmon Observing Facility, they obtained mid-IR data on epsilon and alpha Aurigae. The expected heated side of the disk was not detected, suggesting an optically thick disk with circulation maintaining cooler equilibrium.

A similar effort to capture secondary eclipse was staged by Yaron Sheffer and David Lambert (1999). A low-resolution Hubble Space Telescope GHRS spectrum of epsilon Aurigae was obtained on February. 16, 1996 (orbital phase 0.6971) while the secondary was orbiting toward eclipse by the primary. The UV spectrum covers 1,175 to 1,461 Å and is rich with emission and absorption lines, which include stellar and interstellar components. The emission-

line profiles have the appearance of double-peaked emission with a stronger red component at a radial velocity of +108 km/s, an overlying unresolved absorption component at -20 km/s, and a weaker blue emission bump near -92 km/s. They proposed that the emission originates at the inner radii (about 1.4 AU) of the ~8 AU disk surrounding the enigmatic secondary, but that the high speeds measured move their preferences back toward the higher mass model for epsilon Aurigae.

A final far UV spectrum was obtained by Tom Ake in January 2001, just after nominal end of secondary eclipse, with the Far UV Spectroscopic Explorer (FUSE). This spectrum reinforces the HST spectrum in showing numerous excitation lines, but he interpreted these as due to resonance scattering of photons in the expanding F star wind, or from an occulted UV-bright source, not necessarily in the disk. An analogy with zeta Aurigae UV spectra was examined. Further UV observations with HST are needed to explore this.

This recent work and the historical legacy, sets the stage for renewed efforts in photometry, spectroscopy, interferometry and polarimetry during the next eclipse. The 'Number One' problem remains determination of the mass of the components. Here's a comparison of models:

FACET	HIGH MASS MODEL	LOW MASS MODEL
Eclipse	Large secondary object	
UV features	Hot inner disk of secondary or other UV source	
Distance	625 pc	
Interferometric diameter	2.2 milliarcsec	
Out of eclipse light variations:		
--short term	Cepheid-like	Post-AGB instabilities
--historic shell spectrum	Massive disk	Not consistent
Disk	Surrounds embedded binary	Mass transfer result

Table 2.1 Model Comparison

Derivation of new constraints is called for and given the secular changes eclipse to eclipse, it appears all four eclipses of the 21st century will get more and more interesting (2010, 2037, 2064 and 2091). Excellent summaries of the history of observations related to epsilon Aurigae can be found in the following references:

2.7 References

--Frank Bradshaw Wood (1985 in *The 1982-84 eclipse of epsilon Aur*, NASA Conf. Publication 2384, edited by R. Stencel), http://www.du.edu/~rstencel/NASAcp2384.pdf

--Sean Carroll et al. 1991, http://adsabs.harvard.edu/abs/1991ApJ...367..278C

--Guinan and Dewarf 2002, http://adsabs.harvard.edu/abs/2002ASPC..279..121G

and by

Lucas et al. 2006 Society for Astronomical Sciences Vol. 25, p. 25.

[Journal names are followed by volume and page numbers]:

Ferluga, S. 1990, *"Epsilon Aurigae. I - Multi-ring structure of the eclipsing body"* – Astron. & Astrophys. 238: 270 [http://adsabs.harvard.edu/abs/1990A%26A...238..270F].

Fegluga, S. and Mangiacapra, D. 1991, *"Epsilon Aurigae. II - The shell spectrum"* – Astron. & Astrophys. 243: 230 [http://adsabs.harvard.edu/abs/1991A%26A...243..230F].

Guinan, E. and Dewarf, L. 2002 *"Toward Solving the Mysteries of the Exotic Eclipsing Binary epsilon Aurigae: Two Thousand years of Observations and Future Possibilities"* in "Exotic Stars as Challenges to Evolution" ASP Conference Proceedings, Vol. 279 (IAU Colloquium 187) Eds. C.Tout and W. Van Hamme.

Gussow, M. 1933, *"Über die sekundären Schwankungen im Lichtwechsel von Epsilon Aurigae"* Astronomische Nachrichten, Vol. 250, p.73, http://adsabs.harvard.edu/abs/1933AN....250...73G

Gyldenkerne, K. 1970, *"The Light and Color Variations of Epsilon Aurigae"* - Vistas in Astronomy Vol. 12, p.199 [http://adsabs.harvard.edu/abs/1970VA.....12..199G].

Hack, M. And Selvelli, P., 1979 *"The ultraviolet spectrum of the eclipsing binary Epsilon Aurigae"* - Astron. Astrophys. 75: 316.

Hinkle, K. and Simon, T. 1987, *"Two micron CO absorption lines in the spectrum of Epsilon Aurigae during eclipse"* – Astrophysical Journal 315: 296.

Hopkins, J. and Stencel, R. 2007 "*Recent UBVJH Photometry of Epsilon Aurigae*" in Proceedings of the May 2007 Society for Astronomical Sciences annual conference, eprint arXiv:0706.0891, [http://adsabs.harvard.edu/abs/2007arXiv0706.0891H].

Kemp, J. et al. 1986, *"Epsilon Aurigae - Polarization, light curves, and geometry of the 1982- 1984 eclipse"* – Astrophysical Journal 300: L11 [http://adsabs.harvard.edu/abs/1986ApJ...300L..11K].

Kuiper, G., Struve, O. and Stromgren, B. 1937, "*Interpretation of Epsilon Aurigae*" – Astrophysical Journal 86: 570.

Lambert, D. And Sawyer, S. 1986, *"Epsilon Aurigae in eclipse. II - Optical absorption lines from the secondary"* – Publications of the Astron. Society Pacific 98: 389.

Lissauer, J. and Backman, B. 1985, "*The Epsilon Aurigae secondary - A binary embedded within a disk?"* - Astrophys. Journal 286: L39.

Ludendorff, H. 1904, "*Untersuchungen uber den Lichtwechsel von Epsilon Aurigae*" - Astron. Nachrichten Vol. 164, p. 81

Ludendorff, H. 1912, "*Bearbeitung der Smidtschen Beobachtungen des Veranderlichen Epsilon Aurigae*" - Astron. Nachrichten Vol. 192, p.389.

Nha, I., Lee, Y., Jeong, J. and Kim, H. 1993, *"Extreme Long-period Eclipsing Binary Epsilon Aurigae"* in Proceedings New frontiers in binary star research, eds. Kam-Ching Leung and Il Seong Nha, ASP Conf. Vol. 38, p.291.
http://adsabs.harvard.edu/abs/1993ASPC...38..291N .

Saito, M. et al. 1987, "*Epsilon Aurigae - Rotation curve of the secondary disk and masses of the components"* – Publications of Astron. Society Japan 39: 135
[http://adsabs.harvard.edu/abs/1987PASJ...39..135S].

Sheffer, Y. and Lambert, D. 1999, *"Intereclipse Spectroscopic Snapshot of Epsilon Aurigae with the Hubble Space Telescope"* – Publications Astron. Society Pacific 111: 829 [
http://adsabs.harvard.edu/abs/1999PASP..111..829S].

Shapley, H. 1928, *"On the Variability of the Maximum Light of Epsilon Aurigae"*- Bulletin
Harvard College Obs. No. 858, p.5,
http://adsabs.harvard.edu/abs/1928BHarO.858....5S .

NASA Conf. Publication 2384
[http://www.du.edu/~rstencel/NASAcp2384.pdf].

Wilson, R. 1971, *"A model of Epsilon Aurigae"*- Astrophysical Journal Vol. 170, p.529.

III. 1982/1984 Campaign

3.1 The Campaign

For the 1982 to 1984 eclipse of epsilon Aurigae a world wide campaign was formed to pool observations and comments. Russell m. Genet and on of us (Stencel) started the first Newsletter in January of 1982. Starting with the second Newsletter in March of 1982, one of us (Hopkins) took over for Genet and continued on for the remainder of the Newsletters. Thirteen issues were printed.

Figure 3.1 shows a sample 1982-84 Eclipse Campaign Newsletter.

epsilon aurigae

1982-84 ECLIPSE

CAMPAIGN NEWSLETTER

No. 5

PHOTOMETRY:
Jeffrey L. Hopkins
Hopkins-Phoenix Obs.
7812 West Clayton Dr.
Phoenix AZ 85033

SPECTROSCOPY:
Robert E. Stencel
Code EZ-7
NASA - HQ
Washington DC 20546

December 1982

Dear Colleagues,

We are happy to report that Russell Genet (Fairborn Observatory) has received a modest grant from the American Astronomical Society to support the continued publication and distribution of this Newsletter. This grant should provide us with sufficient working capital to continue this work at least through 1983. We thank all whose individual contributions in the past helped in making previous Newsletters possible. Our present mailing list exceeds 100, with about one-quarter being external to the USA. We have thus achieved the desired ability to be a viable communication medium for this eclipse campaign. Once again we solict reports from active observers for inclusion in this Newsletter.

We plan to publish a directory of persons involved with the E Aur campaign. Suggestions concerning content or format would be welcomed by J.L. Hopkins.

This Newsletter is (partially) supported by a grant from NASA, administered by the American Astronomical Society.

EPS AUR NL 5
1

Figure 3.1 Newsletter #5 Cover

Some of the Newsletters are available as .pdf documents at **http://www.hposoft.com/EAur09/EAurNL.html**.

3.2 American Astronomical Society Meeting

Following the end of the eclipse a workshop was held 16-17 January 1985 in Tucson, Arizona U.S.A. in conjunction with the 165th meeting of the American Astronomical Society. A summation of the meeting including invited papers was published as a NASA Conference Publication 2384 titled ***1982 - 1964 Eclipse of Epsilon Aurigae.*** Figure 3.2 shows a photograph of the billboard outside the Holiday Inn in Tucson. Epsilon Aurigae Workshop takes top billing over the Space Telescope at the American Astronomical Society meeting in Tucson, AZ

Figure 3.2 AAS Tucson, Arizona Meeting Billing

3.3 Workshop Invited Papers

Historical Overview	Frank Bradshaw Wood
Optical Photometry	Jeffrey L. Hopkins
Infrared Photometry	Dana E. Backman
Polarimetry	James C. Kemp
Ultraviolet Spectroscopy	Thomas B. Ake
Optical Spectroscopy	Steno Ferluga
Evolutionary Context	Ronald F. Webbink
Photometric Support for Future Astronomical Research	Douglas S. Hall Russell M. Genet

3.4 Workshop Contributed Papers

UBV Photometry of the 1982-1984 Eclipse	Paul C, Schmidtke
Intermediate/Narrow Band Photometry	R. Donovan ,et. al.
Spectrophotometry, 3295-8880Å	G.W. Lockwood, et. al.
Two Micron CO Observations	K. Hinkle and T. Simon
Scattered Light/UV Excess in IUE Spectra	B. Altner, et. al.
Modeling Without Solid Particles	A. Cheng and N. Wolf
Research at the Hopkins Phoenix Observatory	J. L. Hopkins
Automatic Photometric Observations	L. Boyd, et. al.

These papers are available at:
Stencel, R. 1985 NASA Conference Publication 2384 –
"The 1982-1984 Eclipse of Epsilon Aurigae"
http://www.du.edu/~rstencel/NASAcp2384.pdf

3.5 Workshop Attendees

The following 31 people were registered participants at the 1985 Epsilon Aurigae Workshop, 16 and 17 January 1985:

Imad Ahmad	Imad-ad-Dean, Inc.
Thomas Ake	STSc I/CSC
Bruce Altner	GSFC/Applied Research Corp.
Dana Backman	University of Hawaii
Mary Barsony	CalTech
Robert Burham	Astronomy/Astromedia
Andrew Cheng	Steward Observatory
D. Scott Davis	Steward Observatory
Steno Perluga	Trieste Observatory (Italy)
Robert Fried	Braeside Observatory, IAPPP
Wendy Hagen	University of New Mexico & Wellesley
Douglas Hall	Vanderbilt University
Walter van Hamme	USC-Coastal Carolina College
Wayne Hanson	USAF/Vandenberg AFB
Cleve Hopkins	IAPPP
Jeff Hopkins	Hopkins Phoenix Observatory
Dick Joyce	KPNO

James Kemp	University of Oregon
Wes Lockwood	Lowell Observatory
Barry Lutz	Lowell Observatory
Alan MacRobert	Sky and Telescope
l l-Seong Nha	Yonsei University Observatory Soul, Korea
John Roemmelt	Dearborn, Michigan
Paul Schmidtke	Arizona State University
Theodore Simon	University of Hawaii
George Spagna	Renssalaer Polytech University
Robert E. Stencel	NASA HQ & JILA
Frank Verbunt	Inst. of Astronomy, Cambridge (UK)
Ronald Webbink	JILA & University of Illinois
Robert Wilson	University of Florida
Frank Bradshaw Wood	University of Florida

3.6 Workshop Photographs (by J. Hopkins)

The following are some pictures from the AAS meeting and Epsilon Aurigae Workshop in Tucson, Arizona in January 1985.

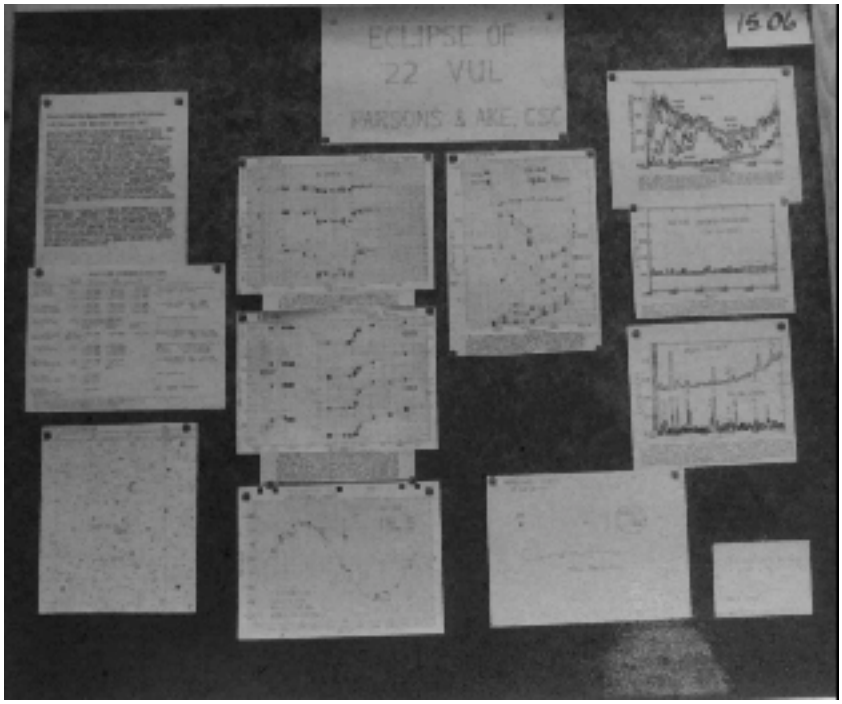

Figure 3.3 AAS Poster Paper

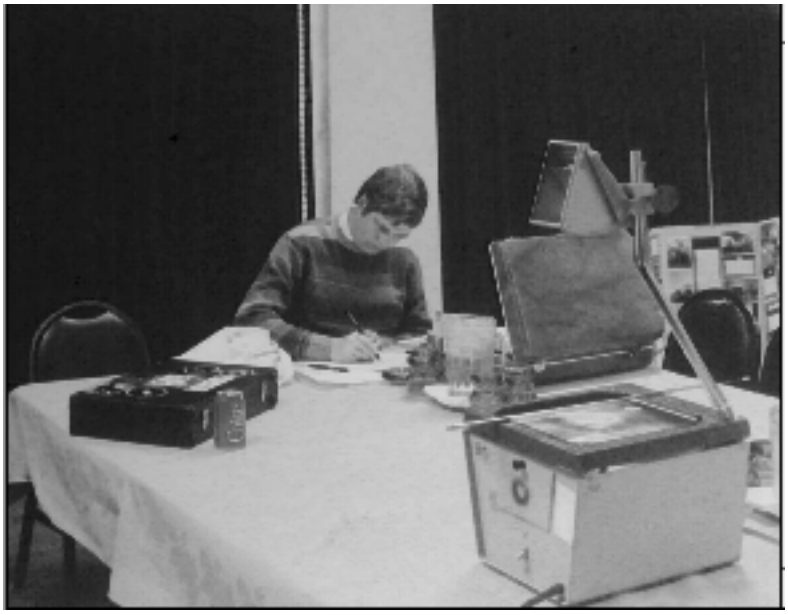

Figure 3.4 Ronald Webbink Preparing Talk

Figure 3.5 Bruce Altner

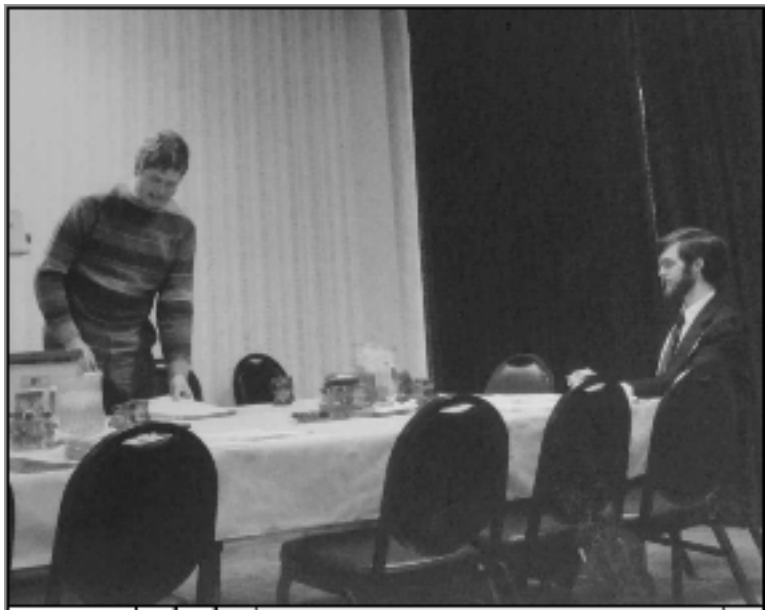

Figure 3.6 Webbink and Stencel

Figure 3.7 F.B. Wood

Figure 3.8 D.S. Hall

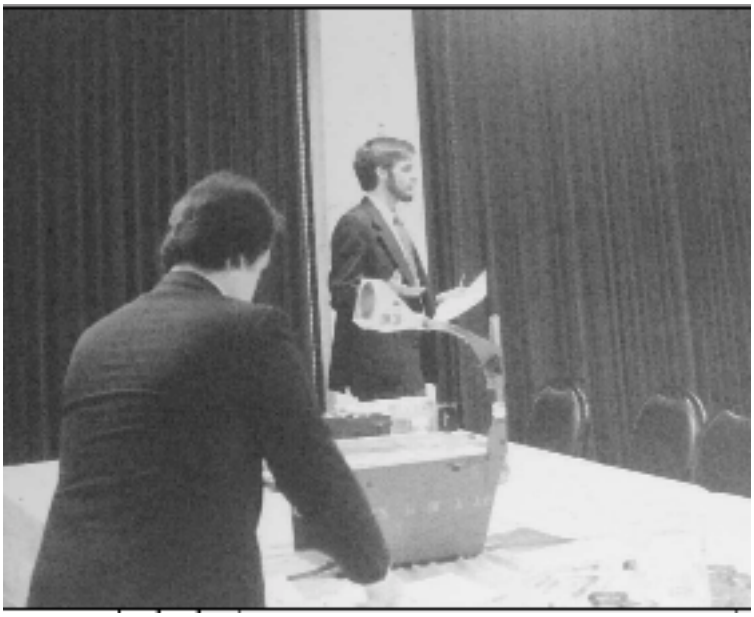

Figure 3.9 R.E. Stencel Introducing a Speaker

Figure 3.10 J.L. Hopkins

Figure 3.11 is a group picture of some 30 workshop attendees. If anyone knows the names of those with ?? please contact one of the authors and the names will be added in future publications.

Figure 3.11 Epsilon Aurigae Workshop Gang

3.7 Workshop Attendee Photograph:

From Figure 4.3, Front Row L-R: ?, A. Cheng, F. B. Wood, J.L. Hopkins, R.E. Stencel, ?, T. Simon, ?, ? Next Row L-R: I. Ahmad, T. Ake, ?, ?, B. Altner, ?, ?, J. Kemp, E. Guinan, ?, K. Hinkle, F. Fekel, ?, L Boyd, ?, ? Last Row L-R: P. Schmidtke, ?, ?, ?, R. Genet, D. Hall

3.8 Photometry Data

3.8.1 Out-of-Eclipse Magnitudes

Average V magnitude: 3.03
Average B magnitude: 3.60
Average U magnitude: 3.73

3.8.2 1982 -1984 Totality Magnitudes

Average V magnitude at totality: 3.74
Average B magnitude at totality: 4.30
Average U magnitude at totality: 4.52

3.8.3 1982 -1984 Depths Magnitudes

V magnitude depth: 0.71
B magnitude depth: 0.70
U magnitude depth: 0.79

3.8.4 Contact Times

Because of the out-of-eclipse variations of the system, precise contact times are a real challenge. Contact times were determined by plotting the magnitudes and using the slope of the ingress and egress to intersect with the average out-of-eclipse magnitude for first and fourth contact times and average totality magnitude for the second and third contact times. See Table 3.1 for the contact times.

Filter	1st	2nd	Mid-Eclipse	3rd	4th
V	5,158	5,300	5,524 / 5,485	5,747	5,812
B	5,170	5,305	5,524 / 5,492	5,742	5,813
U	5,180	5,300	5,528 / 5,495	5,755	5,810

Table 3.1 1982-84 Eclipse Contact Times

Note: Mid-Eclipse dates have two numbers, the first was derived as the midpoint between 2nd and 3rd contact. The second number was derived between first and fourth contact. Dates are PJD + 2,440,000.

3.8.5 1982 -1984 Eclipse Summary of Event Duration

Filter	Ingress	Totality	Egress	Total
V	142 days	447 days	65 days	654 days
B	135 days	437 days	71 days	643 days
U	120 days	455 days	55 days	630 days

Table 3.2 1982-84 Eclipse Event Durations

These data are in fair agreement with others, notably Nha's data for observations during the 1982-84 eclipse.

3.8.6 Photometry Data Plots

Remember this was before CCDs and even PIN diodes. All data were taken with UBV photomultiplier tube photon counting photometers. Plots of the UBV magnitudes are from data obtained by Jeff Hopkins at the at the Hopkins Phoenix Observatory - HPO (Phoenix, Arizona U.S.A.) and Stig Ingvarsson at the Tjorn Island Astronomical Observatory - TAO (Sweden).

Figure 3.12 Stig Ingvarsson TAO - Sweden

Note: First contact and the mid-eclipse were during the summer when the star was low in the night sky and very difficult to observe. Stig Ingvarrson is located at a high latitude which allowed him a longer observing season. Stig was one of the very few who caught part of the mid-eclipse brightening.

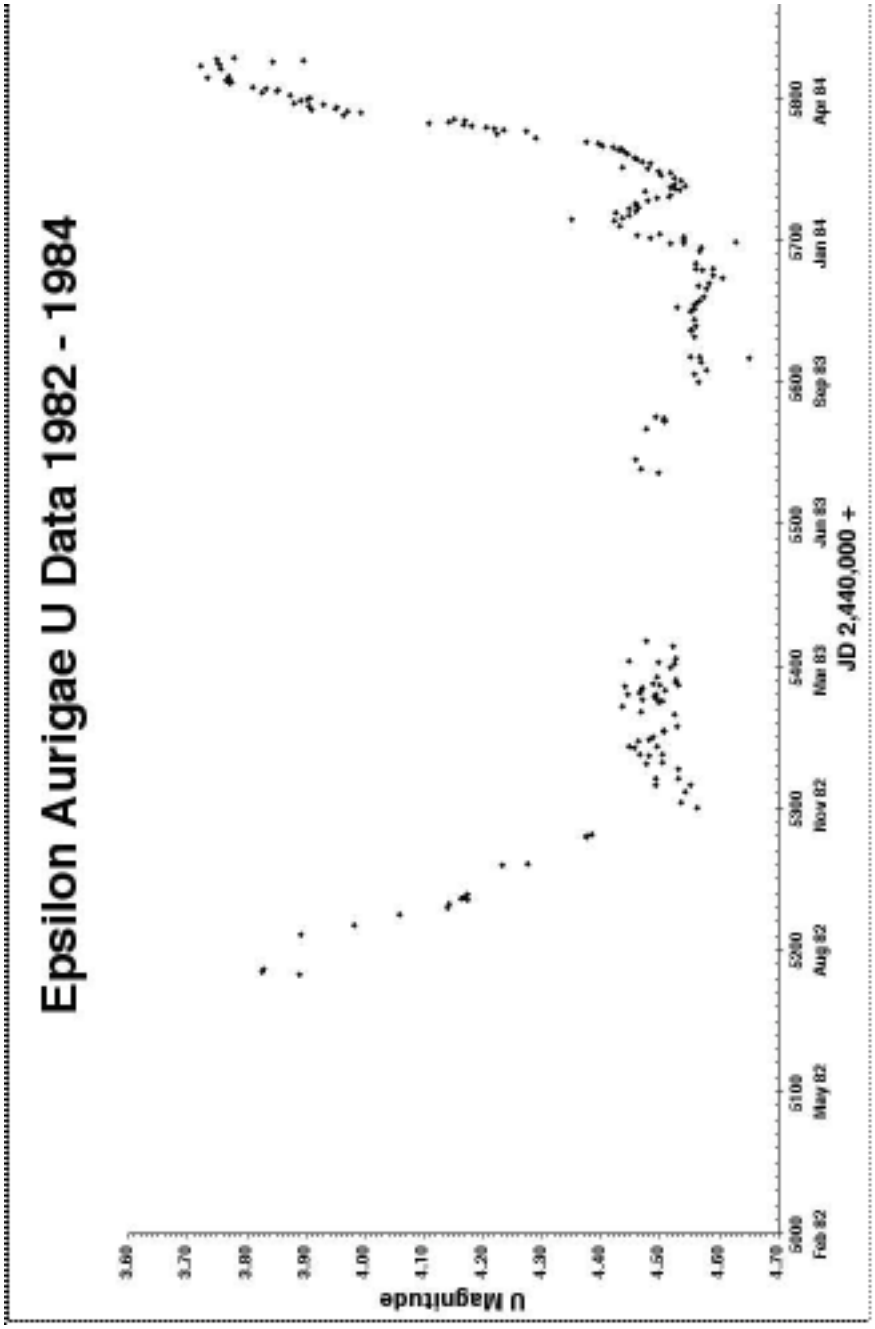

Figure 3.13 1982 -1984 U Band Data Plot

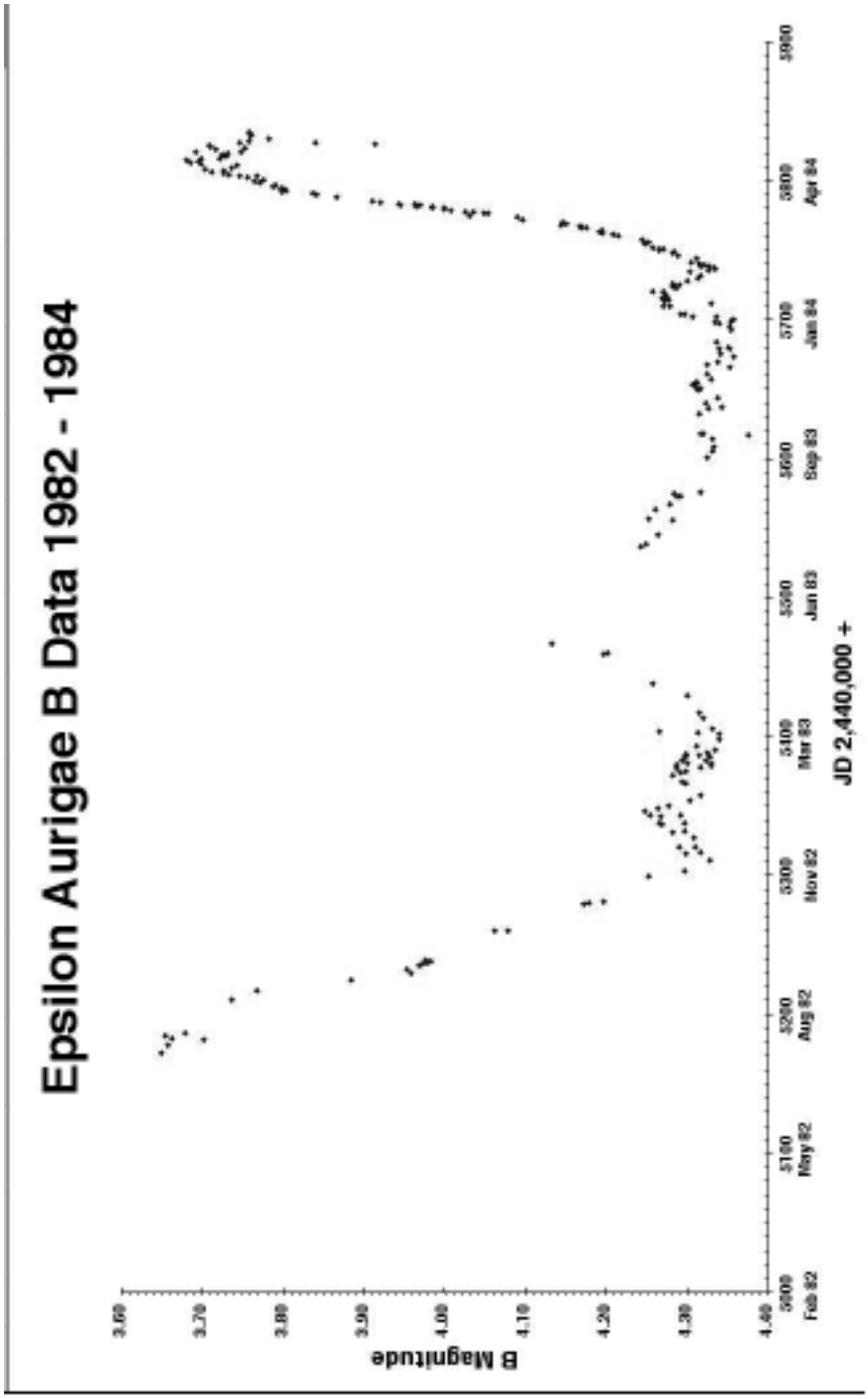

Figure 3.14 1982 -1984 B Band Data Plot

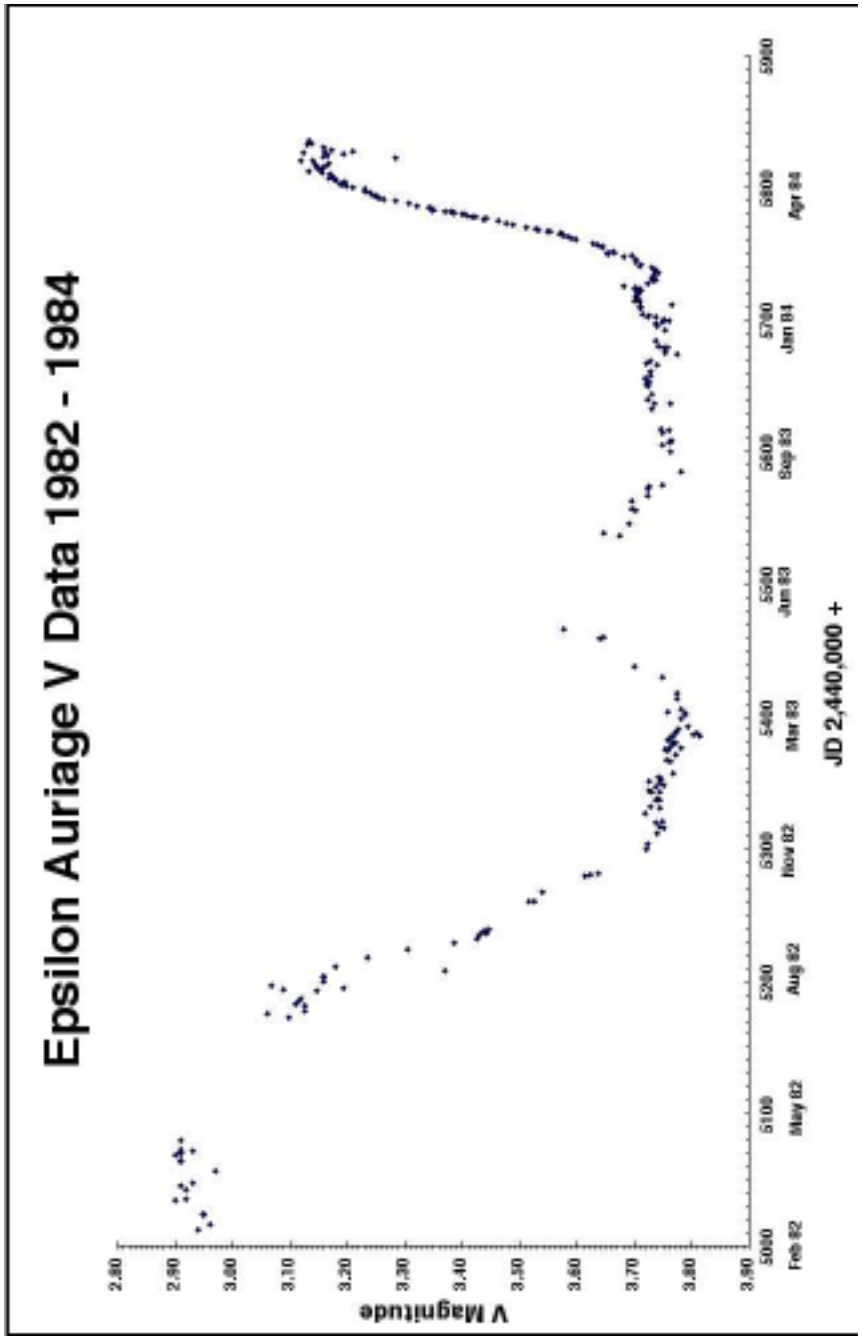

Figure 3.15 1982 -1984 V Band Data Plot

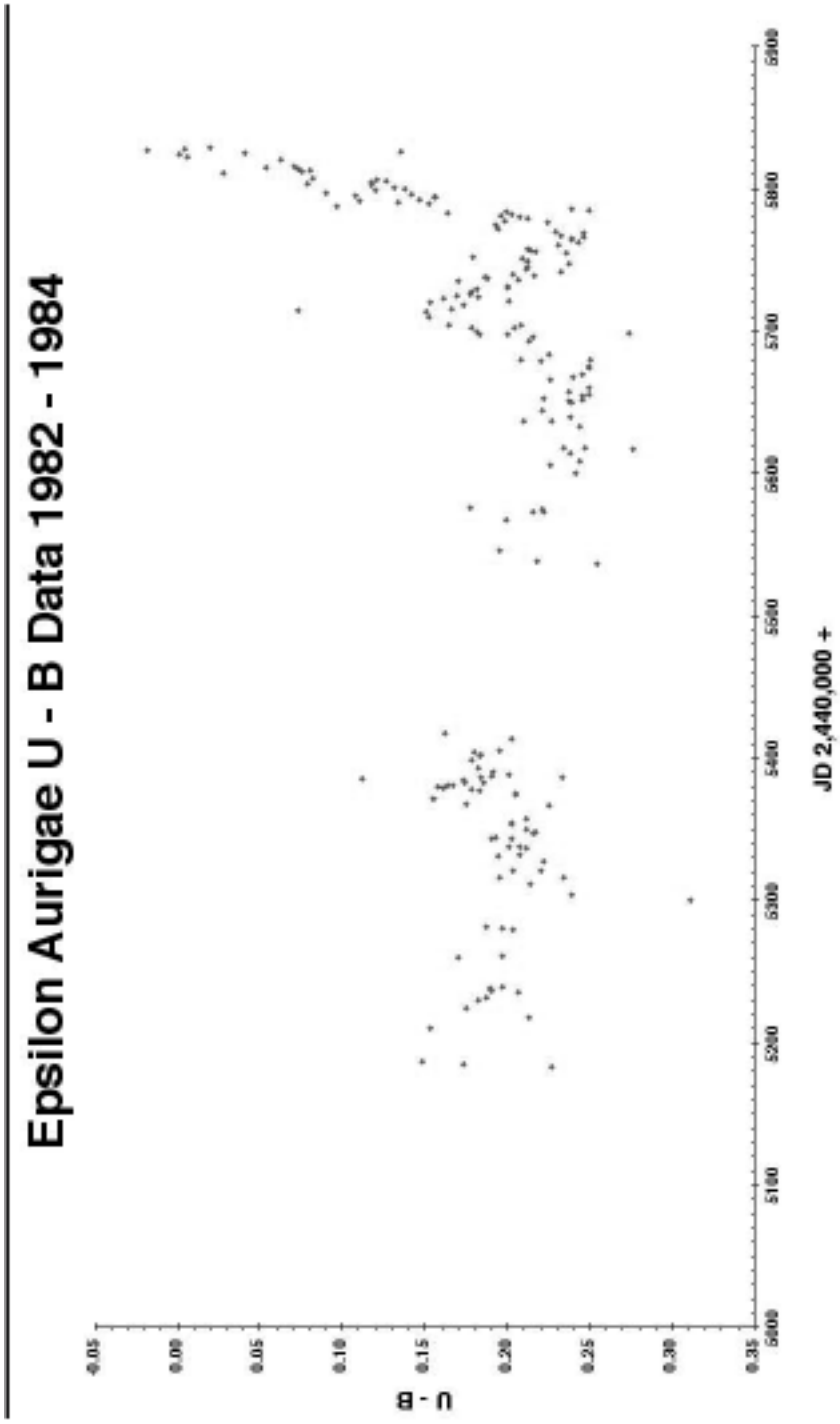

Figure 3.16 1982 -1984 (U - B) Data Plot

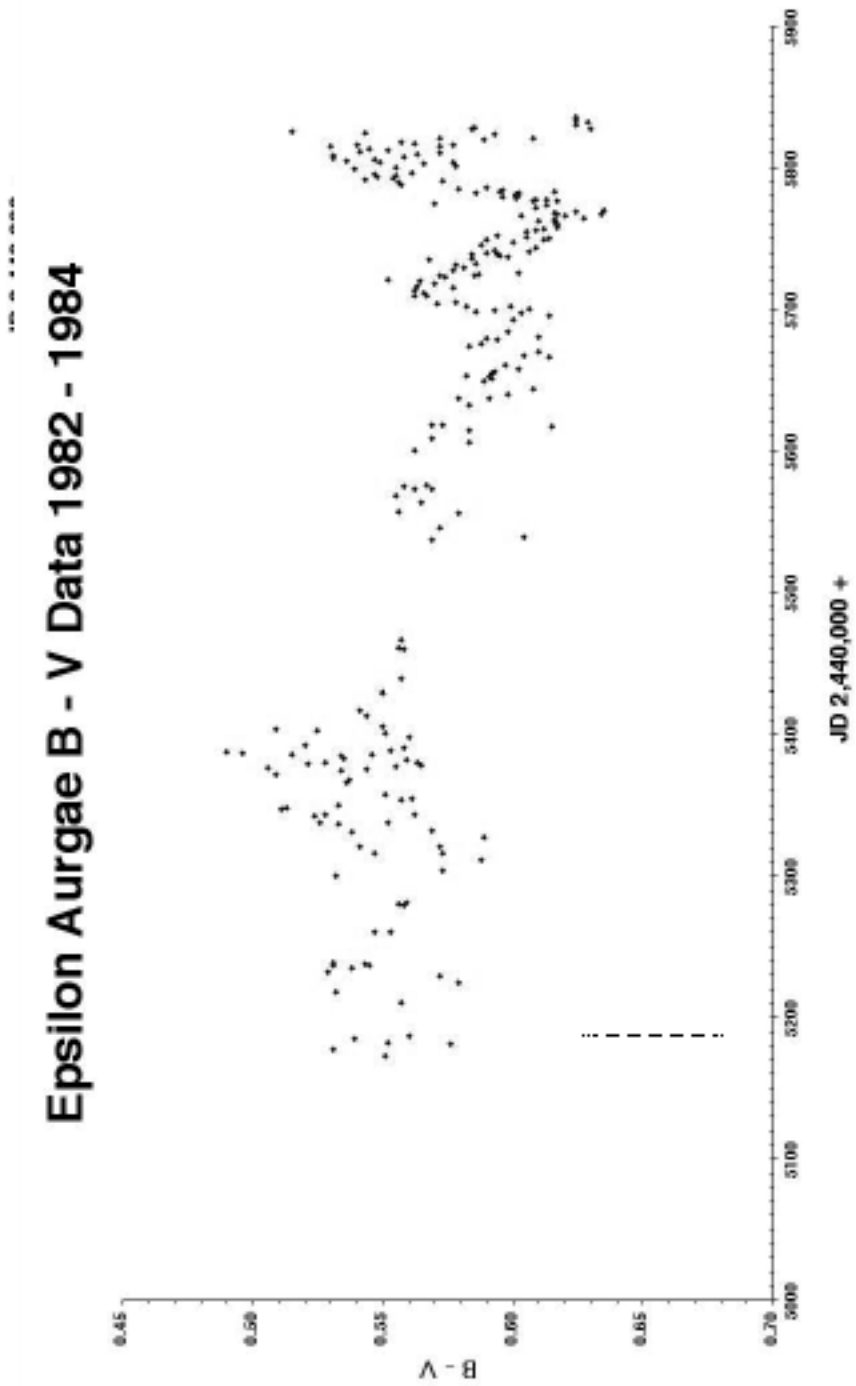

Figure 3.17 1982 -1984 (B - V) Data Plot

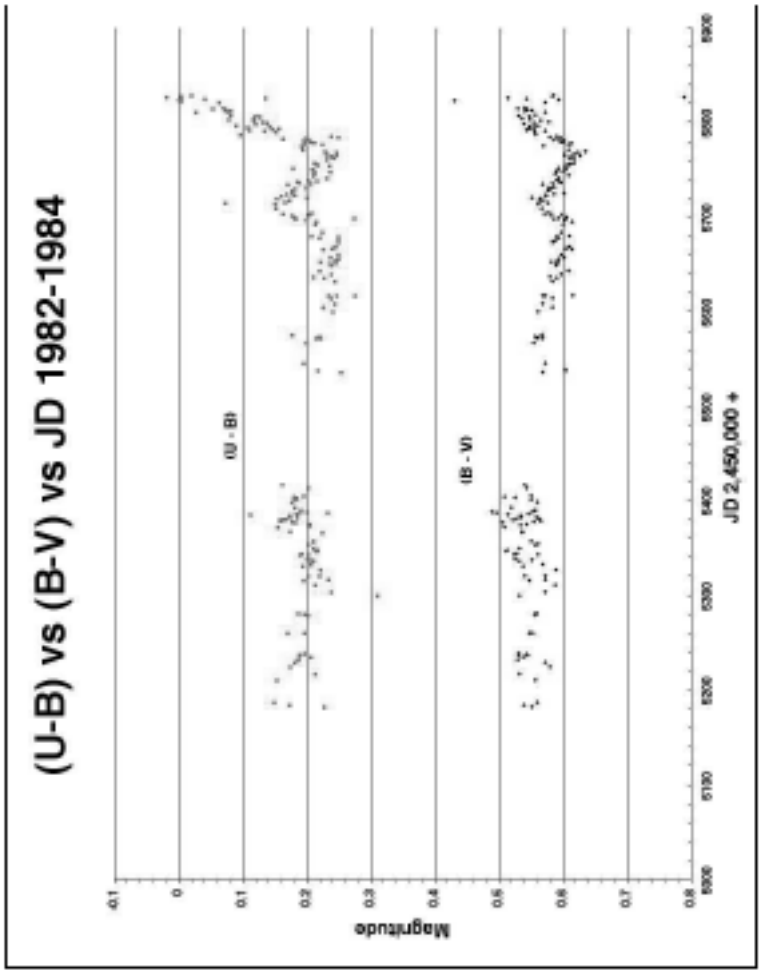

Figure 4.18 1982 -1984 (U - B) vs. (B -V) Data Plot

3.9 Spectroscopy

As mentioned in chapter 9, major advances were made with spectroscopic observations obtained during the 1982-84 eclipse event. These include careful radial velocity observations by Lambert & Sawyer who detected neutral potassium lines from the secondary through eclipse and past 4th contact. They argue this helps support a low mass model for the epsilon Aurigae system. A similar asymmetric behavior was seen in the near-infrared carbon monoxide bands, which strengthened at and after mid-eclipse, as reported by Hinkle and Simon. Finally, a careful study of the shell spectrum through eclipse was reported by Ferluga, who concluded that the eclipsing body is an asymmetric disk with trailing material and shock fronts.

3.10 Polarimetry

3.10.1 Introduction

The principal result in polarimetry of the epsilon Aurigae eclipse was provided by James Kemp and collaborators, in three reports: at the 1985 Workshop, in a short paper in the Astrophysical Journal, and as part of a unpublished Ph.D. thesis by Gary Henson, student of Kemp.

Kemp et. al's work was to monitor linear polarization and state the range of values they found.

With care and precision, they detected eclipse phase dependent polarization changes. These were seen to be asymmetric – greatest during the second half of eclipse.

3.10.2 Interpretation

Their interpretation calls for the secondary resembling a tilted disk, as illustrated in Figure 3.19 (from Kemp et al. 1986 ApJ) and an orbital inclination not exactly 90 degrees (edge-on). They further argue that the next eclipse (2010) might reveal a much greater mid-eclipse brightening as the central hole in the disk precesses into greater view.

Low levels of post-eclipse polarization on the 100 day quasi-period (with fluctuations as fast a 0.5 to 5 days) further argue for asymmetric structure of the primary star – perhaps a chromospheric (UV-emitting) 'belt' tilted as much as 45 degrees from the ring plane. This latter point should be readily testable by interferometry. To date, this has been the last substantive polarimetry obtained and presented concerning epsilon Aurigae.

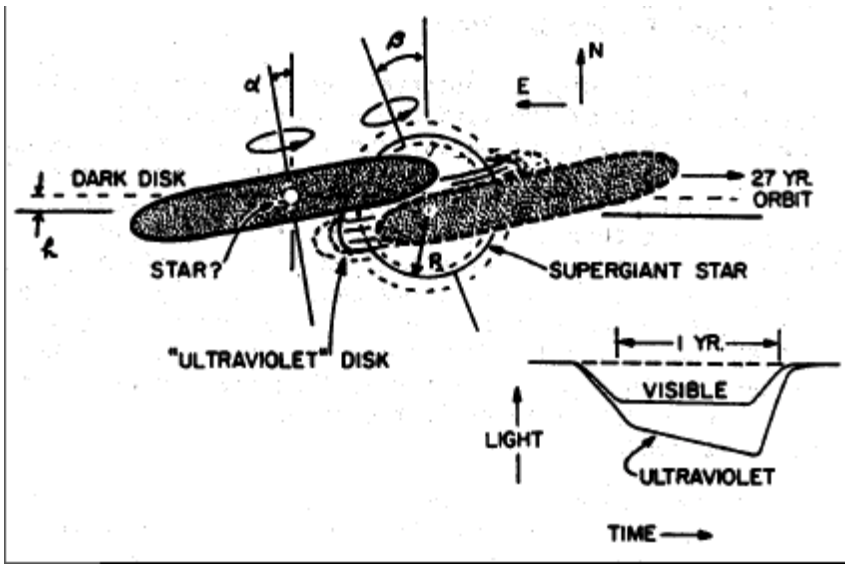

Figure 3.19 Kemp, 1985 Workshop Diagram

3.11 References

Kemp, J., Henson, G., Kraus, D., Beardsley, I., Carroll, L., Ake, T., Simon, T., Collins, G., 1986 Astrophysical Journal, vol. 300, L11 – E*psilon Aurigae - Polarization, light curves, and geometry of the 1982-1984 eclipse"*
http://adsabs.harvard.edu/abs/1986ApJ...300L..11K

Stencel, R. 1985 NASA Conference Publication 2384 –
The 1982-1984 Eclipse of Epsilon Aurigae
http://www.du.edu/~rstencel/NASAcp2384.pdf

IV. Post 1984 Observations

4.0 Introduction

This section will present observational data taken after the 1982 - 1984 eclipse. Some of the plots will contain the 1982-1984 eclipse data for reference.

Data include UBV photometric observations and frequency domain analysis using Peranso software.

Spectroscopic data supplied by Brian McCandless is presented. Analysis of Hα lines and the significance of the Hα profile changes is discusses along with a similarity with Be stars. **S**tan Gorodenski of the Blue Hills Observatory in Dewey, Arizona provides some Hα spectra.

No known polarimetry data exists for the post 1983- 1984 eclipse.

For the first time, interferometry is playing an important role in epsilon Aurigae observations. Interferometry with the Navy Prototype Optical Interferometer (NPOI) located in Flagstaff, Arizona has been used.

4.1 Photometry Data

UBV photometric data obtained at the Hopkins Phoenix Observatory for the periods of 1982 - 1988 and 2003 - 2008 are presented. Data provided by the AAVSO taken by Louis Boyd for the period 1987 - 2005 are presented. In both cases data were taken with 1P21 PMT based photon counters. The HPO data was taken with an 8"C-8 SCT while the Boyd data were taken with an automated robotic 10" Newtonian telescope.

4.1.1 HPO UBV Photometric Data 1982 - 1988

The 1982 - 1988 UBV photometric data were taken at the Hopkins Phoenix Observatory using a Celestron C-8 (8") Schmidt-Cassegrain Telescope and homemade photon counting unit.

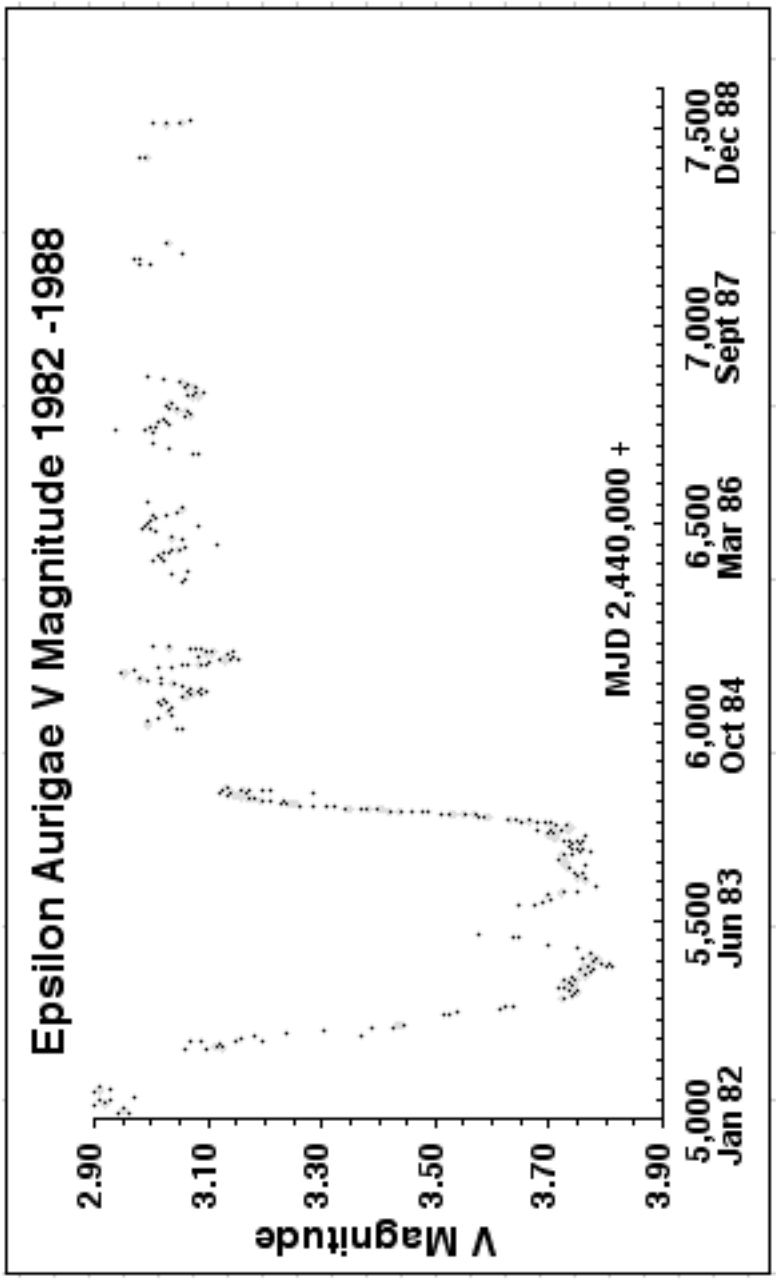

Figure 4.1 HPO V Band Data 1982 - 1988

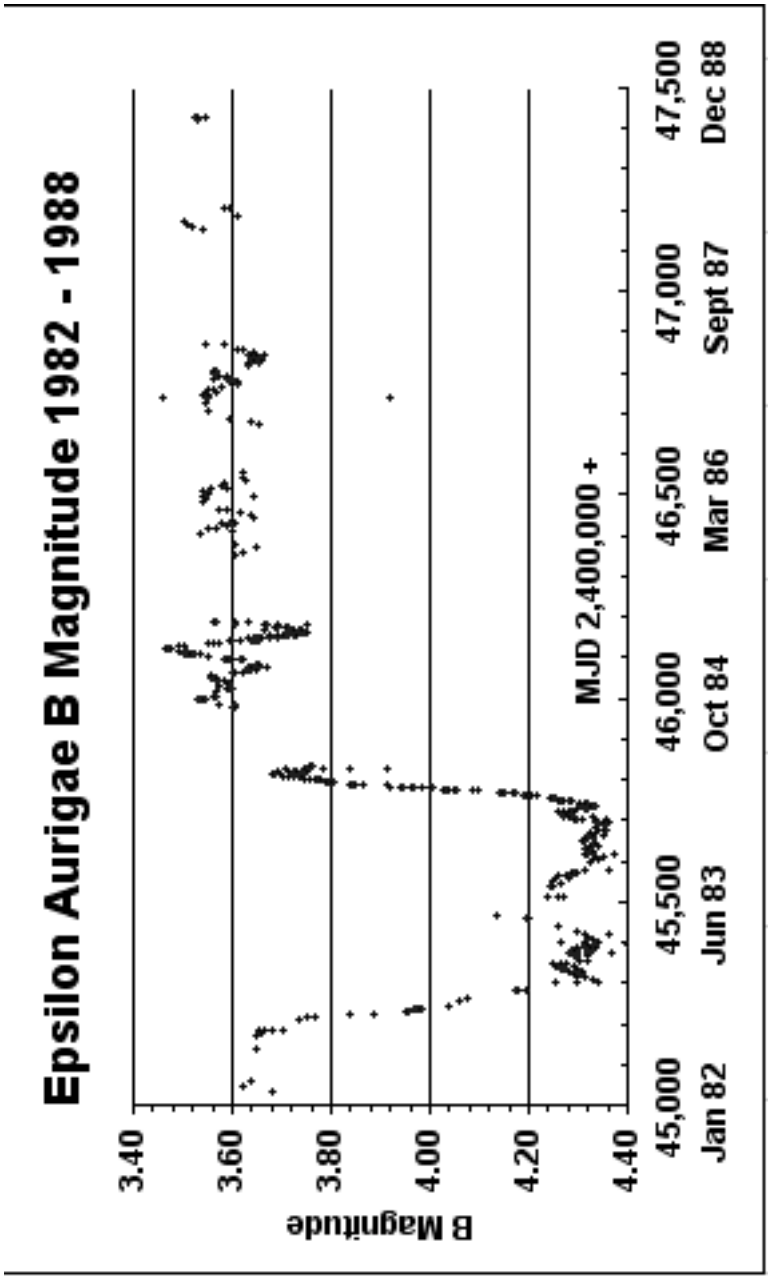

Figure 4.2 HPO B Band Data 1982 - 1988

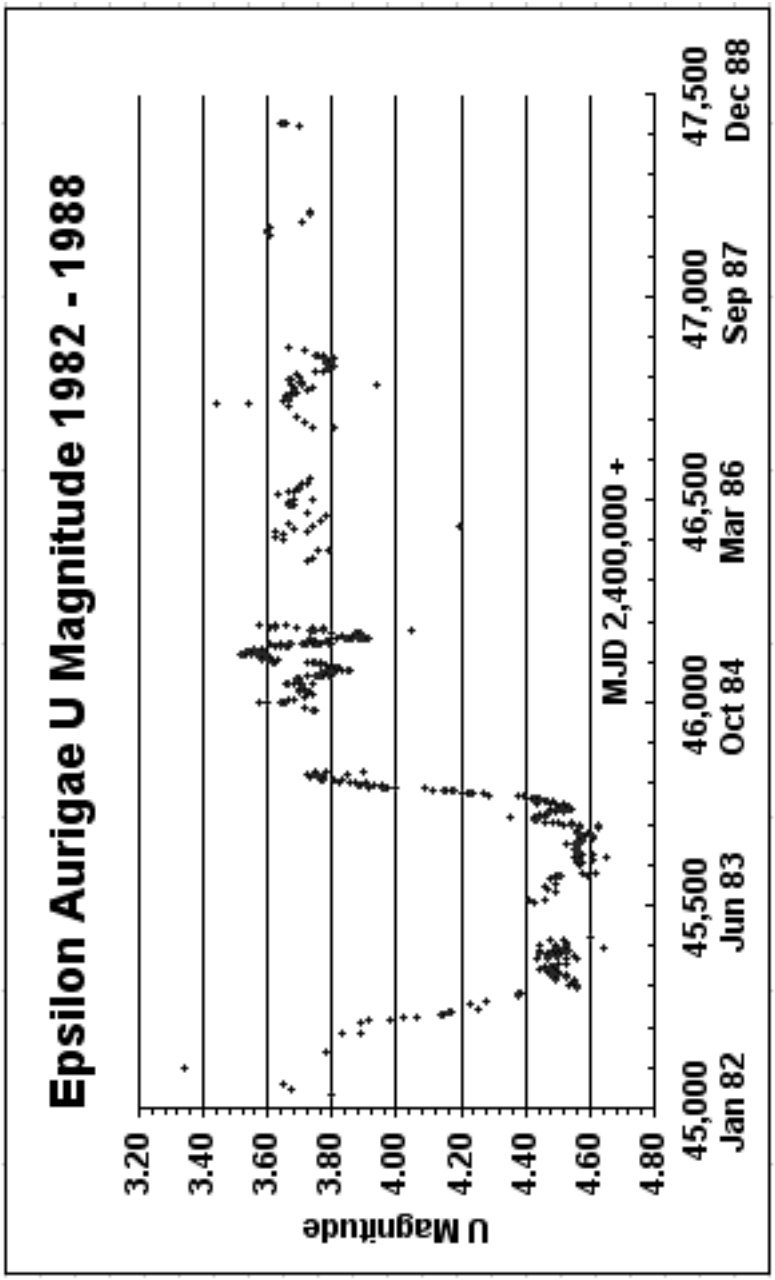

Figure 4.3 HPO U Band Data 1982 - 1988

4.1.2 HPO UBV Photometric Data 2003 - 2008

The 1982 - 1988 UBV photometric data were taken at the Hopkins Phoenix Observatory using a Celestron C-8 (8") Schmidt-Cassegrain Telescope and homemade photon counting unit.

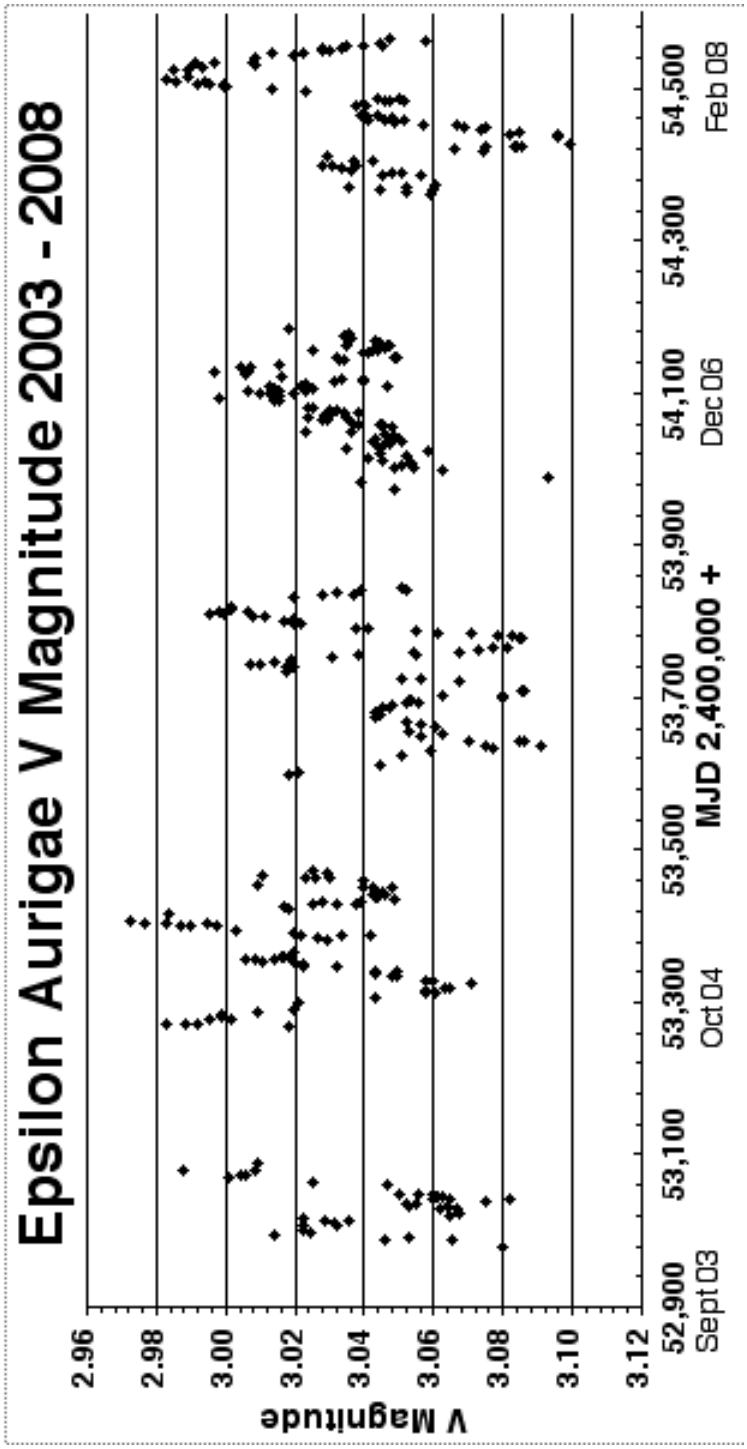

Figure 4.4 HPO V Band Data 2003 - 2008

Table 4.1 is a summary of the V band data taken at the Hopkins Phoenix Observatory from 1982 - 1988 and 2003 - 2008.

Season	Vmin	Vmax	Vavg	ΔV
84/85	3.155	2.945	3.054	0.210
85/86	3.116	2.983	3.029	0.133
86/87	3.094	2.938	3.044	0.156
87/88	3.054	2.972	3.006	0.082
88/89	3.071	2.981	3.023	0.090
03/04	3.082	2.987	3.043	0.095
04/05	3.071	2.973	3.025	0.098
05/06	3.091	2.995	3.046	0.096
06/07	3.093	2.997	3.034	0.096
07/08	3.099	2.983	3.038	0.117

Table 4.1 HPO V Photometric Data Summary

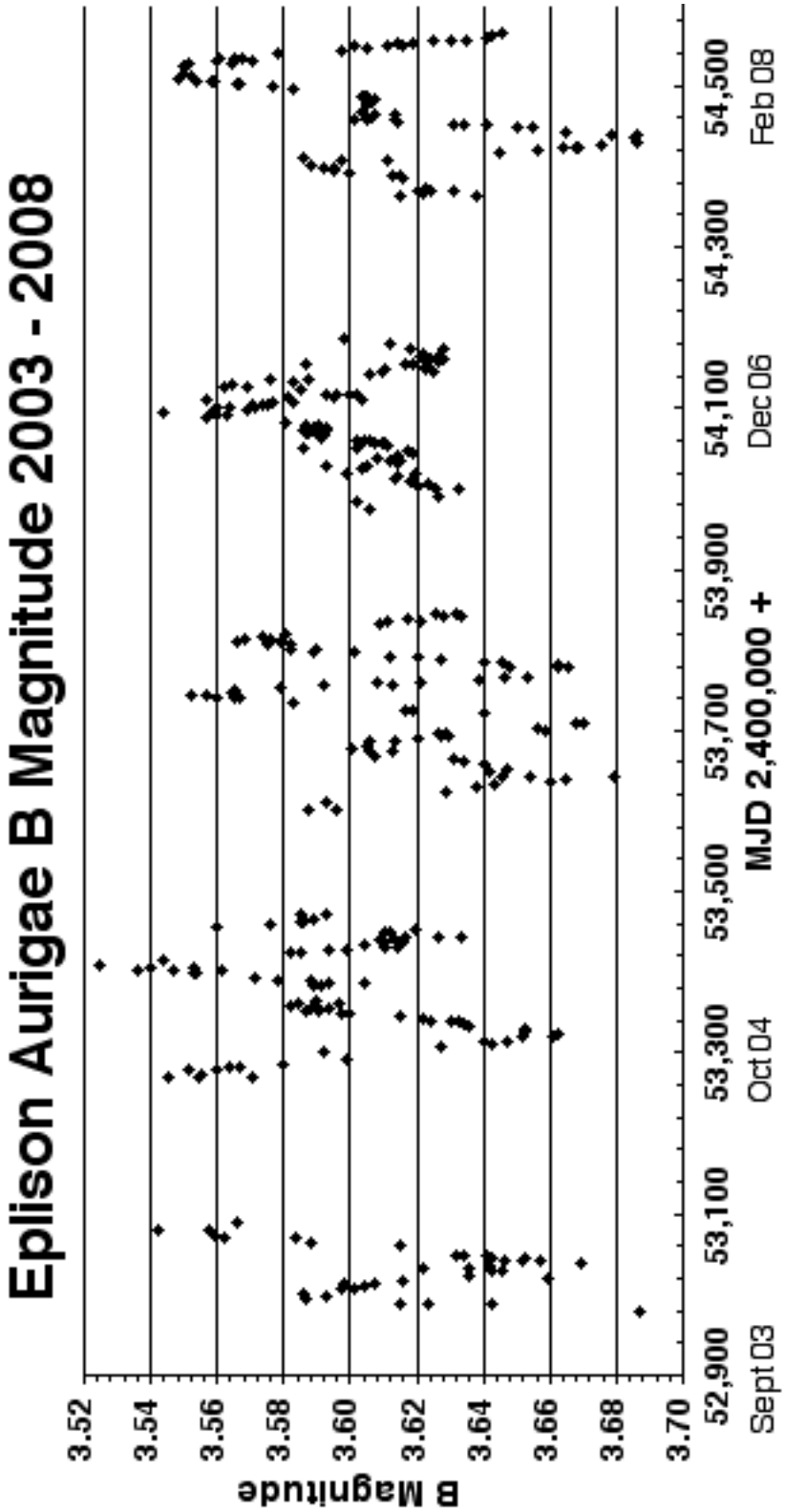

Figure 4.5 HPO B Band Data 2003 - 2008

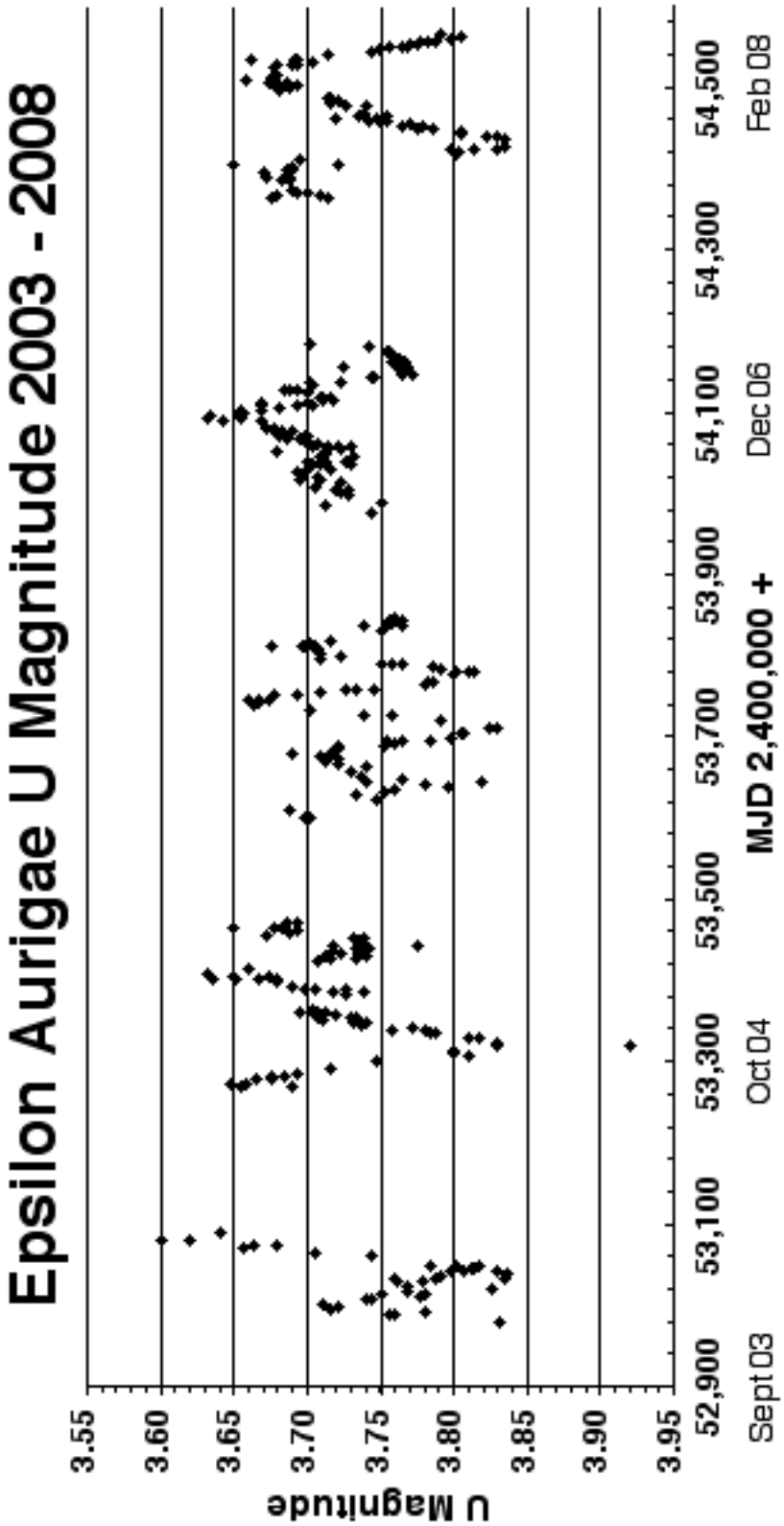

Figure 4.6 HPO U Band Data 2003 - 2008

4.1.3 HPO JH Photometric Data 2006 - 2007

Infrared J and H band data were taken at the HPO during the 2005 to 2007 seasons using an Optec SSP-4 solid state photometer. The 2005 - 2006 season data was of poor quality and the unit's detector was changes from a 0.3 mm to 1.0 mm detector. The data improved considerably and Figures 4.7 and 4.8 show plots of the J and H band data respectively.

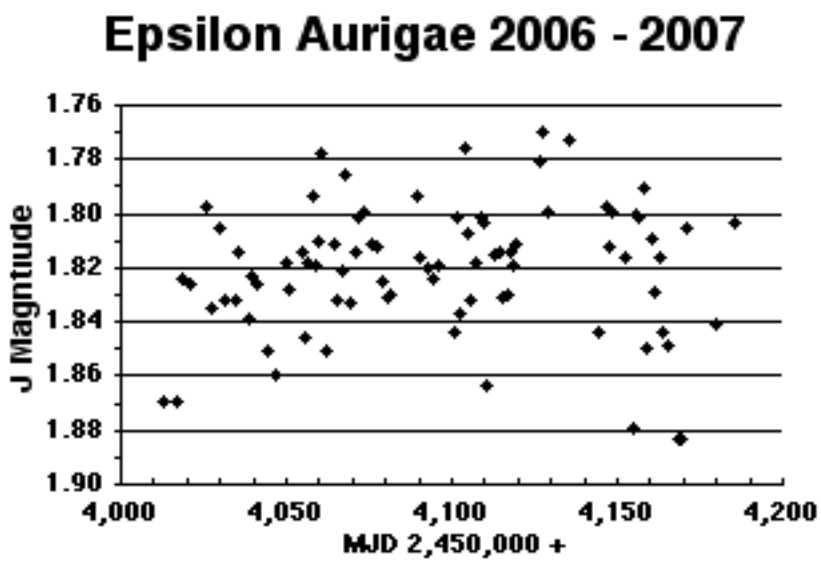

Figure 4.7 HPO J Band Data 2006 - 2007 Season

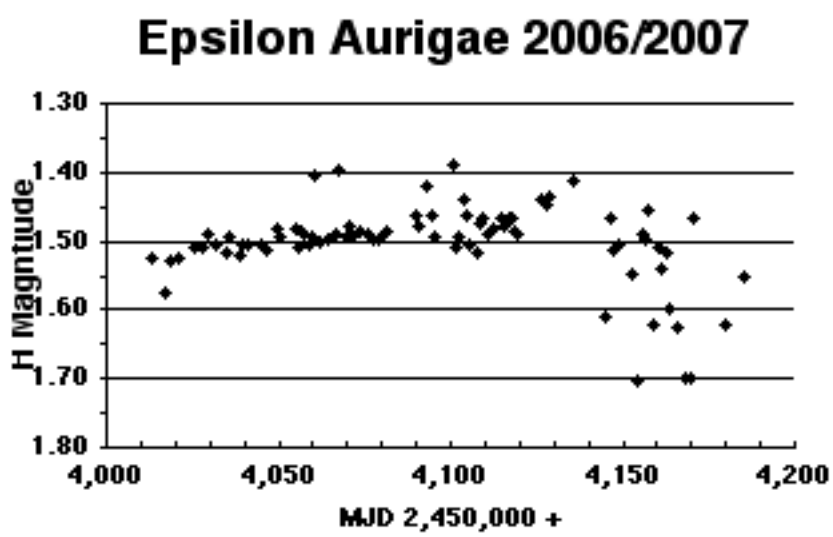

Figure 4.8 HPO H Band Data 2006 - 2007 Season

4.1.4 Boyd UBV Photometric Data 1987 - 2005

The AAVSO was kind enough to provide UBV data taken by Louis Boyd using a home made 10" robotic Newtonian telescope.

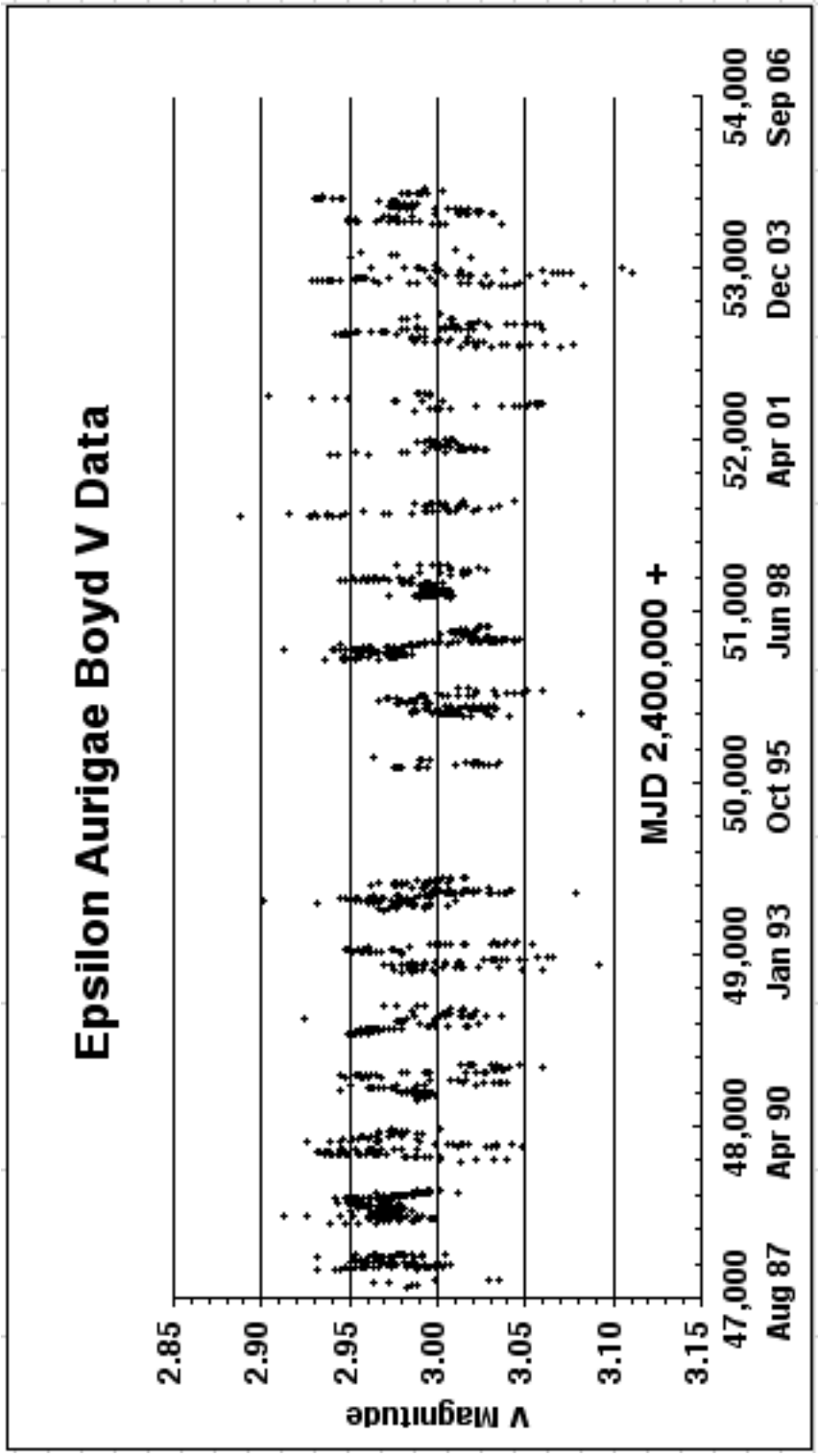

Figure 4.9 Boyd V Band Data 1987 - 2005
Plotted by HPO

Table 4.2 is a summary compiled by HPO of the Boyd V data taken from 1988 to 2005.

Season	Vmin	Vmax	Vavg	ΔV
87/88	3.035	2.931	2.975	0.104
88/89	3.011	2.913	2.971	0.098
89/90	3.048	2.926	2.977	0.122
90/91	3.059	2.945	2.994	0.114
91/92	3.037	2.924	2.983	0.113
92/93	3.092	2.948	3.000	0.144
93/94	3.078	2.901	2.990	0.177
1996	3.035	2.963	3.000	0.072
096/97	3.082	2.967	3.008	0.115
97/98	3.047	2.912	2.989	0.135
98/99	3.027	2.945	2.991	0.082
2000	3.044	2.888	2.983	0.156
00/01	3.028	2.939	3.000	0.089
2001	3.060	2.904	3.008	0.156
02/03	3.077	2.942	3.001	0.135
03/04	3.111	2.929	3.001	0.182
04/05	3.037	2.930	2.983	0.107

Table 4.2 Boyd V Photometric Data Summary

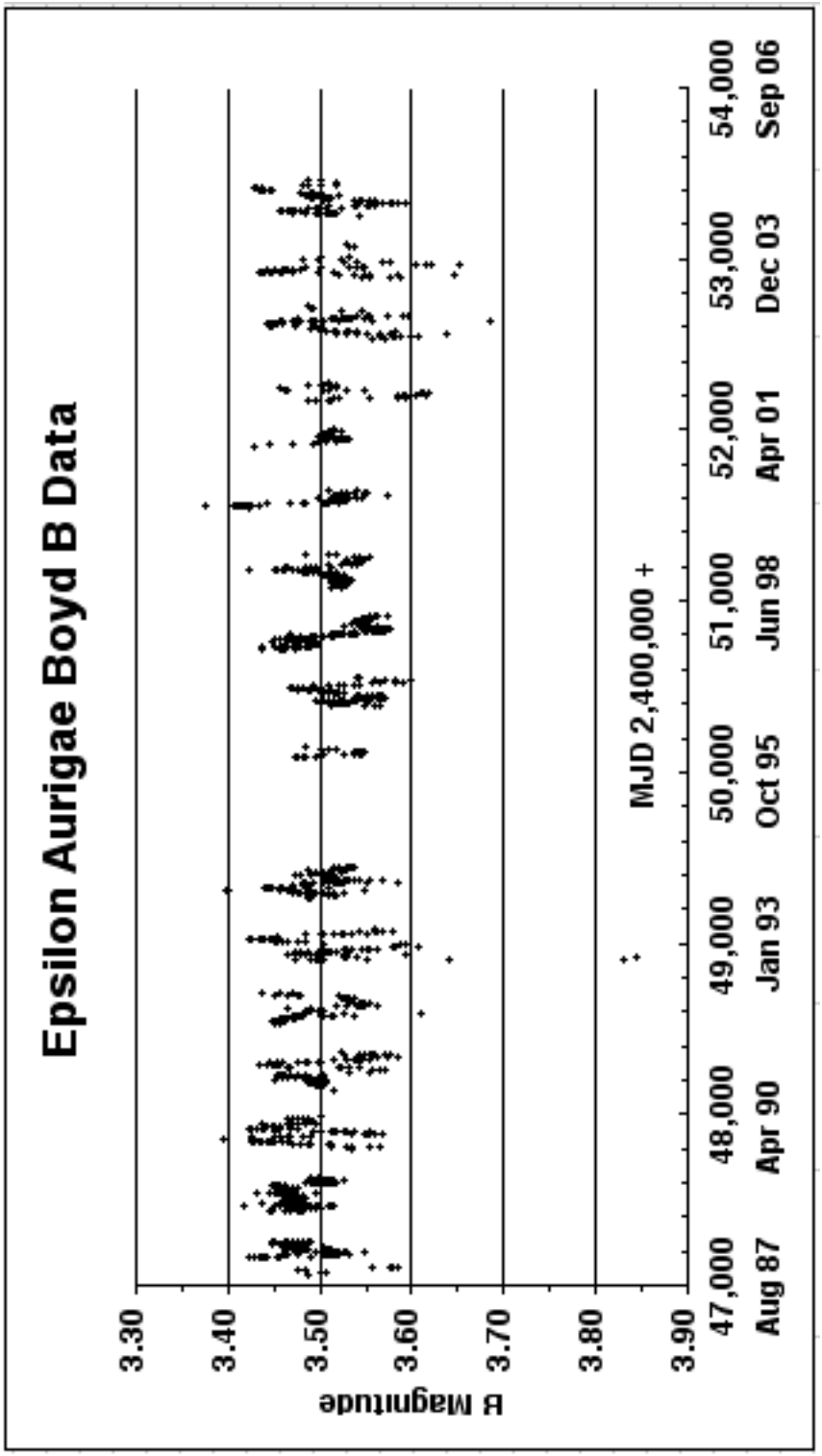

Figure 4.10 Boyd B Band Data 1987 -2005
Plotted by HPO

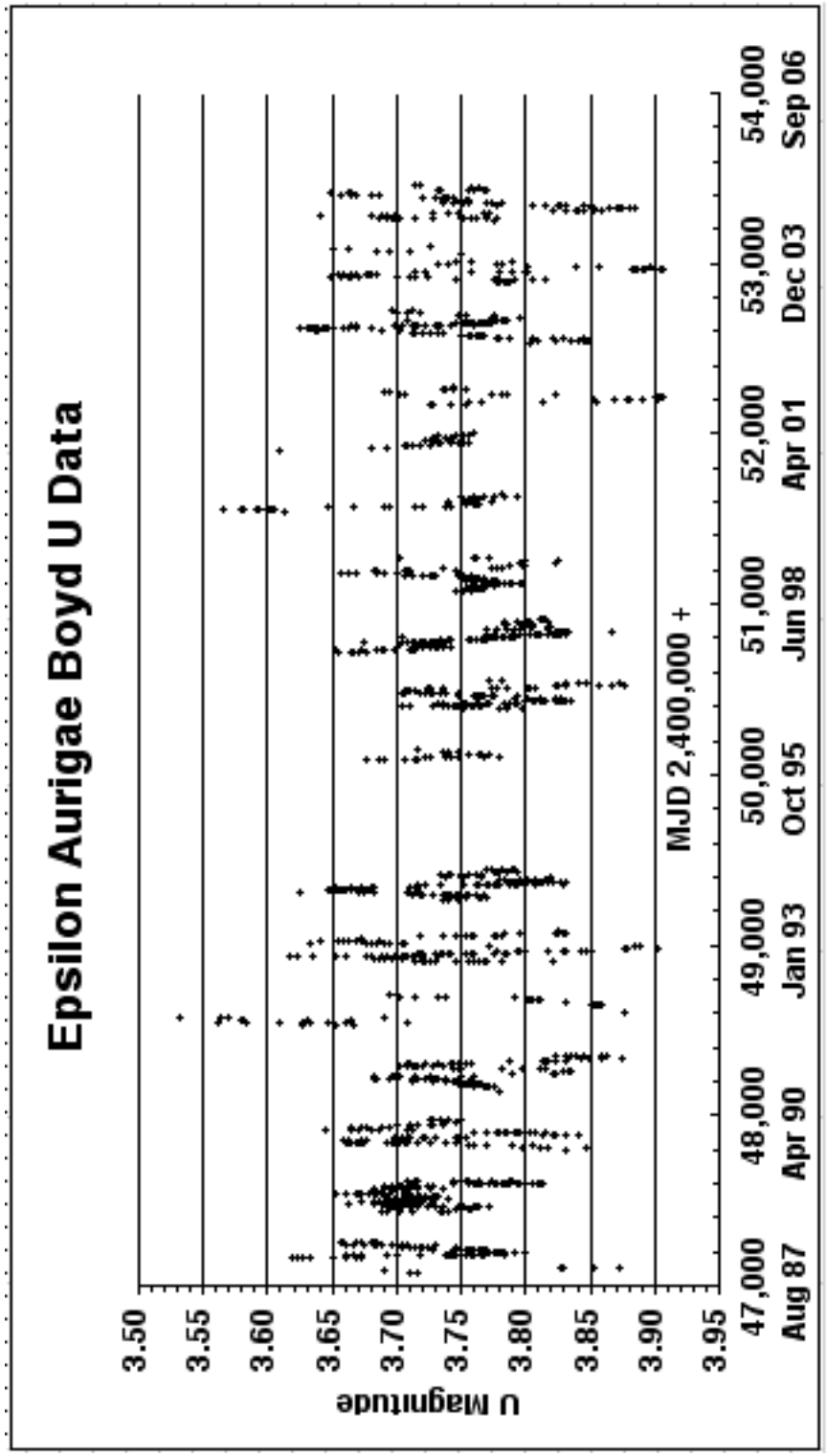

Figure 4.11 Boyd U Band Data 1987 - 2005
Plotted by HPO

4.1.5 Frequency Domain Data

4.1.5.1 Introduction

Several techniques have been used to discern a period for the star system light variations. Taking the data and doing a Fourier transform on them will produce a period or periods, but the value of that is arguable. Taking shorter segments (by season) seems a bit better approach. What has been seen is the period or periods do not appear to be constant and in fact appear to be getting shorter. See Section 9.2.10.4 for more information on techniques.

4.1.5.2 HPO V Band Frequency Domain Data

Figure 4.12 shows a frequency domain plot using the Deeming (DFT) method for 1984 - 1985 HPO V data.

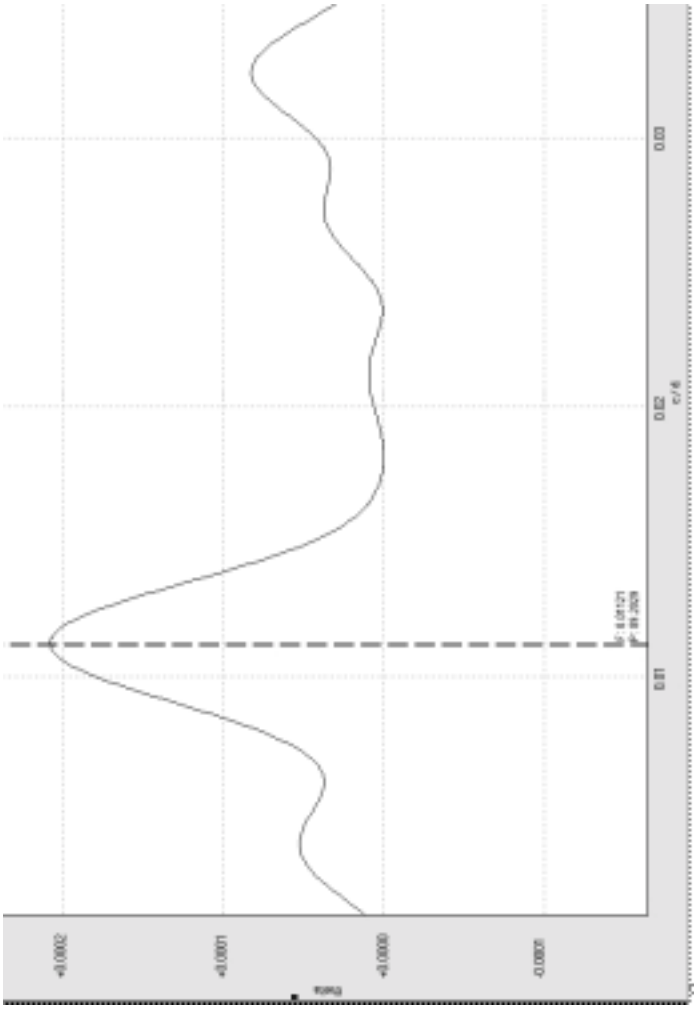

Figure 4.12 HPO V Frequency Domain 1984 - 1985

Note: The 88/89 season only had a few data points and with a large time gap in observations. Some of the primary periods may be aliases of the season rather than true periods.

Figure 4.13 shows a frequency domain plot using the Deeming (DFT) method for 2003 - 2004 HPO V data.

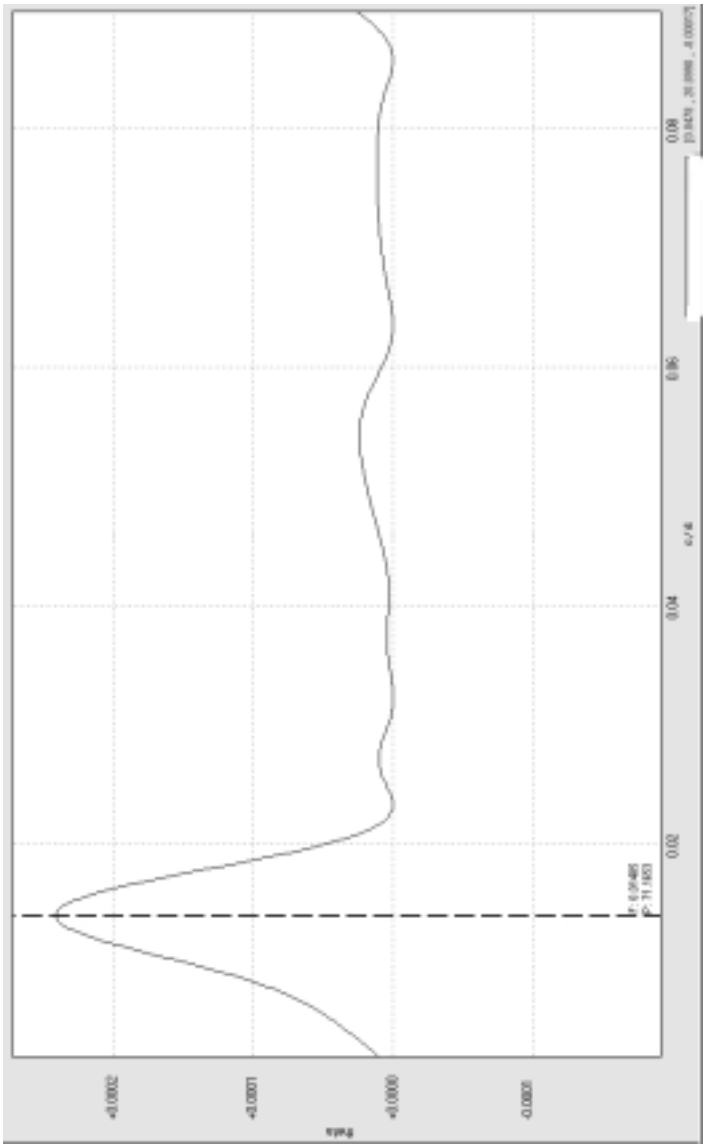

Figure 4.13 HPO V Frequency Domain 2003 - 2004

.

Figure 4.14 shows a frequency domain plot using the Deeming (DFT) method for 2003 - 2008 HPO data.

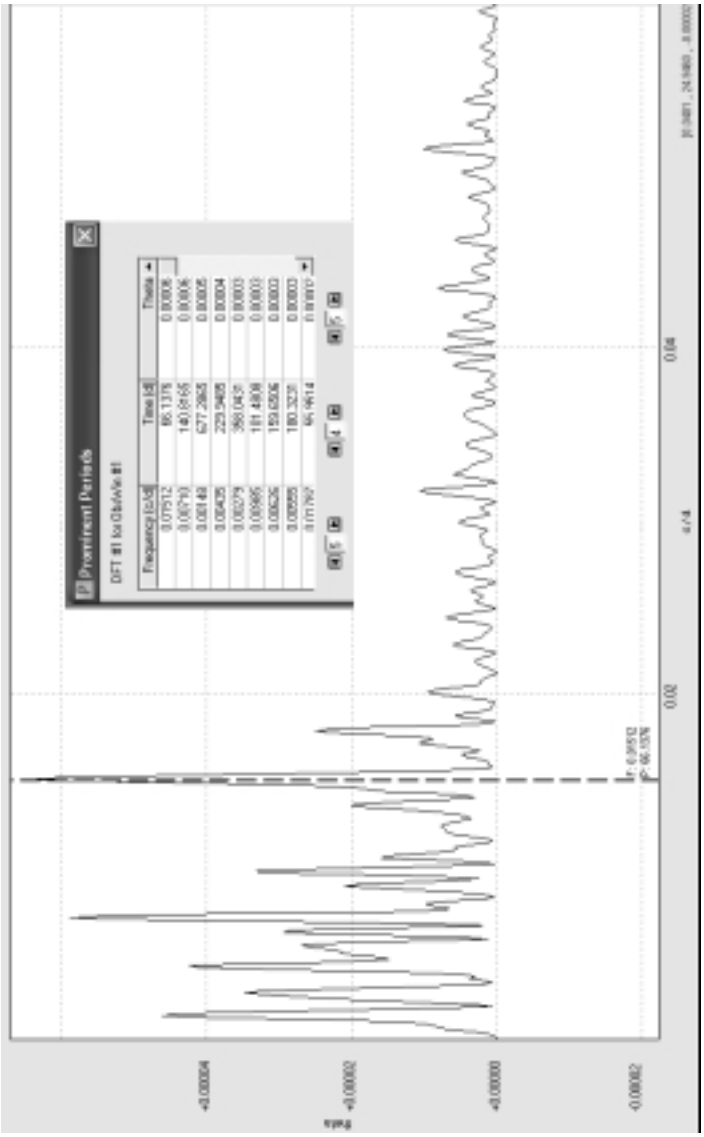

Figure 4.14 HPO V Frequency Domain 2003 - 2008

Figure 4.15 shows a frequency domain plot using the Deeming (DFT) method for 2007 - 2008 HPO data.

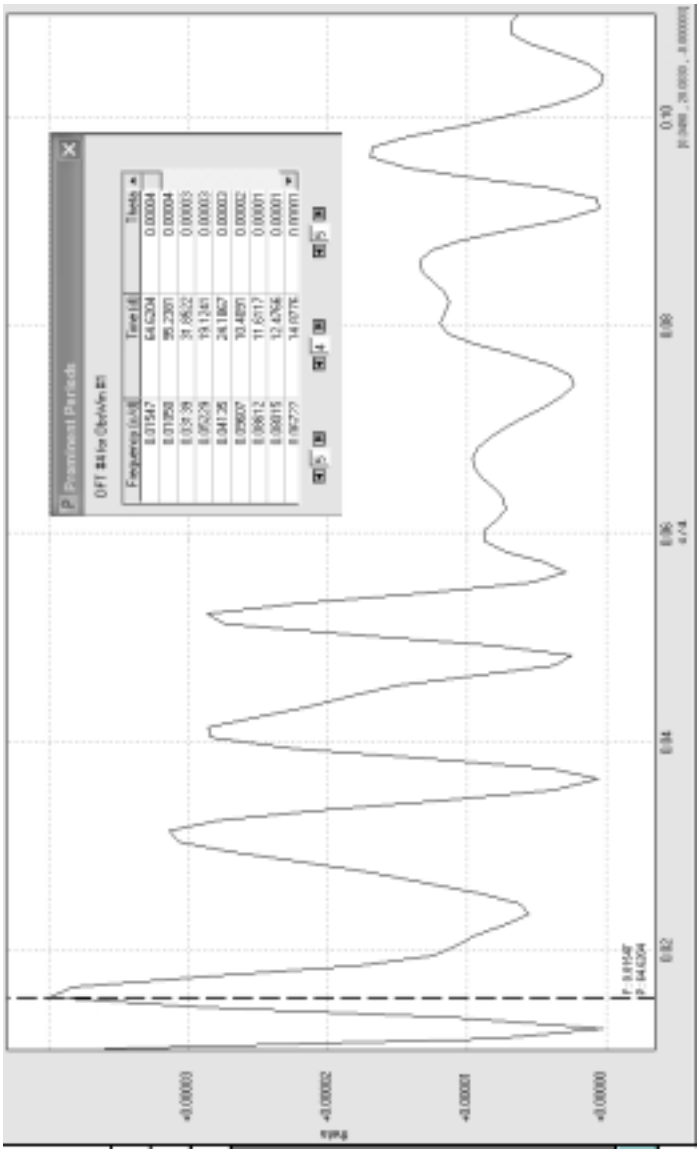

Figure 4.15 HPO V Frequency Domain 2007 - 2008

4.1.5.3 HPO V Band Prominent Period Data

Figure 4.16 shows the prominent period for 1984 - 1985 V is 89.2029 days.

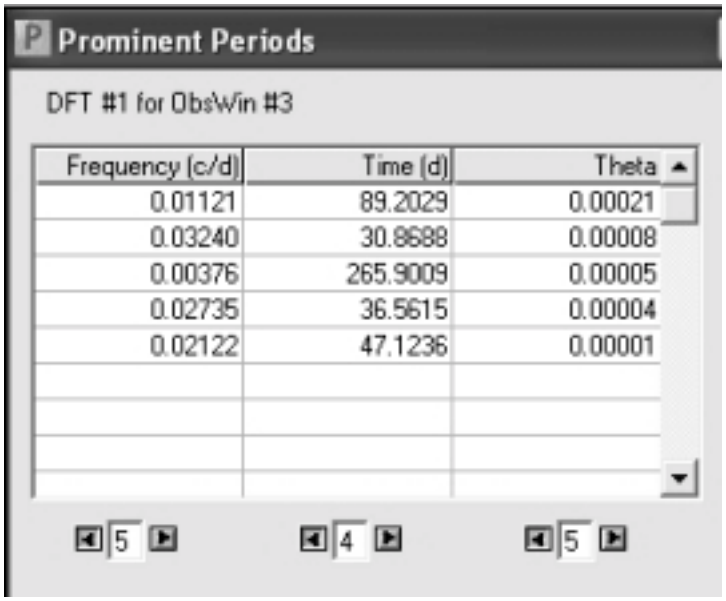

Prominent Periods

DFT #1 for ObsWin #3

Frequency (c/d)	Time (d)	Theta
0.01121	89.2029	0.00021
0.03240	30.8688	0.00008
0.00376	265.9009	0.00005
0.02735	36.5615	0.00004
0.02122	47.1236	0.00001

5 4 5

Figure 4.16 HPO V Prominent Periods 2003 - 2008

Figure 4.17 shows the prominent period for 2003 - 2004 V is 71.1653 days.

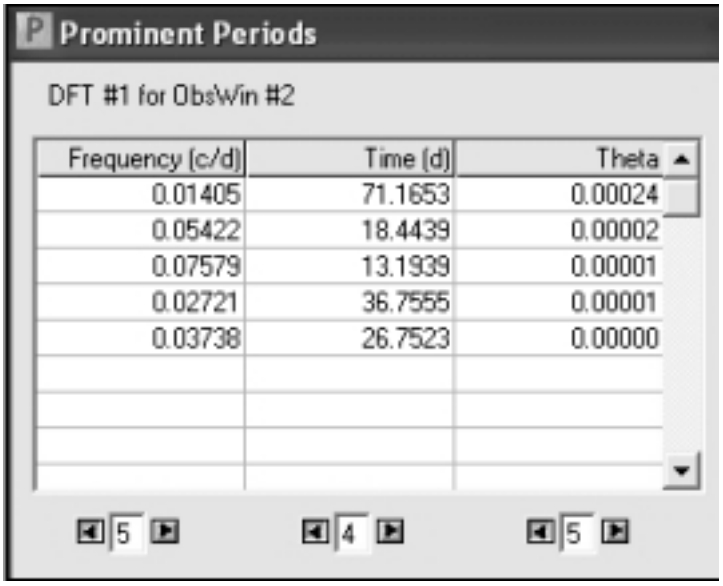

Prominent Periods

DFT #1 for ObsWin #2

Frequency (c/d)	Time (d)	Theta
0.01405	71.1653	0.00024
0.05422	18.4439	0.00002
0.07579	13.1939	0.00001
0.02721	36.7555	0.00001
0.03738	26.7523	0.00000

5 4 5

Figure 4.17 HPO V Prominent Periods 2003 - 2008

Figure 4.18 shows the prominent period for 2003 - 2008 V is 66.1376 days.

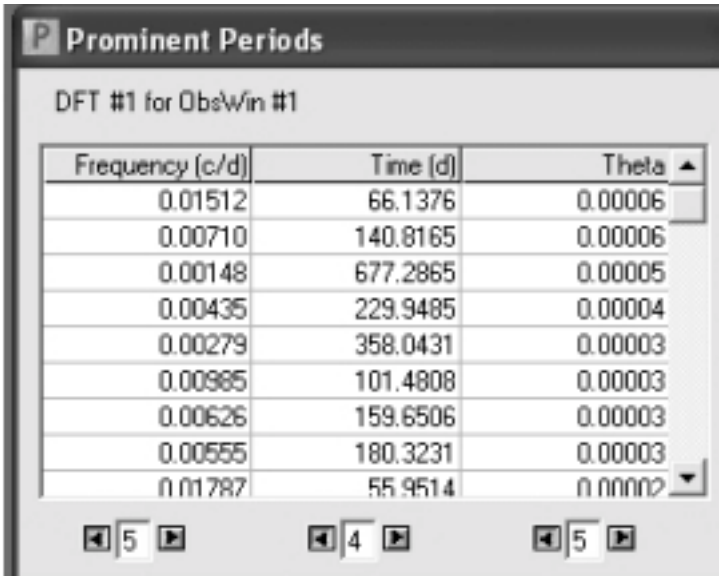

Prominent Periods

DFT #1 for ObsWin #1

Frequency (c/d)	Time (d)	Theta
0.01512	66.1376	0.00006
0.00710	140.8165	0.00006
0.00148	677.2865	0.00005
0.00435	229.9485	0.00004
0.00279	358.0431	0.00003
0.00985	101.4808	0.00003
0.00626	159.6506	0.00003
0.00555	180.3231	0.00003
0.01787	55.9514	0.00002

5 4 5

Figure 4.18 HPO V Prominent Periods 2003 - 2008

Figure 4.19 shows the prominent period for 2007 -2008 V is 64.6204 days.

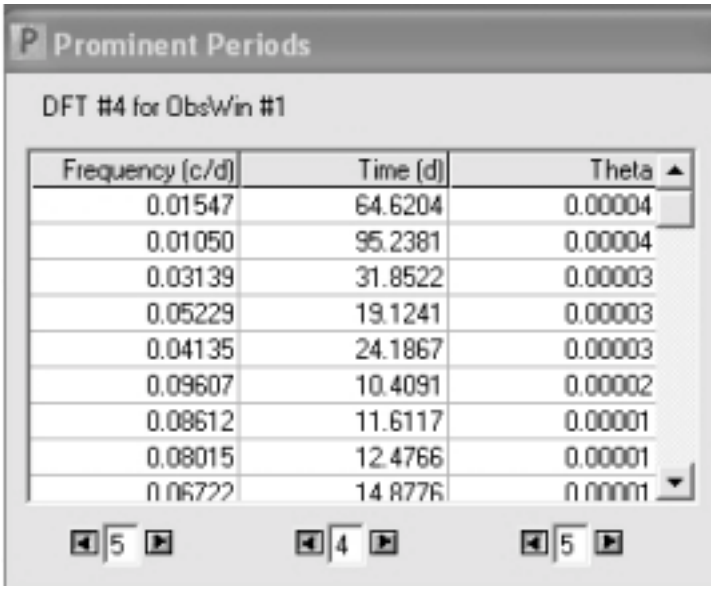

Prominent Periods

DFT #4 for ObsWin #1

Frequency (c/d)	Time (d)	Theta
0.01547	64.6204	0.00004
0.01050	95.2381	0.00004
0.03139	31.8522	0.00003
0.05229	19.1241	0.00003
0.04135	24.1867	0.00003
0.09607	10.4091	0.00002
0.08612	11.6117	0.00001
0.08015	12.4766	0.00001
0.06722	14.8776	0.00001

5 4 5

Figure 4.19 HPO V Prominent Periods 2007 - 2008

As can be seen the period seems to be getting shorter even over just a few years.

1984 - 1985:	**89.2029 days**	**2003 - 2008:**	**66.1376 days**
2003 - 2004:	**71.1653 days**	**2007 - 2008:**	**64.6204 days**

4.2 Spectroscopy Data

Prior to the present decade, the only significant new spectroscopy of epsilon Aurigae was reported by G.-W. Cha et al. (1989 -1992) and Sheffer and Lambert in 1997 using the Hubble Space Telescope, Goddard High Resolution Spectrograph. Sheffer and Lambert reported that their single 16 February 1996 ultraviolet spectrum showed emission features that originate from a heated region near the inner radius of the disk, but could not confirm support for the low mass model for the system. In addition, the Infrared Space Observatory obtained a single Short Wavelength Spectrograph data on 22 August 1997, which shows a largely featureless continuum matching the F supergiant star's output.

4.2.1 Hydrogen Alpha Lines

Several astronomers have used small telescopes to take spectra of epsilon Aurigae out-of-eclipse. One interesting feature found is the hydrogen alpha (Hα) line has some interesting characteristics. Normally stars contain hydrogen and the Hα line is seen as an absorption line in the star's spectrum. A non-Doppler shifted Hα line has a wavelength of 656.281 nanometers (6562.81 Angstroms). The Hα line usually shows an absorption line, but as figure 4.20 shows the Hα line of epsilon Aurigae is complex .

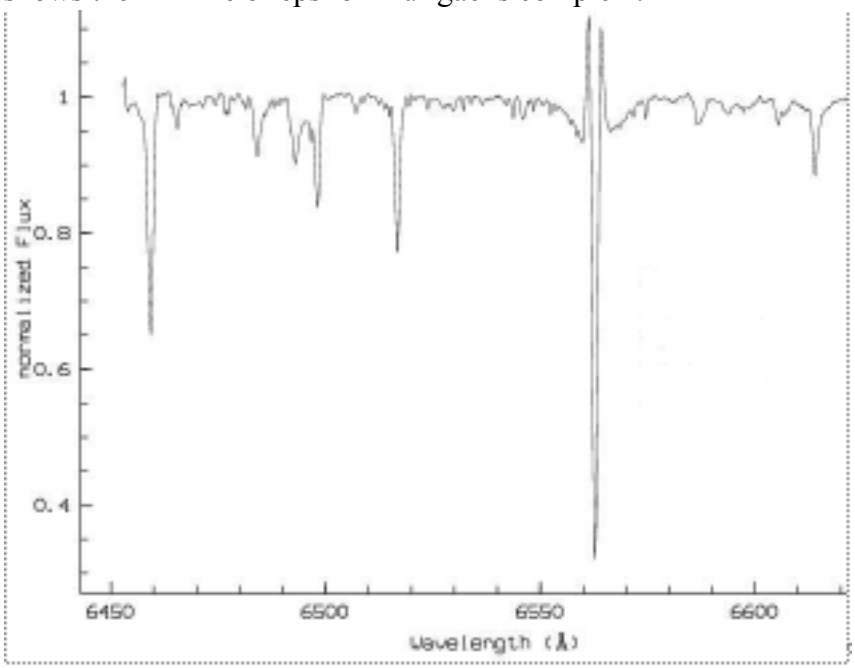

Figure 4.20 Sample Hα Spectrum
Photo Credit: Stan Gorodenski

4.2.2 Be Stars Hα Line

Some stars, e.g., Be stars, have a disk or ring of hydrogen gas around the star that emits in addition to absorbing the Hα radiation. See Figure 4.21.

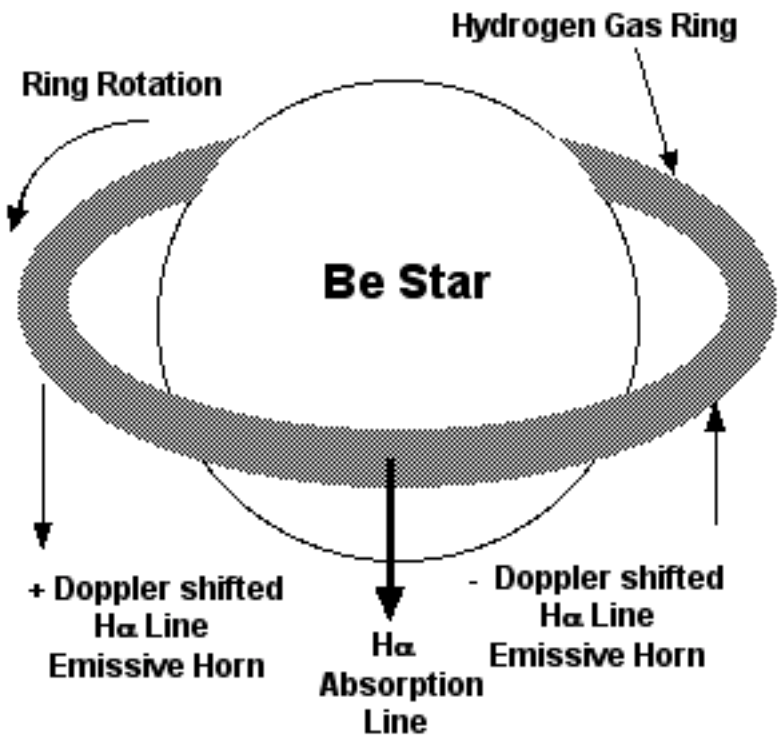

Figure 4.21 Be Star Hydrogen α Lines (not to scale)

The positive Doppler shifted Hα radiation produces the leading higher frequency or shorter wavelength horn/wing while the negative Doppler shifted Hα radiation produces the trailing lower frequency or longer wavelength horn. While there is non-shifted Hα radiation perpendicular to the star there is also a large absorption of Hα radiation from the star thus producing the large absorption line in addition to the leading and trailing horns.

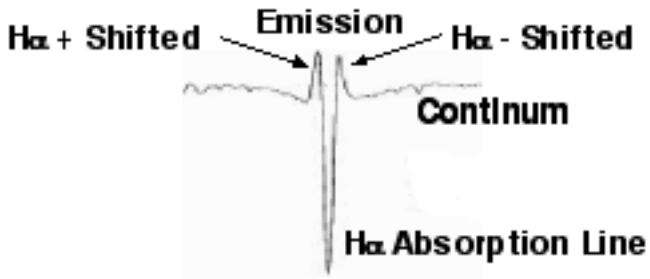

Figure 4.22 Hydrogen α Line Horns

The Hα emission spectra components are Doppler shifted from the leading and trailing side of the disk/ring. This produces horns or wings on the Hα line as seen in Figure 4.22 and 4.23.

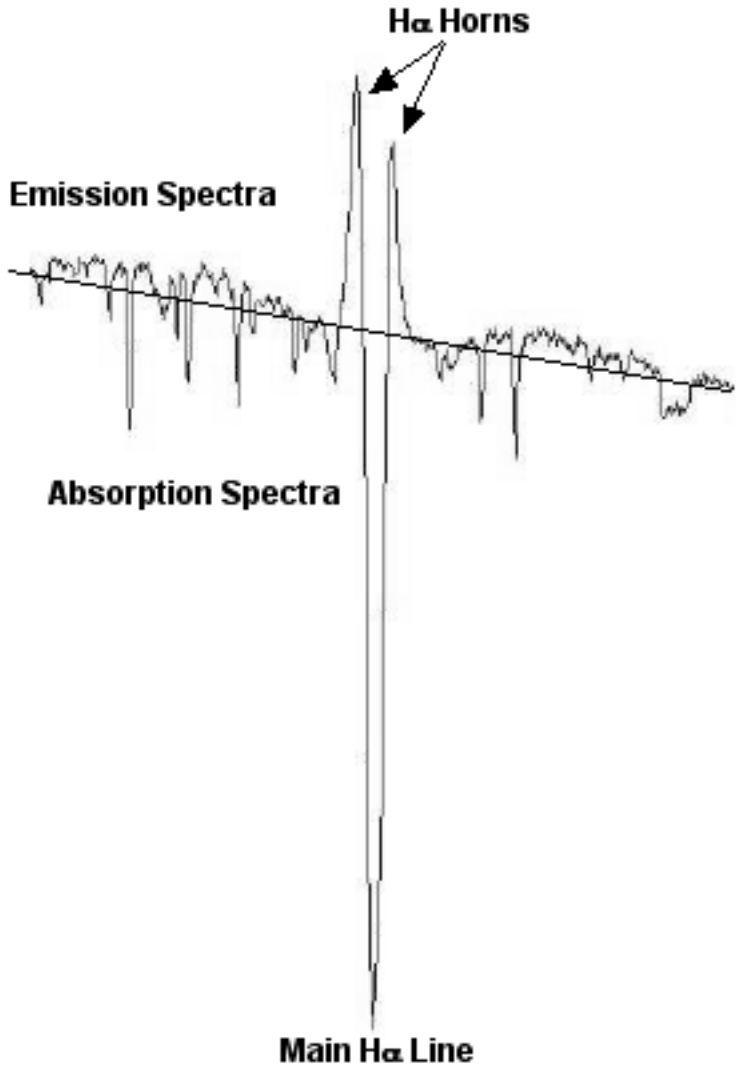

Figure 4.23 Hα Line Parts
Photo Credit: Stan Gorodenski

4.2.3 Epsilon Aurigae Hα Line

What is interesting is while epsilon Aurigae is a F star, not a Be star, it too produces a similar Hα line profile. While the Be star's Hα line horns remain constant and equal amplitude, epsilon Aurigae's Hα horns vary up and down and in addition the main absorption line increases and decreases in amplitude.

Brian E. McCandless of the Institute of Energy Conversion, University of Delaware, provided some spectra of epsilon

Aurigae that illustrates these changes in the Hα profile. See Figures 4.24a and 4.24b.

The 4.24a spectrum taken on 12 December 2005 shows a larger amplitude absorption line as compared with Figure 4.24b spectrum of 24 November 2006. In addition the December 05 spectrum shows a small leading (positive Doppler shifted) horn and a large trailing (negative Doppler shifted) horn.

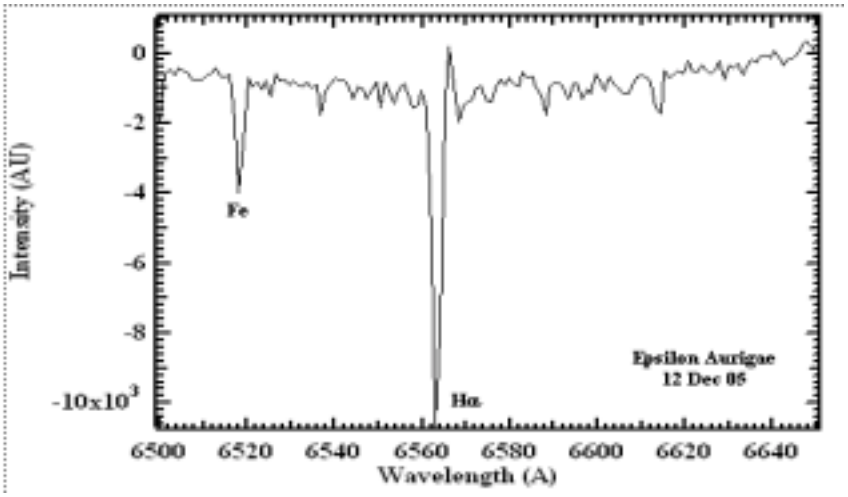

Figure 4.24a Epsilon Aurigae Hα Spectra
(12 December 2005)
Photo Credit: Brian McCandless

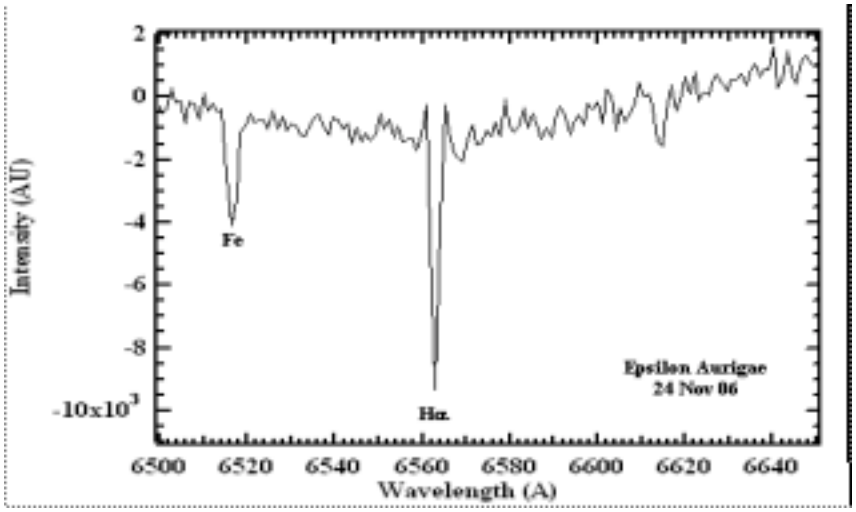

Figure 4.24a Epsilon Aurigae Hα Spectra
(24 November 2006)
Photo Credit: Brian McCandless

One of us, Hopkins, attended a SAS meeting in California in May of 2008. Oliver Thizy of Shelyak gave an interesting and inspiring

talk about spectroscopy of Be stars. The similarity of the Hα profiles between the Be stars and epsilon Aurigae stood out. From some discussions one of us, Hopkins, proposed some ideas for what was causing the profile changes. Figure 4.25 show a possible configuration under the simplifying, but unrealistic assumption that Hα is optically thin..

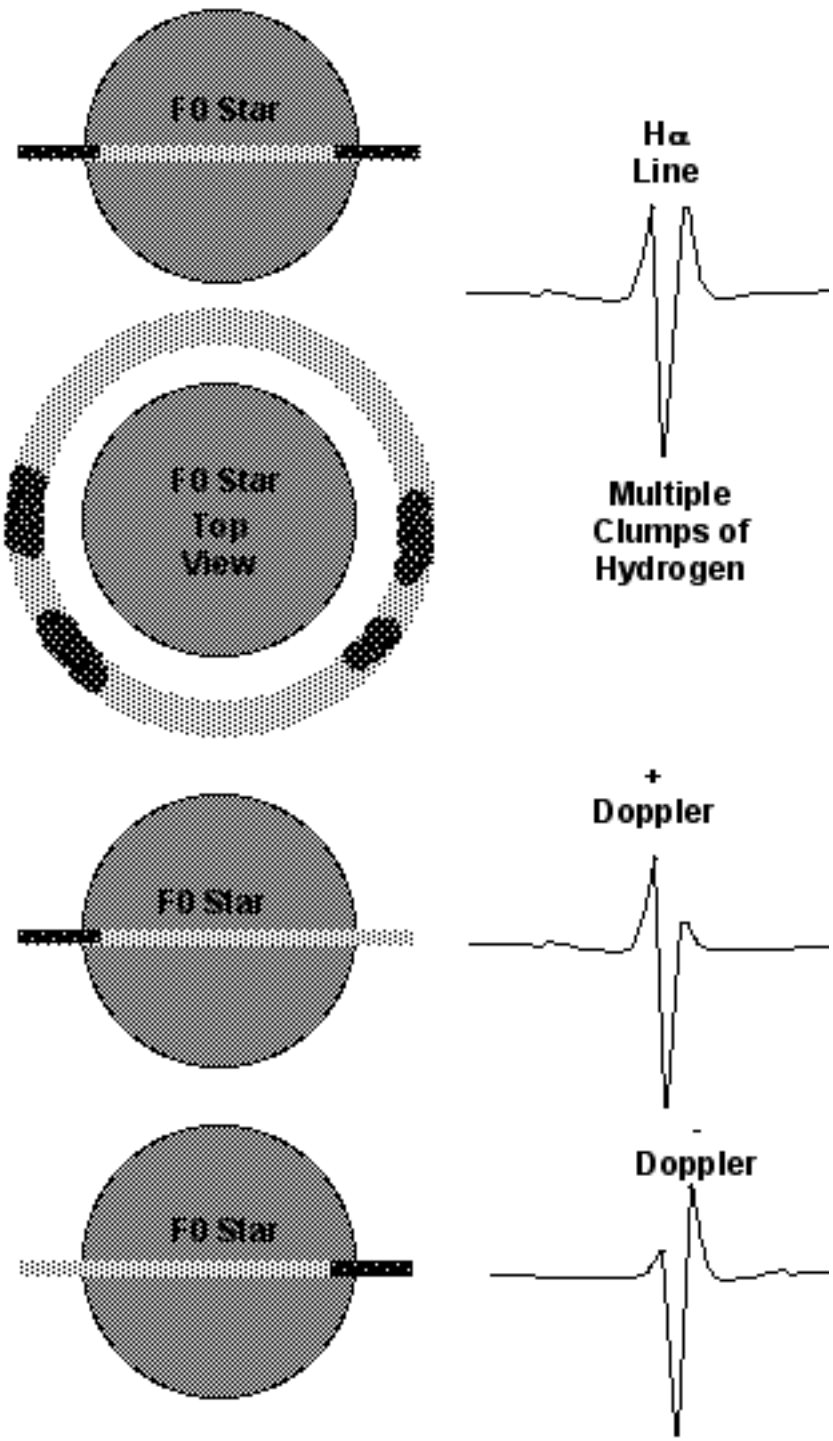

Figure 4.25 Epsilon Aurigae Primary Star Ring

A few weeks later we came across the 1994 paper by Cha that re-enforced the ideas of what causing the Hα profile changes.

In 1994 Cha Guangwel, et al. reported in Astronomy and Astrophysics (284, 874-882, April) the possibility of a circumstellar gas (H II structure) ring circling the primary star with apparent motion of gas within the ring causing the profile changes.

The paper describes out-of-eclipse spectroscopy of the Hα line of epsilon Aurigae. As can be seen from Figure 4.26, it is thought that if the variations of the Hα horns/wings were due to a lumpy disk of hydrogen around the primary F star, one should see periodic effects, unless the lumps form and disappear rapidly. The paper tracks the equivalent widths of the Hα horns and absorption line over several years.

An effort was made at HPO to correlate the variations with the Boyd photometric data of that period. No conclusive results were found. Part of the problem was the data were very scattered and photometric and spectroscopic data did not coincide well.

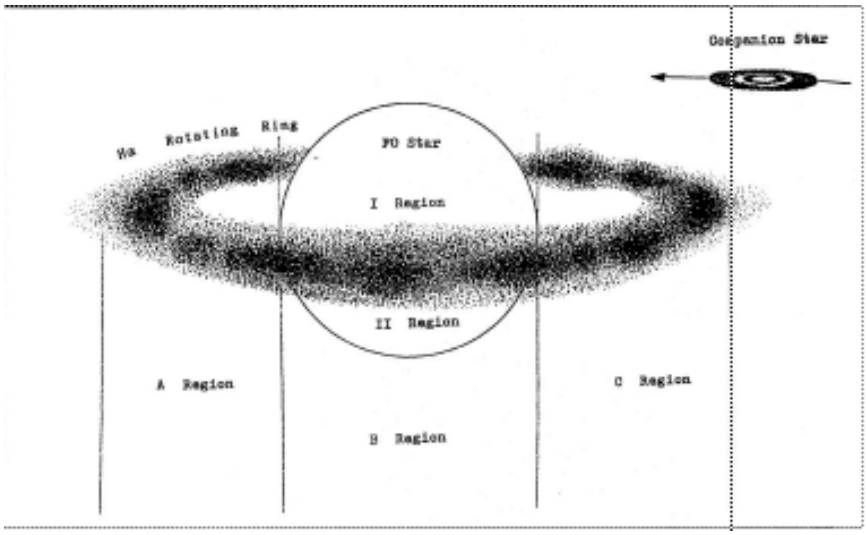

Figure 4.26 Schematic of Epsilon Aurigae Primary Star
Credit: Astron. Astrophys., 284, 874-882 (1994)

4.3 Polarimetry Data

There is no published polarimetry following the 1984 eclipse. A PhD dissertation by Gary Henson completed in 1989 at the University of Oregon, includes details about the eclipse phase observational work published by Kemp et al. in 1986.

4.4 Interferometry Data

4.4.1 Introduction

The bright star, epsilon Aurigae has been known for over a century as an Algol-like eclipsing binary with a very long period. The oddity with the star is that the companion causing the eclipses cannot otherwise be easily detected. During eclipse, the primary star light dims but is largely unchanged in character -- give or take a shell spectrum detected at high spectral resolution optically and/or in the near infrared during the 1983 eclipse (see spectroscopy discussions). Current models for epsilon Aurigae suggest that an opaque disk does the eclipsing. The estimated distance to epsilon Aurigae of 625 parsecs and the maximum binary separation 27.6 AU, imply that the binary should exhibit an angular extent of 44 milli-arcseconds at maximum separation. An F supergiant star has a nominal radius of about 200 solar radii, or nearly 1 AU across, and should exhibit an angular size of nearly 3 milli-arcseconds at the distance of epsilon Aurigae. This is within reach of modern optical interferometers. The secondary – an opaque disk – nominally spans about 10 times the F star dimensions. Additionally, epsilon Aurigae shows an irregular out-of-eclipse light variation of ~0.2 magnitude, which some authors have ascribed to pulsation of the F star, or its equatorial ring.

4.4.2 Navy Prototype Optical Interferometer (NPOI)

NPOI interferometric measurements began in the early 21st century. NPOI is a system of telescopes operating at Lowell Observatory near Flagstaff, Arizona. See Figure 4.27.

Figure 4.27 NPOI Flagstaff, Arizona
(Photo Credit :NPOI)

This interferometer has three separate arms, each of length 250 meters. Up to six 20 inch telescopes may be located at discrete stations along these arms, and their light combined, to provide flexible resolutions. Nordgren et al. (2001) reported a broadband optical diameter for epsilon Aurigae (HR 1605) as 2.18 milli-arcsec (uniform disk) and 2.28 milli-arcsec (limb-darkened) within 4 percent errors. This is slightly smaller than the diameter and distance factors would imply, suggesting the F star is somewhat smaller than the standard 200 solar radii for a supergiant. Instruments like NPOI and others should be capable of examining the predicted changes during the next eclipse of epsilon Aurigae.

4.5 References

NPOI: http://www.nofs.navy.mil/projects/npoi/

Nordgren, T., Sudol, J. and Mozurkewich, D. 2001 AJ 122: 2707 – *Comparison of Stellar Angular Diameters from the NPOI, the Mark III Optical Interferometer, and the Infrared Flux Method* http://adsabs.harvard.edu/abs/2001AJ....122.2707N

V. Current Interpretations

5.1 Epsilon Aurigae System Schematic

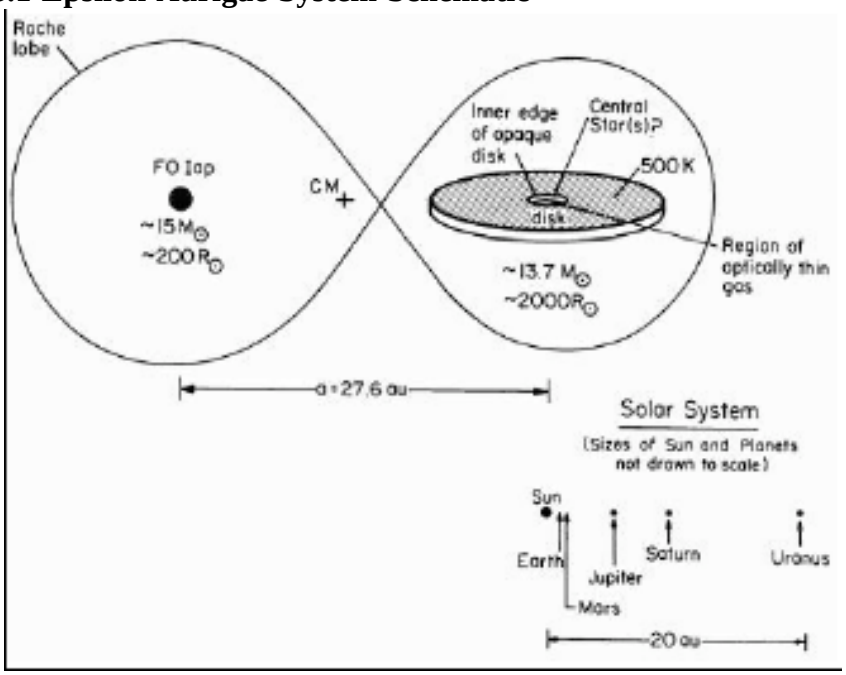

Figure 5.1 Epsilon Aurigae System Schematic
Credit: Caroll et al. 1991 Ap.J367:278

5.2 Next Eclipse Timing

Figure 5.2 shows a graphical representation of the 2009 eclipse timing. First contact is predicted around the end of July 2009, mid-eclipse around July of 2010 and fourth contact in May of 2011.

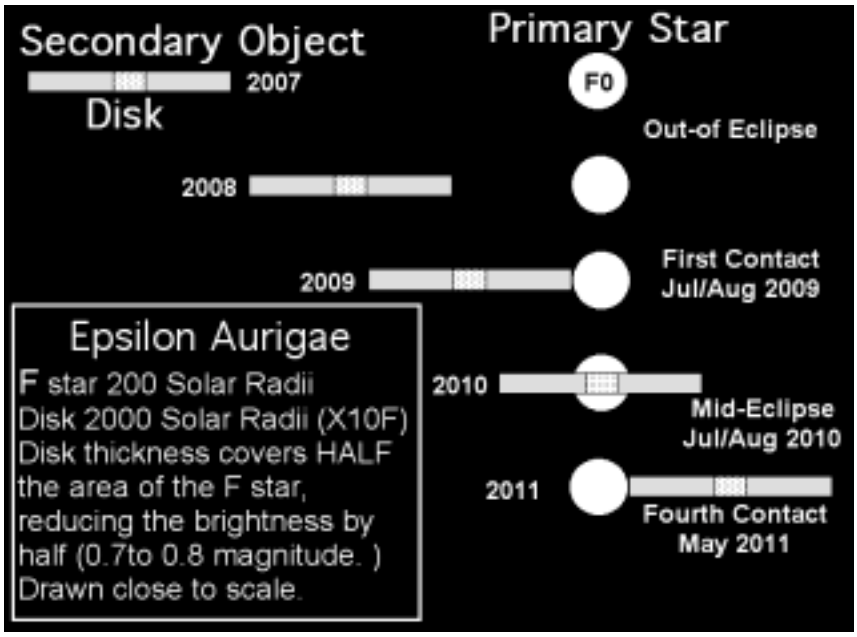

Figure 5.2 2009/2011 Eclipse Timing

5.3 Past Eclipse Timing

One of the interesting results to date from the photometry is preliminary evidence for an evolving quasi-period associated with the low amplitude, out of eclipse, light variations. Data from this decade indicate a predominant 66 day period, with other sub periods present (Hopkins and Stencel 2007). Analysis of data obtained during the decade of the 1990s by Louis Boyd, made available by AAVSO, seems to indicate a 96-97 day period, as mentioned above Post-eclipse observations 1982-1987 by Nha et al., argue for a 96 day periodicity. Even earlier, Shapley reports sparse data over the 1904-11 interval and suggests a 355 day quasi-period, although this cannot be confirmed. Taken at face value, this secular decrease in periods for the low amplitude quasi-variations suggests these will become very fast within a couple of decades, perhaps connected with an accretion death-spiral. Suggestions of changes to periods in epsilon Aurigae were also made by Gyldenkerne who deduced that the 1956 overall eclipse decreased 44 days relative to Gussow's 1933 analysis of 1929 eclipse, while totality was longer by 64 days!

5.3.1 Timing Changes

Saito and Kitamura (1986) commented on shortening eclipse phases and propose that the F star is shrinking at a rate of up to 16% eclipse to eclipse. If continued, this effect should be obvious during the coming seasons.

Table 5.1 shows a summary of best estimates of times of contact during the four eclipses. Data for eclipses prior to the 1982/84 eclipse are assumed to reflect measurements in essentially the V band. We note that duration of totality has apparently INCREASED by ~25% while overall duration and especially egress have been DECREASING. If the trend continues, egress will last only one or two weeks in 2011, whereas ingress will still last 140 or more days! These odd asymmetries suggest dramatic changes on the horizon for epsilon Aurigae in coming decades.

	1874-76	1900-82	1928-30	1955-57	1982-84
Eclipse Duration	**685 d**	**727 d**	**701d**	**670 d**	**V 654 d B 643 d U 630 d**
Totality	**340 d**	**313 d**	**347 d**	**394 d**	**V 447 d B 437 d U 455 d**
Ingress			**182 d**	**135 d**	**V 142 d B 135 d U 120 d**
Egress			**203 d**	**141 d**	**V 65 d B 71 d U 55 d**
Period			**9888 d**	**9885 d**	**V 9863 d B 9875 d U 9885 d**
Amplitude			**0.80 m**	**0.75 m**	**V 0.91 m B 0.73 m U 0.84 m**

Table 5.1 Past Eclipse Timing Summary

Note: Ingress, egress, Period and Amplitude for 1928-30 is an average of the 1900-02 and 1928-30 eclipses.

5.3.1.1 Duration and Totality Change

The difference between the eclipse duration of the 1874-76 and 1900-02 is an increase of 42 days whereas the duration decreases fairly linearly after that with 26 days less between 1900-02 and 928-30, 31 days less between 1928-30 and 1955-57 and 28 days less between 1955-57 and 1982-84. For the 1982-84 eclipse an average value of 642 days was used.

The difference between totality of the 1874-76 and 1900-02 eclipses is a decrease of 27 days where as the totality increases fairly linearly after that with an increase of 34 days between the 1900-02 and 1928-30 eclipses, an increase of 47 days between the 1928-30 and 1955-357 eclipses, an increase of 52 days between

the 1955-57 and 1982-84 eclipses. For the 1982-84 eclipse an average value of 446 days was used.

Figure 5.3 shows the changing times for the past four eclipses for the eclipse duration and totality.

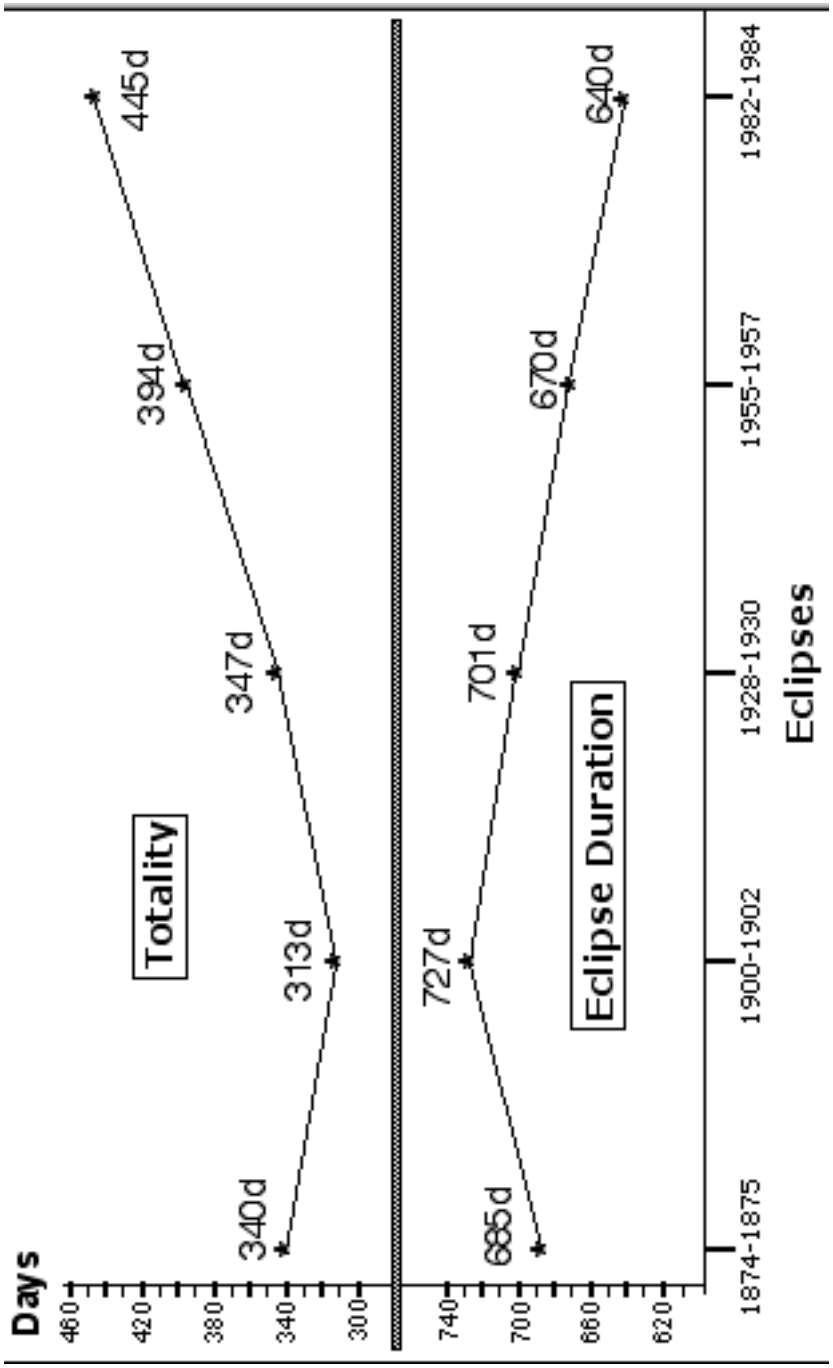

Figure 5.3 Past Eclipse Duration and Totality Time Changes

5.3.1.2 Ingress and Egress Change

Figure 5.4 shows the changing times for the past four eclipses for the eclipse ingress and egress. The difference between the eclipse ingress of the 1902/1930 and 1955-57 eclipse is a decrease of 47 days whereas the difference for the 1955-57 and 1982-84 eclipses is zero days (for B filter data). The difference between the eclipse egress of the 1902/1930 and 1955-57 eclipse, B band, is 62 days whereas the difference for the 1955-57 and 1982-84 eclipses is 76 days (for V filter data).

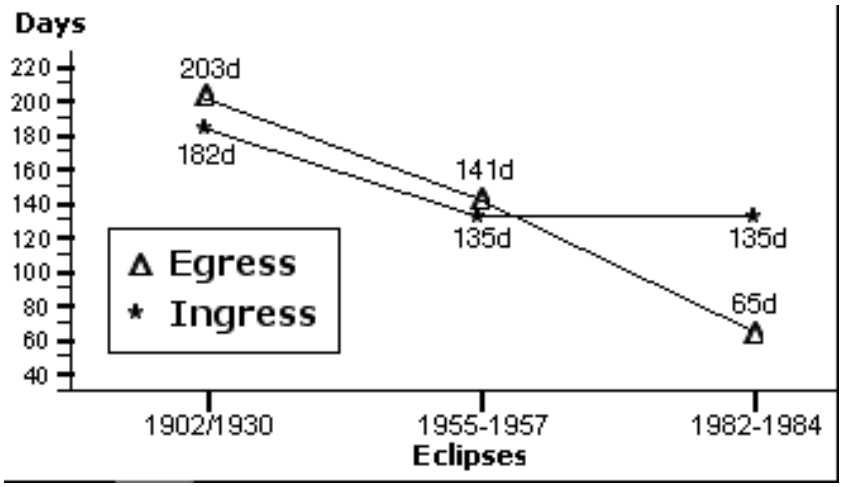

Figure 5.4 Past Eclipse Ingress and Egress Time Changes

5.3.1.3 Eclipse Period Change

The eclipse period seems to be slightly shortening. The 1902/1930 eclipses showed a period of 9888 days while the 1955-57 eclipse appeared to be 3 days shorter at 9885 days. The period to the 1982-84 eclipse appeared to be wavelength dependent with the V band at 9863 days, B band at 9875 days and U band at 9885 days.

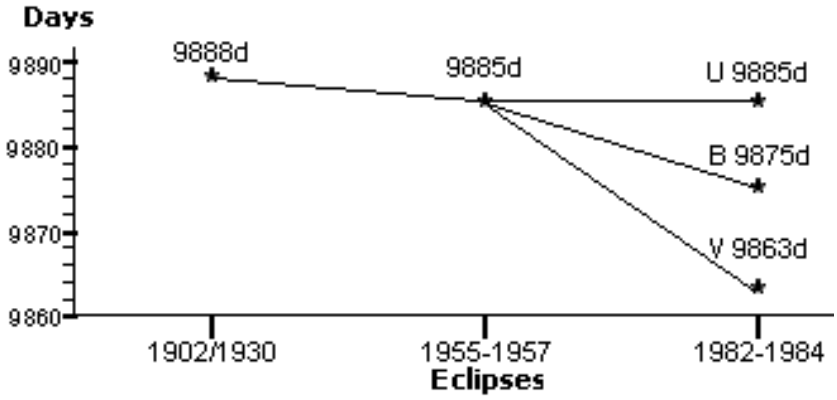

Figure 5.5 Eclipse Periods

5.3.1.4 Eclipse Magnitude Change

The magnitude change during the eclipse appears to have changed slightly. The 1902/1930 magnitude change was 0.80 magnitudes while the 1955-57 eclipse showed a change of 0.75 magnitudes (this is assumed to be close to the V band). The 1983-84 eclipse showed wavelength dependent variation with V = 0.91, B = 0.73 and U = 0.84 magnitudes. See Figure 5.6.

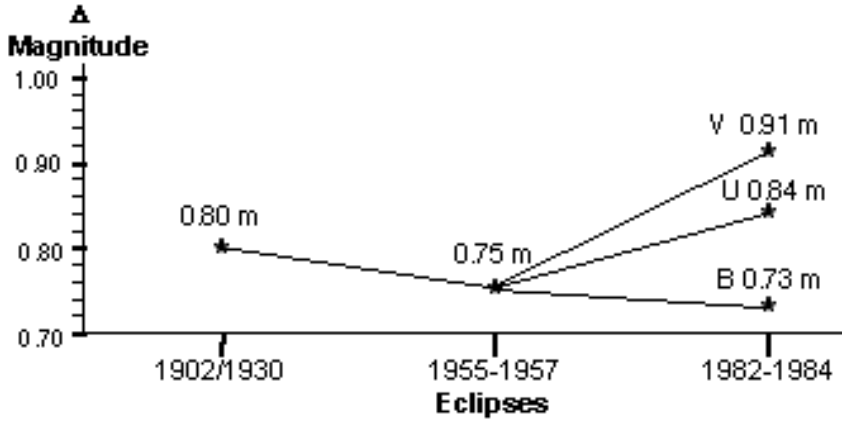

Figure 5.6 Eclipse Δ Magnitudes

5.3.2 Out-of-Eclipse Period Changes

5.3.2.1 Photometric Changes

The star system shows variation of brightens in the photometric bands, The period of these variations appears chaotic, but in general seems to be decreasing from over 300 days to around 63 days currently. Shapley report a possible period of 355 days during a period between 1904 and 1911. Nha et al. mentions a period of 96 days during the period 1984-1987. Boyd data for the 1990's also indicates a 96-97 day period. Boyd and HPO data for the early 2000's indicate a period close to 70 days and for the 2007-2008 season, HPO data indicate a period of 63 days. Obtaining meaningful periods from the photometric data is difficult, but as can be seen there appears to be a trend toward shorter periods.

5.3.2.2 Spectroscopic Changes

While spectroscopic coverage is sparse, what out-of eclipse spectroscopy that has been done on epsilon Aurigae show some interesting changes. The Hα line in particular has been seen to change shape. The wings or horns representing the positive and negative Doppler shifted Hα emissive lines has been seen to alternately go up and down in amplitude. The main Hα absorption line has been seen to change significantly in amplitude. James Kemp appears to have been the first person to suggest a ring of hydrogen gas around the primary star (J. Kemp et al. 1986 Astrophys J. 300, L11). As mentioned in Section V, in 1994 Cha Guangwel, et al. reported the possibility of a rotating ring of gas around the primary star. The rotating ring would account for the Doppler shifted Hα lines, but why the amplitudes of the horns very is still not understood. The ring may be tilted and may wobble. This could account for the varying amplitude of the horns and main absorption line.

5.3.3 Summary and Predictions

The following is from a press release at the June 3, 2008 AAS meeting in St. Louis.

Astronomers are announcing today the prediction that the bright northern star called epsilon Aurigae is headed for a "doomsday event" within a few decades. Observations over the coming three years may hold the secret to the extreme changes detected during the past few decades.

What could be simpler than an eclipsing binary star? As they orbit each other, it is relatively easy to measure brightness change and the duration of change, and, from simple geometric arguments, to obtain size and temperatures for each star in the binary. With the addition of Doppler spectroscopy, which measures orbital velocities, one can solve for mass of each star, using Kepler's third law.

The classic example of this is the so-called Demon Star, Algol, which exhibits 2 hour eclipses every 2.87 days. With such eclipsing binary stars, astronomers can calibrate important parameters that describe a star's structure. The Vogt-Russell theorem says the mass, composition and age uniquely determine the stellar structure, when normal laws of physics are applied. This theorem appears largely true, except for epsilon Aurigae - the real "Demon star". It's behavior has "bedeviled" astronomers for centuries.

The spectrum of epsilon Aurigae looks like a normal F supergiant star, estimated at about 12 to 15 times the mass of the Sun. The orbit data implies that the mass ratio in the binary is close to one, implying that the companion is about 12 to 14 solar masses as well. Epsilon Aurigae exhibits Algol-like eclipses every 27 years, which last for nearly 2 years. The next one starts in August 2009, and should run through May 2011.

The problem? The 12 to 14 solar mass second "star" is largely invisible! The best model (Huang, 1965) says the secondary is a huge dark disk, not a sphere. Such a shape needs a massive central object(s) to stabilize it.

Normal eclipsing binary star analysis suggests that the secondary is about 10 A.U. across (10 times the distance from the Earth to the Sun, or 930 million miles). It does not emit anywhere near the amount of light expected from a star of its size. Scientists are confident that it is not a black hole, because it hasn't been detected with X-ray observations (Einstein, Swift).

Epsilon Aurigae shows low amplitude quasi-periodic light variations, similar to Cepheid variable stars. Cepheid variable stars are close relatives of epsilon Aurigae, being high mass yellow stars prone to pulsation - a useful property in terms of their Period-Luminosity relationship. Currently the light variations in epsilon Aurigae are on a 67 day cycle, but these were nearer to 100 days during the last two decades. Something is accelerating in this

system! At this rate, variations will become very rapid within six decades, perhaps cataclysmically so.

Observations made during the last eclipse suggest that the F supergiant star may be shrinking by about 1/2 percent per year (noted in 1986 by Mamuro Saito and Masatoshi Kitamura at Tokyo Astronomical Observatory
- http://adsabs.harvard.edu/abs/1986Ap%26SS.122..387S).

The duration of total eclipse (during which the F star is partially covered by the disk shaped companion) has increased by about 25 percent between the 1956 and 1983 eclipses. Despite this, the overall length of the total plus partial phases of eclipse - especially the time where the F star moves out from the cover of its partner - has gotten shorter!

If these trends continue, the F star will come out of eclipse (from totality) in only 1 or 2 weeks during 2011. But, it will still take 140 days or so to move from the beginning of the eclipse to totality..

What is changing, and what do the variations mean? Is this binary system preparing for an energetic event? Is the light variation due to changes in the F supergiant star's radius or temperature? Using the well-known correlation among stellar luminosity, radius and temperature, a ten percent change in Luminosity can result from a 5 percent change in Radius, or a 2.5 percent change in Temperature. At an estimated distance of 625 pc, and assuming the F supergiant star is close to the nominal 100 solar diameters appropriate for its type, then the implied angular diameter is 3 milli-arcseconds. Modern interferometers, like the Palomar Testbed Interferometer (PTI, San Diego County, CA), are capable of measuring down to fractions of one milli-arcsecond, close to that 5 percent change anticipated, and these measurements are underway. These measurements would help confirm that the F star could be causing the accelerating light changes.

The best model for the eclipsing object makes a clear, testable prediction that is suitable for interferometry: the F supergiant star

should be Bifurcated (cut in half) by the eclipse-causing disk, if indeed it is a disk. Next generation imaging interferometers like CHARA at Mt.Wilson and MROI at Socorro, should be easily able to monitor this set of changes. If the disk is causing the changes in the system, that should be seen with these measurements.

In summary, the bright northern star, epsilon Aurigae, is exhibiting rapid changes suggestive of dramatic events within one or two eclipse cycles, later this century. "These changes offer a chance to examine the dynamics of rapidly changing stellar disks on a human time scale, and an opportunity for the public to see for themselves that stars change."

5.4 References

Gussow, M. 1933 Astron. Nachrichten 250: 73 - *Über die sekundären Schwankungen im Lichtwechsel von Epsilon Aurigae* - http://adsabs.harvard.edu/abs/1933AN....250...73G .

Gyldenkerne, K. 1970 Vistas in Astron. 7: 199 - *The light and colour variation of Epsilon Aurigae* - http://adsabs.harvard.edu/abs/1970VA.....12..199G .

Hopkins, J. and Stencel, R. 2007 Soc. Astron. Sci. Symposium - *Recent UBVJH Photometry of Epsilon Aurigae* - http://adsabs.harvard.edu/abs/2007arXiv0706.0891H .

Nha, I.S., Lee, Y., Jeong, J. and Kim, H. 1993 Astron. Soc. Pacific Conf. 38, 291 - *The extreme long period eclipsing binary epsilon Aurigae* - http://adsabs.harvard.edu/abs/1993ASPC...38..291N .

Saito, M. and Kitamura, M. 1986 Astrophys. & Space Sci. 122: 387 - *Possible shrinking of the primary component of epsilon Aurigae* http://adsabs.harvard.edu/abs/1986Ap%26SS.122..387S .

Shapley, H. 1928 Harvard Coll. Obs. Bulletin No. 858, p.5 - *On the Variability of the Maximum Light of Epsilon Aurigae* - http://adsabs.harvard.edu/abs/1928BHarO.858....5S .

VI. 2009 Campaign

6.1 Campaign Web Site

To provide rapid information and world-wide availability we created an Eclipse Campaign web site in May of 2006. We also solicited interested parties to join the Campaign. As of May 2008 we have two dozen observers signed up from around the world. In addition we have published five Newsletters for this campaign. These are available on the Campaign web site in .pdf format. As the eclipse draws closer, the frequency of publication of Newsletters will increase. Any one with data or information related to the eclipse is encourage to contact us and the information will be added to the next Newsletter. The campaign web site URL is:

http://www.hposoft.com/Campaign09.html

6.2 Photometry Contact Time Predictions

Table 6.1 shows the contact time predictions based on 1982-84 eclipse contact times (dates are PJD + 2,450,000):

1st	2nd	Mid-Eclipse	3rd	4th
5,055	5,185	5,413	5,640	5,695
Tuesday	Saturday	Wednesday	Saturday	Friday
11 Aug 09	19 Dec 09	04 Aug 10	19 Mar 11	13 May 11

Table 6.1 Official Predicted Contact Times
PJD + 2,450,000

Table 6.2 shows the unofficial contact times for the UBV bands. It appears, first contact will be first at the longer wavelengths. J and H bands infrared as well as CCD R and I bands data may show even earlier contacts.

V band	2,455,043	Thursday, 30 July 2009
B band	2,455,055	Tuesday, 11 August 2009
U band	2,455,065	Friday, 21 August 2009

Table 6.2 Unofficial Predicted First Contact Time
For UBV Bands

6.3 Spectroscopy

The new generation of CCD detectors and optical spectrographs like LHIRES III, enables observers with modest telescopes to conduct eclipse studies that previously required large telescopes using photographic methods. In particular, the following spectroscopic regions deserve study: the blue region (3,600-5,000Å, which includes shell lines reported by Ferluga 1991); sodium D doublet lines (Na D, near 5,892Å); Hα (for reasons mentioned in section 5.2) and neutral potassium (K I, 7,664Å and 7,699Å lines as discussed by Lambert and Sawyer in their 1986 paper). Whereas in previous eclipses, Hα absorption strength tracks the light curve, the shell spectrum and K I lines were strongest after mid-eclipse. It is very important that observers obtain pre- and post-eclipse spectra for comparison and take the ratio, to avoid the effects of short term light variations during eclipse.

6.4 Polarimetry

Polarimetry is challenging, because stars like epsilon Aurigae might show only one or two percent polarization overall.

The last substantive polarimetry data obtained and published concerning epsilon Aurigae were provided by James Kemp and collaborators, in three reports: at the 1985 Workshop, in a short paper in the Astrophysical Journal 1986, and as part of a unpublished 1989 Ph.D. thesis by Gary Henson, student of Kemp. With care and precision, they detected eclipse phase dependent polarization changes. These were seen to be asymmetric -- greatest during the second half of eclipse. Their interpretation calls for the secondary resembling a tilted disk, as illustrated in their paper, and an orbital inclination not exactly 90 degrees (edge-on). They further argue that the next eclipse (2010) might reveal a much greater mid-eclipse brightening as the central hole in the 500K dark disk precesses into greater view. Low levels of post-eclipse polarization on the 100 day quasi-period (with fluctuations as fast a 0.5 to 5 days) further argue for asymmetric structure of the primary star --

perhaps a chromospheric (UV-emitting) 'belt' tilted as much as 45 degrees from the ring plane. This latter point should be readily testable by interferometry, which is being pursued as well. With a combination of observers, technique and wavelengths, we should be able to test this model and fulfill the hope expressed by Kemp in 1986 (paraphrasing) that 'future technology should resolve many of the open issues surrounding this interesting system'.

6.5 Interferometry

6.5.1 Palomar Testbed Interferometer

In preparation for eclipse observations, time was enlisted on the Palomar Testbed Interferometer (PTI), described on their web site and in papers by Michael Colavita and Gerard van Belle in 1999, with the first observations done in October 2007 Figures 6.1, 6.2 and 6.3 show the Palomar Observatory and PTI facility. Figures 6.1, 6.2 and 6.3 from msc.caltech.edu web site.

Figure 6.1 Palomar Observatory

Figure 6.2 Palomar Observatory and PTI Aerial View

Figure 6.3 PTI Aerial View

PTI's near infrared capability in 5 channels (2.0 to 2.4 microns) presented an exceptional opportunity to precisely measure the angular diameter of the primary star. A high resolution near IR spectrum of epsilon Aurigae obtained in 2006 January by Dan Clemens at Lowell Observatory shows a bright continuum plus a moderate strength, narrow absorption Brackett gamma line at 2.16 microns in the K band (Clemens et al. 2007). Figure 6.4 shows the optics bench with optical delay lines.

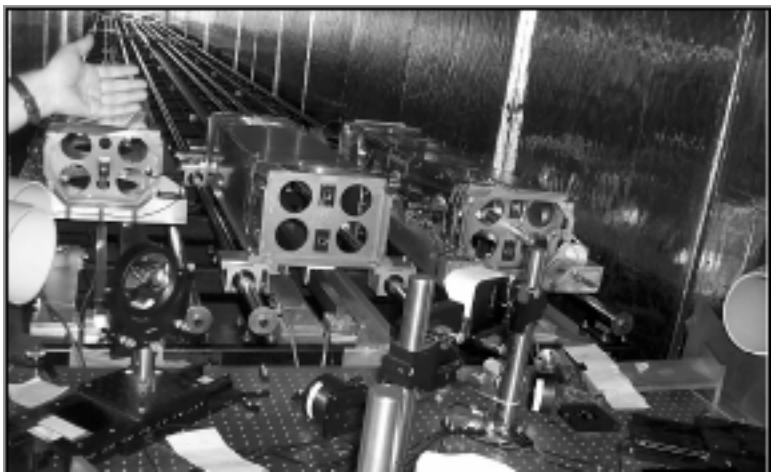

Figure 6.4 Optical Delay Lines

6.5.2 Preliminary Results

An interesting, preliminary result of our ensemble of initial measurements was that the preliminary, error-weighted uniform disk diameter of epsilon Aurigae, at 2.2 microns, was 2.35 +/- 0.15 milli-arcseconds. The PTI result is marginally consistent with, but slightly larger than, the NPOI optical diameter of 2.18 +/- 0.08 mas reported by Nordgren et al. (2001). Given the Hipparcos distance

for epsilon Aurigae of 625 pc, our weighted mean uniform disk diameter suggests a stellar radius of ~150 solar radii. The error on the Hipparcos parallax admits a range of distances from 450 to 850 pc, which formally admits a range of radii from 114 to 213 solar radii. Next generation astrometric satellites like GAIA will hopefully refine the parallax value, but if Saito and Kitamura's estimate that the F star was shrinking 16% over an orbital period, we could detect that effect with a few more years of careful interferometric monitoring.

More intriguing is the prospect for imaging interferometry to actually resolve the secondary disk crossing the F star surface during eclipse, assuming the basic Huang model truly describes the situation. Prior to eclipse, the circularly symmetric diffraction pattern appropriate for the 2.35 milli-arcsecond F star surface should be seen. Using an on-line 2-D Fast Fourier Transform (FFT) tool (Weber 2008) Figure 6.5 shows a predicted FFT image at the left and diffraction pattern at the right for July 2009, just before first contact.

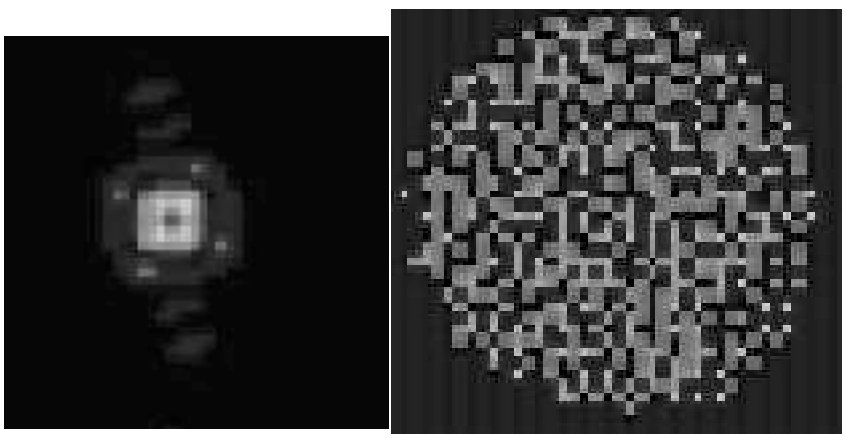

Figure 6.5 FFT Image and Diffraction Pattern
July 2009

As eclipse occurs, the residual bright surface should transform to a pair of smaller stars separated by the occulting disk thickness, causing systematic and measurable changes to the interferometric pattern. Figure 6.6 shows a predicted FFT image at the left and diffraction pattern at the right for October 2009 when the secondary object is about half way through ingress.

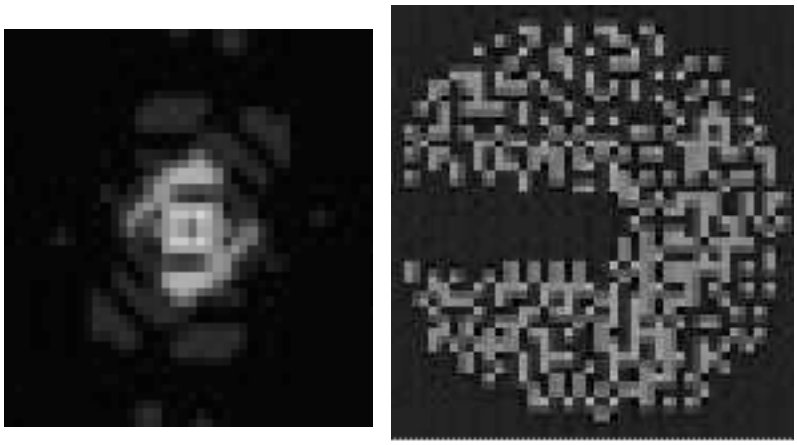

Figure 6.6 FFT Image and Diffraction Pattern October 2009

Figure 6.7 shows a predicted FFT image at the left and diffraction pattern at the right for July 2010 when the star system is in mid-eclipse.

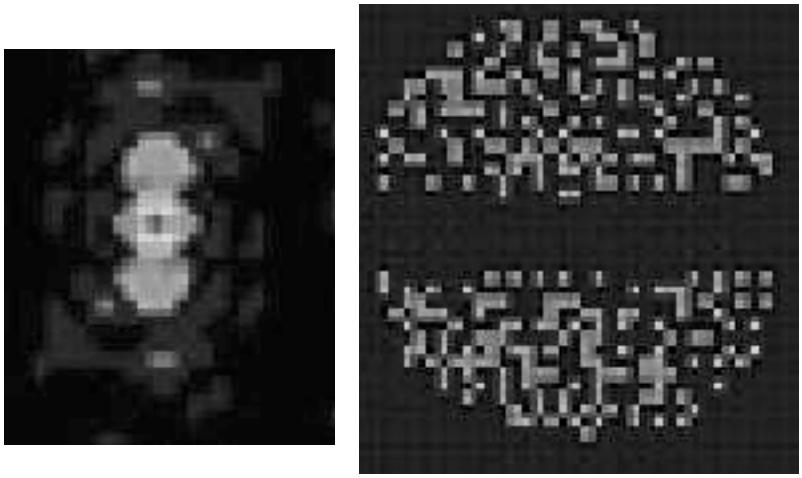

Figure 6.7 FFT Image and Diffraction Pattern July 2010

Reciprocally, the observed interferometric pattern can be transformed into a spatial map – to confirm or refute the occulting disk model, and/or show us something unexpected. The latter is "par for the course" considering this enigmatic star.

Note: Figures 6.4 - 6.7 provide by Dale Mais.

6.6 References

Mais, D., Kloppenborg, B. and Stencel, R. (2008) Proceedings of the Symposium of the Society for Astronomical Sciences.

VII. Similar Star Systems

7.1 Introduction

As chance will have it there are some star systems similar to epsilon Aurigae that are eclipsing during 2009 and offer additional observational opportunities. These stars are zeta Aurigae, VV Cephei, EE Cephei and BM Orionis.

7.2 Zeta Aurigae

7.2.1 Introduction

The zeta Aurigae is a 6th magnitude star system with a period of 2.7 years. Next eclipse is 22 march 2009. It consists of a very hot and luminous blue star plus an even more luminous orange super giant star. Because of the vast difference in sizes, only the primary eclipse where the orange super giant passes in front of the smaller blue star, is observable. Along with the other star systems listed here, the zeta Aurigae system allows observations of the chromospheric, or outermost layers, of the orange super giant star. By careful observations during the ingress and egress phase of the eclipse, information about the super giant's atmosphere can be gained. As might be expected, the UBV observations of the eclipse will produce a small change in the "V" (0.1 to 0.2 magnitudes) but nearly 2 magnitudes of change in the "U" band.

7.2.2 Zeta Aurigae Data

Names: Zeta Aurigae 8 Aurigae HR1612 HD32068 Sadatoni
AAVSO AVID: 000-BCZ-120
R.A. (2000) 05h 02m 28.6s **DEC.** (2000) +41d 4' 33"

Star Component	A	B
Spectral Type	K4	B7
Diameter		
Mass	200 Suns	5 Suns
Luminosity	2,100	400
Absolute Mag	-3.5	-1.6
Temperature	3,500K	12,500K

Table 7.1 Zeta Aurigae Basic Data

I= + 1.77	B= +4..98
R= +2.64	U= +5.34
V= +3.75	

Table 7.2 Zeta Aurigae Magnitudes Out-of-Eclipse

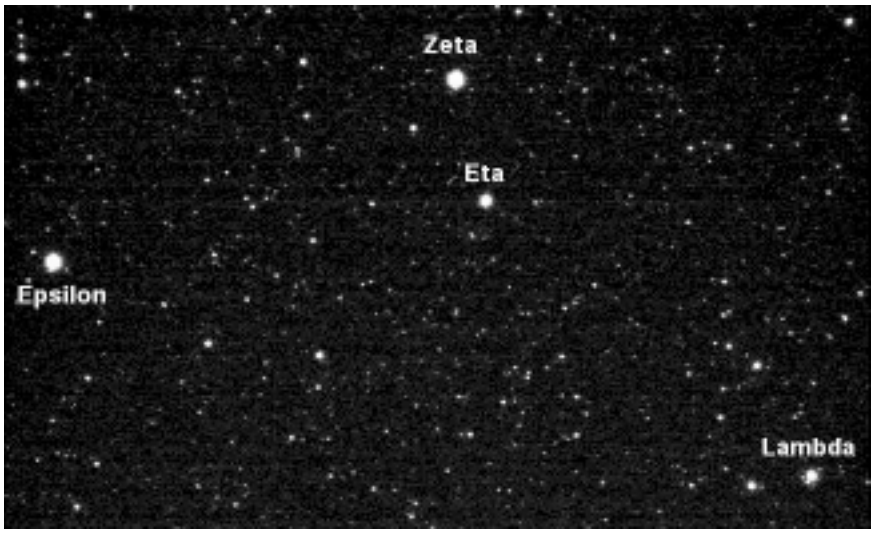

Figure 7.1 Zeta Aurigae Image

Distance: 1300 light years (400 pc)
Epoch: JD 2,438,386.525
Period: 972.164 days 2.7 years
Secondary Eclipse at Phase: 0.27<
Ingress/Egress: 1.5 days
Totality: 37 days
Next Eclipses: HJD= 2,454,913.313 / 22 March 2009
Secondary Eclipses: HJD= 2,455,175.797 / 9 December 2009
Maximum Separation Date - ?

7.2.3 Zeta Aurigae Comparison Star

Lambda Aurigae
HR1729, HD34411, SAO40233
R.A. (2000) 05h 19m 08.4s **DEC.** (2000) +40d 05' 57"

I= + 3.88	B= +5.34
R= +4.19	U= +5.46
V= +4.71	

Table 7.3 Lambda Aurigae Magnitudes

7.2.4 HPO Zeta Aurigae Data

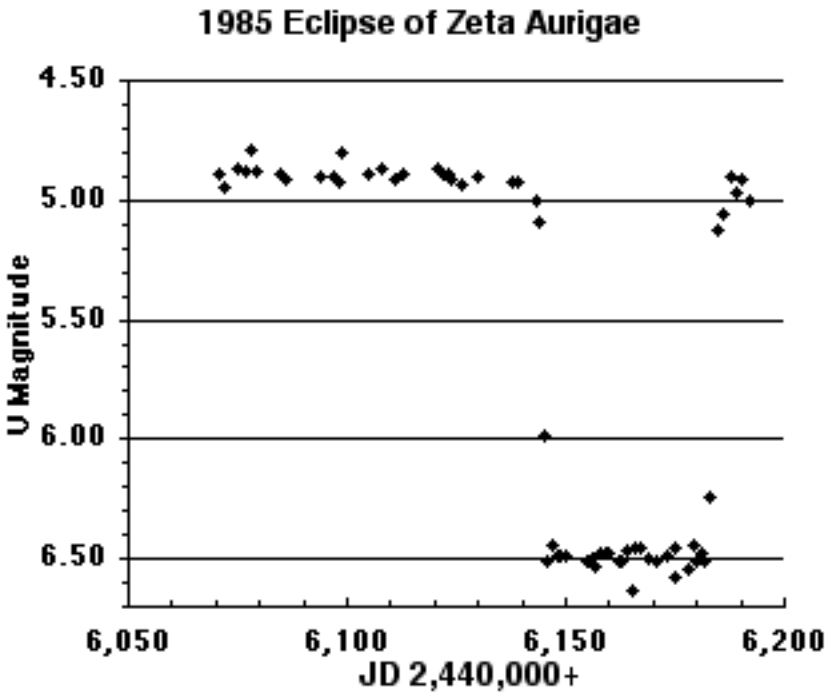

Figure 7.2 U Band Plot of 1985 Zeta Aurigae Eclipse

7.2.5 References

Darling, D., 1983, Astronomy; The Curious Case of Zeta Aurigae, 66-70, March 1983

7.3 VV Cephei

7.3.1 Introduction

VV Cephei is the second longest known (P= 20.3 years) eclipsing binary system. The last eclipse was in 1997-98. The observation of long period eclipsing binaries requires a special kind of dedication. Few of these systems are followed in detail between eclipses. These stars are bright, and so obtaining telescope time for extended periods at professional observatories is nearly impossible. Therefore, amateur photometrists with modest backyard observatories and time to devote can make an important contribution by monitoring these stars.

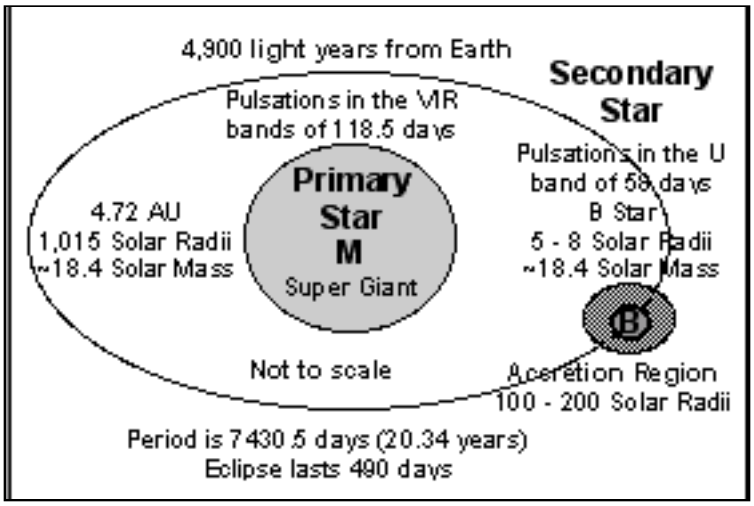

Figure 7.3 VV Cephei System Diagram

7.3.2 VV Cephei Data

Name: VV Cephei, HR8383, HD208816
AAVSO AVID: 000-BCP-658
RA: (2000): 21h 56m 39.1s **Dec (2000):** +63d 37' 33"
M1 = 18.2 M solar (M supergiant mass)
M2= 18.6 M solar (B star mass)
d= 1.5 kpc = 4900 l.y.
R1= 1015 R solar = 4.7 AU
a= 24.8 AU (orbit semi-major axis)
I= 1.86; **R**= 3.21; **V**= 4.91; **B**= 6.68; **U**= 7.07
V-I= +3.04; **R-I**= +1.40; **B-V**= +1.77; **U-B**= +0.39

Epoch: JD**:** 2,435,931.4
Period: 7430.5 days/ 20.34 years
Secondary Eclipse at Phase: ?
Ingress/Egress: 100/200? days
Totality: 490 days
Next Eclipse: (2017)
Secondary Eclipse - Fall/Winter 2005
Maximum Separation Date - ?

7.3.3 Recommended Comparison Star:

20 Cep, HR8426
R.A. (2000): 22h 05m 00.4s **DEC. (2000)**: +62d 47m 09s
I = ?; **R** = ?; **V** = 5.27; **B** = 6.68; **U** = 8.46

Check Star: 19 Cep HR8428
R.A. (2000): 22h 05m 08.8s
DEC. (2000): +62d 16m 48s
R - I = 0.03; **V** = 5.11; **B** = 5.17; **U** =4.33

7.3.4 References

Single Channel UBV Photometry of Long Period Eclipsing Binary VV Cephei, Jeffrey L. Hopkins ,Hopkins Phoenix Observatory, Phoenix, Arizona USA and Philip D. Bennett, Saint Mary's University, Halifax, Canada and Eureka Scientific, Inc. Oakland, California USA, presented at the May 2006 Society for Astronomical Sciences Symposium, Big Bear Lake, California.

Rapid Mass-Loss Transients in VV Cephei, Robert E, Stencel Daniel E. Potter, Wendy H. Bauer, PASP 105:45-50, 1993 January

The 1997/1998 eclipse of VV Cephei was late, L. Leedjarv, D. Graczyk, M. Mikolajewski, and A. Puss, Astronomy & Astrophysics 349,511-514 (1999)

The Distances of VV Cephei and Epsilon Aurigae, Peter van de Kamp, Sproul Observatory, November 1978, Sky and Telescope, 397.

Six Years of HST/STIS Observations of Eclipsing Binary VV Cephei, P.D. Bennett (University of Colorado), W.H. Bauer (Wellesley College), AAS 204th Meeting June 2004, Poser Paper.

118 Day Optical Variations in VV Cep, G. P. McCook, E. F. Guinan,
IBVS Number 1385, 8 February 1978.

Semiregular 58 Day Variations in VV Cep, L. Baldinelli, S. Ghedini, S. Marmi,
IBVS Number 1675, 24 September 1979.

7.4 EE Cephei

7.4.1 Introduction

EE Cephei is an eclipsing binary with a period of 5.6 years and an eclipse lasting 17 days whose nature still remains unclear. The next eclipse is due 9 January 2009. The various features observed during the different eclipses and the lack of any evidence for a star-like secondary are in favor with the hypothesis that the secondary contains a dark, opaque disc covering a central low-luminosity star or binary system.

The most promising model remains that of a dark, precessing disk around a low luminosity central object (Mikolajewski & Graczyk 1999, Graczyk et al. 2003). The precession changes both the inclination of the disk to the line of sight, and the tilt of its cross-section to the transit direction. The unique shape of the eclipse observed in 1969 can be explained by a practically edge-on and non-tilted projection of the disc. Two hypotheses can be considered for such a disc:
(i) it has a proto-planetary origin;
(ii) it is a post-planetary object (a result of planetary disintegration). An important question is the nature of the central body embedded in the disk. It can be a low massive single star or a close binary system. The only similar object previously known with a dark circumstellar disc is epsilon Aur - the longest period (~27 years) eclipsing binary.

7.4.2 EE Cephei Data

Name: EE Cephei
AAVSO AVID: 000-BCQ-039
RA 22h 09m 22.771s **Dec** +55d 45m 324.7s
Vmax 10.72 **Vmin** 12.15
Epoch 2,434,346.0
Period 2,049.53 days/5.6 years
Duration 17 days
Spect B5III-IV+e
Next Eclipse
2,454,841.30, Friday, 9 January 2009

Figure 7.4 HPO EE Cephei V Filter Image

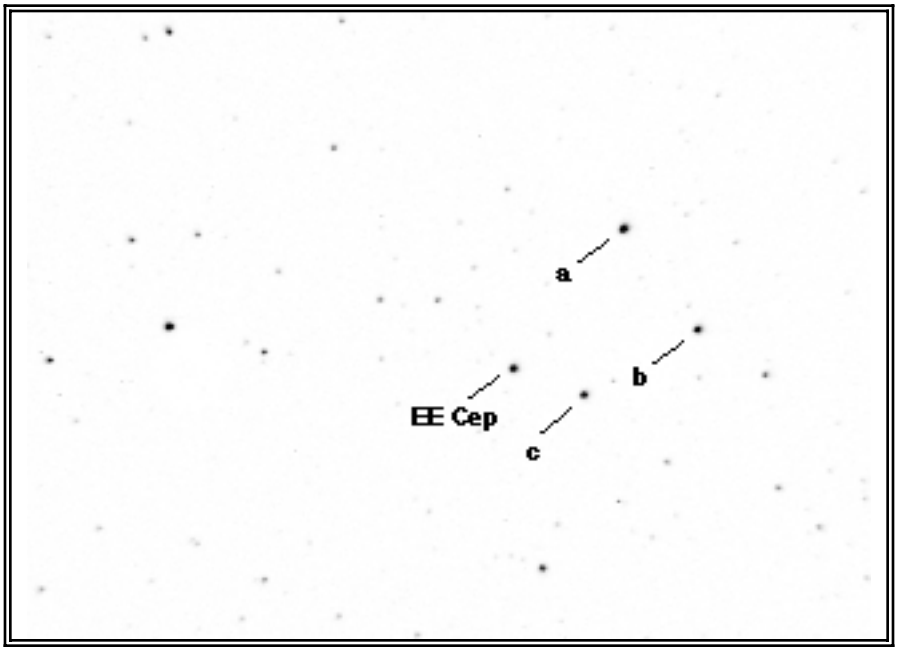

Figure 7.5 EE Cephei Detail

7.4.3 EE Cephei Comparison Stars

Star: a = BD+55°2690

R.A. 22h 09' 07" **Dec.** 55d 47' 25"

U	B	V	R	I
10.86	10.68	10.38	10.09	9.87

Table 7.4 EE Cephei Magnitudes Out-of-Eclipse

Star: b = GSC39732150

R.A. 22h 09' 02" **Dec.** 55d 45' 25"

Magnitudes Out-of Eclipse

U	B	V	R	I
11.31	11.47	11.23	10.99	10.81

Table 7.5 Star b Magnitudes

Star: c = BD+55°2691

R.A. 22h 09' 16" **Dec.** 55d 44' 07"

U	B	V	R	I
11.59	11.47	11.22	10.96	10.75

Table 7.6 Star c Magnitudes

7.4.4 HPO EE Cephei Data

The following is a sample set of data from a single 15 second exposure with the B filer and processed with AutoStar.

```
File Name:                  EE CEP-B-30-1.fts
FITS Header Date:           007-09-26
FITS Header Time:           04:54:05
Exposure Time:              30 seconds
Filter:                     B
Star aperture radius:       6
Sky annulus inner radius:   9
Sky annulus outer radius:   15
Star aperture pixels:       116
Sky annulus pixels:         272
Zero point:                 25.0
Integration time:           15.0
Gain [e/ADU]:               1.0
Readout noise [e rms]:      10.0
Dark current [e/sec/pix]:   1.0
Mid-exposure Date:          007-09-26
Mid-exposure Time:          04:54:20.000

Photometric Data for Individual Stars:
Comp    ADU_Max      Sky_ADU    Star_ADU
 Var    38017.4      8154.6     304661
  C1    43100.0      8159.87    451048.3
  C2    28750.8      8270.55    240568.1
  C3    31058.4      8171.37    220595.5
```

7.4.5 References

Timing of the 1997 Eclipse of the Long Period (5.61 Years) Eclipsing Binary EE Cephei, Edward A. Halbach, 720 Ramshorn Drive, Estes Park, CO 80517-7035, Presented at the 87th Spring Meeting of the AAVSO, June 10, 1998.

The 2003 Eclipse of EE Cephei, Gerard Samolyk, 9504 W. Barnard Ave, Greenfield, WI 53228 and Shawn Dvorak, 1643 Nightfall Drive, Clermont, FL 34711, JAAVSO Volume 33, 2004.

The 2003 eclipse of EE Cep is coming, A review of past eclipses, D. Graczyk, M. Mikolajewski, T. Tomov1, D. Kolev, and I .liev, Astronomy & Astrophysics, A&A 403, 1089–1094(2003)

1980 Eclipse of EE Cephei: Light Curves and Time of Minimum, IBVS 1939, 23 March 1981, L. Baldinelli, A, Ferri, S. Ghedini, "G. Horn D'Arturo" Observatory, C.P. 1630 AD, 40100 Bologna, Italy

7.5 BM Orionis

7.5.1 Introduction

Within the Great Orion Nebula lies four stars that make up what is known as the Trapezium. These stars are labeled A, B, C and D. The distance between the stars are between 9 and 20 arc seconds. See Figure 7.6. Stars A and B are eclipsing binary star systems. BM Orionis is also known as Theta 1 Orionis B. BM Orionis has a period of 6.470525 days and varies between V = 7.96 and V= 8.65.

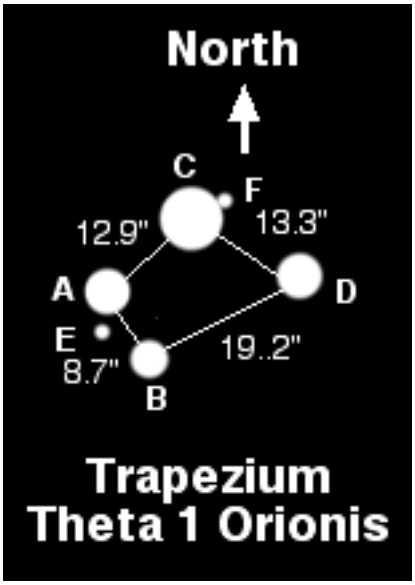

Figure 7.6 Theta 1 Orionis Detail

Figure 7.7 shows a CCD image take with the HPO 12" LX200 GPS and V filter.

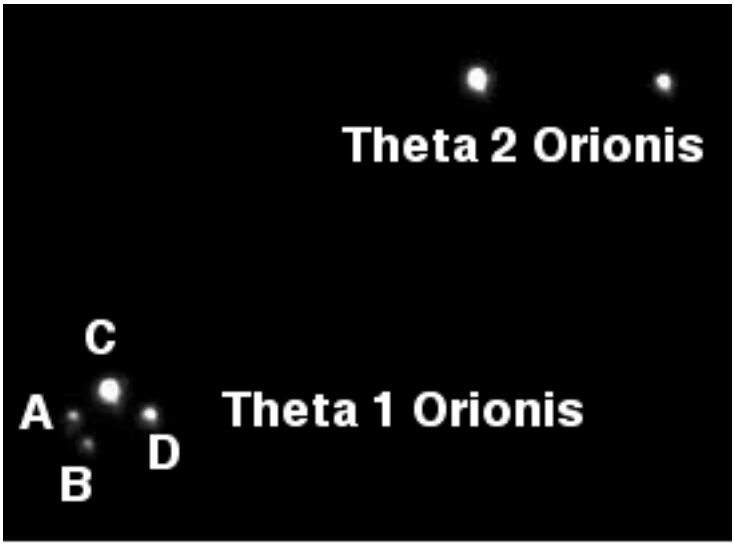

Figure 7.7 Theta 1 Orionis HPO V Image

7.5.2 Theta 1 Orionis Data

Name: Theta 1 Orionis A (V1016 Ori)
HD37020 HR 1893
Period: 65.43233 days (6.72 - 7.65 ~ 20 hours)
2nd @ Phase 0.54

U	B	V	R	I
5.87	6.72	6.72	6.41	6.20

Table 7.7 BM Ori Magnitudes Out-of-Eclipse

Name: Theta 1 Orionis B (BM Ori)
HD37021 HR 1894
AAVSO AVID: 000-BDY-996
Period: 6.470525 days (7.96 - 8.65)

U	B	V	R	I
?	8.20	7.96	?	?

Table 7.8 Theta 1 Ori B Ori Magnitudes

Name: Theta 1 Orionis C
HD37022 HR 1895

U	B	V	R	I
4.188	5.140	5.134	4.914	4.734

Table 7.9 Theta 1 Ori C Ori Magnitudes

7.5.3 BM Orionis Comparison Star

Name: Theta 1 Orionis D
HD37023 HR 1893

U	B	V	R	I
5.96	6.78	6.70	6.41	6.22

Table 7.10 Theta 1 Ori D Ori Magnitudes

Figure 7.8 show a plot by D. Hall of a 1969 eclipse of BM Orionis.

7.5.4 References

Publications of the Astronomical Society of the Pacific, 22 July 1969, ***BM Orionis, The Eclipsing Binary in the Trapezium***, Douglas S. Hall, Dyer Observatory, Vanderbilt University and Loring M. Garrison Jr., Kitt Peak National Observatory.

Astrophysics and Space Science, 19 (1972) 165-171, ***The Case for Black Hole in BM Orionis,*** Robert E. Wilson, Department of Astronomy, University of South Florida, Fl, U.S.A..

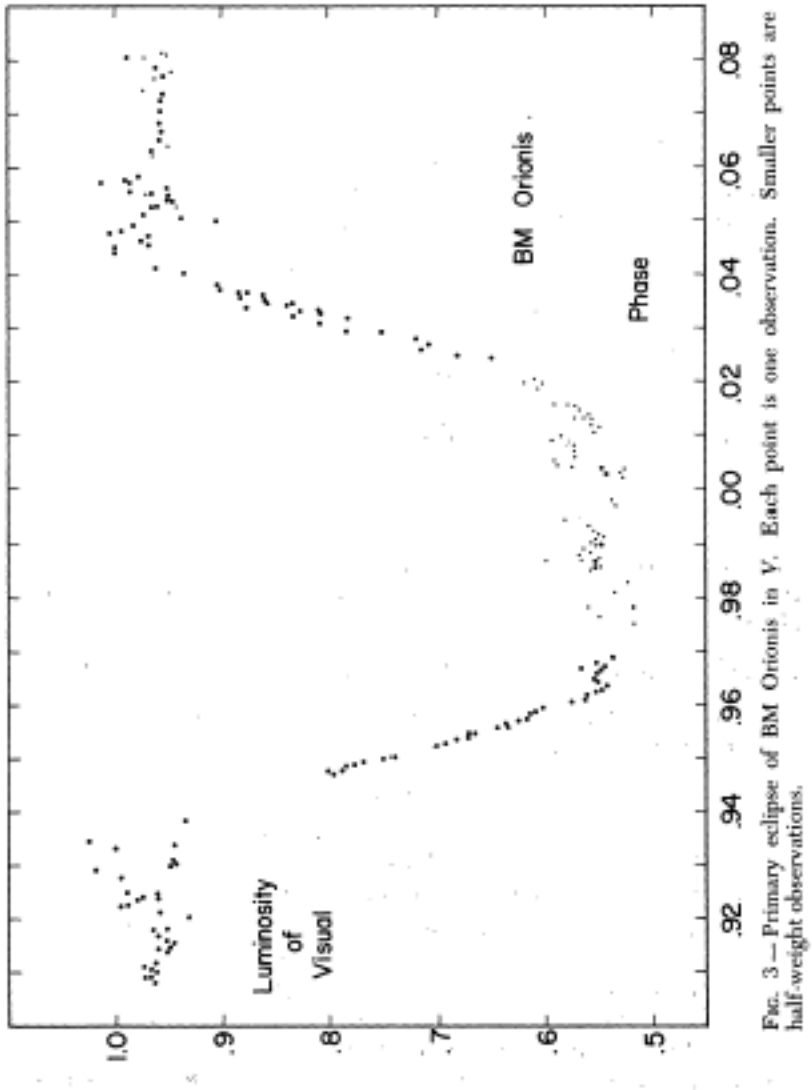

FIG. 3 — Primary eclipse of BM Orionis in V. Each point is one observation. Smaller points are half-weight observations.

Figure 7.8 Eclipse of BM Orionis

VIII. Prospects

8.1 Interferometry Diameter Measurement

Interferometric studies are just getting serious with respect to epsilon Aurigae. A campaign with the Palomar Testbed Interferometer revealed an average diameter of 2.3 milli-arcseconds, with an indication of variation on time scales of days and weeks – but the latter needs verification. After the 1984 eclipse ended, Saito and Kitamura (1986) provided evidence that the F supergiant star was shrinking at a rate of 16 percent eclipse to eclipse (27.1 years), based on duration of eclipse phases.

At face value, this would result in a decrease of angular diameter of about 5 percent over the PTI interval reported. Within the dispersion of PTI measurements, there was no confirmation of any decrease, nor evidence for significant changes in diameter over the past 10 years, based on archival data. However, the 2.3 milli-arcsecond angular size reported, when combined with the 625 pc Hipparcos distance, implies a primary star diameter of 77 solar diameters. This is smaller than the classically derived diameter for an F0 Ia star, 100 solar diameters.

Further progress in the study of epsilon Aurigae should be possible by applying interferometric imaging to the eclipse event during 2009-2011. If the Huang model is basically correct, the passage of a dark disk, bisecting the F star surface, should produce a straightforward change in the fringe patterns - from circular symmetry of a single disk, to an asymmetry from a close pseudo-binary star pair of bright limbs during totality, modulo pulsation phenomena. Observers with suitable resources have been asked to make this star a priority for frequent observation.

8.2 Changing Eclipse Timings

As previously discussed in detail, observations during last eclipse were used to argue that the F star is SHRINKING by about 1/2% annually! The details are that the duration of totality has

apparently INCREASED by ~25% while overall duration of eclipse - and especially egress - has been DECREASING. If the trend continues, eclipse egress will last only one or two weeks in 2011, whereas eclipse ingress will still last 140 or more days! These odd asymmetries also suggest dramatic changes on the horizon for epsilon Aurigae in coming decades.

8.3 Out -of -Eclipse Variations

As mentioned above, the strongest evidence for a shortening period of the low amplitude variations seen out of eclipse in the light of epsilon Aurigae come from the pair of studies by Nha et al. 1993 and Hopkins et al. 2007. Nha reported frequency analysis for 1982-89 and find a 95.5 day periodicity prominent in their data, which they associated with pulsations of the primary. Hopkins determined the same variations were characterized by a predominant 66 day period with data obtained after 2003. If this period decrease can be confirmed to accelerate, it could imply some kind of accretion event in the coming decades, perhaps associated with changes in the overall eclipse timing. As noted after the 1984 eclipse, when the "new thing" was to add "jets" to every binary system, today the "new thing" is the demise of "hot Jupiters" - large planets detected very close to their host star, spiraling into the central object. Among the questions concerning the disk in the epsilon Aurigae system is whether proto-planetary bodies are forming therein. Light variation changes might be the first hint of this actually happening. This does not exclude that the F supergiant is the cause of said variations, but the rapid changes also suggest interesting changes for the F star if that is indeed the case.

8.4 Hα Emission Wing Variability

The coordinated work of Lothar Schanne and Jeff Hopkins provides the first tangible correlations between the profile of the Hα line and the broad band light variations. For example, In April and May 2005 (JD 2,453,462 to 2,453,502), the absorption component almost disappeared and a fairly symmetrical pair of emission wings formed next to the line center (as reported in IBVS

5747). Since JD 2,454,400, the Doppler shifts of the absorption cores of Hα lines have been measured, and it was found that the radial velocity had increased in parallel with the rapid increase in V band brightness at that time. However, much of the time monitored to date, the correlations are less pronounced. Continued monitoring through the 2009-11 eclipse is anticipated and the results eagerly awaited.

8.5 Polarimetry

The results of Kemp et al. (1986) represent the gold standard for polarimetric study of the epsilon Aurigae system. Modern methods need to be applied to the next eclipse opportunity, to improve on the results so far.

8.6 Your Role

Cosmic coincidence and design have combined epsilon Aurigae's first eclipse of the millennium with the observance of the International Year of Astronomy 2009, in celebration of the 400th anniversary of Galileo's use of the telescope to discover astronomical wonders - craters, sunspots, moons of Jupiter, etc. Among the events being planned is a "citizen science" opportunity for interested public to use the magnificent optics and detectors now available to enable participation in the monitoring of the eclipse light curve, spectrum changes and beyond. We encourage the reader to seek out and participate in these opportunities. We, the authors, stand ready to provide any help we can to make your participation a positive learning experience - about the joys of observing the cosmos! As Jack Horkheimer, the 'StarGazer' of PBS fame, says, "Keep looking up!"

IX. Observational Methods

This final chapter summarizes a variety of methods that observers can use to monitor epsilon Aurigae and related objects

9.0 Magnitudes

The magnitude of a star is determined relative to another star by the following equation:

$$\textbf{Magnitude Difference } (\Delta M) = -2.5 \log_{10}(\text{Star 1}/\text{Star 2})$$

Star 1 and Star 2 are some quantitative measure of the star's brightness. This could be an analog voltage level, marking on a strip chart recorder or digital count.

Using a photometer to measure the stars, Star 1 might have been 365,324 counts and Star 2 = 18,332 counts. To determine the magnitude difference between the two stars:

$$\begin{aligned} \Delta M &= -2.5 * \log_{10}(365{,}324 / 18{,}332) \\ \Delta M &= -2.5 * \log_{10}(19.9282) \\ &= -2.5 * (1.2995) \\ \Delta M &= -3.2487 \end{aligned}$$

The minus sign indicates that Star 1 is 3.2487 magnitudes brighter than Star 2.

Note: There are several factors that determine the extraterrestrial magnitude. The atmospheric extinction can have a large effect and increases rapidly the further from the zenith a measurement is made. The color sensitivity of the system also comes into play. The biggest factor and one that remains constant once determined is the system's zero point (defined below).

Since many times it is desirable to determine a star's magnitude without having to measure a second star. The same basic equation is used, but only one measure value is used and a special zero point constant is added to adjust the equation for the sensitivity of the

system being used. Obviously a 6" telescope will produce a much lower reading for a given star than say a 16" telescope using the same photometer. The zero point adjust for that.

For example: Using a given system we measure the star Vega with a V filter and get 493,879 counts. Vega has a magnitude (M) of approximately 0.0 in the V band.

$$M = -2.5\ (\mathrm{Log}_{10}(493{,}879)) + Zv$$

$$Zv = 2.5\ (\mathrm{Log}_{10}(493{,}879)) - M$$

Since M is 0.0 $Zv = +14.2341$

Thus our system has a zero point of +14.2341

If we used this system to measure Star 1 above and got 365,324 counts, that would mean: the Instrumental Magnitude

$$IM = -2.5\ \mathrm{Log}_{10}(365{,}324\ ) + 14.2341$$

$$IM = -13.9067 + 14.2341 = 0.3274$$

Thus Star 1 has an Instrumental Magnitude of +0.3274.

Note: The Instrumental Magnitude is the magnitude before applying correction for extinction and color.

9.1 Naked Eye Techniques

You do not need a computer or fancy electronic equipment to observe variable stars. Long before any of the electronic devices were available amateur astronomers were contributing to science by making visual estimates. With practice some of these observers produced very good results. Information on variable star observers in the 1800's and early 1900's can be found at:

http://www.aavso.org/aavso/history/webhist1.shtml.

In 1911 the American Association of Variable Star Observers (AAVSO) was formed at Harvard College Observatory to coordinate these efforts and archive the data. For more information about the AAVSO see:**http://www.aavso.org**

The technique of naked eye measurements is to find close stars of known brightness and then estimate the star of interest's brightness by comparing to the known stars. With practice observers can get close to 0.1 magnitude accuracy. To date the AASSO has close to

15 million variable star observations from around the world. With members from 45 countries the AAVSO is very active today with many observers still making valuable naked eye estimates.

Many interesting star systems have magnitude variations that are smaller than can be seen by naked eye techniques. A new field of astronomy was created called astronomical photometry to allow finer measurements to be made.

For those wishing to do naked eye observations of epsilon Aurigae a modest telescope or binoculars are suggested. There are four close stars that can be used to base brightness estimates of epsilon Aurigae on. While zeta Aurigae is an eclipsing binary system it will be out-of-eclipse and steady during epsilon's eclipse and eta Aurigae will be steady enough to use too. Refer to Figure 9.1 for the position of the stars. Use the following visual magnitudes for the estimates:

Zeta Aurigae = 3.8	Eta Aurigae = 3.2
Lambda Aurigae = 4.7	Capella = 0.1

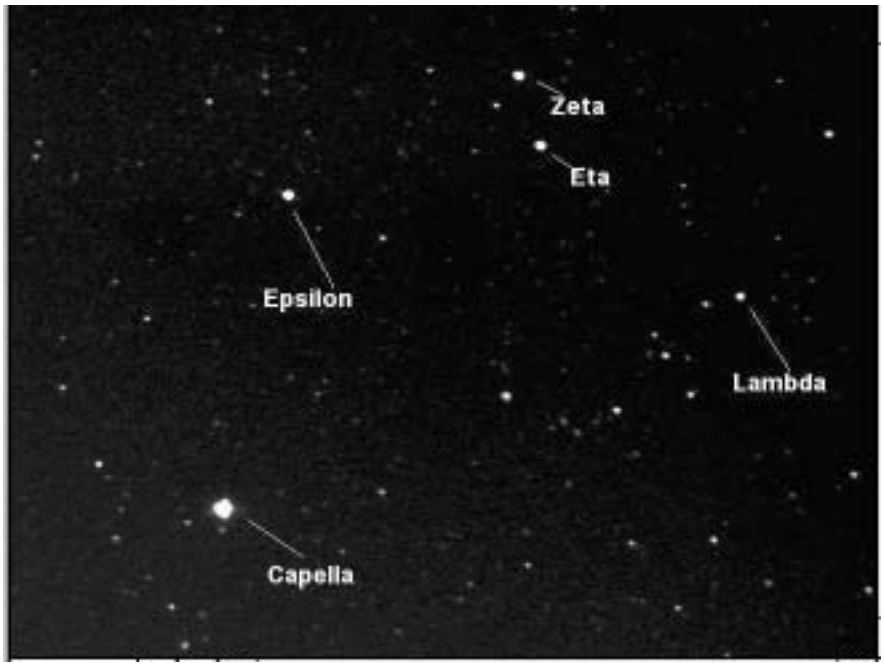

Figure 9.1 The Stars of Aurigae

9.2 Photometry

9.2.1 Introduction

Astronomical photometry is the precise measurement of the brightness of astronomical objects. The most popular of objects are stars. Why measure the brightness of stars? Aside from being able to classify the brightness of stars, much can be learned about stars and star systems (multiple gravitationally connected stars). Various means have been used to do this. Photographic emulsions of star fields have been studied and the density of star images used as an estimate of the star's brightness. A calibrated attenuating wedge has been used to see at what point a star can no longer be seen due to the attenuation. Technology has provided much better means now.

9.2.2 Photomultiplier Tubes

With further understanding of Einstein's photoelectric effect, very sensitive electronic photometers were developed. Among the first of these devices were photomultiplier tubes. These tubes are glass vacuum tubes, but unlike most glass vacuum tubes do not have a filament that gets hot and essentially do not wear out. They do require a high direct current voltage of around -1000 VDC, but at a very low current, around 1.0 milliampere. Figure 9.2 shows a 1P21 photomultiplier tube. This is the tube used to develop the initial standard star magnitudes beginning in the 1950's.

Figure 9.2 1P21 Photomultiplier Tube

The way the photomultiplier tube works is a photon strikes the surface of a sensitive photometric material called the photocathode. Due to the photoelectric effect an electron is knocked off. This is the first stage of many (typically nine stages) and at a high negative potential usually around -1,000 VDC. The next stage is at a slightly lower potential so the electron is accelerated toward it. When the electron hits the second stage multiple electrons are knocked off. These are then accelerated toward a third stage. And so on. In the 1P21 there are nine stages. At the last stage a small current pulse is produced. A special voltage divider network on the tube's socket produces the stepped voltages for each stage.

There are two modes in which a photomultiplier tube can be operated in. One is an analog mode where the current produced is stored in a capacitor and as the charge builds up the voltage is read out as a function of the rate of photons striking the photocathode. A second way is to use a pulse forming network on the voltage divider on the tube socket to shape the pulse into a narrow single pulse. This pulse is then amplified and fed to a frequency or pulse counter. This is known as photon counting. One count means 1 photon. A million counts per second means a million photons. Not every photon striking the photocathode results in a pulse,. however. The efficiency, known as Quantum Efficiency (QE), of the tube is very constant so the results can still be very accurate. Another factor with photon counting is known as dead time. If multiple photons hit simultaneously only one will be counted. This is not a problem with the analog mode, but can be easily compensated for with the photon counting mode. With large telescopes and bright stars another serious consideration is saturation. While an 8" telescope can be used to measure stars as bright as magnitude 2, anything brighter may saturate the tube. When the tube saturates the data becomes nonlinear and worthless. The larger the telescope the fainter the stars must be. A good rule of thumb is to observe stars that produce a maximum count of under 1,000,000 counts per second.

Figure 9.3 shows a schematic of a 1P21 photomultiplier with the voltage divider designed as a pulse forming network. The resistors

provide a voltage divider so each stage has an increasing voltage level. The capacitors at the bottom form the pulse forming network and shape the output pulse. Because pulse widths, rise and fall times are in the nano second region, high frequency techniques should be followed. This means keeping leads as short as possible.

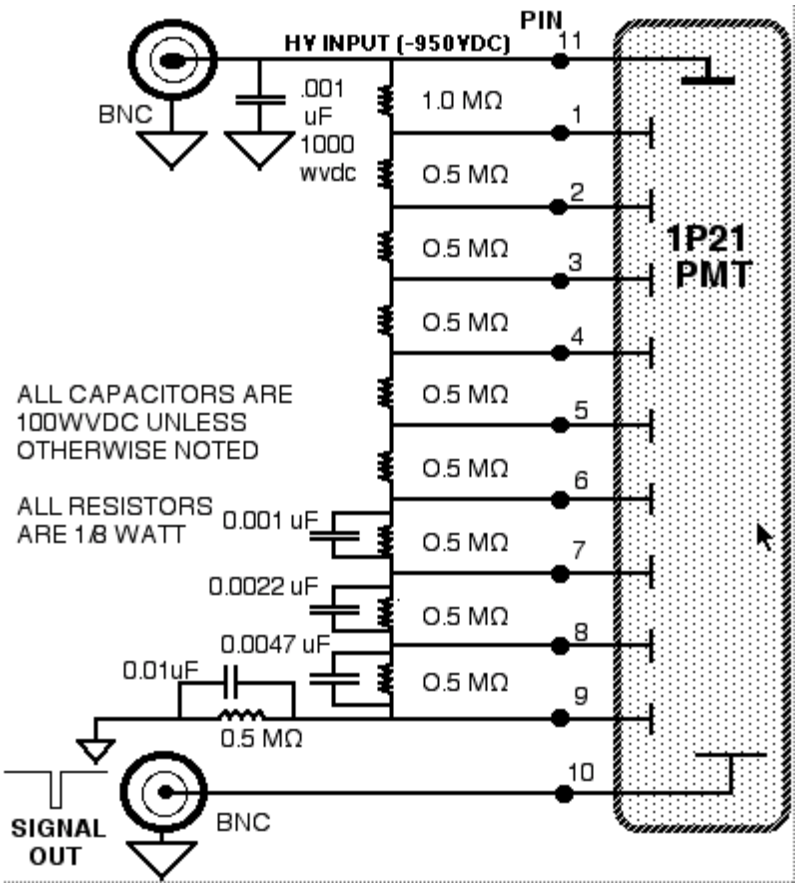

Figure 9.3 PMT Pulse Forming Voltage Divider

While the PMT can operate at voltages greater than -1,000 VDC, it has been found that operating at -950 VDC is about optimum. Higher voltage will increase the sensitivity, but also increase the dark counts. At -950 VDC the sensitivity is excellent and dark counts minimized. As the voltage is raised, the dark counts increase rapidly.

A 1P21 photomultiplier tube has an effective spectral range of 300 nanometers (ultraviolet region) to 650 nm (visual region). Figure 9.4 shows a set of response curves for various types of photocathodes. A 1P21 uses a bialkali photocathode.

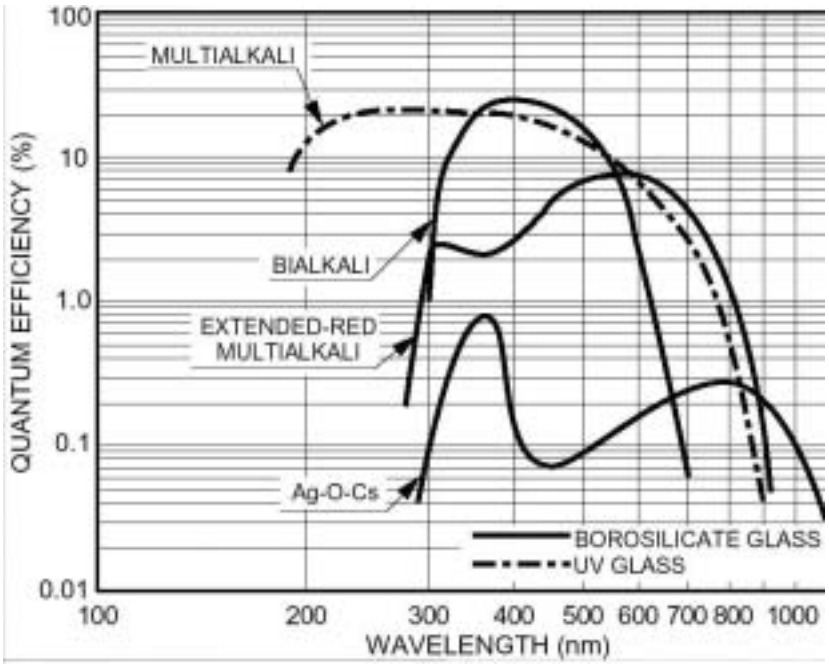

Figure 9.4 PMT Spectral Response
Photo Credit: RCA PMT Handbook

An interesting historical note is that during the 1950's the 1P21 photomultiplier tube became very important for the automotive industry. It was used with luxury cars as a detector for an automatic headlight dimmer. There are many other types of photomultiplier tubes uses for many applications, particularly high energy physics. A 931A is the same tube as a 1P21 except the 1P21 is supposed to be a selected version with increased sensitivity and lower dark current or noise. This is not necessarily always the case, however. Some 931A tubes are better than the 1P21s. Aside from physical damage of the glass tube and jarring the delicate internal parts of the tube, the tube should last indefinitely. One very important thing, contrary to its automotive use, it should never be exposed to bright light (even ambient room light) with power on. Keeping the tube in the dark with power on will increase the sensitivity and decrease the dark current and sometimes bring a poor tube back to life.

Two very big advantages of a 1P21 photomultiplier tube photon counting photometer are it can easily produce data in the ultra violet region and secondly it has a very large dynamic range, in excess of a 10^6.

Figure 9.5 shows a diagram of the HPO Photon Counting Photometer. Star light from the telescope enters the unit via the telescope coupler. A flip mirror is set to reflect the light to an eyepiece so the star can be centered in the diaphragm opening. The diaphragm slide starts with a large opening and the star is centered. The diaphragm sizes are reduced and the star centered more accurately. The flip mirror is then flipped out of the way and the star light passes tot he fixed mirror. The fixed mirror reflects the light through a Fabry lens, the desired filter and into the photomultiplier tube.

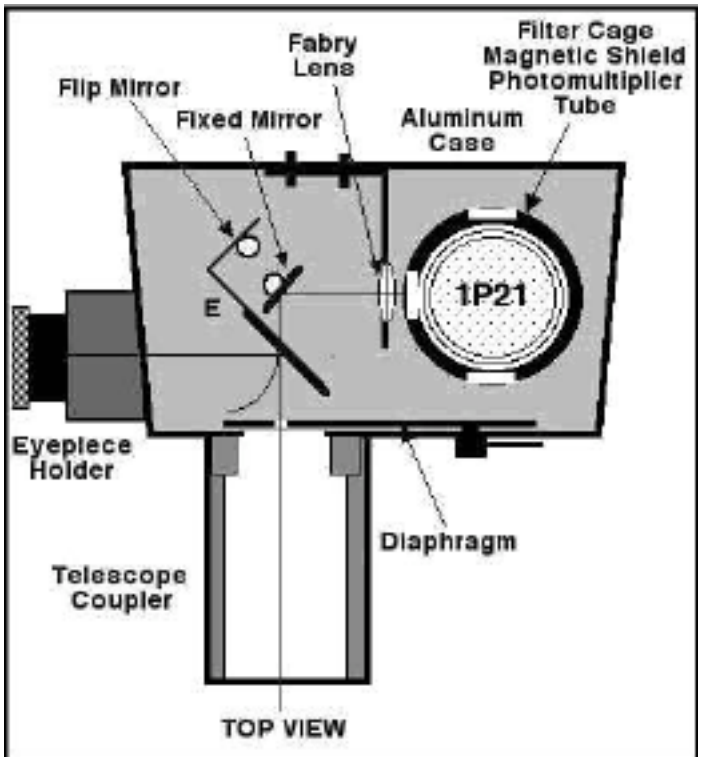

Figure 9.5 HPO Photon Counting Photometer

The unit is machine from a die cast aluminum box. Machining requires a skilled machinist as the box sides are all sloping and getting precise positions requires skill.

Figure 9.6 shows the HPO photometer mounted on a C-8. The unit is smaller than a 35 mm camera body. The four position filter switch can be seen at the bottom (VBUD) where D is dark (no filter, no light). The knob right above the filter switch is for the flip mirror. The white box on the back is just a battery box that houses two AA batteries for the illumination of the dual crosshair reticule

in the eyepiece. Originally the eyepiece had a self illuminating system with a small battery. Typically turning off the battery at the conclusion of a night's observations would be forgotten. Next time the battery would be low or dead. The external battery box provides space for two inexpensive AA batteries plus an LED power on indicator. It is very obvious that the power is on so turning off the unit is seldom overlooked.

The unit slides into the back of the telescope in place of an eyepiece. Counter weights are used to balance the telescope for optimum tracking.

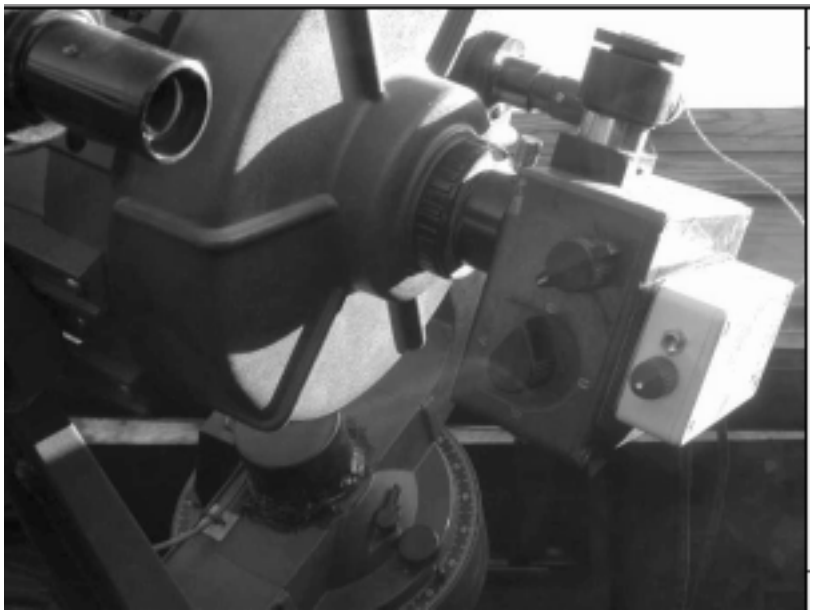

Figure 9.6 HPO Photometer on C-8

Compared to other PMT based photometers the HPO photometer is extremely light and compact. As such, even on an 8" telescope, balancing requirements are minimized.

Figure 9.7 shows the HPO photometer with the back cover removed. To the left is the rotatable filter cage. In the middle are the flip mirror and fixed mirror. The eyepiece is to the right. At the bottom are BNC connectors for the high voltage (-950 VDC) and output pulse.

The 11 pin tube socket has a special pulse forming network built on top of the voltages divider network to create a narrow pulse for

each detected photon. If the unit were to be used in analog mode, the pulse forming network would not be needed and a simple capacitor used to create a current level proportional to the photon detection. In the photon counting mode it is very important to determine and factor in the system dead time. See paragraph 9.2.7.1.1.4 for more information on dead time.

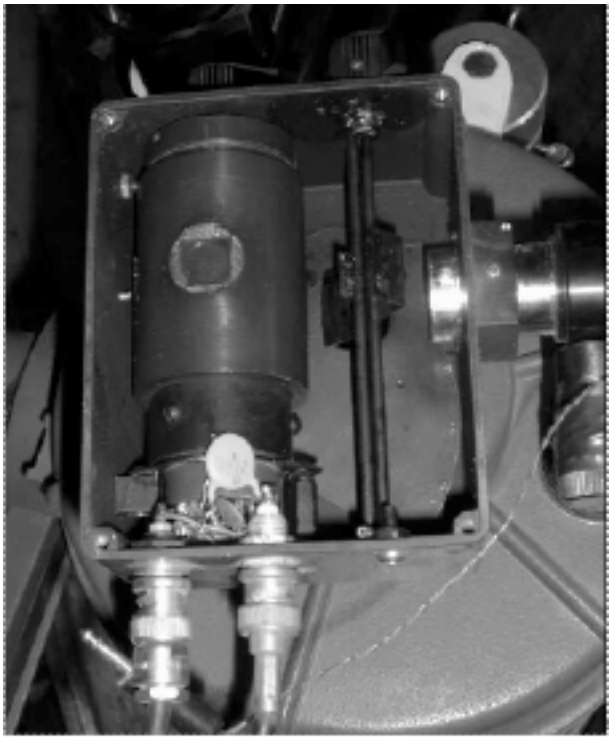

Figure 9.7 Inside HPO Photometer

The filter cage to the left has 1/4" holds machined in it to allow small 1/2" pieces of filter glass to be secured with RTV. The filter cage is machine from aluminum and black anodized. In fact all metal parts are black anodized. Inside the filter cage is a magnetic shield. This is important as the gain of the PMT is affected by even slight changes in the magnetic field, e.g., change in position to the Earth's magnetic field. Inside the shield is the PMT.

9.2.3 Solid State Detectors

With the advent of semiconductors, PIN diodes were developed that are very sensitive to light. The diodes require extremely high gain amplifiers (called electrometers) with gains exceeding 10^{12}.. These high gain amplifiers require very special design to avoid current leakage. These detectors work best on brighter stars and can be useful in the red and near infrared regions. The dynamic range of PIN diode detectors is considerably smaller than the photon counting detectors and require several different amplifier gains to be useful.

9.2.4 Charge-Coupled Device (CCD) Detectors

While the photomultiplier tube and PIN diode detectors are single-channel devices, a CCD is a multi-channel device, but usually is just referred to as a CCD detector as opposed to a single channel detector. With digital cameras becoming very popular development of the CCD detectors has come a long way and prices have plummeted. Many of these devices that are used in digital cameras also work well in photometers. The CCDs are very sensitive, even more so than the PIN diodes and work well for detecting faint star light. An added bonus is these detectors produce images. Each pixel is essentially a single channel detector, but because the star is spread over many, the pixels can be summed to produce an accurate means of determining the stars magnitude. Because the individual pixels are read out with a computer much software magic can be performed to make the data even more accurate and useful.

As with the PIN diode detectors the CCD detectors are sensitive in the red and near infrared spectrum. Except for some very specialized units they are insensitive in the ultra violet region. CCDs can be thought of as a large array of detectors, some into the millions of pixels. Each pixel is a detector and acts like a well. When a photon hit the detector an electron is knocked into the well. The well fills up with electrons and the circuitry reads the level of electrons and empties the well making it ready for the next reading. CCDs have a higher Quantum Efficiency (QE) than photomultiplier tubes. While photomultiplier tube have a QE of around 30, CCDs are around 60. For a CCD 100 photons coming in

will knock off 60 electrons whereas only 30 knock off electrons with the photomultiplier tube detector. This makes CCDs more sensitive than the photomultiplier tubes. CCDs are great for observing faint stars and other astronomical objects.

9.2.5 Photometric Filters

To make the observed data more useful special bandpass filters are used. By placing a filter in front of the detector (or CCD array) light within that bandpass falls on the detector. This is essentially a poor man's spectrometer, but produces very useful data. Stars vary differently at different wavelengths and using filters can provide data for clues as to what is happening. While there are many different filters used by professionals, the most popular are known as UBVRI and more recently JH have been added. The U filter is the ultra violet filter and has an effective bandpass of 300 to 400 nm. The B filter is the blue filter with an effective bandpass of 400 to 500 nm. V is the visual filter (usually yellow or green to simulate what is seen by the naked eye) with an effective bandpass of 500 to 600 nm. The R band or red filter has an effective bandpass of 600 to 800 nm. The I band (near infrared) has an effective bandpass of 800 to 1000 nm. Further into the infrared region a special PIN diode detector is used with J and H band filters. The J filter has an effective bandpass of approximately 1,200 to 1,300 nm. The H band filter has a bandpass of approximately 1,400 to 1,800 nm.

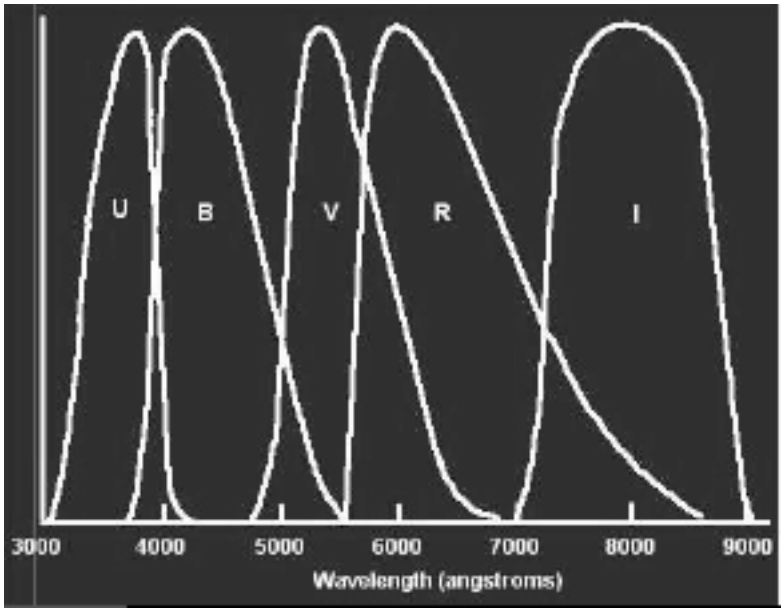

Figure 9.8 UBVRI Band Passes

Figure 9.9 shows the different photometric filter bands from the ultraviolet to the infrared K band.

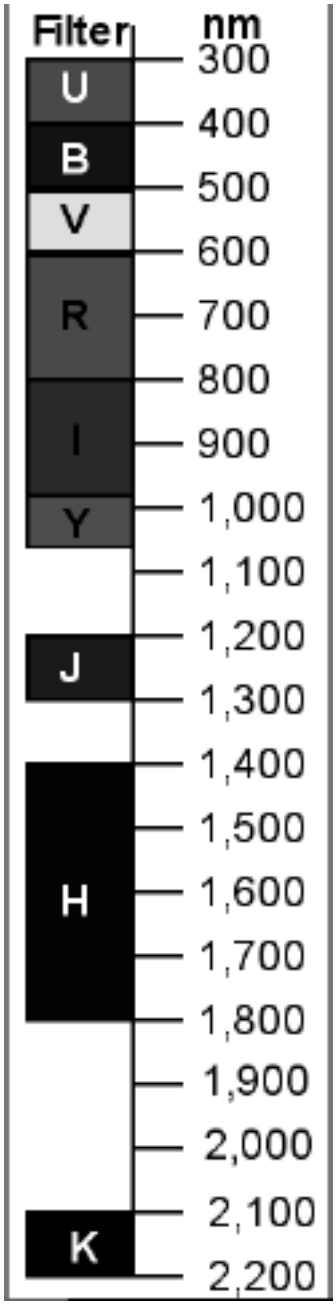

Figure 9.9 Photometric UBVRIYJHK Filter Bands.

UBVRI CCD Astrodon-Schuler photometric filters can be purchased at:

http://www.astrodon.com/products/filters/photometric/

J and H filters work with an SSP-4 photometer. It may be possible to use a Y band filter also. The K band is beyond the sensitivity of the SSP-4 photodiode.

9.2.6 Photometric Techniques

There are basically two types of astronomical stellar photometry, all-sky and differential. All-sky is used when calibrating a system and sometimes under other special circumstances. Differential photometry is much more accurate and easier. For differential photometry a star of interest is measured along with a comparison star close in color and magnitude and not too far away in the view of the stars. For single channel photometry a comparison star is measured in each of the filters used, then a sky measurements made in each filter (in a close area with no visible stars). This is repeated for the star of interest, called the program star. The comparison star sequence is again done. Then the program star. There will be three sets of program star measurements each bracketed by a comparison star set. Because observing is done through the atmosphere and the fact that photons do not arrive in a constant stream it has been found that each observation should last 10 seconds. This is sometimes known as the integration time. The 10 seconds is not arbitrary, but has been found to be about right for best results.

The above technique is used for single channel photometry. CCD photometry is usually easier because both the comparison star,. sky background and program star are all in the same image.

There are several commercial sources of astronomical photometers. Optec, Inc. is the only one that offers singe channel units. Most any monochrome CCD camera can be used for CCD photometry once suitable filters are coupled with it. Even the Meade DSI Pro series can be used for good photometry at a very reasonable price.

9.2.7 Photometry Equipment

9.2.7.1 Single Channel Photometry Equipment

9.2.7.1.1 PMT Based Photometers

9.2.7.1.1.1 HPO Photon Counter Photometer

At HPO our UBV PMT based photometer uses a photon counting system connected to a C-8 telescope. Close scrutiny will show that the mount for the C-8 optical tube assembly (OTA) is not a Celestron mount, but a Meade LX-90 mount. The reason for this is that the original Celestron mount wore out and would not track well. Despite trying to fix it, it still would not track acceptably. Meade had a sale on 8" SCT LX -90 telescopes so one was purchased.

All went well until U band data show detection levels at about half of what the C-8 produced. Repeated test verified this. Since the U band is of great interest it was decide to use the C-8 OTA on the Meade LX-90 mount With a little experimentation and adjustment of the counter weights this has worked well. Tracking is now excellent and the system is a GOTO system now. Figure 9.10 shows the Celestron C-8 OTA on a Meade LX-80 mount.

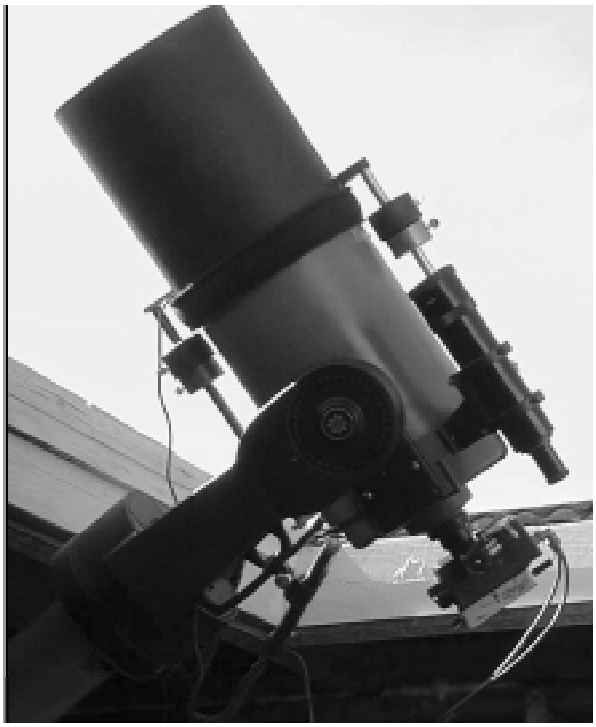

Figure 9.10 HPO C-8 UBV Photon Counting System

9.2.7.1.1.2 Optec SSP-5 Analog Photometer

The only commercial offering of a UBV PMT base photometer is the SSP-5 offered by Optec, Inc.

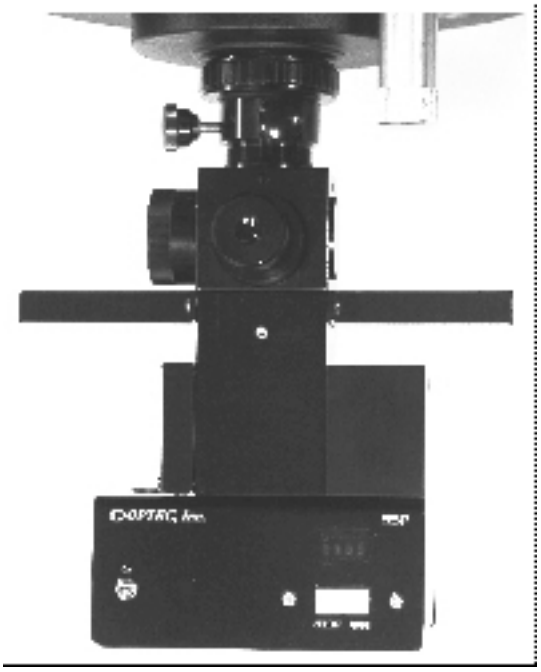

Figure 9.11 Optec PMT Analog SSP-5 System
Photo Credit: Optec Inc.

From the Optec web site: The SSP-5 photomultiplier-based single channel photometer provides greater sensitivity than the SSP-3 and faster response time for occultation work. The SSP-5 has nearly 5 magnitudes greater sensitivity compared to the SSP-3. Using an optional extended red-sensitive PMT and Optec filters, the SSP-5 can provide accurate photometric measurements in the Johnson U, B, V and R bands. Optec also stocks filters for the Strömgren u v b y bands and H-beta band. Like the SSP-3, the SSP-5 has been extensively upgraded with PIC microcontroller technology and a direct computer serial interface. The SSP-5 can also be ordered with the optional motorized 6-filter slider for robotic operation. This model is referred to as SSP-5A.

Information on the Optec units can be found at:

http://www.optecinc.com/.

9.2.7.1.1.3 PMT Saturation

With single channel PMT based photometers there are some factors that must be considered that are not factors for solid state or CCD photometry. With a PMT, saturation is the point where the PMT out is no longer linear. The larger the telescope, the more important this consideration is. Typically the brightest star you

can detect with an 8" is about second magnitude. If you are using a larger telescope, experiment to see if you are close to saturation. Integration time is not a factor. Taking shorter measurements will not help. This is true for both photon counting and analog PMT based units.

9.2.7.1.1.4 Dead Time

For photon counting units, dead time must be factored in. When observing bright sources, a photon-counting system tends to under-count the number of photons, i.e., the number of pulses counted becomes increasingly non-linear as the number of photons increases. This is because the output pulse has a given pulse width (say 150 nanoseconds). When the pulse rate increases to the point where there are more pulses than one per 150 nano seconds then the additional pulses do not get counted. Since pulse counters usually use a rising or falling edge as an event to count, a second rising edge occurring during a pulse will not be seen. To correct for this a dead time factor is used.

Assume the following:

N= True number of pulses per second.

n= Number of pulses per second observed.

δ= Time needed before another pulse can be counted.

Thus for each pulse observed, **δ N** photons are not counted. The rate at which photons are counted is:

$$n = N(1 - \delta N)$$

Because the factor desired is the True number of pulses per second (**N**) an approximation of the above equation yields the following:

$$N = n / (1 - \delta N) \sim n / (1 - \delta n)$$

or

$$N = n(1 + \delta n)$$

Perhaps the easiest way to determine a system's dead time is to use the complete system to measure a pair of stars. One star should be 3 to 4 magnitudes brighter than the other. It should also be bright enough to cause significant dead time (**Mv** = 3 for an 8" aperture), but not so bright as to cause saturation of the PMT. Saturation will produce a non-linear relationship that will invalidate the dead time

calibration. A diaphragm with many small holes (0.5" to 1.0" diameter holes) that fits over the end of the telescope tube can be made out of card board or thin plywood. The diaphragm should reduce the effective aperture by about 80%, e.g., for an 8" aperture (area = 50.27 sq. in.) the sum area of all the small holes should be 10.05 sq. in. (.20 X 50.27). For 0.75" holes there should be 23 holes (23 X 3.14 X $(0.75/2)^2$ = 10.16 sq. in. The holes should be place in an irregular pattern to avoid diffraction effects.

Pick stars that are close to the zenith and close together. Make all the measurements as quickly as possible to reduce any extinction change effects. First measure the bright star and then the faint star with out the diaphragm. Next measure the faint star and then the bright star with the diaphragm. Finally measure the bright star and then the faint star without the diaphragm. Average the measurements of the faint star without the diaphragm (call this number of count **F**). Next average the counts for the bright star without the diaphragm (call these counts **B**). Determine the ratio (**R**) of the averaged faint star's count without the diaphragm to that of the faint star's count with the diaphragm (call this **FD**).

R= F / FD

The true counts (**N**) for the bright star without the diaphragm should now be the bright star's count with the diaphragm (**BD**) times the ratio (**R**).

N= BD * R

Make several determinations of **R** using different sets of stars and then average the values of **R**.

The following is an example of dead time determination:

Average faint star counts without the diaphragm	**F= 27,500**
Faint star counts with the diaphragm	**FD= 1,222**
R= 27,500 / 1,222 = 22.50	
Bright star counts with the diaphragm	**BD= 54,500**
Averaged bright star counts without the diaphragm	**B= 987,500**

True counts for the bright star without the diaphragm

N= 54,500 * R = 1,226,250

The approximate dead time (**δ**) can now be determined by:

δ= (N - B) / (B * B)

or

δ= (1226250 - 987,500) / (987,500 * 987,500)

δ= 245 nanoseconds (nS)

To correct for dead time use the following equation:

N= n(1 + δ * n)

Where: **N=** True counts in counts per second
n= Observed counts in counts per second
δ= Dead time in seconds

Example: **n=** 987,500 counts per second
δ= 0.000000245 seconds
N= 987,500(1 + 0.000000245*987,500)
or
N= 1,226,413 counts per second

9.2.7.1.1.5 Threshold Adjustment

Again for photon counting units another adjustment must be made. The output pulse from the PMT is very small and must go to a pulse amplifier/conditioning circuit. In the conditioning circuit there is a threshold adjustment. Pulses from the PMT will vary in amplitude. Some times pulses are generated by thermal electrons and do not go through the nine stages resulting in a lower level pulse. The threshold adjustment is used to limit only pulses of a certain size or greater from being out putted from the circuit. Follow the directions for the circuit used for the proper setting.

9.2.7.1.1.6 Photon Counting Data Reduction

Unless there is a computer interface or some other means of auto data acquisition, data can be easily recorded manually. It is suggested that a data entry form be created and copies used. Figure 9.12 is a form used by HPO for entry of epsilon Aurigae UBV data. Similar forms can be used for other star systems and other types of photometry.

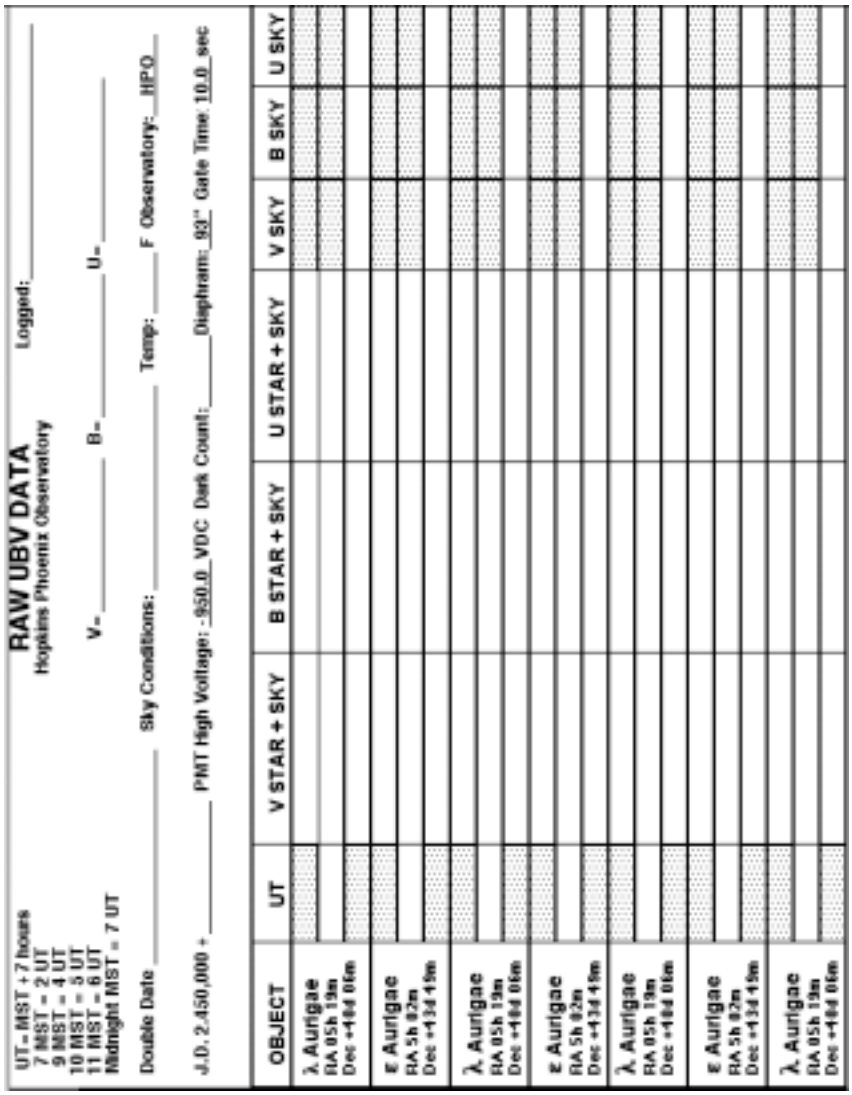

UT = MST + 7 hours
7 MST = 2 UT
9 MST = 4 UT
10 MST = 5 UT
11 MST = 6 UT
Midnight MST = 7 UT

RAW UBV DATA
Hopkins Phoenix Observatory

Logged: _____

V= _____ B= _____ U= _____

Double Date _____ Sky Conditions: _____ Temp: _____ F Observatory: HPO

J.D. 2.450,000 + _____ PMT High Voltage: -950.0 VDC Dark Count: _____ Diaphram: 93" Gate Time: 10.0 sec

OBJECT	UT	V STAR + SKY	B STAR + SKY	U STAR + SKY	V SKY	B SKY	U SKY
λ Aurigae RA 05h 19m Dec +404 06m							
ε Aurigae RA 5h 02m Dec +43d 49m							
λ Aurigae RA 05h 19m Dec +404 06m							
ε Aurigae RA 5h 02m Dec +43d 49m							
λ Aurigae RA 05h 19m Dec +404 06m							
ε Aurigae RA 5h 02m Dec +43d 49m							
λ Aurigae RA 05h 19m Dec +404 06m							

Figure 9.12 HPO UBV Photon Counting Data Entry Form

Once the data has been entered in the form the form can be set aside for later entry into a computer program for data reduction. Typically data reduction is done the next day. At HPO we used a database application development program called FileMaker Pro (FMP). FMP runs on Windows or MacOS and programs developed will run on both operating systems also. See:

http://www.filemaker.com/

Many people use spreadsheet programs, but a database program is much more powerful and versatile. It is encouraged that a database program be developed as it will give the observer great flexibility in how data is handled and displayed. Figure 9.13 shows part of a data entry screen. Similar screens for each star's date are in the program.

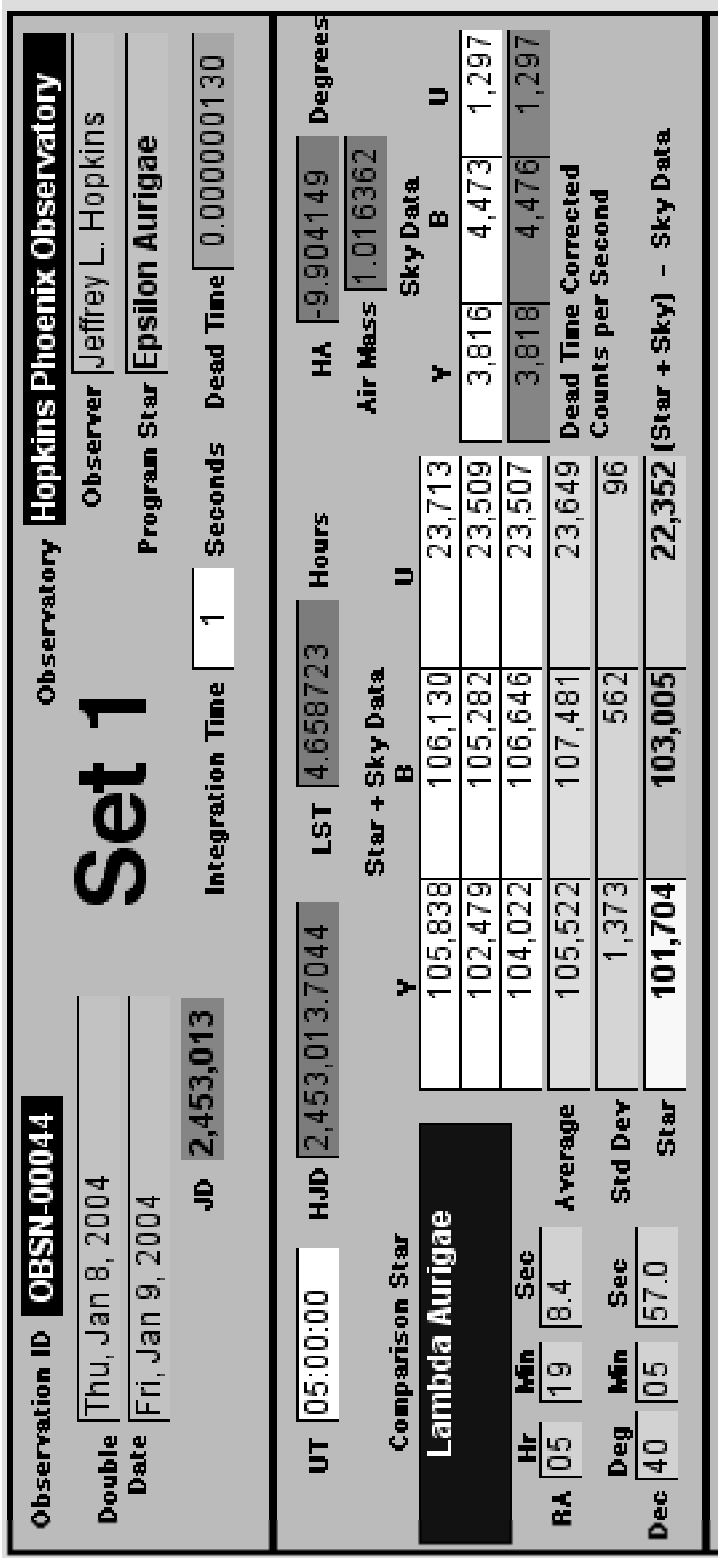

Figure 9.13 FMP UBV Data Entry

This is the first set of data for the comparison star lambda Aurigae. The Heliocentric Julian Date (HJD) and air mass are calculated. Dead time is factored in and sky readings for each filter subtracted.

Figure 9.14 shows a sample FMP window of a night's data summary.

Average HJD

2,453,013.7213

Summary

Average Net Comparison Star Counts

UT	Y	B	U	Air Mass
05:00:00	101,704	103,005	22,352	1.016362
05:10:00	101,722	102,710	22,332	1.012053
05:21:00	101,585	102,924	22,211	1.008773
06:32:00	102,492	103,415	22,419	1.023885

Average Net Program Star Counts

UT	Y	B	U	Air Mass
05:06:00	485,410	524,167	109,513	1.018014
05:15:00	484,011	518,554	109,641	1.016742
05:26:00	479,826	520,329	109,375	1.016496

Net Star Counts have been corrected for Deadtime, Normalized to 1 second and have corrected Sky Counts subtracted.

Nightly Extinction Coefficients

	Counts Per Second		Comparison Raw Mag
Average Y Comp Counts	101876	Y	-12.5202
Average B Comp Counts	102767	B	-12.5296
Average U Comp Counts	22329	U	-10.8721
Extinction Air Mass	1.0153		

Globals

	Color Coeff		Zero Points		Comp Mag
Epsilon	-0.1625	Zy	17.4269	Y	4.7100
Mu	0.8580	Zby	0.7493	B	5.3400
Psi	0.9870	Zub	-1.4298	U	5.4600
				BY	0.6300

Observation Extinction Coefficients

K'y	0.0929	K'by	0.0940	K'ub	0.0837

K'y= (Yrm + Epsilon * BY + Zy - Ystd) / Extinction Air Mass

K'by= (Mu * (BYrm) + Zby - (BY))/ Extinction Air Mass * Mu

K'ub= (Psi * (UBrm) + Zub - (UB))/ Extinction Air Mass * Psi

Figure 9.14 FMP Data Summary Screen

In addition to the same calculations a spreadsheet program provides there are numerous text handling and scripting possibilities with the database program. Data can be easily archived, data sets found and sorted and the exported or lists printed. Exported data can be used in a graphics program to create plots of the data. Figure 9.15 shows a FMP screen with the UBV data reduction results.

Julian Date	2,453,013		
Double Date	Thu, Jan 8, 2004		
	Fri, Jan 9, 2004		
	ETIM V	ETIM B	ETIM U
Comp Star	4.6236	5.1791	5.2026
Prog Star	2.9363	3.4319	3.4959
Comp Star	4.6238	5.1825	5.2042
Diff Mag 1	1.6874	1.7488	1.7075
Star Mag 1	3.0226	3.5912	3.7525
Comp Star	4.6238	5.1825	5.2042
Prog Star	2.9395	3.4426	3.4939
Comp Star	4.6256	5.1813	5.2114
Diff Mag 2	1.6851	1.7393	1.7139
Star Mag 2	3.0249	3.6007	3.7461
Comp Star	4.6256	5.1813	5.2114
Prog Star	2.9490	3.4408	3.4984
Comp Star	4.6145	5.1729	5.1968
Diff Mag 3	1.6710	1.7363	1.7057
Star Mag 3	3.0390	3.6037	3.7543
Avg Mag	3.0288	3.5985	3.7510
SD	0.0089	0.0066	0.0043
# Obs	3	3	3

Figure 9.15 FMP UBV Data Reduction

Figure 9.16 shows a FMP report with a list of UBV observations.

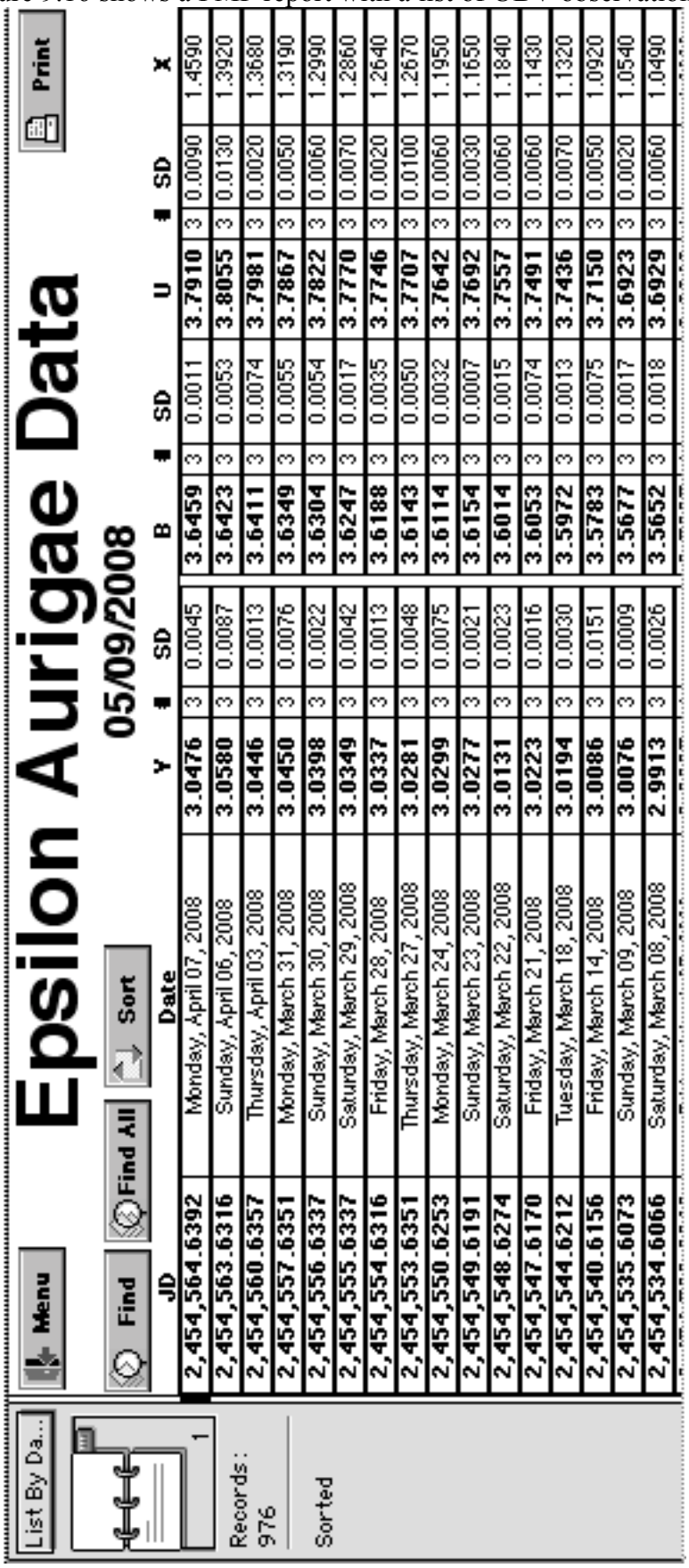

Epsilon Aurigae Data

05/09/2008

JD	Date	Y	#	SD	B	#	SD	U	#	SD	X
2,454,564.6392	Monday, April 07, 2008	3.0476	3	0.0045	3.6459	3	0.0011	3.7910	3	0.0090	1.4590
2,454,563.6316	Sunday, April 06, 2008	3.0580	3	0.0087	3.6423	3	0.0053	3.8055	3	0.0130	1.3920
2,454,560.6357	Thursday, April 03, 2008	3.0446	3	0.0013	3.6411	3	0.0074	3.7981	3	0.0020	1.3680
2,454,557.6351	Monday, March 31, 2008	3.0450	3	0.0076	3.6349	3	0.0055	3.7867	3	0.0050	1.3190
2,454,556.6337	Sunday, March 30, 2008	3.0398	3	0.0022	3.6304	3	0.0054	3.7822	3	0.0060	1.2990
2,454,555.6337	Saturday, March 29, 2008	3.0349	3	0.0042	3.6247	3	0.0017	3.7770	3	0.0070	1.2860
2,454,554.6316	Friday, March 28, 2008	3.0337	3	0.0013	3.6188	3	0.0035	3.7746	3	0.0020	1.2640
2,454,553.6351	Thursday, March 27, 2008	3.0281	3	0.0048	3.6143	3	0.0050	3.7707	3	0.0100	1.2670
2,454,550.6253	Monday, March 24, 2008	3.0299	3	0.0075	3.6114	3	0.0032	3.7642	3	0.0060	1.1950
2,454,549.6191	Sunday, March 23, 2008	3.0277	3	0.0021	3.6154	3	0.0007	3.7692	3	0.0030	1.1650
2,454,548.6274	Saturday, March 22, 2008	3.0131	3	0.0023	3.6014	3	0.0015	3.7557	3	0.0060	1.1840
2,454,547.6170	Friday, March 21, 2008	3.0223	3	0.0016	3.6053	3	0.0074	3.7491	3	0.0060	1.1430
2,454,544.6212	Tuesday, March 18, 2008	3.0194	3	0.0030	3.5972	3	0.0013	3.7436	3	0.0070	1.1320
2,454,540.6156	Friday, March 14, 2008	3.0086	3	0.0151	3.5783	3	0.0075	3.7150	3	0.0050	1.0920
2,454,535.6073	Sunday, March 09, 2008	3.0076	3	0.0009	3.5677	3	0.0017	3.6923	3	0.0020	1.0540
2,454,534.6066	Saturday, March 08, 2008	2.9913	3	0.0026	3.5652	3	0.0018	3.6929	3	0.0060	1.0490

Figure 9.16 FMP UBV Data Report

9.2.7.1.2 Single Channel Solid State Photometers

Optec offers two PIN diode detector photometers the SSP-3 and SSP4. Both units have a digital readout, but can only go to 9,999 counts. Using the data acquisition software, the counts can be up to 65,535 which is the maximum count the 16 bit analog-to-digital converter (ADC) can handle. Because there is a voltage-to-frequency converter in the unit that has a maximum rate of 15,000 Hz. This means that with an integration time (gate time) of 1.0 second, the maximum count is 15,000. So at 1.0 integration that is a limit. For a 10 second integration it would be 150,000, but the ADC limit is 65,535 counts.

9.2.7.1.2.1 Optec SSP-3 PIN Diode Photometer

Figure 9.17 shows the UBVRI SSP-3 photometer. This is ideally suited for someone starting out. In addition to being battery operated the PIN diode is nearly indestructible and the unit has a computer interface for logging data. While the U band filter is offered, sensitivity in that band is very low, but BVRI works well.

Figure 9.17 Optec SSP-3 Photometer
Photo Credit: Optec Inc.

From the Optec web site: "The SSP-3 solid-state photometer is an entry level instrument for measurement of stellar magnitude. Durable and well constructed, the SSP-3 and SSP-3A automated model have been used by amateurs, students, and professional astronomers worldwide since 1983. With a spectral response from the UV to the near-infrared, the SSP-3 can used for UBVRI photometry using Optec's Johnson standard filters. The SSP-3 has been upgraded with PIC microcontroller technology and direct computer serial interface. It is now referred to as generation 2."

9.2.7.1.2.1.2 Optec SSP-4 Infrared Photometer

Figure 9.18 shows the infrared JH band SSP-4 photometer. This is an amazing unit. Previously photometry in these bands was reserved for major observatories with exotic and expensive equipment. While similar to the SSP-3 this unit is not battery operated. As with the SSP-3 the unit has a computer interface for logging data. While the software allows selection of the filter, the SSP-4 does not have an automated filter selector and changes must be made manually. The software note is just to help keep track which filter was used.

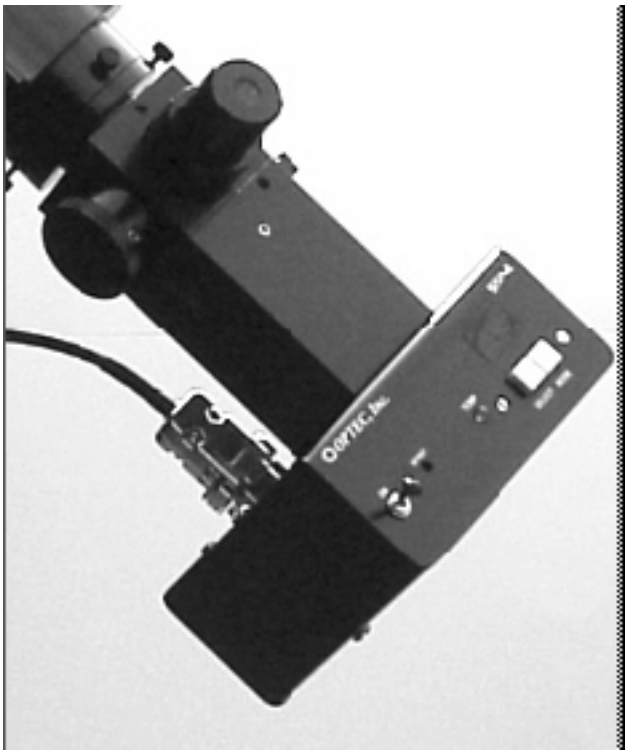

Figure 9.18 Optec SSP-4 Photometer
Photo Credit: Optec Inc.

From the Optec web site: "The SSP-4 Infrared photometer uses an InGaAs PIN photodiode detector and is the first off-the-shelf infrared photometer available to amateur and professional astronomers. This instrument allows accurate measurements of very cool stars in the J and H standard photometric bands. A two-stage temperature control Peltier cooler keeps the detector at a presetable temperature down to -40 degrees. This instrument was developed in part with the help of the AAVSO."

Information on the Optec units can be found at:

http://www.optecinc.com/.

A SSP-4 has been used at HPO for two epsilon Aurigae observing seasons.

Figure 9.19 HPO 12" LX200 GPS and SSP-4

Initially the SSP-4 was tried on a C-8 telescope. It was found that lambda Aurigae was not detectable and had the same reading as a sky reading. To solve this problem a 12" LX200 GPS telescope was obtained. While the signal to noise was much better, it soon became apparent that even the 12" was marginal and a 14" or 16"

would be a better choice. For more information on using the SSP-4 see: **http://www.hposoft.com/Astro/IR.html**

When purchased the SSP-4 came with the smaller 0.3 mm detector. This was suppose to be more sensitive. As it turns out it produced poor data. Data was not repeatable even over short time frames. The unit was returned to Optec and the larger 1.0 mm installed. Further testing showed a vast improvement. Figure 9.20 shows J band data for the 2005/2006 (at the left) and 2006/2007 (at the right) seasons. The H band data had a similar data spread. The data for the 2005/2006 season was taken with the 0.3 mm detector and is widely scattered. The data for the 2006/2007 season was taken with the 1.0 mm detector and resulted in a much smaller data spread.

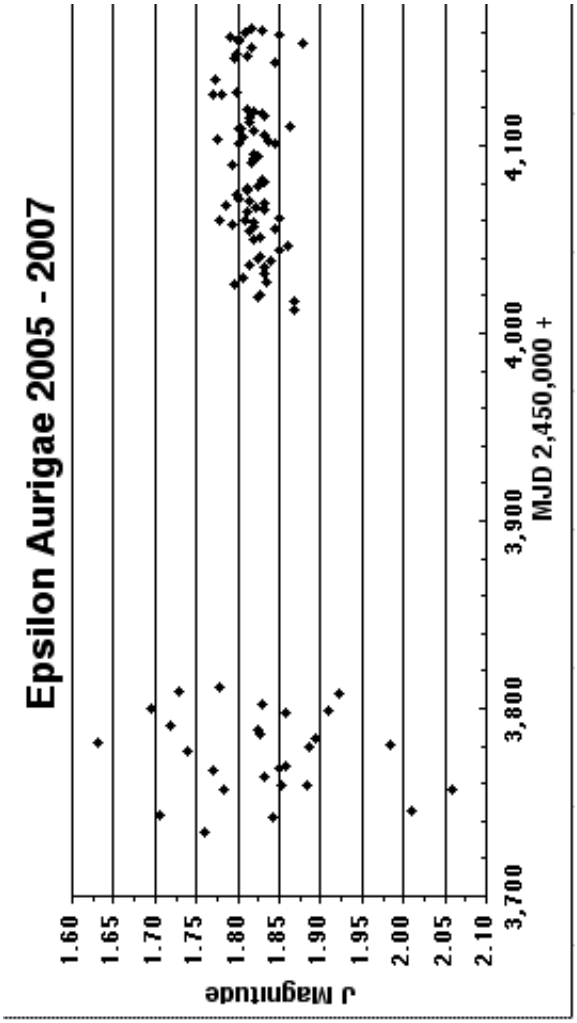

Figure 9.20 SSP-4 Detector Comparison

Table 9.1 shows a typical computer report of JH band data. Dark counts were taken between each movement of the telescope to keep track of the drift. Only one sky measurement was made for each filter and star set of measurements.

EPSILON AURIGAE
RAW OUTPUT DATA FROM SSP4
DATA ACQUISITION PROGRAM
UT DATE= 03/06/2007
TELESCOPE=12"LX200 GPS OBSERVER=JLH HPO
CONDITIONS= CLR NW NM -40.0

UT	OBJECT	F	------COUNTS		-----INT	SCLE	
01:59:50	SKY	D	04846	0	0	10	100
02:00:05	SKY	H	05080	0	0	10	100
02:00:52	COMP	H	05977	05971	05962	10	100
02:01:36	COMP	J	05507	05494	05476	10	100
02:02:05	SKY	J	04828	0	0	10	100
02:02:24	SKY	D	04555	0	0	10	100
02:03:11	SKY	H	04916	0	0	10	100
02:03:53	VARIABLE	H	09595	09578	09555	10	100
02:04:36	VARIABLE	J	07977	07949	07944	10	100
02:05:15	SKY	J	04634	0	0	10	100
02:05:33	SKY	D	04513	0	0	10	100
02:06:11	SKY	H	04729	0	0	10	100
02:06:55	COMP	H	05637	05618	05609	10	100
02:07:37	COMP	J	05106	05091	05071	10	100
02:08:08	SKY	J	04431	0	0	10	100
02:09:09	SKY	H	04538	0	0	10	100
02:09:50	VARIABLE	H	09186	09176	09182	10	100
02:10:32	VARIABLE	J	07564	07554	07523	10	100
02:11:01	SKY	J	04232	0	0	10	100
02:11:20	SKY	D	04128	0	0	10	100
02:12:01	SKY	H	04344	0	0	10	100
02:12:47	COMP	H	05242	05232	05227	10	100
02:13:28	COMP	J	04688	04672	04657	10	100
02:13:58	SKY	J	04001	0	0	10	100
02:14:16	SKY	D	03917	0	0	10	100
02:15:17	SKY	H	04100	0	0	10	100
02:16:01	VARIABLE	H	08761	08744	08733	10	100
02:16:42	VARIABLE	J	07125	07099	07073	10	100
02:17:12	SKY	J	03783	0	0	10	100
02:17:28	SKY	D	03586	0	0	10	100
02:18:00	SKY	H	03902	0	0	10	100
02:18:50	COMP	H	04784	04772	04751	10	100
02:19:35	COMP	J	04216	04207	04195	10	100
02:20:04	SKY	J	03550	0	0	10	100
02:20:20	SKY	D	03485	0	0	10	100

Table 9.1 Sample SSP-4 Data

As with the UBV data a FMP program was written to handle the JH data. While similar, the program is significantly different. Figure 9.21 shows a FMP screen of RAW JH band summary data.

Average HJD 2,454,170.6074

Summary

Average Net Comparison Star Counts

UT	J	H	Air Mass
02:34:33	0.613000	0.953000	1.026269
02:39:04	0.606000	0.947000	1.029619
02:43:24	0.619000	0.898000	1.033094
02:47:40	0.629000	0.871000	1.036769

Net Counts are adjusted for gain, integration time with sky subtracted. Counts are per second with Gain of X1

Average Net Program Star Counts

UT	J	H	Air Mass
02:36:38	3.181000	4.526000	1.050789
02:41:12	3.202000	4.490000	1.055211
02:45:38	3.227000	4.489000	1.059782

Dark Counts

Not used for data reduction. Used to monitor Sky only

6649	6888
6714	6890
6784	6834
6906	6732

Net Sky Counts (Sky -Dark)

UT	J Sky	H Sky
02:34:33	-0.0310	0.3330
02:36:38	-0.0420	0.3540
02:39:04	-0.0490	0.3520
02:41:12	-0.0220	0.3250
02:43:24	-0.0350	0.3090
02:45:38	-0.0110	0.3090
02:47:40	-0.0290	0.2650

Figure 9.21 FMP JH Band Summary Data

9.2.7.2 Potential Problems

One advantage of single channel photometry is the ability to see the data immediately. These are also true for CCD photometry except the drifting in the diaphragm (there is no diaphragm used in normal CCD photometry}. Have an idea what the reading should be for the star. If they vary greatly, look for problems. The following is a list of the potential problems:

1. Looking at the wrong star. Make test runs, double check the star fields. More than one expert has taken data on a wrong star.

2. Star drift in the diaphragm. Or with the solid state detectors drifting off the detector. If counts drop off quickly, do a check to see if the star is still centered. Otherwise the data will be of no value.

3. Watch for thin clouds and contrails. Sometimes everything looks fine except the readings are jumping up and down. Many times you cannot see the clouds or contrails, but the reading tell the story. Just wait until the reading stabilize before continuing. If they don't, give up for the night as it will be a waste of time to continue.

4. Dew. While Arizona is very dry, even here there are nights where dew can be a problem. The effect can be subtle and usually only seen on SCT type telescopes with a glass corrector plate. If a gradual decrease in counts of both the comparison and program star is seen, consider dew as the reason. While it is possible to de-dew the telescope with a hair dryer, it is better to eliminate the problem to begin with. This can be accomplished by using a dew heater on the front of the telescope. These are like small electric blankets and heat the corrector plate slightly so dew will not form. a dew shield also helps, but if it is windy, it tends to act like a sail and disrupt tracking.

5. Dark Current Drift. This is only a concern with the SSP-4. Because of the very high gains involved (10^{12}) the zero point for the amplifier tends to drift. If the signal-to-noise is high enough,

this may not be significant. This is another reason to use a large telescope with the SSP-4 or observe very bright stars.

9.2.8 CCD Photometry

While typical CCD photometry is done with a CCD camera connected to a telescope, when observing epsilon Aurigae this presents a couple of big problems. First, at 3rd magnitude epsilon Aurigae is very bright for CCD cameras. Second, most telescopes do not have a field of view capable of showing both epsilon and the comparison star lambda Aurigae in the same image. To get around this we at HPO experimented with using a DSI Pro (monochrome version) CCD camera with a Mogg adapter coupled to a wide angle 50 mm F.2.0 camera lens. The stock filter slide, while far from ideal, was used to hold the BVRI photometric filters. A filter wheel was tried, but focus could not be reached. The assembly was mounted on a 12" LX200 GPS telescope that acted as a tracking platform.

Figure 9.22 shows the Mogg adapter. The adapter has a 1/4" - 20 mounting hole in it to mount the assembly to the telescope. There are a multitude of different Mogg adapters for various camera lens and CCD cameras. For more information on the DSI Pro and Mogg adapters see:

http://www.meade.com/dsi_ii/index.html and
http://www.webcaddy.com.au/astro/adapter.asp

Figure 9.22 DSI Pro/Mogg Adapter/Camera Lens

Figure 9.23 shows the DSI Pro CCD/ with camera lens assembly and filter slide with BVRI filters.

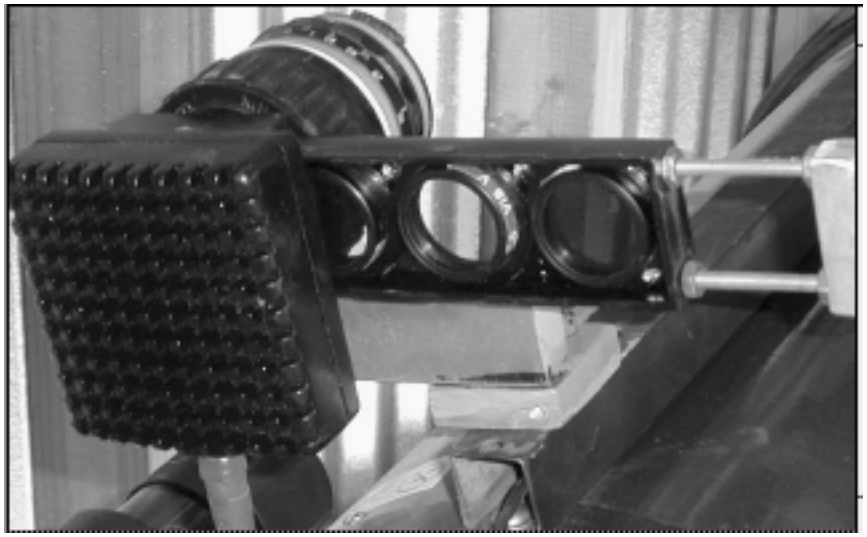

Figure 9.23 HPO Wide Angle BVRI Photometry

9.2.8.1 CCD Observing

9.2.8.1.1 AutoStar Software

When purchasing a DSI Pro CCD camera the unit comes with AutoStar software. While not perfect, AutoStar does a very respectable job of telescope control, CCD camera control and image processing. There is also a planetarium program included with millions of stars. When connected to a proper telescope (such as the Meade LX200 series telescopes), just clicking on a star will move the telescope to that position. When setup properly, this is very accurate. The part of AutoStar that is used for image acquisition and CCD camera control is called Envisage.

Details on doing CCD photometry with AutoStar can be found in the book *AutoStar CCD Photometry* details at:

http://www.hposoft.com/ASCCD.html

There is also a CCD Mentor Project for those wishing to learn CCD photometry at:

http://www.hposoft.com/SZHER/Mentor.html

9.2.8.1.2 CCD Photometry Technique

Perhaps the most important part of CCD photometry of epsilon Aurigae is to experiment before taking serious or usable data. Much frustration can be avoided by working out your technique with sample data. This can avoid lost time and useless data. Since the filed of view of the DSI Pro CCD camera and 50 mm F/2.0 camera lens is sufficient to capture epsilon, zeta and lambda Aurigae all in the same image, initial adjustments of the positioning should be done to approximately center the stars. Try not to have any stars of interest too close to the edge of the image. This will make image processing and the acquisition of the star information easier. Stars too close to the edge will produce poor data. Figure 9.24 shows a typical field of view with this arrangement.

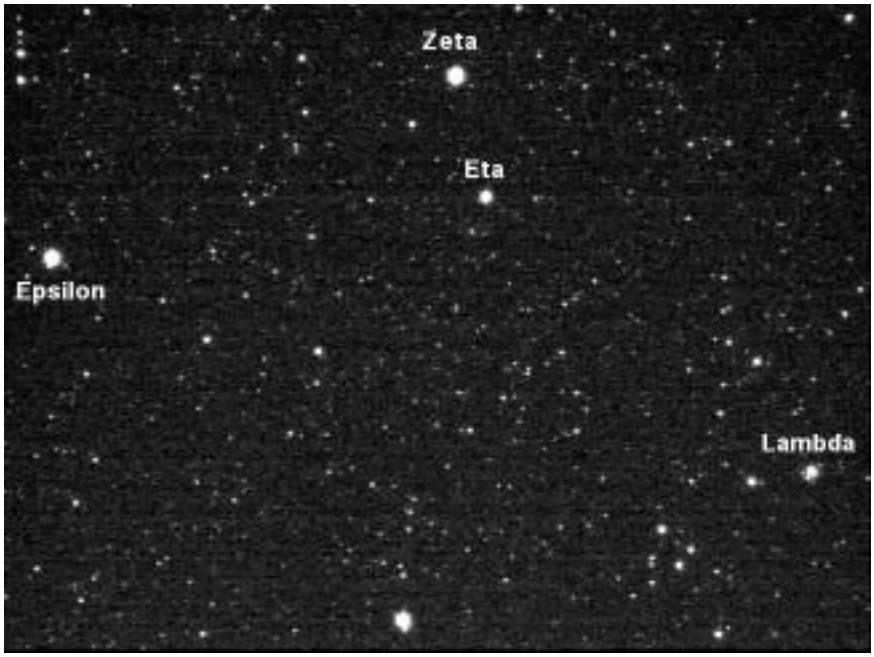

Figure 9.24 Wide Angle Field of View

9.2.8.1.2.1 Darks

Unless the ambient temperature is close to freezing, a set of 2.0 second darks should be taken, averaged and stored. Select "Take Darks" from the "Image Process" pull down menu. Set "First Exp" and "Last Exp" both to 2.0. Set the "Avg Exp" to the number of darks you want to use. Delete old darks "Del Existing Darks" and take 5 to 20 dark images. When taking the exposure, the subtract darks "Dark Sub" should be checked to provide automatic dark frame subtraction of the images.

9.2.8.1.2.2 Exposure

It was found that for epsilon Aurigae, a defocused 2.0 second exposure was about right. Twenty-five or thirty images were stacked/combined to provide an effective exposure of 50 or 60 seconds. This will average out the atmospheric scintillation effects. It is recommended for photometry to set the "Min Quality %" to zero and as well as the "Evaluation Count." Make sure the "Combine" box is checked. Save the images in FITS format. If other formats are used the photometric data will be lost.

9.2.8.1.2.3 Defocusing

Because of the very short focal length, star images on the CCD detector will be severely undersampled. This means a high percent of the light will be lost to the area between the pixels. To avoid his, the image must be defocused. This seems a bit against nature, but defocusing spreads the light out over more pixels and greatly reduces the undersampling.

To adjust the focus, it was found the following procedure worked well. First select the filter of interest. Next setting the exposure to 1.0 second. Adjust the focus for a peak reading on the AutoStar Histogram (See Figure 9.25). Typically this can be 55,000 to 60,000 ADU (Analog-to-Digital Units) counts (number at the upper right). Now re-adjust the focus so the counts to be about 1/3 that value or 15,000 to 20,000 ADU counts. Now set the exposure to 2.0 seconds and start the imaging.

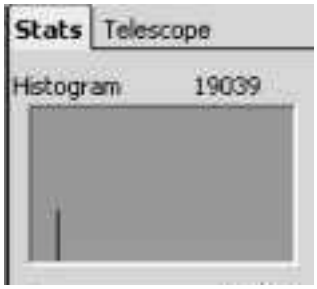

Figure 9.25 AutoStar Histogram

9.2.8.1.2.4 Flats

Flats provide a calibration of the optical system. While properly obtained flats will improve the accuracy, it is debatable how

important they are for the scheme used here. The user is encouraged to at least experiment with flats to see how much improvement if any can be made.

9.2.7.2 Image Processing

9.2.8.2.1 AutoStar Image Processing

The Image Processing part of AutoStar is separate from the Envisage part and must be opened.. A large part of the image processing is devoted to making pretty pictures and for photometry can be ignored.

Click on one of the image files in the new folder. The AutoStar Image Processing program will open the file.

Close the file, but not the image processing program.

To make working on similar files (same filter) a Group can be created that will have all the calibration done on the members of the Group automatically.

Click on the Group pull down menu and select New.

The Photometry selection is a bit misleading. It's designed to automate time series projects where you may have hundreds of images in each filter. For starting out, this can cause more problems than it solves. Ignore it for now. Also ignore the rest of the item from this pull-down menu as the mainly apply to astro imaging and not photometry.

Select all the images of a given filter (e.g., the V filter images in the V Raw Data folder).

This will create a new text file called ImageGroup.lst. Do not move or rename this file. This is not a text file and cannot be opened. Just let it be as it defines the files in the Group.

From the Group pull down menu select Calibrate.

A Calibrate window will be displayed where you can select and include a Bias, Dark Frame and a Flat field image. If you have used the auto dark subtraction while taking images or if the exposure time is less than 1 second you do not need to use another dark frame. If you have used a dark frame when taking the images the Bias image is not needed.

This will create a new file called NewImageGroup.lst. Do not move or rename this file. This is not a text file and cannot be opened. Just let it be as it defines the Calibration for the files in the Group.

Select the Flat Field you wish to use to calibrate with (e.g., Select Flat Field and find the flat field for the filter used for the images to be calibrated, e.g., FB). Click the Include Flat Field box and if desired the Include Bias button (after selecting the Bias image). Remember the Dark Frames have already been used on the fly when the images were exposed. Remember also that the Bias Frame data is part of the Dark Frame. Click on OK.

The program will now automatically calibrate all the images and save the new calibrated images with a new name (Calibrated_"file name"). The original images will be left untouched.

To organize the files make a new folder within the current folder. Call the folder "Cal Filter Name Data" (Cal V).

Repeat these steps for each filter. You now have sets of calibrated data ready to have the star magnitudes determined.

9.2.8.2.1.1 Differential Magnitude

The best and most accurate way to do photometry is to use differential photometry where program star magnitudes are compared to comparison star magnitudes and then normalized to produce a magnitude. This means you must know the comparison star magnitude accurately for each band.

9.2.8.2.1.2 Setting the Reference Magnitude

From within the image processing program select File and Open.

From within a folder with the images of interest select the first image to be processed. Make sure the file name has a Calibrated in from of it.

AutoStar automatically adjusts the display contrast so even if the images look faint, the data should be okay. If the star image is too faint you can adjust the contrast manually. the adjustment only affects the display. You can also expand the image to full screen if it helps.

Draw a small box around the comparison star. There will be a diagonal line across the box. The line should be approximately across the middle of the star. This is not critical as the software will find the center of the star. See Figure 9.26

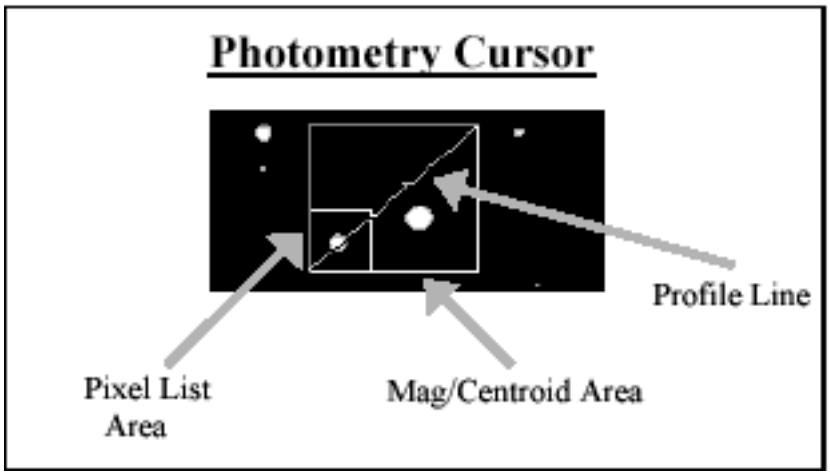

Figure 9.26 AutoStar Photometry Cursor

The Magnitude/Centroid rectangle bounds the entire area used in the magnitude and/or centroid calculations. This is a bit confusing as to properly determine the magnitude of a star, only draw the small box to the lower left (Pixel List Area) around the star of interest. The Profile line delineates the pixels that will be displayed when the Draw Profile function is selected.

You will see the term "centroid" appear many times when reading about CCD photometry. This is a bit of magic. The centroid of a

star's image is essentially its center of gravity or center of brightness. The CCD software can find this center very precisely. This is important because when selecting the star for processing, you do not need to select it exactly. Just as long as you are close the software will find the center of the star and reference everything about the star relative to that center. This is also important when using the CCD camera for tracking. The star image's center can be determined precisely and used for tracking.

In the pop up window select Set Reference Magnitude. See Figure 9.27. While for accurate photometry, the use of a reference star to do differential photometry at this point is only good for an approximation. No extinction or color correction has been done. In order to set up the software and proceed the Set Reference Magnitude must be selected

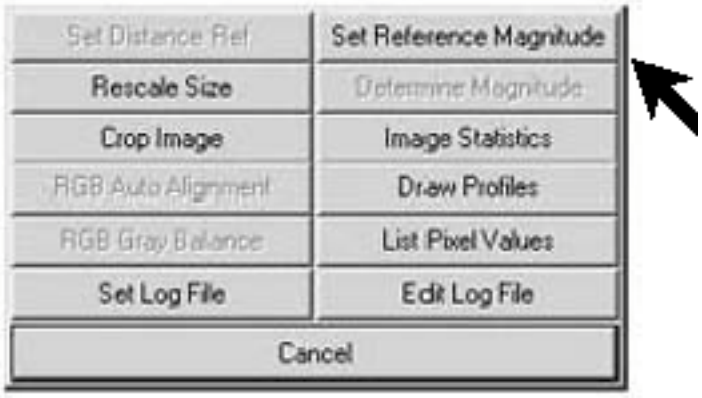

Figure 9.27 Setting Reference Magnitude

Set the Reference Magnitude for the comparison star for that filter.

This will set the reference magnitude for the comparison star. This must be done with each image. Other star measurements will now produce a magnitude referenced to the comparison star magnitude. This will create a new text file in the folder called ImageInfo. All the data that is acquired from the images will be logged into that file. Do not move or rename the file until all data has been entered.

The Aperture Diameter, Annulus and Centering Box Size can be changed, but unless you want to experiment or know what you re

doing, it is best to leave these values at their default settings of 8, 15 and 15 pixel diameters respectively. See Figure 9.28. It is important to remember that these are diameters. AIP4WIN does something similar, but it uses radii so the same values in AIP4WIN will be half. While there are several other values in the Magnitude Reference window, the only ones of interest at this point are the Aperture Diameter, Annulus Diameter and Centering Box Six (please excuse the software misspellings). It is recommended that the default values be used to start with. Experiment to see if better data can be obtained with other settings. Different stars and different conditions can benefit from adjusted settings.

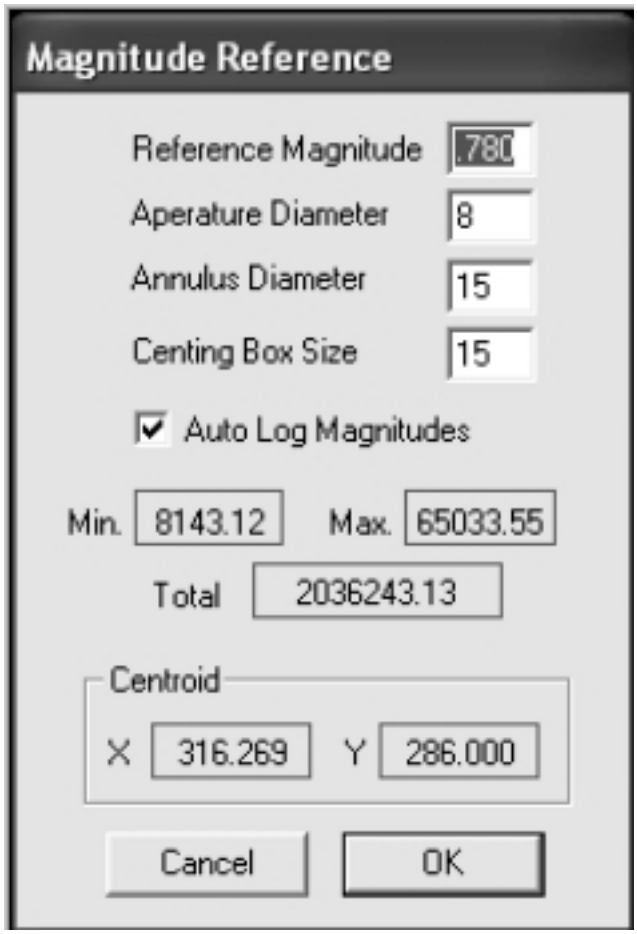

Figure 9.28 Setting Aperture and Annulus Diameters

9.2.8.2.1.3 Raw Magnitude Determination

Draw a box around the first program star. A widow will pop up. Select Determine Magnitude.

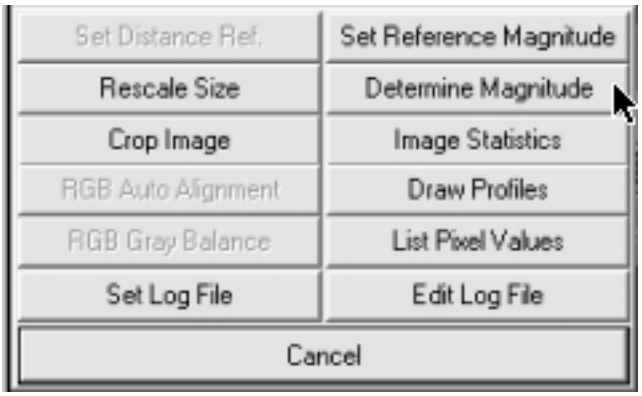

Figure 9.29 Selecting Determine Magnitude

While the Determine Magnitude option is selected, we are not primarily interested in the magnitude at this point. What is of interest is the Total Flux (1,516,860.37 ADU) and the Max value (64,716.73 ADU) for the star. The Max value in this case is too high and the exposure should be adjusted to reduce that value into the linear range (under 40,000 ADU).

The Magnitude Determination window with be shown, See Figure 9.30.

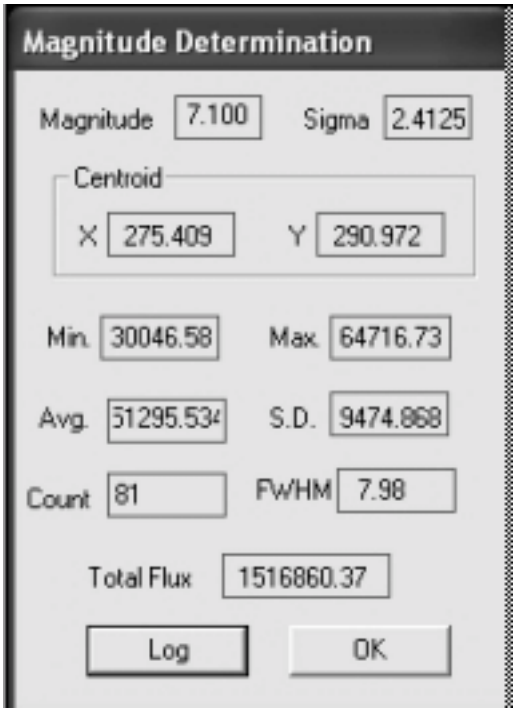

Figure 9.30 Determine Max Pixel and Total Flux

While the Magnitude determine can be used, it must be understood that extinction and color transformations have not been accounted for.

It may be better to use the Total Flux value as the ADU counts and let the data reduction software determine the raw magnitude and account for the extinction and color transformations. Once corrected magnitudes have been determined then differential magnitudes can be calculated and the program star's magnitude determined.

9.2.8.2.2 AIP4WIN Image Processing

While AutoStar Image processing does a good job of getting magnitude data, AIP4WIN is a step up, but even more important is the software comes with a 640 page handbook that is excellent. Even though AIP4WIN does not control the camera or acquire images, it is still a must for the serious CCD photometrist.

AIP4WIN can be purchased for $99.95 from Willmann-Bell at:

http://www.willbell.com/aip/index.htm

After loading the program, from the File pulldown menu select open and the image file you wish to process. Next from the Measure pulldown menu select photometry. The window as shown in Figure 9.31 will be seen.

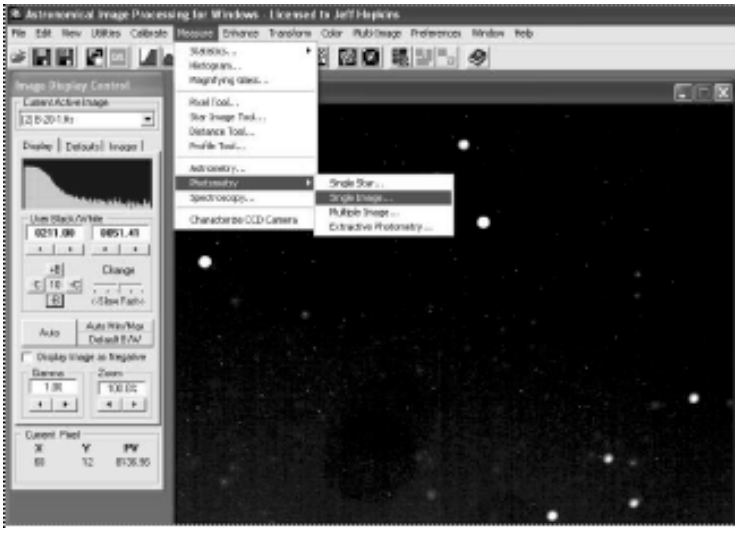

Figure 9.31 AIP4WIN Initial Display

From the Photometry selection another popup will allow you to select Single Image. See Figure 9.32.

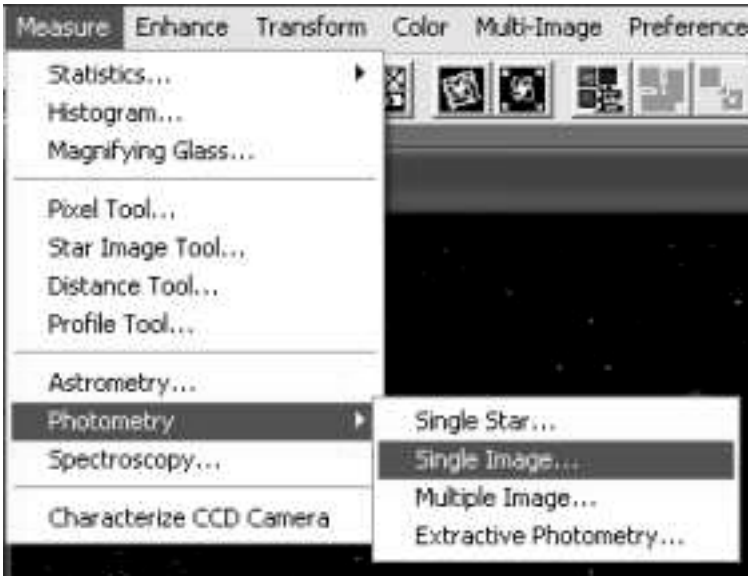

Figure 9.32 AIP4WIN Single Image Selection

Next the Single Image Photometry window will be seen. Select the Settings tab. See Figure 9.33.

Figure 9.33 Single Image Photometry Window

The Setting window will show the image processing cursor radii. See Figure 9.34. Remember these are radii pixels of the Aperture (7.0 pixel radii default), Inner Annulus (9.0 pixel radii default) and Outer Annulus (15.0 pixel radii default). It is suggested you start with the default values and experiment. The instrument Parameters are also shown, but not normally used. If the default settings are changed be sure the select Save.

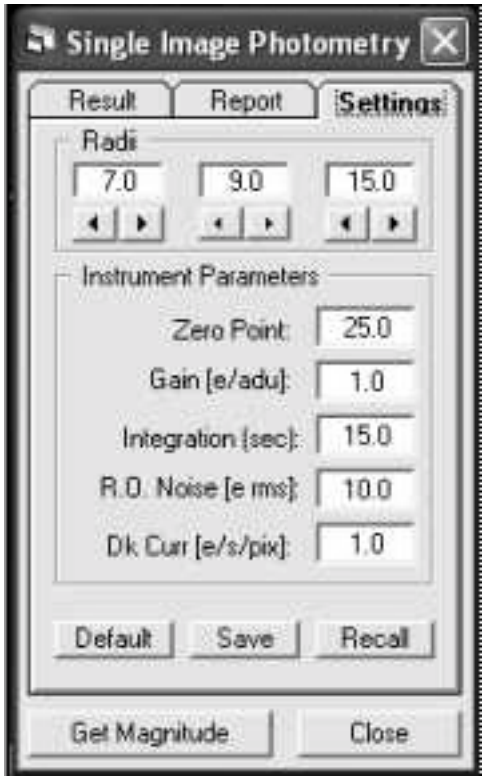

Figure 9.34 AIP4WIN Aperture and Annulus Settings

Next you must first select the Program Star (V) and then at least one Comparison Star (C1). Now selecting Get Magnitude will show the results as seen in Figure 9.35.

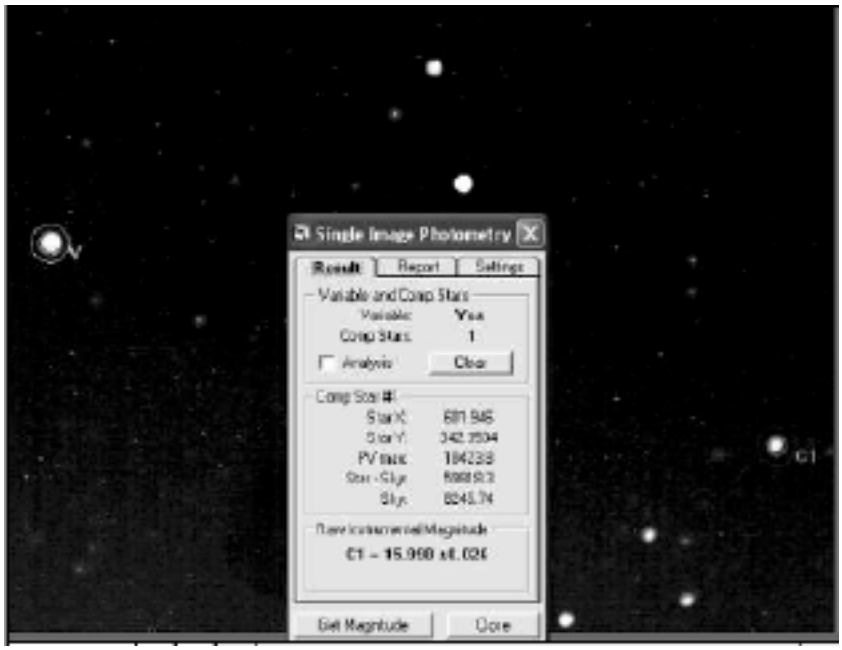

Figure 9.35 AIP4WIN Photometry Results

Figure 9.36 shows the results in detail. The value of interest is the Star- Sky value, here 59,818.3 ADU. The PV Max value should be also noted to make sure the maximum pixel count for the star is in the linear region (usually below 40,000 ADU) Here is well within that value at 10,423.8 ADU.

Figure 9.36 AIP4WIN Photometry Results Detail

9.2.9 Data Reduction

As mentioned earlier, many people use a spreadsheet program to do the data reduction. While that certainly works a database program works much better. There are several commercially available database programs, but FileMaker Pro (FMP) wins hands down for ease of learning and use. It is somewhat confusing as these programs are really application building programs. What you develop with FMP still needs FMP to run it. There is an option whereby you can create what is known as a runtime program so you do not need FMP. The downside is you cannot make any design changes without FMP. So it is usually best to just use a normal program. As you use the program you will be continually modifying it to make it better and more suited for your use. Once you learn it you will not understand how you got around without it before.

At HPO we have several data reduction programs created. One for UBV photon counting, one for BVRI single channel photometry (for use with an SSP-3), one of JH infrared band photometry (for use with an SSP-4) and one for BVRI CCD photometry. While multiple program stars can be all handled within a single program we have found it best just to duplicate the program for the technique used and dedicate it to a single star system. While this may seem inefficient it actually makes everything easier. Each program can be considered a unique project.

Databases are like a living being, they can grow, get sick and die. It is very important to periodically backup the program with its data. External CDs or memory sticks are inexpensive and ideal for this. A procedure should be developed to do periodic maintenance such as the backup.

At HPO we have several tables (or file depending on the version you are using to develop your program) in each program. Beginning with FMP Version 7.0 multiple files were replaced with a single file which contained tables that are similar to what used to be the individual files.

9.2.9.1 Star Information

The first part to develop is a table for Star information. This will have star names, RA, Dec, and published color magnitudes. This data will be used later each time you create a new record for a nights observation. The star's data needs to be entered just the one time. This file can help when it comes time to write reports or a paper on a project. While the brighter stars are fairly easy to find data on, with CCD and the faint star work, fainter than say magnitude 12, star data becomes very scarce. One can spend many hours trying to find magnitudes and even coordinates of a faint star system. Because some of the fainter stars usually do not have a name and do not even have a standard designation, the program creates a unique Star ID that is only used within the program to identify the star.

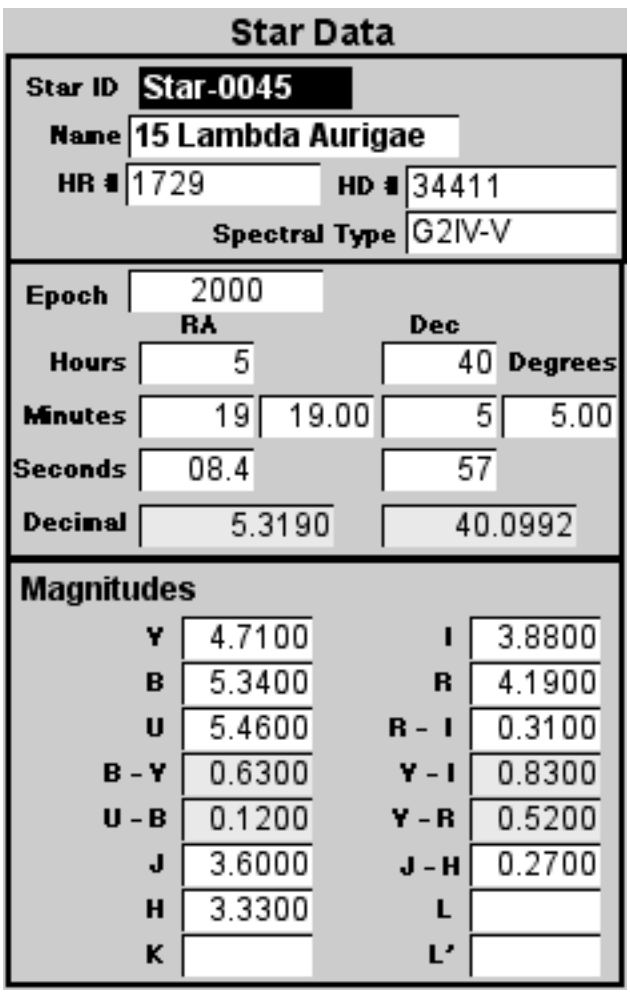

Star Data

Star ID	Star-0045		
Name	15 Lambda Aurigae		
HR #	1729	HD #	34411
Spectral Type	G2IV-V		
Epoch	2000		
	RA	Dec	
Hours	5	40	Degrees
Minutes	19 / 19.00	5	5.00
Seconds	08.4	57	
Decimal	5.3190	40.0992	

Magnitudes

Y	4.7100	I	3.8800
B	5.3400	R	4.1900
U	5.4600	R - I	0.3100
B - Y	0.6300	Y - I	0.8300
U - B	0.1200	Y - R	0.5200
J	3.6000	J - H	0.2700
H	3.3300	L	
K		L'	

Figure 9.37 FMP Star Data

9.2.9.2 Observatory and Equipment Information

Next you should develop a table for your observatory, equipment and calibration constants. This table will contain the observatory latitude and longitude as well as elevation. Instrument zero points and color transformation coefficients should also be entered.

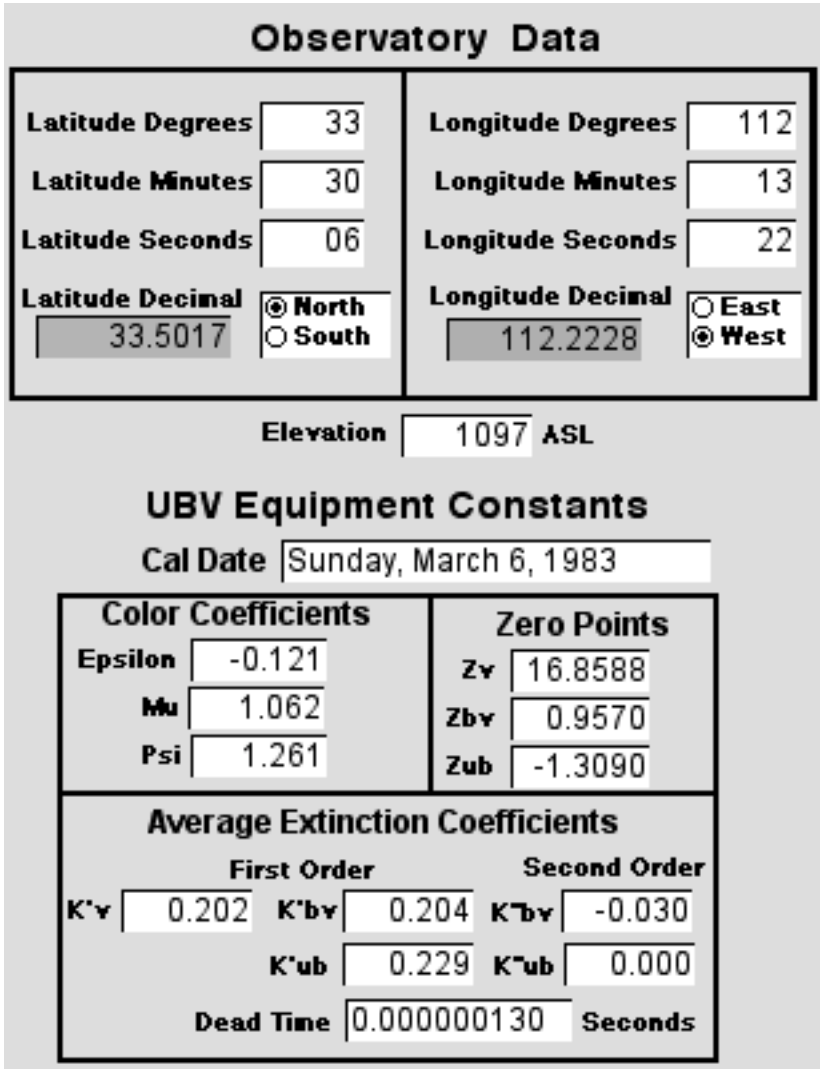

Figure 9.38 FMP Observatory and Equipment Data

It is important to have accurate data for the observatory's location (latitude and longitude)> Several evenings should be set aside to do calibration of the equipment. This includes determining the system dead time(for photon counting), the system zero points, color transformation coefficient and an average set of extinction coefficients. For best accuracy the extinction coefficients should be determined nightly, but the average can be used if the nightly extinction was not determined.

9.2.9.3 Observation Data Entry

This table should allow you to enter a nights observations and calculate things like air mass, extinction, heliocentric Julian Date, the sky and star + sky's net counts. A double date should be used bracketing the night of the observation. This helps avoid confusion when observations start one day and go past midnight into the next day. Heliocentric Julian Date should be calculated. There should be data fields for each raw star + sky and sky count. The net counts should have dead time (photon counting system), gain and integration time adjustments made. The corrected sky counts are then subtracted from the corrected star + sky counts. This data will be archived with one record per set of observations (usually one set per night). In cases when multiple sets of data are taken each night (time series on a fast changing system) each set will be record.

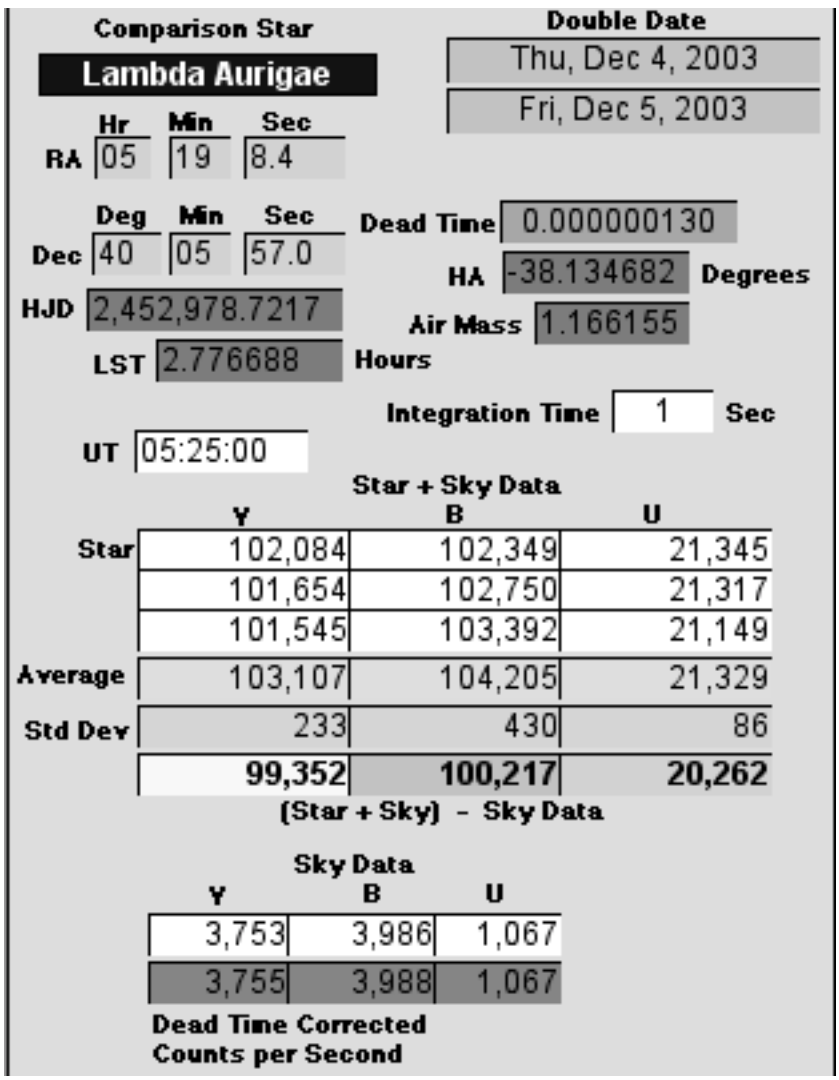

Figure 9.39 FMP Observation Data Entry

9.2.9.4 Final Data Reduction

While it will be tempting to use the same table as used for the data entry for final data reduction, it is better to create a separate table for the final reduction. All the observation data can be automatically entered into the data reduction table and all calculations performed automatically. This table can be an archive and data can be found, sorted and exported as well as lists printed.

Julian Date	2,453,013		
Double Date	Thu, Jan 8, 2004		
	Fri, Jan 9, 2004		
	ETIM V	ETIM B	ETIM U
Comp Star	4.6236	5.1791	5.2026
Prog Star	2.9363	3.4319	3.4959
Comp Star	4.6238	5.1825	5.2042
Diff Mag 1	1.6874	1.7488	1.7075
Star Mag 1	3.0226	3.5912	3.7525
Comp Star	4.6238	5.1825	5.2042
Prog Star	2.9395	3.4426	3.4939
Comp Star	4.6256	5.1813	5.2114
Diff Mag 2	1.6851	1.7393	1.7139
Star Mag 2	3.0249	3.6007	3.7461
Comp Star	4.6256	5.1813	5.2114
Prog Star	2.9490	3.4408	3.4984
Comp Star	4.6145	5.1729	5.1968
Diff Mag 3	1.6710	1.7363	1.7057
Star Mag 3	3.0390	3.6037	3.7543
Avg Mag	3.0288	3.5985	3.7510
SD	0.0089	0.0066	0.0043
# Obs	3	3	3

Figure 9.40 FMP Final Data Reduction

9.2.10 Data Analysis

9.2.10.1 Plotting Data

Reduced photometric data consists of a star's extraterrestrial magnitude (as would be seen outside the Earth's atmosphere) as observed through a photometric filter versus time. The time is usually expressed in Julian Date or Heliocentric Julian Date.

There are three types of plots used with photometric data, time domain, phase (which is a form of a time domain plot) and frequency domain plots.

9.2.10.2 Time Domain

A time domain plot is a plot of magnitude (vertical or y axis) versus time (horizontal or X axis). This shows how the star system's magnitude varies over time. The plot can extend over many cycles. The Y axis is usually reversed so that toward the top is more negative indicating a brighter data point. If data is in the form of a text file with date as Julian Date to a few decimal places and the second column the corresponding magnitude, the data can be imported directly into a graphics program or spreadsheet program like Excel. In Excel, by selecting the two columns of imported data they can be used to generate a plot. Labels can be added and scales arranged.

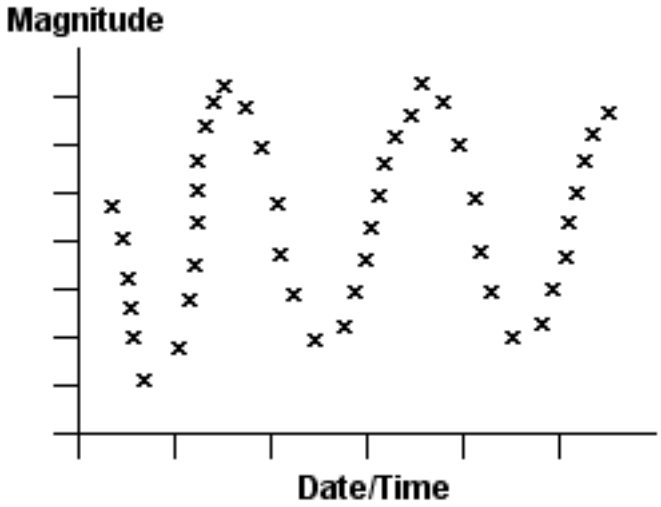

Figure 9.41 Time Domain Plot

9.2.10.3 Phase

A phase plot is like a time domain plot except that only one cycle is shown. Data from multiple cycle is added to the plot to create a folded plot to show the actual phase more accurately. To create a phase plot it is necessary to know the period accurately. It is also necessary to have a star that has a repeatable period. A star that varies randomly or that the period changes rapidly cannot have a meaningful phase plot generated. Figure 9.42 shows a sample phase plot.

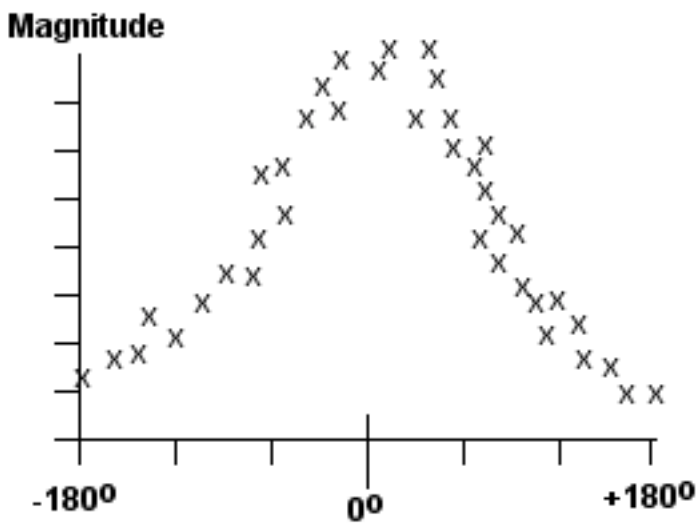

Figure 9.42 Phase Plot

If the data do not form a nice plot the period may be wrong. A slightly off epoch can shift the zero point right or left of the center. While in itself the phase plot does not tell much, it is more of a confirmation of the correct epoch and period. It can show a good representation of what the shape of the variation is, however. If the plot is very scattered then probably the period assumption is wrong or the data is not a fixed period data set.

9.2.10.4 Frequency Domain

A frequency domain plot is a plot of magnitude (vertical or y axis) versus frequency (horizontal or X axis). See Figure 3.43. This shows how the star system's variation frequencies vary in magnitude. This is useful for determining the period or periods of star system variations. Some variable stars have complex periods and careful analysis of the data must be made to obtain useful information. With care, frequency domain analysis can produce useful information.

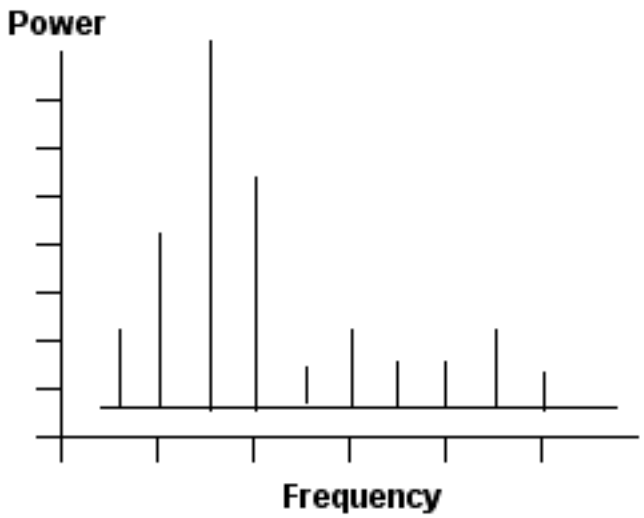

Figure 9.43 Frequency Domain Plot

Wave shapes, whether electrical or those created by data plots can be thought of as being created out of one or more since waves. Adding multiple sine waves together can produce different wave shapes.

Much can be learned about data by studying the frequency domain part of it. This is done extensively for Radar and other electronic signals. Electronic spectrum analyzers can display the spectral line of an electronic signal. If in place of a signal there are data points, the same can be done using a mathematical transform that finds the frequencies that make u the shape of the data. This is known as Fourier Transform. While difficult to calculate manually, computers do this easily. As an illustration of the transform, four types of time series data are used. One produces a sine wave pattern, another a square wave pattern, another a triangular wave

pattern and finally a sawtooth wave pattern. These all have a base frequency of 100 Hz. The top part of the diagrams show a time series plot while the bottom shows the frequency domain plot.

9.2.10.4.1 Sine Wave

A pure sine wave (see Figure 9.44) will have a frequency domain plot of a single narrow line at the frequency of the sine wave. There will be no other peaks. This is because the sine wave has only that one frequency sine wave in it.

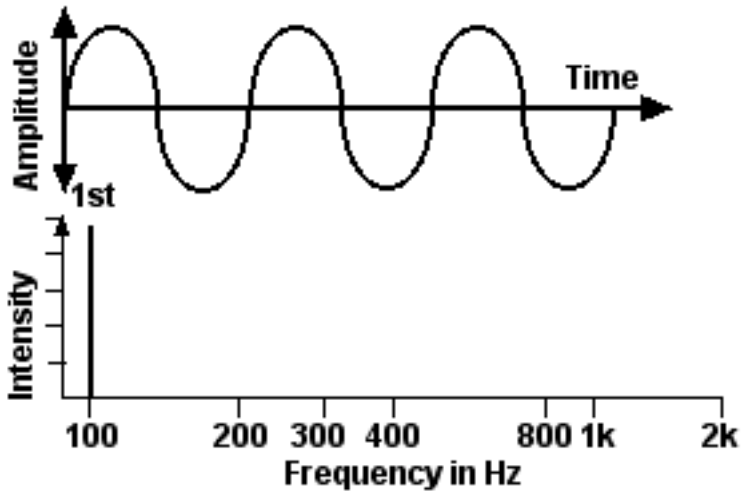

Figure 9.44 100 Hz Sine Wave

9.2.10.4.2 Square Wave

A more complex wave is a square wave. see Figure 9.45. A square wave consists of only odd harmonics.

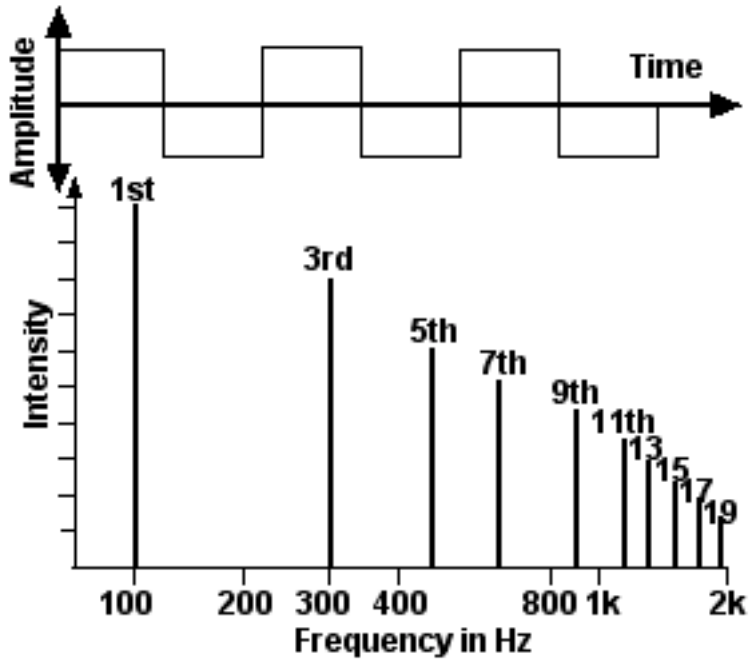

Figure 9.45 100 Hz Square Wave

9.2.10.4.3 Triangular Wave

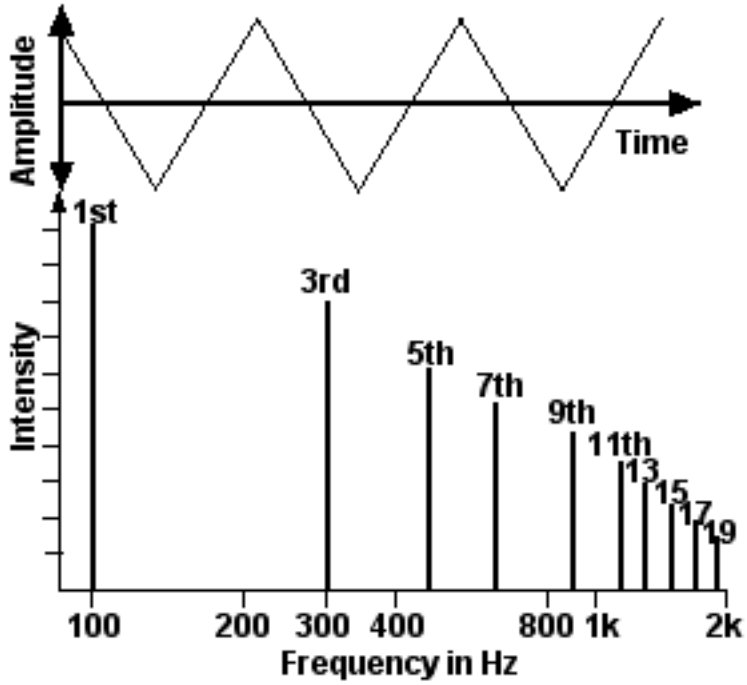

Figure 9.46 100 Hz Triangular Wave

Note: The square wave and triangular wave frequency domains look the same. Indeed, they both contain only odd harmonics. With the triangular wave the higher harmonics (not shown in the figure) roll off much faster than the square wave (proportional to the inverse square of the harmonic as opposed to just the inverse).

9.2.10.4.4 Sawtooth Wave

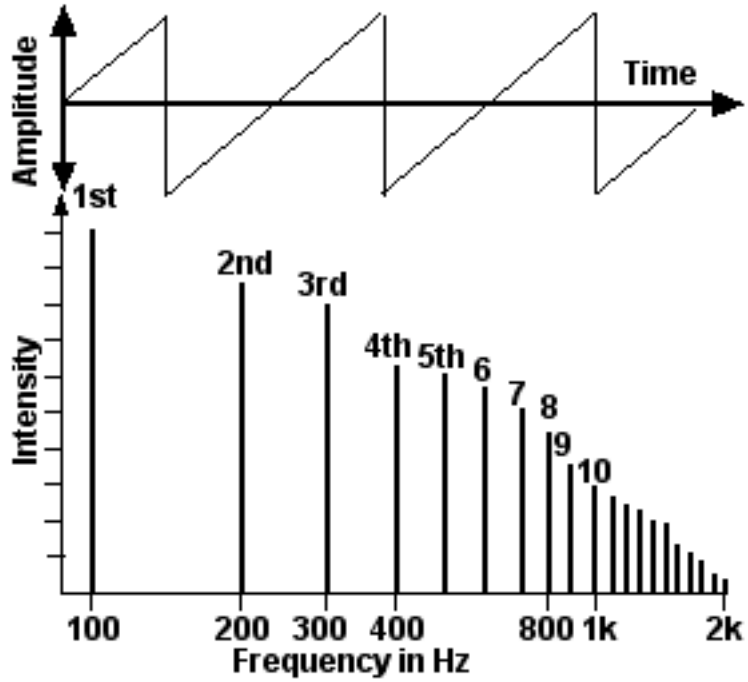

Figure 9.47 100 Hz Sawtooth Wave

9.2.10.4.5 Peranso

Peranso, a light curve and period analysis software program, is specifically designed to take data such as photometric data points of a varying star system and analyze the data an produce a frequency domain plot also known as a Period Plot. This is a windows based program. A demonstration program and more information can be found at:

http://www.peranso.com/

To use Peranso you must first import data from a txt file. The file name must have a .txt at the end and it must be a text only file. It should have a date and magnitude for each line. Date and magnitude should be separated by a tab. Line should be delimited by a carriage return (paragraph mark).

Figure 9.48 shows a time domain (time series) plot of HPO V data for the 2007/2008 season.

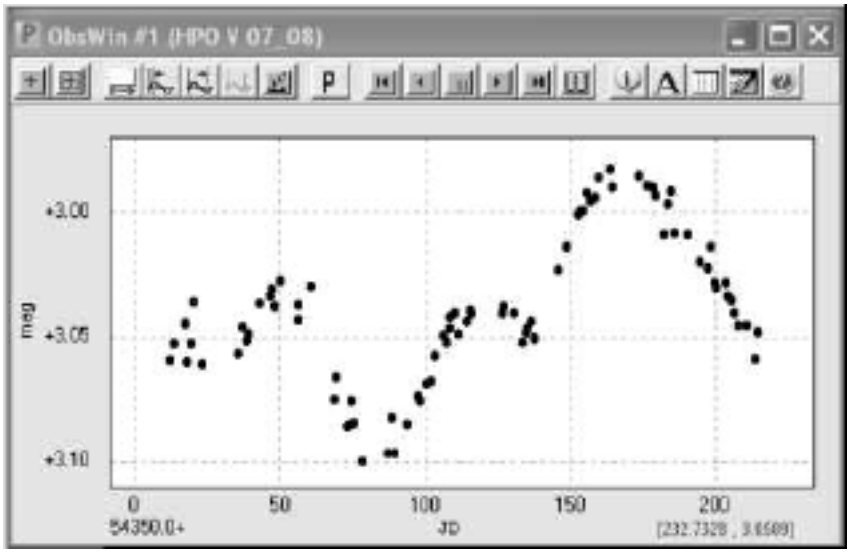

Figure 9.48 Peranso V Data

Figure 39.49 shows a resulting frequency domain plot of period window. The Discrete Fourier Transform DFT (Deeming) method was used to create this. The vertical dashed line is a cursor that can be mover back and forth to display the frequency or period at that point.

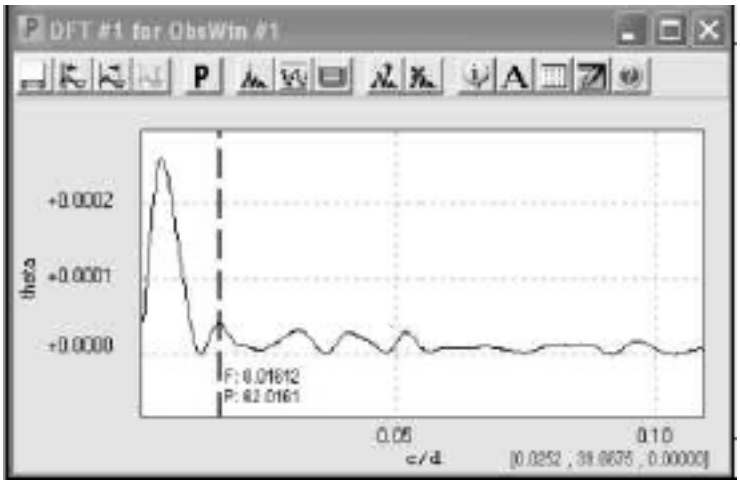

Figure 9.49 DFT Frequency Domain

Once the transformation has been calculated a list of the prominent periods in the frequency domain plot can be listed. While there may be a large spike, many times that is due to the seasonal period rather than the actual variation of the data. Figure 9.50 shows the Prominent Period list for the above data.

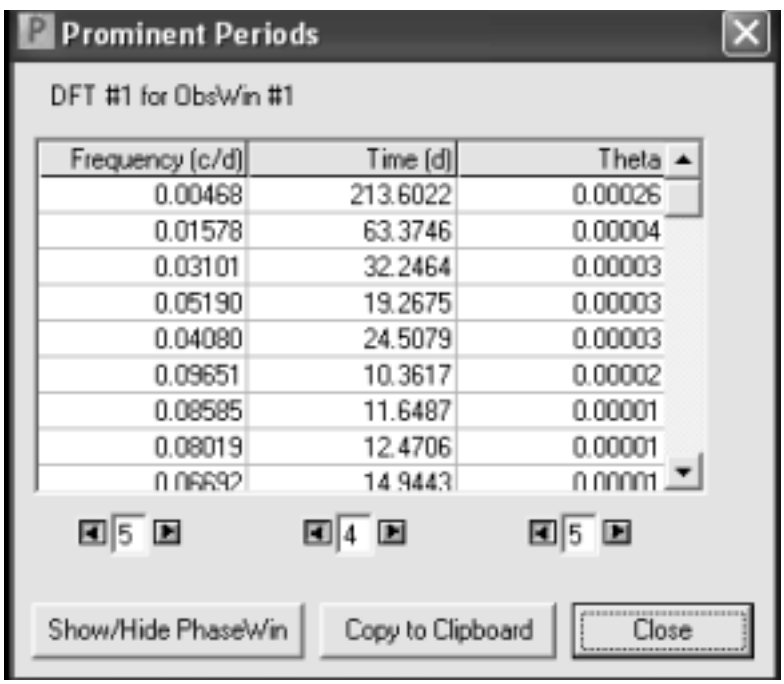

Frequency (c/d)	Time (d)	Theta
0.00468	213.6022	0.00026
0.01578	63.3746	0.00004
0.03101	32.2464	0.00003
0.05190	19.2675	0.00003
0.04080	24.5079	0.00003
0.09651	10.3617	0.00002
0.08585	11.6487	0.00001
0.08019	12.4706	0.00001
0.06692	14.9443	0.00001

Figure 9.50 Prominent Periods

An extensive set of period analysis methods to detect periodicities in variable star and asteroid time-series data is provided in Peranso. The following is a list of different methods that can be selected. Most of the work done on the epsilon Aurigae

photometry data uses the Discrete Fourier Transform created by Deeming.

The following is a Peranso Processing Techniques List

Lomb-Scargle

Bloomfield,

Discrete Fourier Transform DFT (Deeming)

Date Compensated Discrete Fourier Transform DCDFT (Ferraz-Mello),

CLEANest (Foster), Jurkewich,

PDM (Phase Dispersion Minimization)

Dworetsky, Renson, Analysis of Variance ANOVA (Schwarzenberg-Czerny)

Phase-binned AoV (Schwarzenberg-Czerny)

Lafler-Kinman, EEBLS (Kovacs) for exoplanet transits, FALC.

9.3 Spectroscopy

9.3.1 Introduction

Anyone who has looked at a rainbow has surely found them interesting and beautiful, but few people understood what they were seeing. It took Sir Isaac Newton (1642 - 1727) to show what caused the rainbow and some deeper characteristics of light. Newton took a glass prism and allowed a sliver (light through a small slit) of light to fall on it. What was seen on the other side of the prism was a rainbow of colors. White light was broken down into rainbow colors.

9.3.2 Spectra

What Newton then did was to focus the rainbow of colors with a lens and pass the resulting beam through another prism which then produced the original beam of white light. He carried this further with his famous blue light experiment. He blocked all the rays (colors) coming out of the first prism except the blue portion. He then fed the blue ray through the lens and into the second prism. What came out of the second prism was not white light, but the unchanged blue ray. From this he deduced that light is composed of many single colors and when put together produced white light. This was the beginning of spectroscopy, a very slow beginning.

Physicists and astronomers continued to experiment with light. Experiments were performed with different elements. Some elements gave off different colored light. By examining this light it

was discovered that each element gave of a unique spectrum, a unique set of bright lines. For example, holding salt crystals (sodium chloride) in a flame produce a yellow flame. Examining the yellow light showed two very bright yellow lines. These are now known as the sodium D lines (with wavelengths of 588.9950 and 589.5924 nanometers).

In the early 1800's German physicist Joseph von Fraunhofer (1787–1826) noted that the expanded spectra of the Sun had some dark lines in it. These are now known as Fraunhofer lines. Also during the early 1800's British astronomer William Hyde Woollaston (1766-1828), using a prism, observed that the Sun emitted a continuous spectrum that had 784 dark lines. These were the lines Fraunhofer had noted. Fraunhofer realized that some of these dark lines were at the same position in wavelength as bright emission lines of spectra of various elements which were studied in the laboratory. It is now known that there are thousands of these lines and they represent 67 different elements found in the Sun.

In the mid-1800's German physicist Gustav Kirchoff (1824 -1857) experimented with the spectra of light. He formulated three empirical rules of spectra analysis:

Rule 1
A hot opaque solid, liquid or gas which is under high pressure will emit a continuous spectrum.

Rule 2
A hot gas under low pressure (i.e. much less than atmospheric) will emit a series of bright lines on a dark background. Such a spectrum is called a bright line or emission spectrum.

Rule 3
When light from a source that has a continuous spectrum is shone through a gas at a lower temperature and pressure, the continuous spectrum will be observed to have a series of dark lines superimposed on it. This kind of spectrum is known as a dark line or absorption spectrum.

For many years science did not understand how the bright and dark spectra lines were created. Almost all the ideas were from empirical efforts.

It wasn't until 1913 that Danish physicist Niels Bohr (1885 - 1962) managed to explain the spectrum of the element hydrogen. In a simplified model of the hydrogen atom the nucleus (a single proton) is orbited by a single electron. The atom can have different states where the electron's orbits are different. When the orbit changes from a higher or more energetic orbit to a lower orbit, a photon is emitted with energy equal to the difference of the energy levels. When a photon of the right frequency interacts with an electron, the electron's energy state is raised and the photon absorbed. Only discrete jumps are permitted and none between these specific levels. This means only photons of specific wavelengths/frequencies can be absorbed.

According to the Bohr model of the hydrogen atom, electrons exist in quantized energy levels. These energy levels are described by a principal quantum number **n**. Where n is an integer 1, 2, 3, ... Electrons may only exist in and may transit between these states.

The energy (**E**) of the photon emitted or absorbed is equal to Planck's Constant (**h**) times its frequency (**ν**).

$$\mathbf{E = h * \nu}$$

Planck's Constant $\mathbf{h = 6.626 \times 10^{-27}}$ **erg-sec**

The frequency of the photon is inversely proportional to its wavelength and equal to the speed of light **c** divided by the wavelength **λ**. Because of the extremely high frequencies of light, photons are usually described by their wavelength in Angstroms or nanometers. One Angstrom is equal to 0.1 nanometers or 1×10^{-10} meters.

$$\nu = c/\lambda$$

Thus

$$E = h * c/\lambda$$

A convenient relationship to know when transforming from wavelength (λ) to energy (E) is E(eV) ~ 1240 / λ (nm).

Hydrogen has several series or sets of energy states. See Table 9.2. They are known as the Lyman, Balmer, Paschen, Brackett, Pfund and Humphreys Series.

.

Series	n	λ(nm)		Series	n	λ(nm)
Lyman	2	122		Brackett	5	4050
	3	103			6	2630
	4	97.2			7	2170
	5	94.9			8	1940
	6	93.7			9	1820
	∞	91.1			∞	1460
Balmer	3	656		Pfund	6	7460
	4	486			7	4650
	5	434			8	3740
	6	410			9	3300
	7	397			10	3040
	∞	365			∞	2280
Paschen	4	1870		Humphreys	7	12372
	5	1280			8	7503
	6	1090			10	5129
	7	1000			11	4673
	8	954			13	4171
	∞	820			∞	3282

Table 9.2 Hydrogen Series

See Figure 9.51 for an energy diagram of the Lyman, Balmer, Paschen and Brackett Series.

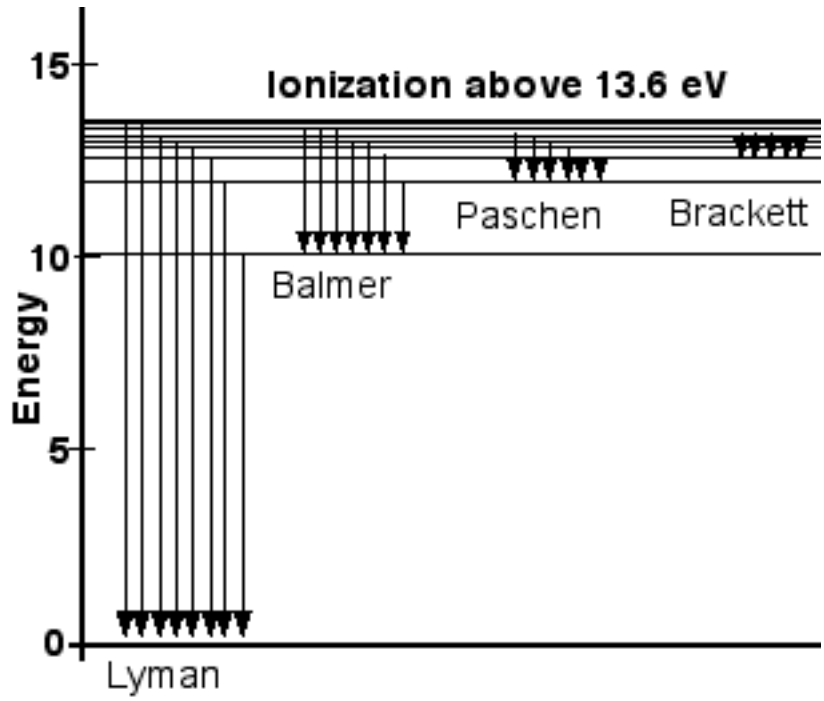

Figure 9.51 p/o Hydrogen Transition Series

In the Balmer Series, transition from n= 3 to n= 2 is called the hydrogen alpha (Hα) transition. The Hα line has a specific wavelength of 6562.8 Angstroms or 656.28 nanometers. This is visible in the red part of the electromagnetic spectrum. See Figure 9.52.

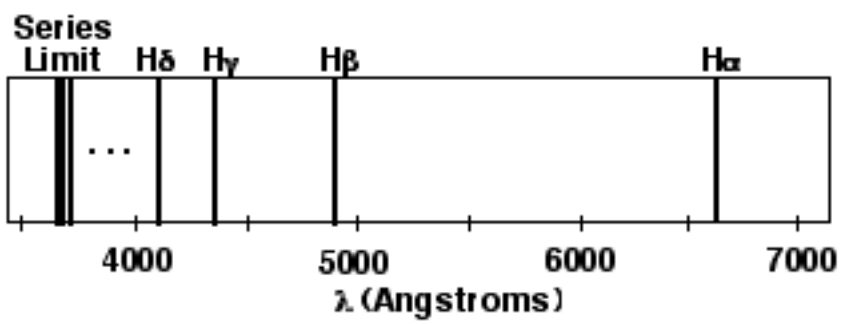

Figure 9.52 Hydrogen Balmer Spectrum

Since it takes nearly as much energy to excite the hydrogen atom's electron from n = 1 to n = 3 as it does to ionize the hydrogen atom, the probability of the electron being excited to n = 3 without being removed from the atom is very small. Instead, after being ionized, the electron and proton recombine to form a new hydrogen atom. In the new atom, the electron may begin in any energy level, and

subsequently cascades to the ground state (n = 1), emitting photons with each transition. Approximately half the time, this cascade will include the n = 3 to n = 2 transition and the atom will emit Hα light. Therefore, the Hα line occurs where hydrogen is being ionized.

9.3.3 Types of Spectra

There are three types of spectra, Continuous, Emission and Absorption Spectra.

9.3.3.1 Continuous Spectra

A Continuous Spectrum such as that produced by the Sun is the result of very hot gases containing atoms with high kinetic energy in collision. While elements produce their discrete spectral lines, the lines get blurred and as a result a continuous spectrum without individual emission lines is produced.

9.3.3.2 Emission Spectra

An Emission Spectrum is produced when atoms are less excited as with the Continuous Spectra gas. An individual atom's unique spectral lines or the lines of many different elements can be seen as the atom's electron states drop to lower levels and emit photons. These lines are seen against a dark background.

9.3.3.3 Absorption Spectra

When photons from a continuous spectrum pass through a gas made up of one or more elements, the specific lines for each element will absorb photons of the wavelengths for those specific lines. This produces a continuous spectrum with holes in it, dark lines where photons of that frequency were absorbed. These are the Fraunhofer lines seen in the spectrum of the Sun. The Sun produces a continuous spectrum, but as the light goes through the

atmosphere of the Sun, elements in the atmosphere absorb photons that are of their specific energy levels.

9.3.3.4 Stellar Spectroscopy

Since the spectrum of a light source can tell so much about the source, spectroscopy is ideal for studying distant astronomical objects.

Stellar Spectroscopy is the study of the spectra of starlight. Much can be learned about distant stars by analyzing the star's spectrum. Remember, like our Sun, other stars will produce a continuous spectrum, but the star's atmosphere acts like a filter and shows what elements are in the atmosphere as well as a host of other information.

In many cases multiple lines for a given element can be seen. The lines are shifted slightly up or down in wavelength due to the stars motion and other phenomena. When seen, this is an indication of a multiple star system even though only one star can be resolved visually from Earth. When two sets of lines are seen this is known as a spectroscopic binary star system. By analyzing the spectral lines much more information can be learned. The spectroscopic binary systems are also good candidates for photometric study as they may be eclipsing binaries.

9.3.4 The Shape of a Spectral Line

The shape of a spectral line is influenced by a number of processes occurring in the stellar atmosphere. According to its intensity a line's shape or profile is described as being weak, strong or very strong .

The three main processes that affect the shape of a spectral line are collisional broadening, Doppler broadening and rotational broadening. In addition a lesser effect called the Zeeman effect can also cause splitting of the spectral lines as well as a Stark effect.

9.3.4.1 Collisional Broadening

If two atoms collide, the electrons of each atom will repel each other and distort their respective energy levels. If a collision happens when one of the electrons is interacting with a photon, then the photon's energy will be altered from the value it would have had if the atom was in an undisturbed state. In a gas that is at a moderate temperature and density, collisions between atoms are infrequent and so interaction is likely to happen when the atom is undisturbed. Higher temperatures and pressures cause the photon energies to vary over a considerable range. This spread of energies relates to a spread of frequencies/wavelengths and causes the spectral line to be widened or broadened.

9.3.4.2 Doppler Broadening

Due to their thermal energy, atoms in a star's atmosphere have random velocities. At any instant some of the atoms travel towards us and others away when they emit or interact with photons. This produces a Doppler shift of the absorption lines. Doppler broadening is a lesser effect than collisional broadening.
The approximate broadening is given by:

$$\Delta\lambda = \lambda_0 * v / c$$

Where is the change in the wavelength is $\Delta\lambda$, λ_0 is the stationary spectral line wavelength, **v** is the velocity of the atom that interacted with the photon and **c** is the velocity of light.

9.3.4.3 Rotational Broadening

A star that is rotating will produce a Doppler shift of each absorption line of the star's atmosphere's spectrum. The amount of broadening depends on rotation rate and the angle of inclination of the axis of rotation to the line of sight. This effect can be used to calculate the rotation rate of the star. Assuming the axis of rotation is perpendicular to the line of sight with Earth. If the change in wavelength of a line at wavelength λ is $\Delta\lambda$, then the velocity **v** of atoms on the limb of a rotating star is given by:

$$v = c * \Delta\lambda / \lambda$$

If we know the radius **R** of the star then the period **P** of rotation can be calculated from:

$$P = 2 * \Pi * R / v$$

Astrophysicists have found that, in general, the hottest stars (type O and B) rotate the fastest with periods as fast as 4 hours. G-type stars like the sun rotate fairly slowly at about once every 27 days.

9.3.4.4 Zeeman Effect

Electrons in atoms are moving charges that constitute rings of electric current. This produces a magnetic field similar to that of a bar magnet. This causes the spectral lines to become split and is called the Zeeman Effect.

It is possible to relate the degree of splitting to the strength of the external magnetic field and astrophysicists can obtain information about a star's magnetic field distribution. Zeeman splitting is particularly useful in the study of sunspots which have very intense magnetic fields and produce pronounced splitting in the absorption spectrum of the sun.

9.3.4.5 Stark Effect

Like the magnetic field of the Zeeman Effect, an electric field produces a similar spilt and is called the Stark Effect. This is not normally seen in astronomical spectroscopy.

9.3.5 Stellar Spectra Classification

The changes in intensity of the absorption lines with temperature allows creation of a spectral classification system. The first person to attempt to do this was the Italian astronomer P.A. Secchi who in 1860 classified stars into four distinct groups based on their spectral features. The modern scheme is called the MK system (devised by W.W. Morgan, and P.C. Keenan). To be classified, a star is assigned a Spectral Type and a Luminosity Class.

9.3.5.1 Spectral Type

The spectral type of a star is designated by one of seven letters O, B, A, F, G, K, M, starting with the hottest type (O type) to the coolest type (M-type). The table below shows the temperatures and characteristic features in the star's spectrum that distinguish spectral types. Table 9.3 shows a list of MK of Spectral Types.

	Surface Temp/K	Spectral Type
O	20 000	ionized helium (He II)
B	20 - 10 000	neutral helium, hydrogen lines start to appear
A	10 - 7000	strong neutral hydrogen (Balmer lines) visible
F	7000 - 6000	ionized calcium (Ca II) visible, hydrogen lines weaker
G	6000 - 5000	ionized Ca II very prominent, much weaker neutral H lines, also other metallic lines such as Iron (the sun is a G-type star)
K	5000 - 3500	neutral metals such as Ca and Fe prominent, molecular bands visible
M	3500 - 2000	molecular bands very visible, those particularly of Titanium Oxide (TiO)

Table 9.3 MK of Spectral Types

The classification of stars into spectral types is actually more complex . Each type can be subdivided into at least 10 subdivisions so that one might refer to a star of type A5 lying halfway between type A0 and F0. The spectral type order is commonly remembered by the mnemonic 'Oh Be a Fine Girl (or Guy) Kiss Me'!

3.3.5.2 Luminosity Classes

For a given temperature, some stars are more luminous than others. This is usually because the star is larger and its outer atmosphere more tenuous and at a lower pressure than a fainter star. The spectral lines of very luminous stars are much narrower since the effects of line broadening due to collisions is much less and the line profile is sharper. Stars can be further classified for each spectral type in terms of luminosity on the basis of the 'sharpness' of their spectral lines. These luminosity classes are denoted by Roman

numerals and are divided into seven star-types: Table 9.4 shows a list of Luminosity Classes

I	Supergiant Stars
II	Bright Giant Stars
III	Giant Stars
IV	Subgiant Stars
V	Main Sequence Dwarf Stars
VI	Sub Dwarf Stars
VII	White Dwarf Stars

Table 9.4 Luminosity Classes

Some luminosity classes, particularly those of the supergiants, are subdivided into suffixes **a**, **ab** and **b** and a class written as III-IV means a star with characteristics midway between the two classes.

The full spectral classification thus consists of [Spectral type] [number] [Luminosity Class] [suffix (if any)].

For example, the sun is classified as a G2V star. Betelgeuse, a red giant is classified M2Iab. epsilon Aurigae is classified F0I.

A good source of spectral types of stars can be found in many astronomy textbooks and on the web at:
http://simbad.u-strasbg.fr.

9.3.5.3 Chemical Composition

The dark spectral lines observed in a star's spectrum arise from the chemical elements present in the stellar atmosphere. Each element leaves its 'signature' in the form of a pattern of dark spectral lines corresponding to its electron shell structure.

At first it may seem that the more intense the spectral line pattern is, then the more of that element the star contains. However, a faint set of absorption lines can be due to the fact that the high temperature of a star means that not all the electrons of an element are in the correct initial energy levels in order to produce a particular line.

In order to calculate the relative abundances of the chemical elements in the stars, for an element, it is necessary to estimate what fraction of atoms are in the first excited state, what fraction in the second and so on.

It is found that for the majority of stars, the chemical composition is very nearly the same. By mass, most stars contain about 72% hydrogen, 26% helium and the remaining 2% is made up of other elements (notably iron) in roughly equal abundances.

9.3.5.4 Radial Velocities

The wavelength of a spectral line is affected by the relative motion of the star and the observer. Due to the Doppler effect, light from a star will be shifted to the blue end of the visible spectrum if it is approaching the observer and shifted to the red end if it is receding. The same equation used for the Doppler Broadening above applies for a Doppler shift due to a radial velocity.

$$\Delta\lambda = \lambda_0 * v / c$$

where v is the radial velocity (the velocity of the star as measured along the line of sight of the observer in the manner of a 'radius' drawn from the earth to the star). A negative v (a star moving away from the observer) will produce a shift in wavelength to a longer wave length. A positive v (a star moving toward the observer) will produce a shift toward a shorter wavelength.

9.3.6 Spectroscopy Equipment

9.3.6.1 Introduction

While photometry can be done on faint stars with most equipment, spectroscopy is much more demanding., because the light of a spectrum is spread out, modest sized telescopes can only produce good spectra of very bright stars. Even with a 16" telescope, using a high resolution grating (e.g., 2,400 lines/mm)), stars fainter than 7th magnitude become a challenge. For spectroscopy, aperture rules. Since epsilon Aurigae is a 3rd magnitude star, even an 8" telescope is sufficient to produce good spectra in a short time. While there are several means used to produce stellar spectra, the most popular is to use a diffraction grating. Prisms can be used, but

diffraction gratings are usually preferred. Assuming you have a suitable telescope, commercial spectroscopy equipment is available. These devices are called spectrographs.

What are the differences between spectrum analyzers, spectrometers, spectroscopes and spectrographs?

Spectrum Analyzer

Spectrum analyzers are usually designed to operate at lower frequencies (radio and microwave bands) and use electronic tunable filters to display the energy in specific areas of the microwave or radio bands on an oscilloscope display.

Spectrometer

A spectrometer is designed to measure properties of light over a specific portion of the electromagnetic spectrum, typically in the optical region. It may use a prism or diffraction grating.

Spectroscope

A spectroscope may use either a prism or diffraction grating and is designed for the spectrum to be viewed directly by the eye.

Spectrograph

A spectrograph usually uses a diffraction grating and is usually (not necessarily, however) defined to be used with a camera., digital or film. Generally a spectrograph is more accurate than a spectrometer. The following sections provide a review of some commercially available spectrographs.

9.3.6.2 Star Analyser 100 (under $200.00)

Certainly the Star Analyser spectrograph is by far the simplest and least expensive. While it will not produce high resolution spectra, it can provide a good starting point.

The Star Analyser 100 is a high efficiency 100 lines/mm transmission diffraction grating, blazed in the first order. It is mounted in a standard 1.25 inch diameter threaded cell. It has been designed to make the production of low resolution spectrum images

of stars as easy as possible. It complements a wide range of types of camera used in astro-imaging. A locking ring is supplied to lock the grating in the desired orientation. The Star Analyser 100 provides an excellent and low cost approach for the amateur to astronomical spectroscopy. See Figure 9.53 and
http://www.patonhawksley.co.uk/staranalyser.html

Figure 9.53 Star Analyser 100

Star Analyser spectra of Delta Virginis (Top) and Vega (Bottom) can be seen in Figure 9.54

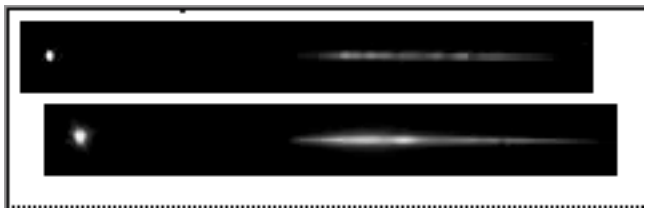

Figure 9.54 Star Analyser Spectra

The Star analyzer can be fitted directly to the bottom of an eyepiece threaded for filters. Note that, since the device is designed primarily for small camera sensors, the spectrum image will be rather short. The length of spectrum can be increased by increasing the distance between the Star Analyser and the eyepiece.

9.3.6.3 SBIG SGS ($4,995)

The Self-Guiding Spectrograph is designed to be used with an ST-7E camera. The spectrometer and ST-7/8 are coupled and mounted as a unit onto the telescope (See Figure 9.55). The system is quite handy for collecting spectra since both the object of interest and the spectrometer entrance slit are simultaneously imaged onto the

tracking CCD, allowing the object to be viewed and accurately placed onto the slit. The slit is backlit by an LED during the setup so it clearly shows on the tracking CCD. Once the object is maneuvered onto the slit, self guiding will then hold the object on the slit. See **http://www.sbig.com/sbwhtmls/online.htm**

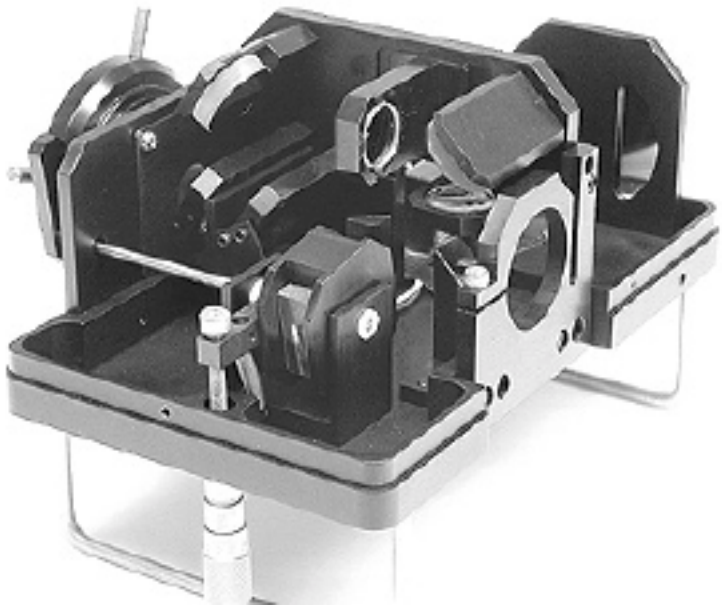

Figure 9.55 SBIG SGS Spectrograph
Photo Credit: SBIG Web Site

Input F/number	F/6.3 x F/10
Dispersion	High Res = 1.07 Å / pixel
	Low Res = 9 Å/ pixel
Resolution with	High Res = 2.4 Å
9u pixels (ST-7)	Low Res = 9 Å
Spectral Range	High Res = 820 Å
(ST-7)	Low Res= 3290 Å
Projected width of narrowest slit on CCD	18 microns
Blur perpendicular to slit	~ 100 microns
Lower resolution slit choices	72 microns
Relative Sensitivity for dim extended objects near Hα	1X

Dimensions 3 x 4 x 7 in ; Weight (excluding camera) 1.5 lb.

Figure 9.56 shows three sample spectra taken with the SGS. The top one is of Betelgeuse, second is Aldebaran and bottom is Sirius.

A spectra is Hβ line at 4,861.3 Angstroms

B spectra is Mg lines at 5,167.3 and 5,172.7 Angstroms

C spectra is Hg emission line at 5,460.7 Angstroms

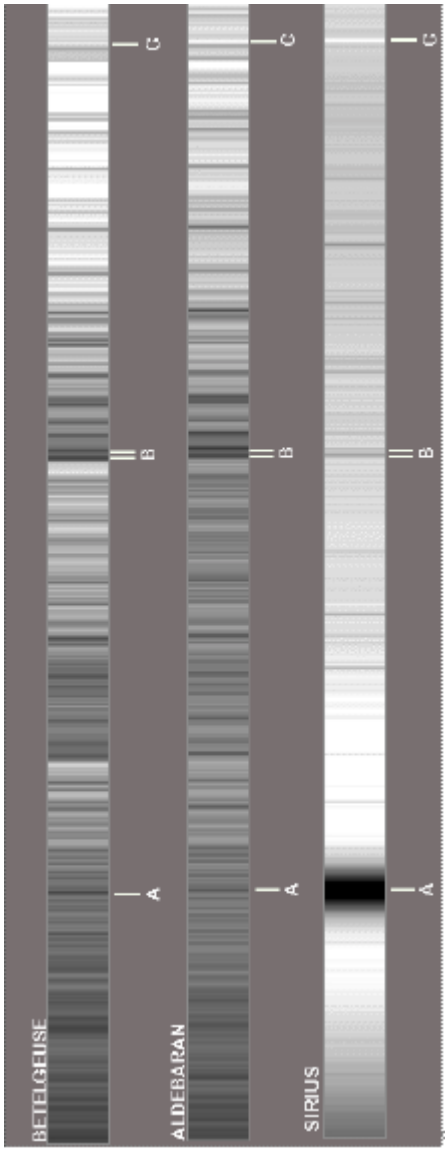

Figure 9.56 Sample High Resolution Spectra
Photo Credit: SBIG Web Site

9.3.6.4 SBIG DSS-7 ($1,595)

SBIG's Deep Space Spectrograph (DSS-7) is a spectrograph optimized for the types of spectral observations that amateur astronomers have been interested in, from stellar classification to nebular analysis to galaxy red shifts. It is a more general purpose instrument than the Self Guided Spectrograph (SGS), which is optimized for stellar work. It is optimized for the ST-7XME or the low cost ST-402, and will work well with ST-8/9/10/2000 cameras and ST-237s. It will not work with the STL series due to their deeper backfocus required by the built in filter wheel. See Figure 9.57, 9.58 and **http://www.sbig.com/sbwhtmls/online.htm**

Figure 9.57 SBIG DSS-7 Spectrograph
Photo Credit: SBIG Web Site

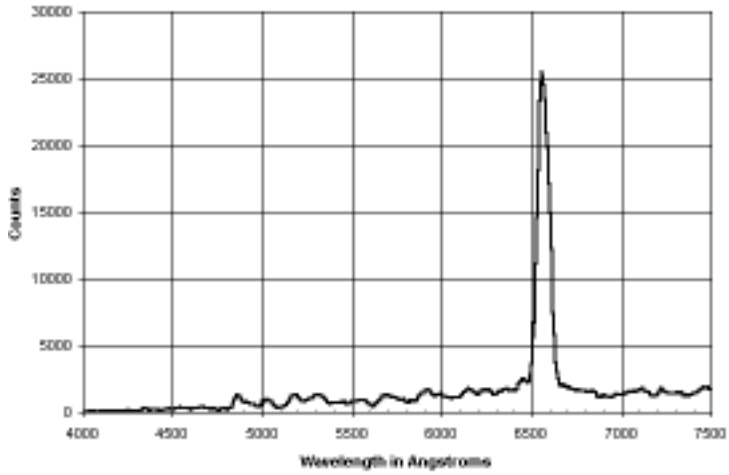

Figure 39.58 Spectrum of Nova Scorpii-2
Photo Credit: SBIG Web Site

Figure 9.58 reveals a huge hydrogen α emission line obviously broadened by the power and heat of the explosion. Visually, this star is probably a cherry red color!

Figure 9.59 shows the inside of the DSS-7.

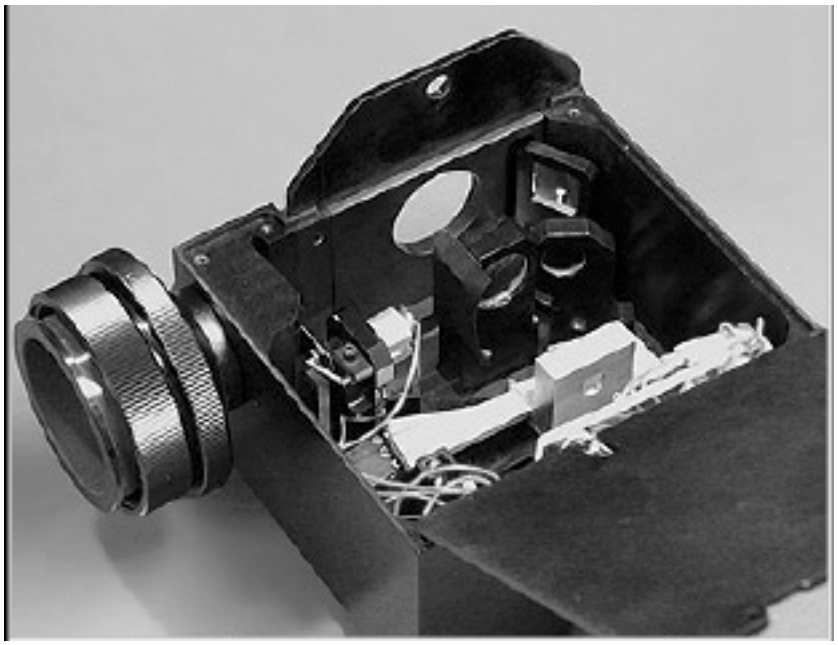

Figure 9.59 Inside the DSS-7
Photo Credit: SBIG Web Site

Input F/number	F/10
Dispersion	5.4 Å /pixel
Resolution with 9u pixels (ST-7)	15 Å
Spectral Range (ST-7)	4130 Å
Projected width of narrowest slit on CCD	25 microns
Blur perpendicular to slit	~ 25 microns
Lower resolution slit choices	50, 100 and 200 microns
Relative Sensitivity for dim extended objects near Hα	5 - 10X

Dimensions 2.2 x 4 x 4.3 in; Weight (excluding camera)1.5 lb.

9.3.6.5 Shelyak Instruments
Lhires III Spectrograph ($3,395.00)

Following a pro-am meeting in Oleron in 2003, Christian Buil and others within the AUDE association developed the Lhires III. Lhires stands for **L**ottrow **H**igh **RE**solution **S**pectrograph. See Figure 9.60, 39.61 and
http://www.astrosurf.com/thizy/lhires3/index-en.html

Figure 9.60 Lhires III Spectrograph
Photo Credit: Shelyak User Manual

Lhires III is a Littrow type reflection spectrograph, allowing high-resolution spectra to be recorded on 6-8 magnitude stars with a 8"-16" telescope on one hour or less, and with a minimum of space and weight. The dimensions of the Lhires III are 250mm x 200mm x 83mm and the weight is 1.7kg - 1.9kg (without CCD cameras). This makes the Lhires III an ideal spectrograph for amateur telescopes and mounts. A highly polished reflective slit is used for long-exposure guiding with a second camera, (webcam, video, etc.), while maintaining high spectral throughput and efficiency.

The spectral resolution of the Lhires III can be modified. The standard version uses a 2,400 lines/mm grating, giving a resolution R=17,000. With the KAF400 family of CCD cameras (Audine,

ST7,...), the spectral range is approximately 80Å with a dispersion of around 0.12Å/pixel. These values are ideal for instruments with focal ratios of f/10 and the acceptable range is f/8 - f/12. For amateurs with faster optical systems a Barlow lens can be employed to increase the f-number, but sufficient back-focus, should be checked particularly if using a Newtonian reflector. Other resolution grating units can be purchased for 1,200 lines/mm, 600 lines/mm, 300 lines/mm and 150 lines/mm. Each grating unit sells for $535.00.

A neon calibration lamp is integrated in the spectrograph for reference emission line comparison. This can be powered by an external 12 VDC power source or two 9 V batteries in series.

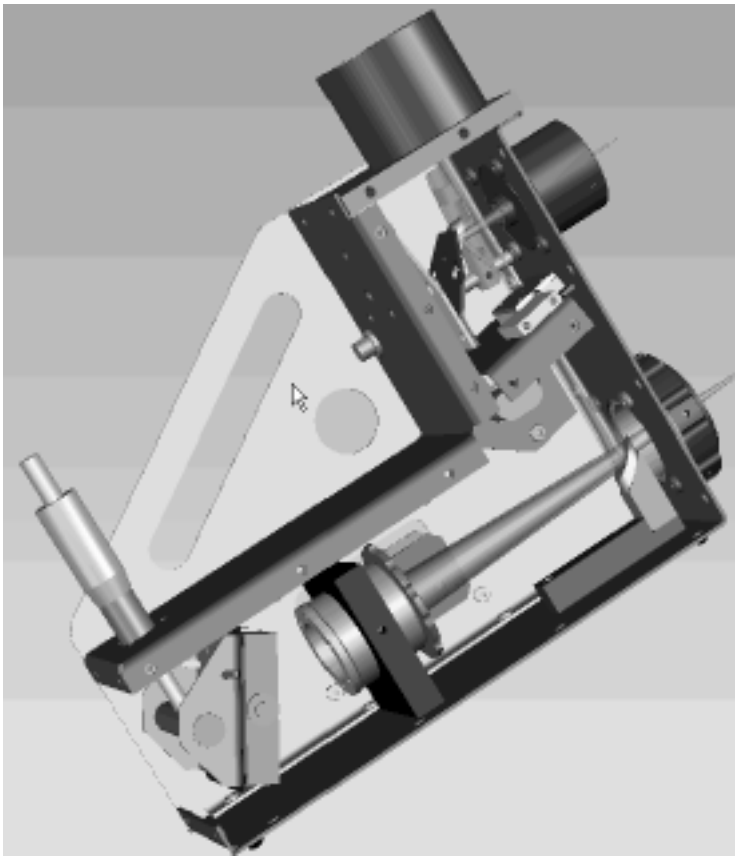

Figure 9.61 Inside the Lhires III Spectrograph
Photo Credit: Shelyak User Manual

Lhires III spectrograph has been designed for small telescopes (typically 8" f/10 telescope) and is well adapted for backyard astronomy. It can be used with several types of CCD cameras, webcams, or SLR cameras.

Figure 9.62 shows the Lhires III with two Meade DSI Pro cameras, The top camera used for guiding is a DSI Pro series 1 and bottom camera is a DSI Pro II used for imaging the spectrum.

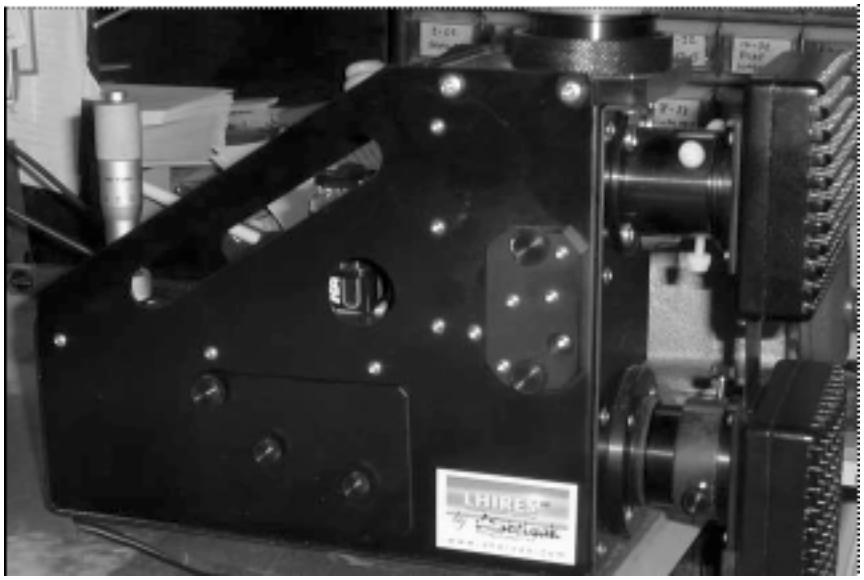

Figure 9.62 Lhires III with DSI Pro CCD Cameras

		Grating - Lhires III (lines/mm)				
		2400	**1200**	**600**	**300**	**150**
Field of View	nm	8.5	25	55	110	230
Limiting Magnitude		5.0	6.8	7.5	8.4	9.2

Table 9.5 Lhires III Parameters
(200 mm F/10 Telescope, 30 μm Slit)
From Lhires III User Manual

Telescope	**Limiting Mag S/N = 50**	**Limiting Mag S/N = 100**
128 mm F/ 8	6.5	5.6
200 mm F/ 10	6.7	5.9
280 mm F/10	7.1	6.2
355 mm F/11	7.2	6.3
600 mm F/8	8.1	7.2

Table 9.6. Lhires III Performance
(2400 line/mm, 25 μm Slit, 1 hr Exposure)
From Lhires III User Manual

9.3.7 Spectroscopy Techniques

9.3.7.1 Introduction

To use a spectrograph with a grating and slit, two CCD cameras are required. One is used to guide the telescope and keep the star centered in the slit. The other camera is used to take the exposure of the spectrum. Because the spectrum is faint even for bright stars, a time exposure of several minutes or more may be required. The slit may have a mirror finish on the telescope side and provide the star image for guiding. The Star Analyzer is different because it does not use a slit and thus only one camera is required.

Each spectrograph has its own instructions. A serious consideration is a means to calibrate the spectrum. Many people use a neon bulb to provide a set of calibrated spectral lines. The Lhires III has a built-in Neon calibrator. The calibrator uses an external 12 VDC supply, but two 9 V batteries in series works well and reduces the cabling. The batteries can be tied inside the bracket on the Lhires III.

9.3.7.2 Obtaining a Spectrum

Once the spectrograph has been adjusted the actual taking of the spectral image is straight forward. Darks should be taken and subtracted and for best result a light frame also. A calibration spectrum should be taken before and after the star spectrum to assure nothing shifted.

Figure 9.63 shows a Lhires III on the HPO 12" LX200 GPS with two Meade DSI Pro cameras. The camera closest tot he telescope (on the right) is a DSI Pro series I monochrome camera and is used as a guiding camera. It is also used to find and center the star on the spectrograph's slit. The camera to the left is a DSI Pro II monochrome camera. This is used for the acquisition of the spectrum. One reason a DSI Pro I was not used is the I series has a smaller field of view (FOV) and for hydrogen α work with a 2,400 l/mm grating the two bracketing Neon calibrations lines could not both be seen. While it is possible to calibrate with just one, a wider

FOV was desired. The DSI Pro cameras worked well for this application.

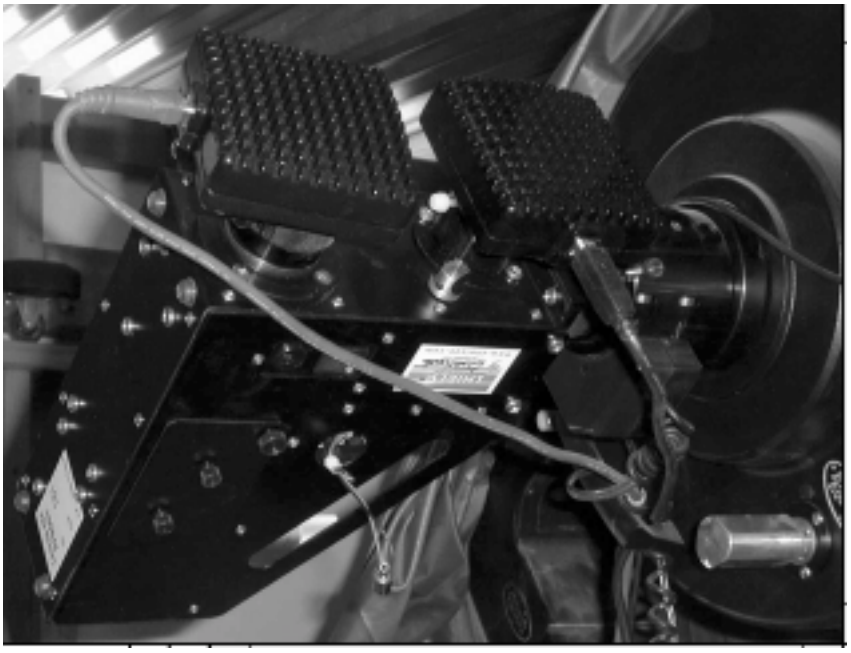

Figure 9.63 Lhires III on 12" LX200 GPS

The Lhires III is designed for work with a 12" F/10 telescope. It will work fine down to F/8. What is interesting is the limiting magnitude difference is less than one between an 8" F/10 and 16" F/10 telescope. The reason is because the star image is bigger with the 16" telescope and more of the light does not enter the slit. The unit comes with a recommended slit width of 20 μm, but can be increased up to 35 μm for a larger telescope. This will allow more of the star light to enter the slit. Increasing the slit width decreases the resolution so there is a limit as to how wide it can be and going beyond 35 μm is not recommended. Seeing also has a large effect on how much light gets through the slit.

9.3.7.3 Spectroscopy Software

There are several freeware software programs.

Iris

Iris is available http://www.astrosurf.com/buil/us/iris/iris.htm. and a tutorial at http://www.astrosurf.com/aras/tutorial1/pipeline.htm

SpcAudACE

SpcAudACE is available http://bmauclaire.free.fr/spcaudace/. This is a French version, but there is an English translation available. Documentation and a tutorial are also on the web site.

VSpec

VSpec (Visual Spec) is available at: http://astrosurf.com/vdesnoux/ and a tutorial at http://astrosurf.com/vdesnoux/tutorial.html. Each program has its own features, but generally they do similar things. The software allows spectral analysis of an object and includes several categories of operations

* Identification of the lines
* Modification of the spectral response, absolute flux, normalization, correction of the continuum, Planck's Law
* Measurements: center of the line, equivalent width, full width at half-maximum
* Identification of the lines is done based on their wavelengths.

9.3.7.3 Plancks Law

The Black Body temperature of a star obeys Planck's Law.

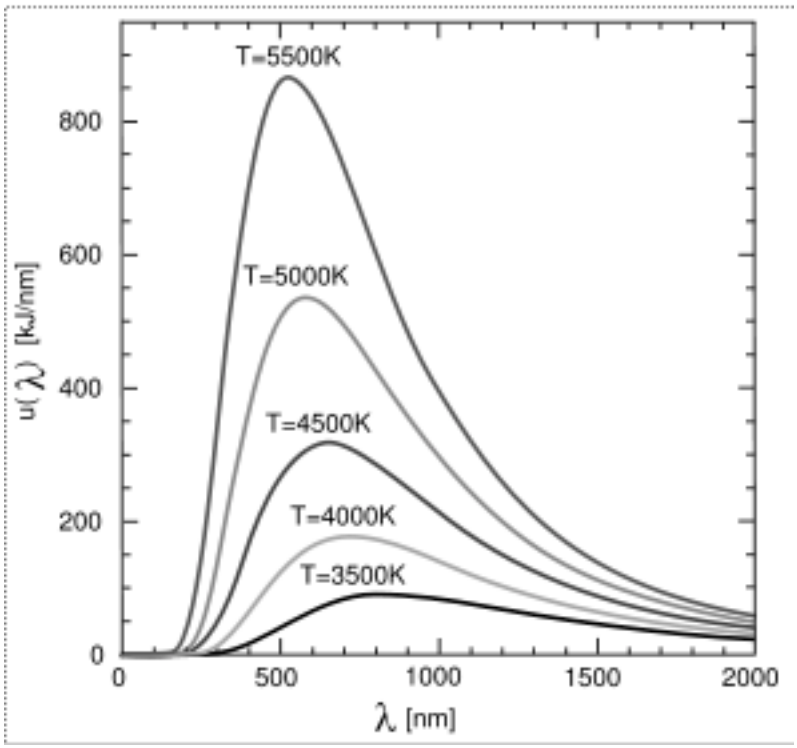

Figure 9.64 Black Body Spectrum
Photo Credit: Wikipedia

Knowing the temperature of a star allows the software to calibrate the spectrum.

9.3.7.4 Full Width Half Mean (FWHM)

Specifying a FWHM for a wave shape allows a description of that wave shape. This is useful when spectral discussing line profiles. To determine the FWHM of a curve the peak is determined. Then the width of the curve halfway to the bottom is the FWHM of the curve.

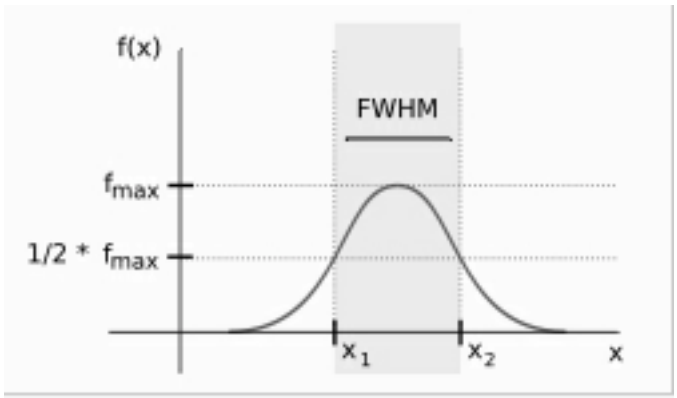

Figure 9.65 Full Width Half Mean
Photo Credit: Wikipedia

9.3.7.4 Equivalent Width (EW)

Expressing a line profile's parts Equivalent Widths allows expressing of the part's significance. The area under the curve between the profile part and the continuum is the EW of that part. The area is equal to the Intensity (normalized to 1.0 for the continuum) times EW in angstrom (Å).

Figure 9.66 show a diagram of an emission spectral curve. The area between the curve and the continuum is the EW of the curve. There is some debate on the sign of the EW. In the days of film spectroscopy it seems areas below the continuum (absorption lines) were considered positive while curves above the continuum (emission lines) were considered negative. This is a bit against common sense as usually values above a line a positive and negative below the line. In fact many professional papers in the last few years use the emission EW as positive and absorption EW as

negative. The bottom line is it is best to specify what convention is used when reporting EW.

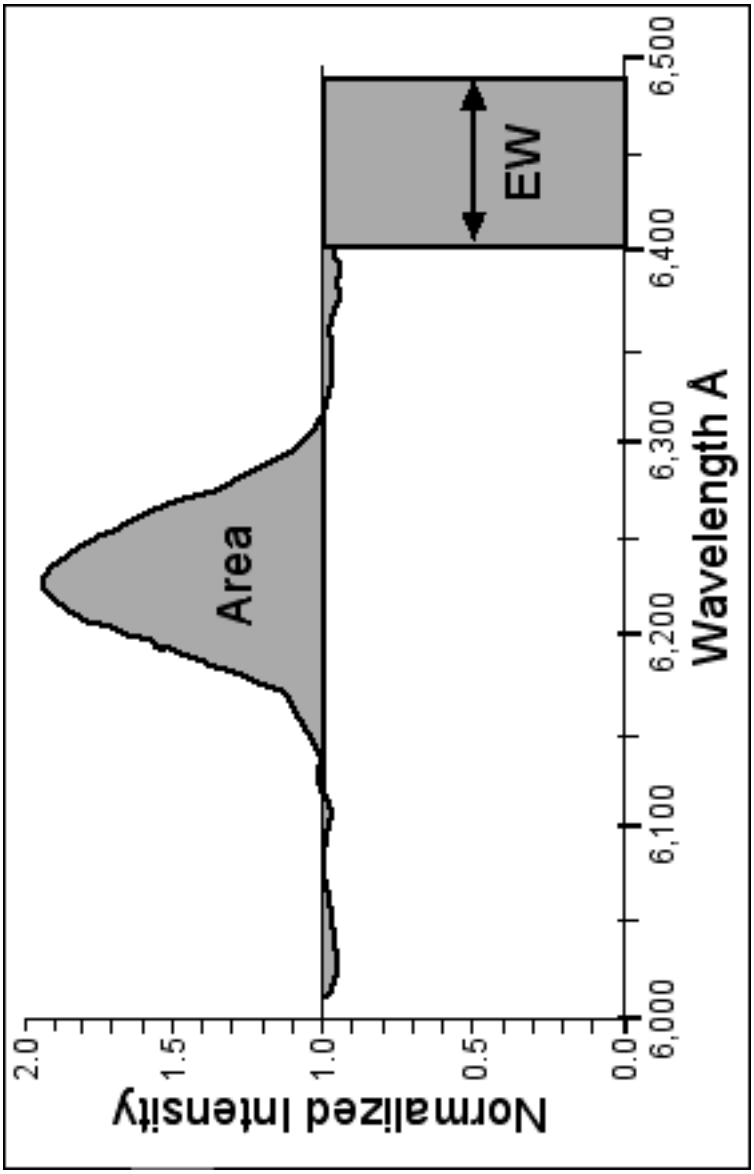

Figure 9.66 Equivalent Width

Figure 9.67 shows a hypothetical hydrogen α spectrum. The blue absorption curve has an EW of -0.1, the blue emission curve has an EW of +0.2, The main absorption line has an EW of -0.6 and the red emission curve has an EW of +0.3. The values can then be checked against other spectra for changes.

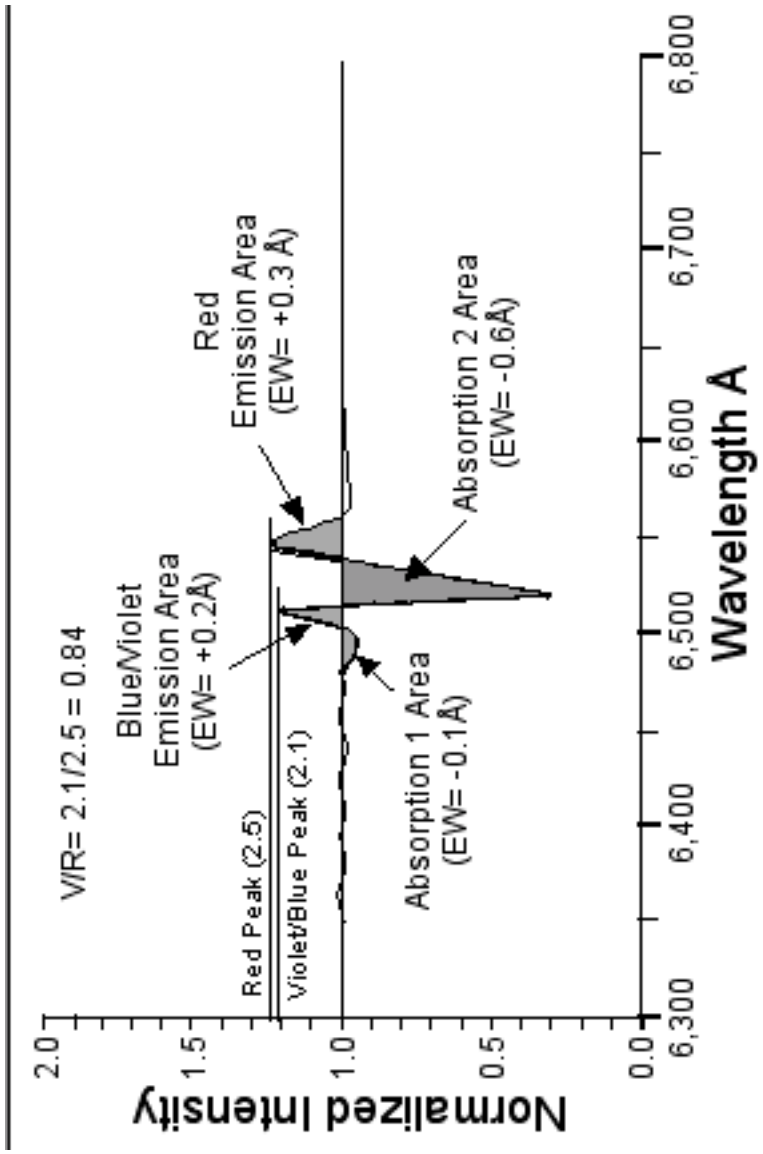

Figure 9.67 Equivalent Widths of Hydrogen α

Along with the EW a term called the VR ratio can be specified. This the ratio of the violet (V) or blue emission line to the red (R) emission line level. In this case the V/R is 0.84.

9.3.7.5 Atmospheric Lines (Telluric Lines)

When radiation passes through the Earth's atmosphere photons with wavelengths equal to the elements in the atmosphere can be absorbed. The higher the density of the atmosphere and the higher the humidity the more profound the absorption. Since these lines aren't normally of interest and confuse the stellar line, a method of eliminating the Telluric lines is provided by the software. Figure

9.68 shows the Telluric lines for Oxygen and Water from 6,800 Å through 7.700 Å.

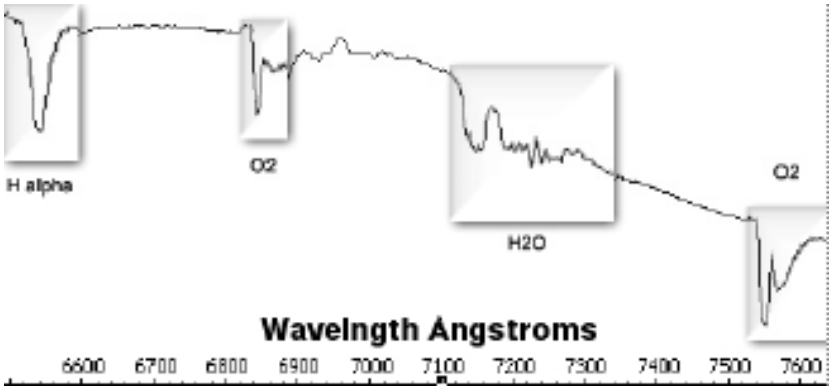

Figure 9.68 Atmospheric (Telluric) Lines
Credit VSpec Tutorial

9.3.7.6 Spectral Resolution

The resolution of a spectrograph depends on the grating characteristics, slit width and spectrum order. The spectrograph plus camera spectral resolution can be approximately characterized by the FWHM (in pixels) of the narrowest spectrum lines observed (e.g. weak neon calibration lines or interstellar features like the Na D lines), assuming you have derived the dispersion (A/pixel). An insufficient resolution impedes determination of the chemical elements having lines in this area. To help identify lines, Visual Spec includes a database of spectral lines between 3000 and 11000 angstroms for elements with atomic numbers less than or equal to that of Iron.

As mentioned above, spectral resolution is dependent on the number of lines per millimeter of the grating and the width of the slit in micrometers (μm or microns).

9.3.7.7 Spectral Intensity

The intensity of a spectrum is affected by:

The spectral response of the CCD

Its own continuum, distribution of energy into wavelength as a function of temperature (Planck's Law)

Atmospheric extinction

For a tutorial on using Iris and VSpec see:
http://www.hposoft.com/Spectra.pdf

Analysis of stellar spectra is not limited to the visible portion of the electromagnetic spectrum. There are spectral lines of interest that range above the visible bands into the ultraviolet and X-ray regions down the other side through the far infrared band into the radio frequency region. Figure 9.69 shows the electromagnetic spectrum .

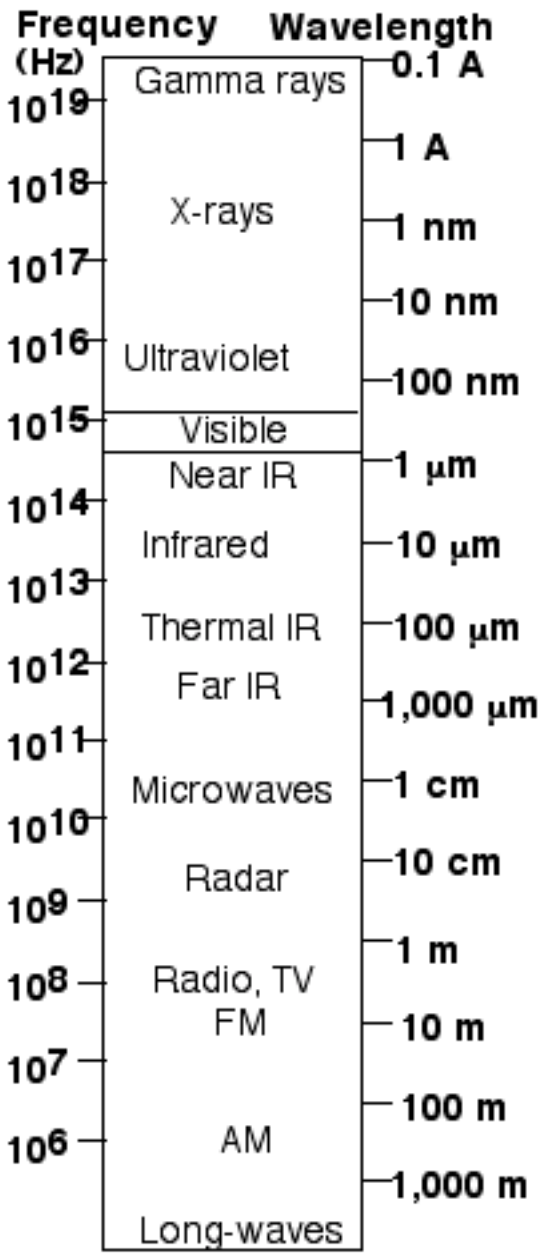

Figure 9.69 Electromagnetic Spectrum

9.4 Polarimetry

9.4.1 Introduction

One of the fundamental methods in astronomy is called polarimetry – measuring the polarization of light. Polarized light (see Figure 9.70) occurs because the electromagnetic waves can be enough "out of alignment" to "arrive" differentially, measurably so through polarizing materials. Why is starlight polarized at all? Two primary causes include scattering from an asymmetric structure of the source, or radiation passing through magnetically aligned particles between source and observer. The latter case is seen as a result of dust grains in the interstellar medium aligned by weak galactic magnetic fields.

The great observer, Albert Hiltner, and collaborators exploited this fact as long ago as 1949 to map the weak, chaotic magnetic fields of the Milky Way, by observing the non-variable polarization toward hot stars in many directions. The great theorist, Subramanyan Chandrashekar, had previously proven that spherically symmetric stars should have no net polarization, and thus any non-zero, non-variable polarization must be caused by the interstellar medium. James Kemp and collaborators further demonstrated the correctness of these predictions by measuring polarization differences in the eclipsing system Algol, during partial phases when the overall symmetry is broken.

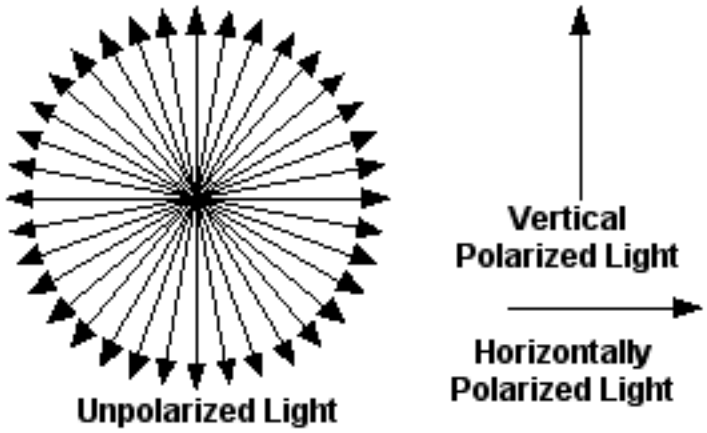

Figure 9.70 Polarized Light

The other cause of polarization is due to geometry. This should be familiar to anyone who uses polarized sunglasses – the vertical polarization orientation of the lenses is designed to cancel polarized light scattered from horizontal surfaces in the view ahead. Tilt of the head reveals rapid changes to the degree of light passing the lenses. This same principle is used in the measurement of astronomical polarized light, except that the magnitude is usually much, much less – a few percent polarization signal in astronomy is headline news, because astrophysical sources are intrinsically complex structures. However, detecting even slight polarization tells us about major structural elements in space.

In an unpolarized light field, the electric field oscillations of the arriving light waves are randomly oriented with respect to the plane of the observer, defined by his eye, a film plane, a detector surface, or a CCD array. When polarization is present, some of the arriving electric fields are aligned along a specific direction; if the alignment remains constant over time, then the light is said to be linearly polarized, but if it varies, then elliptical or circular polarization is present, depending on whether or not the intensity of electric field also changes over time.

Polarimetry is the measurement of these properties and contains information related to both the origin of the light and to scattering events the light wave has experienced along its path to the observer.

What is sought is:

1) The type of polarization;.
2) The optical axis of the polarization;.
3) The degree of polarization.

A polarimeter is the device used to measure the optical axis and degree of polarization. The type of polarization which can be measured dictates the design of the polarimeter, but it always comes down to measuring an intensity or set of intensities of light at different angular settings of an analyzer or modulator. The

simplest device, for measuring linear polarization, employs a filter or birefingent crystal (like calcite) which only allows the electric field to pass along a specific direction or axis within the material. Because sky light is sunlight scattered off the Earth's atmosphere, and since reflected light becomes partially polarized, such a tool can be used to deduce the location of the light source (i.e., the Sun), even on an overcast day. Similarly, light waves emanating from a distant star may scatter in the outer reaches of the star's atmosphere or in an interstellar cloud and become partially polarized. From basic scattering principles and geometrical models we can deduce something about the nature of the cloud by the polarization we measure. The wavelength dependence of the polarization contains clues pertaining to the size and dielectric nature of the particles in the scattering medium. For example, silicate or graphite dust grains only 50 nm in diameter can measurably influence polarization at near infrared wavelengths (McCall and Hough, 1980).

Linearly polarized light will become elliptically polarized when it is reflected from a dielectric medium. Elliptical polarization can also originate at the star by the synchrotron process and by the action of strong magnetic fields. To quantify elliptical polarization, a more sophisticated optical arrangement is required so that the phase properties of the arriving electric fields may be measured. For this a waveplate is used to modulate the arriving light, in front of a linear polarizer (called the analyzer) which is located in front of the sensor.

Four quantities, called the "Stokes vectors", which fully describe elliptical (and thus linear and circular) polarization can be determined by measuring the intensity of the electric field through a fixed analyzer at different positions of a half-wave or quarter-wave plate modulator. The optical arrangements and mathematical treatments needed to carry out Stokes vector analyses can be found in the textbook on astronomical polarimetry by J. Tinbergen (2000) and in review articles such as that by Serkowski (1974).

9.4.2 Polarimetry Techniques

Observational polarimetry is conceptually simple, but challenging in practice. The basic idea is to equip your photometer with a rotating polarizer or "wave plate" in the beam. Polarizers have a preferred orientation due to their fabrication history, much like a picket fence. In one orientation, polarized photons (like flat disks – "Frisbees") will either align and pass through, or not align and bounce off. By rotating the polarizer, one can measure any preferred plane of orientation for the arriving photons. See Figure 9.71 for a block diagram of a basic astronomical polarimeter.

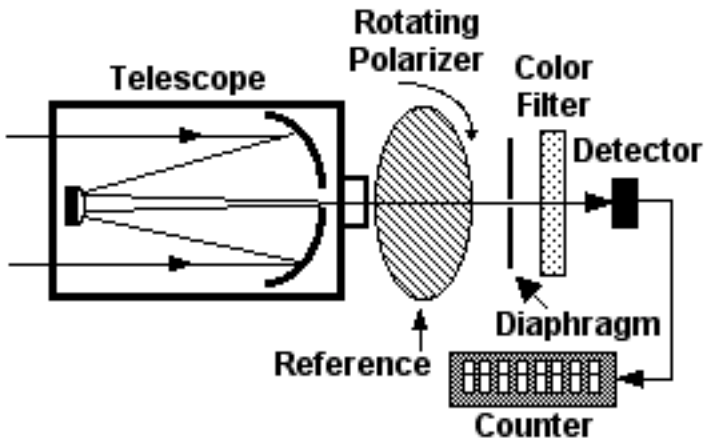

Figure 9.71 Astronomical Polarimeter

Generally, this means recording the photometric intensity as a function of polarizer angle, to determine orientation for minimum and maximum transmission. However, each optical reflection in a telescope can introduce polarization too, and the instrumental contribution can vary with optical axis orientation. Hence, mapping the instrumental polarization is a pre-requisite.

Measuring polarization is "straightforward" for highly polarized sources, like parts of the daytime sky, but astronomical sources are rarely more than 1% polarized, and this means that for good signal to noise fidelity, integration times need to be hundreds of times longer than simple images to make precision polarization measurements. The reduction of data can make use of so-called "Stokes parameters" to help evaluate the degree of linear and/or circular polarization, but the reader is invited to explore these topics on his/her own.

9.4.3 Polarimetry Equipment

Finding commercial astronomical polarimetry is equipment is difficult. Most astronomers doing polarimetry construct their own equipment. A suitable detector and possible filters are easily obtained. A rotatable polarizing disk that can be calibrated and placed in the optical path is perhaps the most challenging aspect of the equipment.

9.4.4 References

Chandrashekar, S. 1946 Astrophysical Journal, vol. 103, p.351 – "On the Radiative Equilibrium of a Stellar Atmosphere. X." http://adsabs.harvard.edu/abs/1946ApJ...103..351C

Hiltner, A. et al. 1949 Astrophysical Journal 109: 471 – "On the Presence of Polarization in the Continuous Radiation of Stars. II." - http://adsabs.harvard.edu/abs/1949ApJ...109..471H

Kemp, J., Henson, G., Barbour, M., Kraus, D., Collins, G., 1983 Astrophysical Journal, vol. 273, L85 – „Discovery of eclipse polarization in Algol"
http://adsabs.harvard.edu/abs/1983ApJ...273L..85K

A. McCall and J. H. Hough, "Near Infrared Polarimetry of Cool stars," *Astron. Astrophys. Suppl. Ser*. 42 141-154 (1980).

K. Serkowski, In: *Planets, Stars and Nebulae Studied with Photopolarimetry*, Univ. of Arizona Press (1974).

J. Tinbergen, *Astronomical Polarimetry*, Cambridge University Press (1996).

9.5 Interferometry

9.5.1 Introduction

Interference phenomena are seen by everyone when looking at the colors swirling on a bubble's surface or on an oil slick on wet pavement. This occurs because the thickness of the soap or oil layer matches the wavelength of selected colors of light. Similarly, when the light from two different telescopes is combined, it can constructively interfere, but only when the exact path difference between telescopes is zero, causing all wavelengths to combine. Small changes to telescope positions then will produce destructive or constructive combinations of the light, depending on the ratio of wavelength to distance separating the telescopes. This effect is analogous to the well-known "double slit experiment" causing light and dark bands on a screen placed behind the illuminated double slits. Numerous articles exist on this "Young's double slit" subject for the reader to pursue independently.

9.5.2 Interferometry Techniques

Given a known wavelength and separation of two telescopes, one obtains angular resolution equivalent to a telescope with an effective diameter equivalent to the separation. This is exactly the same as with a single mirror telescope, but in combination, apertures of 100 meters and more are possible, yielding angular resolution of milli-arcseconds. The unit of arcseconds is 1/3600 of a degree -- in the scheme of angular measure called degrees, minutes, seconds (this, in contrast to radian measure, where an arcsecond is about a micro-radian). Radio astronomy has used this multiple antenna method much longer, and has achieved micro-arcsecond resolution with very long baseline interferometry – using antenna separations of thousands of miles. That is possible only by recording signals independently, with an atomic clock reference, and recombining the results in a computer afterwards. With optical instruments, the work so far is simultaneous and real-time, with milli-arcsecond resolution achieved only along a one dimensional cut across the star, set by the baseline orientation of the pair of telescopes. See Figure 9.72 for a block diagram of a typical optical interferometer. As such, a single diameter measurement along one

azimuth (compass) direction can be obtained, per observation. To construct an image requires continuing observation over many baselines with multiple telescopes, and/or using earth's rotation to sample more azimuth information on the star. This technique, called aperture synthesis, is highly evolved among radio astronomy practitioners, but is under development for optical interferometry. A single mirror essentially does this too, but only on numerous "baselines" defined by the mirror's extent.

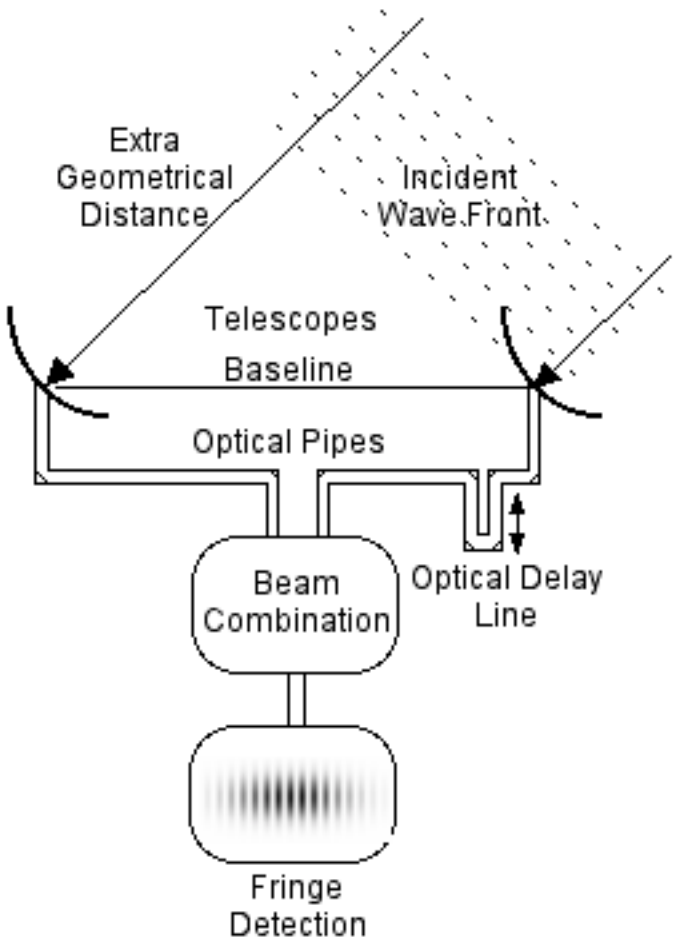

Figure 9.72 Optical Interferometer

9.5.3 Interferometry Equipment

The geniuses Fizeau and Michelson get credit for 19th and early 20th century interferometry theory and experiments, culminating with Michelson's interferometer atop the Mt. Wilson 100 inch , where angular diameters of alpha Orionis and other red supergiant stars were first measured in 1920. The method developed slowly until the advent of computers, digital detectors and precision

metrology in the 1980s and is progressing quickly, particularly with the European investment of over $500M in the Very Large Telescope Interferometer at Paranal, Chile which features combined light from four 8 meter telescopes. The key to modern optical interferometry involves the ability to position moving mirrors to micrometer precision with kilohertz speed corrections, in order to combine light from separate telescopes, matching the effective distances of separation to an integer multiple of wavelengths of light. Figures 9.73 shows a picture of the interferometer beam attached to the Mt. Wilson 100" Hooker telescope.

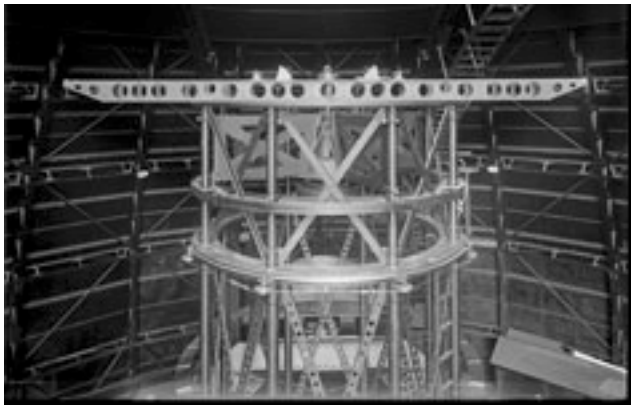

Figure 9.73 Mt. Wilson Interferometer
(Photo Credit: Wikimedia)

Figure 9.74 show a diagram of the Mt. Wilson interferometer.

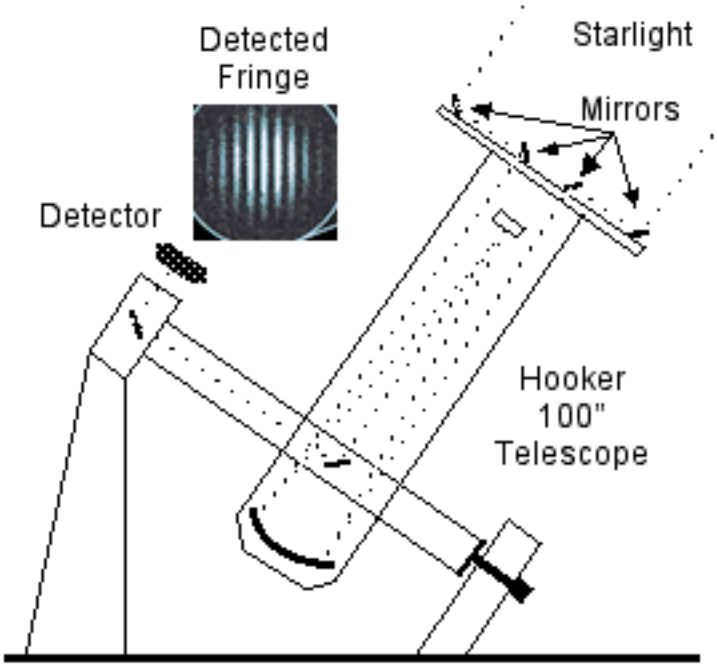

Figure 9.74 Mt. Wilson Interferometer Detail

The Large Binocular Telescope in Arizona, combining light from twin 8 meter telescopes, is a modern incarnation of the Mt.Wilson experiment.

9.5.4 References

About Albert Michelson:
http://msc.caltech.edu/about/aaMichelson.html
Michelson, A. and Pease, F. 1921 Astrophysical Journal, vol. 53, p. 249 – "Measurement of the diameter of alpha Orionis with the interferometer" http://adsabs.harvard.edu/abs/1921ApJ....53..249M

9.6 Astronomical Dates

Keeping track of dates over long periods when there are leap years involved and even changes in calendars can be a big problem. This is especially true for astronomy when you may want to go back in time hundreds of years to an event and know how much time there was between then and now. To make this task easier, a system using Julian Date was devised.

9.6.1 Julian Date

Keeping track of dates over long periods when there are leap years involved and even changes in calendars can be a big problem. This is especially true for astronomy when you may want to go back in time hundreds of years to an event and know how much time there was between then and now. To make this task easier, a system using Julian Date was devised.

Julian Date is the number of days that have elapsed since noon on 1 January 4713 B.C. and is given in the form of decimal days, not in hours, minutes, and seconds. The Julian Day begins at noon Greenwich time or 12^h UT. Leap years and calendar changes do not matter.

Examples of Julian Dates are:

11 January 1988 at 2^h45^m UT,
JD = 2,447,171.6146

11 January 1988 at 12^h2^m UT,
JD = 2,447,172.0333

15 January 1988 at 23^h55^m UT,
JD = 2,447,176.4965

16 January 1988 at 1^h0^m UT,
JD = 2,447,176.5417

What is the origin of the Julian Date system? Contrary to some beliefs, Julian Date has no connection with the Julian Calendar and was not named after Julius Caesar. Instead Joseph Justus Scaliger, in 1583, developed the Julian Period. He multiplied the lengths of three cycles: the 28-year solar cycle, the 19-year lunar cycle, and the 15-year cycle of the Roman Indiction (used in calculating the date of Easter). The resulting period (28 x 19 x 15) is 7980 years, which passed through zero in the year 4713 BC. This is a very convenient date because all recorded history, including documented astronomical events, has occurred after this date. Astronomers adopt Julian Dates because the time interval between events is independent of the day of the week, month, or year.
If a table is not available, such as those in the Astronomical Almanac, then Julian Date can be calculated using the formula

$$\mathbf{JD = 367 * Y - Int\,(\,7 * (Y + Int\,((M + 9) / 12))) / 4)}$$
$$\mathbf{+ Int\,(275 * M / 9) + D + 1721013.5 + UT / 24}$$

where Y, M, D, and UT are the year, month, day of month, and Universal Time (in 24-hour, decimal format), respectively. The function **int** is the integral part of the quotient resulting from the division of two integers (i.e., Int(3/4)=0 and Int(5/4)=1). The formula for JD is valid for the years 1901 through 2099.

Example: What is the Julian Date corresponding to $4^h\ 25^m\ 16^s$ UT on September 9, 1990?

Y = 1990
M = 9
D = 9
UT = 4.42111^h

JD = 367 x 1990 - Int(7 (1990 + Int(18 /12)) / 4)
+ Int(275 x 9 / 9) + 9 + 1721013.5 + 4.42111 /2 4
JD = 730330 - 3484 + 275 + 9 + 1721013.5 + 0.18421
JD = 2,448,143.68421

If time is recorded to the nearest minute or second, the JD can be calculated to the nearest 0.001 or 0.00001 day, respectively.

9.6.2 Heliocentric Julian Date

Because the speed of light is finite and the earth is traveling around the sun with an orbital diameter of nearly $3x10^8$ km, it is both convenient and necessary to adopt a time system that removes the effects of the earth's motion. In a geocentric reference frame, the light from a star in the general direction of the sun (i.e., near conjunction) requires approximately 16 additional minutes to reach the earth compared to a star at opposition. By using the center of the sun as reference point for all time measurements (i.e., a heliocentric system) the errors due to light-travel time across the earth's orbit are eliminated. For observations where timing to the minute or second is important, it is essential to apply this heliocentric correction. For astronomical photometry, precise timing information is specified in terms of Heliocentric Julian Date, or HJD. The correction to HJD can be found using the following equations:

$$\mathbf{HJD = JD_{Hel} = JD_{Geo} + \Delta t}$$

$$\mathbf{\Delta t = - T\ R\ (\cos\lambda\ \cos\alpha\ \cos\delta + \sin\lambda\ (\sin\varepsilon\ \sin\delta + \cos\varepsilon\ \cos\delta\ \sin\alpha))}$$

where

T = Light-travel time for 1 A.U.
(= 499 sec or 0.0057755 days)
R = Earth - Sun distance in A.U.
λ = Longitude of the sun
α = Right Ascension of the star
δ = Declination of the star
ε = Obliquity of the ecliptic (= 23.45 degrees)

Appropriate values for R and λ can be found in the Astronomical Almanac for each observing night. Because R and λ change rather slowly, a unique value of Δt can be calculated for each star and applied to all observations of that star on a given night. There are alternative expressions for Δt that use the rectangular coordinates of the sun, X and Y, rather than R and λ.

9.6.3 Modified Julian Date

There is some debate as to what Modified Julian Date (MJD) and Reduced Julian Date (RJD) mean. The purpose is to provide a focus on the more important and changing numbers. Plotting data using the full Julian date can take up much space. For periods of a decade or less or even a few decades, the first several digits may be dropped since they don't change. Only the last digits that change are used. Although the Modified Julian Date (MJD) and Reduced Julian Date (RJD) have precise definitions, we elect to plot data using a "partial" Julian Date (PJD) which is the Julian Date minus a fixed quantity, e.g., PJD = JD - 2,450,000.

JD	**PJD**
2,456,127.13	127.13
2,456,128.12	128.12
2,456,129.15	129.15
2,456,130.14	130.14
or	
2,454,129	4,129
2,454,458	4,458
2,454,691	4,691
2,454,873	4,873

Where the 127.13 ... or 4,129 ... are used as major tick points on a graph. This is handy when plotting data so each date does not need to be 7 or more digits long. If the plot covers many years, it is also helpful to put periodic dates (e.g., 12 July 2008 or just July 08) on the plot. If the plot is for a long period system, the decimal digits may be left off.

To avoid confusion it is suggested that the major tick marks of the X-axis be labeled with the partial JD with a statement below such as:

Partial Julian Date (PJD)
JD = 2450,000 + PJD

9.6.4 Julian Date List

Julian Dates for the first of each Month from 1 January 2008 to 1 December 2013. Remember, the Julian Day begins at noon Greenwich time or 12^h UT.

1 January 2008	**JD= 2,454,467**
1 February 2008	JD= 2,454,498
1 March 2008	JD= 2,454,527
1 April 2008	JD= 2,454,558
1 May 2008	JD= 2,454,588
1 June 2008	JD= 2,454,619
1 July 2008	JD= 2,454,649
1 August 2008	JD= 2,454,680
1 September 2008	JD= 2,454,711
1 October 2008	JD= 2,454,741
1 November 2008	JD= 2,454,772
1 December 2008	JD= 2,454,802
1 January 2009	**JD= 2,454,833**
1 February 2009	JD= 2,454,864
1 March 2009	JD= 2,454,892
1 April 2009	JD= 2,454,923
1 May 2009	JD= 2,454,953
1 June 2009	JD= 2,454,984
1 July 2009	JD= 2,455,015
1 August 2009	JD= 2,455,046
1 September 2009	JD= 2,455,076
1 October 2009	JD= 2,455,103
1 November 2009	JD= 2,455,137
1 December 2009	JD= 2,455,167

1 January 2010	**JD= 2,455,198**
1 February 2010	JD= 2,455,229
1 March 2010	JD= 2,455,257
1 April 2010	JD= 2,455,288
1 May 2010	JD= 2,455,318
1 June 2010	JD= 2,455,349
1 July 2010	JD= 2,455,379
1 August 2010	JD= 2,455,410
1 September 2010	JD= 2,455,441
1 October 2010	JD= 2,455,471
1 November 2010	JD= 2,455,502
1 December 2010	JD= 2,455,532
1 January 2011	**JD= 2,455,563**
1 February 2011	JD= 2,455,594
1 March 2011	JD= 2,455,622
1 April 2011	JD= 2,455,653
1 May 2011	JD= 2,455,683
1 June 2011	JD= 2,455,714
1 July 2011	JD= 2,455,744
1 August 2011	JD= 2,455,775
1 September 2011	JD= 2,455,806
1 October 2011	JD= 2,455,836
1 November 2011	JD= 2,455,867
1 December 2011	JD= 2,455,897
1 January 2012	**JD= 2,455,928**
1 February 2012	JD= 2,455,959
1 March 2012	JD= 2,455,988
1 April 2012	JD= 2,456,019
1 May 2012	JD= 2,456,049
1 June 2012	JD= 2,456,080
1 July 2012	JD= 2,456,110
1 August 2012	JD= 2,456,141
1 September 2012	JD= 2,456,172
1 October 2012	JD= 2,456,202
1 November 2012	JD= 2,456,233
1 December 2012	JD= 2,456,263
1 January 2013	**JD= 2,456,294**
1 February 2013	JD= 2,456,325
1 March 2013	JD= 2,456,353
1 April 2013	JD= 2,456,384
1 May 2013	JD= 2,456,414
1 June 2013	JD= 2,456,445
1 July 2013	JD= 2,456,475
1 August 2013	JD= 2,456,506
1 September 2013	JD= 2,456,537
1 October 2013	JD= 2,456,567
1 November 2013	JD= 2,456,598
1 December 2013	JD= 2,456,628

Glossary

AAVSO – American Association of Variable Star Observers, web site www.aavso.org

Absorption Spectra – the presence of dark portions in a bright continuum spectrum due to absorption of photons by elements present in the source that absorb specific wavelengths

ADC – Analog to Digital Converter

ADU - Analog Digital Unit. These are counts that relate to the number of photo electrons in a CCD pixel.

Air Mass – an approximation for fractional column of additional air along the line of sight, relative to straight up (zenith) defined to be one air mass. Air mass varies approximately with the inverse cosine (90 degrees minus elevation angle)

Arcsecond – an angular unit which is one 60th of an arcminute, which in turn is one $60t^{h}$ of one degree; Sun and Moon subtend about 30 arcminutes as seen from earth

Atmospheric Lines - Spectral absorption lines due to photon absorption of oxygen, water and carbon dioxide in the Earth's atmosphere. Also known as Telluric lines.

AU – Astronomical Unit, the average earth-sun separation, 93 million miles, 150 million km

AutoStar – AutoStar or more correctly AutoStar Suite is a suite of software by Meade to display a planetarium program, provide CCD camera control and image acquisition, provide telescope control for got and tracking options and contains an image processing part to process images and extract net ADU counts for a star.

Balmer Series – A sequence of spectral lines formed when electrons in hydrogen atoms transition between level 2 and higher levels – visible part of the spectrum

Black Body - A black body is an object that absorbs all light that falls on it. No electromagnetic radiation passes through it and none is reflected. Because no light is reflected or transmitted, the object appears black when it is cold.

Brackett Series - A sequence of spectral lines formed when electrons in hydrogen atoms transition between level 4 and higher levels – near infrared part of the spectrum

CCD – charge coupled device, a silicon based array detector found in many digital cameras

Collisional Broadening – The effect of electron pressure/motion on spectral line width.

Continuous Spectra – The brightness versus color distribution arising from dense materials; the color pattern is predicted by Planck's radiation law.

Continuum - The spectrum of a star created by the star's internal nuclear reactions before and absorption due to the star's atmosphere or other absorption.

Dark Frame – A digital camera image obtained when no light is allowed to reach the detector, useful in calibrating the background contribution in the images

Data Acquisition – The acquiring of star data either by single channel or CCD photometry.

Data Reduction – Taking raw counts and producing a calibrated magnitude.

Diffraction Grating - A surface with ruled lines used to produce a spectrum.

Dead Time – The time in which an addition photon cannot be counted due to the pulse width of the PMT output.

Emission Spectra – Discrete bright colors corresponding to the electron energy release in elements present in the source of the light

Envisage – A program by Meade used for control of a DSI CCD camera and acquisition of images.

EW - Equivalent Width. The area under a curve representing the power of the curve referenced to one unit of Intensity.

Extinction – The decreased brightness of stars when they are measured at lower elevations in the sky, due to particles in earth's atmosphere scattering part of the light

Extra-Terrestrial Magnitude (zero air mass) – An extrapolation of measured magnitudes with air mass variation to estimate the brightness of starlight arriving at the top of our atmosphere

FITS – Flexible image transport system, a file format specification used in astronomy to convey both large bit array images and extended header information not possible with other formats like JPEG, etc.

Flat Fields – A calibration field taken with uniform light which is then divided into the star image.

Fourier Transform – A mathematical theorem that enables any continuous function to be represented by a series of sine or cosine functions, which can be more readily analyzed

FOV - Field of View

Fraunhofer Lines - Some 700 absorption lines in the spectrum of the Sun, or of another star, first studied and named by Joseph von Fraunhofer in 1814.

FWHM - Full Width Half Mean

Heliocentric Julian Date – Correcting an earth-based observation for the light travel time to the Sun's center, in order to be able to precisely intercompare observations at different times of year

Huang Model – The basic hypothesis concerning the eclipses of epsilon Aurigae

Hydrogen Alpha – The first Balmer series transition in hydrogen, from level 2 to level 3

IAPPP – International Amateur-Professional Photoelectric Photometry organization.

Image processing – The processing of an image to obtain the raw net ADU counts for a star.

Interferometry – A method of combining light from two of more telescopes to achieve the equivalent resolution of a telescope as large as the separation of the component telescopes

IRIS - Image processing software used for processing spectra. A French freeware program written by Christian Buil.

Julian Date – A sequential date counting system in astronomy, useful for easy intercomparison of observations (see http://www.aavso.org/observing/aids/jdcalendar.shtml)

Linearity – The ability to fill a CCD pixel well with electrons in a linear way.

Luminosity Classes – distinctions made among types of stars based on surface gravity, arising from different interior evolutionary states; includes supergiant, giant, dwarf and white dwarf stars (the Sun is a dwarf star)

Lyman Series – A sequence of spectral lines formed when electrons in hydrogen atoms transition between level 1 and higher levels – ultraviolet part of the spectrum

MK System – A method of classifying stars in terms of spectral type and luminosity class, based on their spectrum appearance; the Sun is a G2 dwarf in this system; epsilon Aurigae resembles an F0 supergiant.

Modified Julian Date - Modified Julian Day (MJD) – number of days that have elapsed since midnight at the beginning of a defined, cardinal number Julian Date like 2,400,000.5.

OTA – Optical Tube Assembly.

Partial Julian Date- When plotting data, for clarity a "partial" Julian Date (PJD) which is the Julian Date minus a fixed quantity, e.g., PJD = JD - 2,450,000 may be used.

Parsec (Parallax Second) – A natural unit of triangulation, relating earth's orbit (AU) as a baseline, and a 1 arcsecond angular deviation, equivalent to 3.3 light years or 31 trillion kilometers

Peranso – Period Analysis Software.

Photometry – The measurement of the flux or intensity of an star's electromagnetic radiation

PIN diode – A diode with a wide, lightly doped 'near' intrinsic semiconductor region between a p-type semiconductor and an n-type semiconductor regions, hence the layers are labeled PIN.

Planck's Law - Planck's Law describes the relation of a black body's temperature to the intensity of the radiation.

PMT – Photomultiplier tube

PMT Saturation – A limit on the number of electrons that a PMT can transport due to large input

Polarimetry – Methods for measuring the polarization of light in order to deduce source geometry and/or magnetic effects

Radial Velocity – S spectroscopic measurement of the Doppler shift of light due to motion of the source toward or away from the observer; same principle as is used in traffic radar measurement

Reduced Julian Date - Reduced Julian Day (RJD) counts days from nearly the same defined day as the MJD, but lacks the additional offset of 12 hours used in MJD.

Rotational Broadening – Spectroscopic method for determining rotation of a source based on Doppler widening of spectral features in proportion to rotation speed and orientation

Scintillation – Scintillation or twinkling are terms for rapid variations in apparent brightness or color of a star viewed through the atmosphere.

Single Channel Photometry - The use of a single detector, PMT, PIN diode or other such detector to produce an electrical signal as a pulse or voltage/current level. The number of pulses per second is proportional to the star's brightness. The level of the electrical voltage or current for an analog system is proportional to the star's brightness.

Spectroscopy – The method of dispersing light into component colors (e.g. rainbows); analysis of the spectrum can yield information about the temperature, motion and chemical composition of the source of light

SpcAudACE - A Software program for processing spectra. French freeware program written by Benedict Maugis.

Stark Effect – A type of spectroscopic line broadening due to strong electric fields near the source of the light being measured

Stokes Parameters – As used in polarimetry, measurements of the amplitude of perpendicular components of the electromagnetic field mutually perpendicular to the direction of light travel

Telluric Lines - Spectral absorption lines due to photon absorption of oxygen, water and carbon dioxide in the Earth's atmosphere. Also known as atmospheric lines.

Threshold Adjustment – For a photon counting system the threshold adjust allows setting the level to eliminate the thermal pulses and only produce pulses resulting from photons.

Time Domain – A plot of amplitude with respect to time.

Transformation of Coefficients – Because different filter and detectors as well as telescopic optics can have different bandpasses for light, a calibration using color transformation coefficients adjust the magnitude to a standard.

UBVRIJHK Bands – A system of filters defined in astronomy by selection of particular colored glass to match specific wavelengths between near-ultraviolet and near-infrared

Undersampling – With very low power or fast optics the size of the star projected onto the CCD can be too small and a significant portion of the image can fall between the pixels and be lost.

VSpec - Visual Spec, software used for processing spectra.French freeware written by Valerie Desnoux.

Zeeman Effect – A type of spectroscopic line broadening due to strong electric fields near the source of the light being measured

Zero Point – The sensitivity of a photometric system. This includes the detector and telescope. It is a calibration factor to adjust the magnitude value for the system's sensitivity.

Meet the Authors

Jeffrey L. Hopkins
Hopkins Phoenix Observatory

Jeff has been interested in astronomy most of his life. His first telescope was a 2.4" Unitron refractor which he still has today. He began observing epsilon Aurigae with the 1982 eclipse. This has resulted in several thousand high precision photometric UBVRIJH observations of the star system. He was in charge of the last Eclipse Campaign Newsletter and the focal point for the photometry data from that eclipse. He has a BS from Syracuse University with graduate work in Physics at the University of Wyoming, University of Arizona and Arizona State University. He was a Radar Systems Engineer for General Electric Company for 13 years and a Senior Engineer for Motorola for 10 years. He has written or co-authored over three dozen professional astronomical papers as well as three other books on photometry, *Zen and the Art of Photoelectric Photometry*, *Workbook for Astronomical Photoelectric Photometry* and *AutoStar CCD Photometry*. Jeff is originally from upstate New York, but now resides in Phoenix, Arizona. During the cooler nights he spends his time in one of his two backyard observatories.

He can be reached at: phxjeff@hposoft.com or visit his web site at: http://www.hposoft.com/Astro/astro.htm

Robert E. Stencel
University of Denver

Robert Stencel is the William Herschel Womble Professor of Astronomy at Denver University. He became interested in Astronomy as a result of Sputnik, and was fortunate to have as a mentor during high school Ed Halbach, one of the founders of the Astronomical League. Following graduate study in astronomy at the University of Michigan, Dr. Stencel worked at NASA Houston and Greenbelt sites and NASA Headquarters in Washington DC, prior to joining Denver University in 1993 where he teaches astronomy and astrophysics. He is also the Director of the DU Observatories: Chamberlin and Mt.Evans.

He can be reached at rstencel@du.edu

INDEX

Subject **Page**
AAVSO
(See American Association of Variable Star Observers)
Absorption Spectra
ADC (See Analog-to-Digital Converter)
ADU (See Analog Digital Unit)
AIP4WIN
Air Mass
Algol
Alpha Aurigae
American Association of Variable Star Observers
Analog Digital Unit
Analog-to-Digital Converter
Analysis
ATIK
Atmospheric Lines
Aurigae
AutoStar
AVID
Backyard Science
Balmer Series
Binary Star Systems
Black Body
BM Orionis
Bohr, Niels
Boyd, Louis
Brackett Series
BVRI
Camera Lens
Campaign 1982 -1984
Campaign 2009 - 2011
Capella
Carroll, Sean M.
CCD
Charioteer
Collisional Broadening
Comparison Star
Continuum
Continuous Spectra
Counts
Dark Frames
Data Reduction
Deep Sky Imager
Defocusing
Diffraction Grating
Doppler Broadening

DSI Pro
Eclipsing Binary Star Systems
EE Cephei
Emission Spectra
Envisage
Epsilon Aurigae
Equivalent Width
Erechtheus
Eta Aurigae
Excel
Exposure
Extinction
Extraterrestrial Magnitude
Linearity
FileMaker Pro
Filter Slide
Filter Wheel
FITS Header
Flare Observation
Flat Fields
Focusing
Fourier Transform
Fraunhofer, Joseph von
Fraunhofer Lines
Frequency Domain
Fritsch, Johann
Full Width Half Mean
Growth Curve
Guinan, Edward E,
Heliocentric Julian Date
Hephaestus
Hopkins Phoenix Observatory
Hopkins, Jeffrey L.
HPO (See Hopkins Phoenix Observatory)
Huang, Su-Shu
Hydrogen
Hydrogen Alpha
IAPPP
Imaging
Infrared
Interferometry
International Year of Astronomy
Iris
JH
Julian Date
Kemp, James
Kids
Kirchoff, Gustav
Kuiper, Gerald

Lambda Aurigae
Lhires III
Light Curve
Ludendorff', Hans
Luminosity Classes
Lyman Series
Magnitude
Maximum Pixel Value
Mentor Project
MK System
Modified Julian Date.
Naked Eye
Neon
Newton, Sir Issac
Optec
Paschen series
P Cygni
Peranso
Period
Phase
Photometric Filters
Photometry
Photometry Equipment
Photomultiplier Tube
Photon Counting
Planck's Law
Plots
PMT
Polarimetry
Prism
Profile
Program Star
Radial Velocities
Raw Magnitude
Rotational Broadening
SAS (See Society of Astronomical Sciences)
Sawtooth Wave
Scaliger, Joseph Justus
Secchi. P.A.
Sine Wave
Society of Astronomical Sciences
Spectral Intensity
Spectral Type
Spectral Resolution
Spectroscopy
Spectroscopy Equipment
Spectrum
SpcAudACE
Square Wave

SSP-3
SSP-4
SSP-5
Star Analyser 100
Star Systems
Stark Effect
Stellar Spectra Classification
Stencel, Robert E.
Stoke's Parameters
Peranso
Stromgren, Bengt
Struve, Otto
Telephoto Lens
Telescope
Telluric Lines
Theta 1 Orionis B
Threshold Adjustment
Time Domain
Triangular Wave
Transformation
Coefficients
UBV
Ultraviolet
Under Sampling
Visual
VSpec
Vulcan
VV Cephei
Wide Angle Lens
Woollaston, William
Hyde
Zeeman effect
Zeta Aurigae